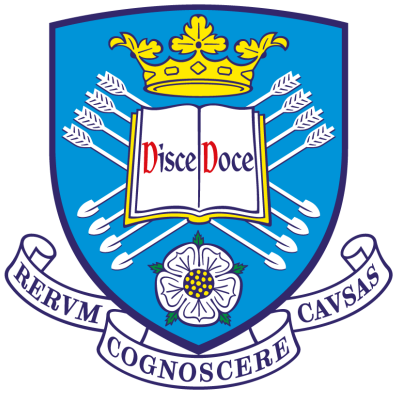

The University Of Sheffield.

Manipulation of Endoplasmic Reticulum Folding and Assembly Machinery for Improved Production of Complex Biotherapeutics

Author: Oscar Swindley

PhD Thesis

A dissertation submitted for the degree of
Doctor of Philosophy

Department of Chemical & Biological Engineering
University of Sheffield
United Kingdom

Research conducted in association with AstraZeneca

May, 2021

Declarations

Deceleration of Originality

I, Oscar Swindley, in accordance with the University of Sheffield regulations, hereby declare that this thesis was solely composed by myself and that data presented is the product of my own efforts. Results generated in collaboration have been clearly stated and are duly acknowledged. The contents of this document are original and have not been submitted in part or whole for any other degree or qualification.

Statement of Confidentiality

This document contains information confidential to AstraZeneca and must not be copied or distributed. Any unauthorised use or disclosure of this file or its contents is not permitted and may be unlawful.

"We cannot solve problems with the same thinking we used to create them"

Albert Einstein

Abstract

Chinese Hamster Ovary (CHO) cells ability to produce complex glycoproteins which do not illicit an immune response in humans makes them ideal hosts cell factories for the production of recombinant therapeutic proteins. Their responses are well characterised through extensive use in biopharmaceutical platforms, simplifying regulatory approval. Modern therapeutics are shifting towards unnatural multi-specific and fragment-based antibody modalities, presenting new challenges to host CHO cell factories. Cellular production bottlenecks can prevent promising therapeutics from progressing to market, due to diminished product titre or quality. Despite diverse cell engineering approaches to facilitate production, solutions are often highly context specific and unique to individual molecule and CHO hosts evaluated.

This thesis is divided into two research branches aiming to facilitate the rapid identification of context specific solutions to aid the production of modern therapeutics.

Through the design of an industry applicable transient Simultaneous Overexpression and Silencing Co-transfection (SOSC) gene screening platform, a High Throughput (HTP) workflow is developed. This facilitates rapid identification of product specific genetic engineering targets, providing insights into context specific sensitivity of effector gene manipulation. This platform was applied, evaluating stable Monoclonal Antibody (mAb) producers of opposing expression difficulty, identifying several molecule specific and one host cell engineering target. Despite this, relation of the experimental results back to the host specific transcriptomics dataset was unsuccessful.

In parallel, compounds which alleviate pathologic protein aggregates in disease models were evaluated as novel tools to reduce aggregation rate in Difficult to Express (DTE) mAbs. This aimed to demonstrate whether aggregate formation in proteopathic disease is mechanistically similar to that of modern DTE therapeutics. An initial Proof of Concept (POC) study evaluating a small library of proteostasis regulators found most compounds resulted in non-toxic growth arrest. Upon delayed supplementation, this resulted in several product specific titre and Specific Productivity (qP) increases. Next, a diverse library of compounds associated with disaggregation in models of proteopathic disease was identified. Preliminary assessments identified 53 hits, and the subsequent evaluation found 20 % of the total library improved and/or titre of a model DTE mAb.

Keywords: Cell culture enhancers, CHO cell engineering, Folding and assembly processes, High throughput screening, Monoclonal antibody aggregation, Proteopathic disease, RNA interference.

"Dīvide et imperā"

Philip of Macedonia

Acknowledgements

This thesis is dedicated to my grandfather, Practoor Subramaniam, whom I hope gets many hours of pleasure reading this book.

First, I would like to thank my supervisor Professor David James, for his continuous advice and guidance throughout the duration of my Ph.D studies. I would like offer a special thanks Dr. Emma Kelsall for her invaluable time and support, going above and beyond to maximise the success and impact of my project. I would also like to thank Dr. Andrew Peden for his guidance and for taking the time to discuss the finer implications of experimental results. I am also grateful to AstraZeneca for funding the project, and for the opportunities provided by everyone involved in the collaboration with the University of Sheffield.

A special mention goes to all current and past members of the DCJ lab, who were of great professional and personal support. In particular, I would like to thank Dr. Yash Patel, Dr. Joe Cartwright and Dr. Devika Kalisi for their mentorship and guidance at various stages of my Ph.D journey.

A huge thank you to all my friends and family, for the ongoing support, encouragement and patience over the last four years. A particular mention goes to a dear friend Dr. Romain Guicherd, whose guidance and patience whilst learning computer programming were invaluable.

Finally, thank you to my partner Lucy, for being my rock, keeping me sane and for the endless hours spent proofreading.

"If I have seen further it is by standing on the shoulders of Giants"

Isaac Newton

Contents

List of Figures

List of Tables

Glossary

This glossary contains a complete list of acronyms, excluding genes and proteins, used throughout this thesis. Acronyms are defined upon first use in each chapter.

Abbreviation	**Description**	**Page**
Δ-StD	Change in Standard Deviation	183, 184
Δ-%CV	Change in Coefficient of Variation	184
ΔCV	Change in Coefficient of Variation	183, 184
%CV	Percentage Coefficient of Variation	72, 184
E. coli	*Escherichia coli*	29, 30
4-PBA	4-Phenylbutyrate	17
ALS	Amyotrophic Lateral Sclerosis	17, 113, 117, 118, 131, 145, 146
BLAST	Basic Local Alignment Search Tool	14, 31
BSA	Bovine Serum Albumin	35
cDNA	Complementary Deoxyribonucleic Acid	12, 16
CDR	Complementary Determining Region	2
CDS	Coding DNA Sequence	29

Abbreviation	Description	Page
CHO	Chinese Hamster Ovary	v, xii, xix, xx, 5–7, 9, 10, 14–16, 19–21, 24–27, 33, 34, 40, 44, 46, 47, 57, 59, 63, 69, 70, 73–75, 78, 84, 89–91, 94–97, 107, 109–111, 113–115, 118, 120, 132, 142, 144–146, 149–155, 174, 182
CJD	Creutzfeldt-Jakob disease	117, 118
CV	Coefficient of Variation	68, 72, 121, 124, 126, 133, 134, 183, 184
DMSO	Dimethyl Sulfoxide	xvi, 17, 25, 31, 98, 99, 101–103, 106, 107, 109, 111, 121, 152
DNA	Deoxyribonucleic Acid	5, 11, 20, 29, 30, 33, 34, 44, 46–49, 56–59, 65, 66, 69–71, 79, 82, 83, 91, 149, 153
dsRNA	Double Stranded Ribonucleic Acid	xii, 10–12, 14, 91, 150, 151, 153, 154
DTE	Difficult to Express	v, xi, xii, 3, 7, 18–21, 24, 44, 73, 75, 78, 89, 92, 93, 95–97, 100, 103, 110, 111, 113, 115, 126, 145, 149, 151–156
DVD	Duel Variable Domain	4
DWP	Deep Well Plate	20, 25, 32, 33, 55, 58, 60, 61, 64, 65, 71, 97, 106, 150, 158

Abbreviation	Description	Page
ELISA	Enzyme-Linked Immunosorbent Assay	180, 184
ER	Endoplasmic Reticulum	xvi, 7, 9, 10, 17–19, 58, 73, 74, 76, 78, 82, 83, 93, 94, 96, 109, 114, 120, 135, 144, 145, 151, 152
ERAD	ER-Associated Protein Degradation	9, 93, 127
ERDJ	ER localised DNA-J homologue	78, 92
esiRNA	endoribonuclease prepared small interfering Ribonucleic Acid	xv, xvi, 12, 13, 31, 33, 55, 57–60, 67, 70, 78–81, 91, 92, 150, 153, 158
ETE	Easy to Express	xi, 19–21, 24, 73, 75, 78, 84, 90, 92, 93, 95–97, 99, 104, 105, 109, 150, 151, 153, 154
FAB	Fragment, Antigen Binding	2, 3
FBS	Fetal Bovine Serum	46, 69
Fc	Constant Domain of Antibody	2, 181
FCS	Fetal Calf Serum	46, 69
FDA	U.S. Food and Drug Administration	2, 5
FP	Fluorescence Polarization	28, 181, 182, 184
FPKM	Fragments per Kilo-base of Transcript per Million mapped reads	70, 76
FSC	Front Scatter	34, 50
FTD	Fronto-Temporal Dementia	117, 131
ftRNA	Fluorescent-Tagged Small Interfering Ribonucleic Acid	34, 49–54, 56–58, 69, 70
Fv	Antibody Variable Domain	2
GC	Guanine and Cytosine	14
GO	Gene Ontology	73, 76, 77, 90, 159
GOI	Gene of Interest	11, 14, 44, 78, 153

Abbreviation	Description	Page
HCP	Host Cell Protein	43, 59–61, 71
HEK293	Human Embryonic Kidney 293	6, 20, 109
HEPA	High-Efficiency Particulate Absorbing	23, 33
HMWS	High Molecular Weight Species	38
HPL-SEC	High-Performance Liquid Size Exclusion Chromatography	xvi, xvii, 121–123, 142, 147, 162
HPLC	High-Performance Liquid Chromatography	33, 37, 38, 40, 180, 184
HTP	High Throughput	v, 19, 20, 44, 56, 65, 66, 71–73, 91, 101, 106, 115, 125, 142, 147, 149, 150, 152, 155, 156
HTP	High Throughput Screening	120, 121
ITCD	Integral Total Cell Density	134
IVCD	Integral Viable Cell Density	xvii, 20, 73, 78–85, 87, 88, 90–92, 101–105, 107, 109–111, 121, 122, 126, 133–135, 142, 143, 145–147, 153, 161
mAb	Monoclonal Antibody	v, xi, xii, xx, 1–7, 19–21, 24, 28, 44, 46, 55, 62–64, 69, 73–78, 84, 88–101, 103–107, 109–111, 113–115, 121–123, 126, 135, 139, 142–147, 149–155, 159, 162
MER	Mutant Oestrogen Receptor Domain	19
MFI	Median Fluorescence Intensity	34, 51, 53, 54, 57, 58, 70
miRNA	micro Ribonucleic Acid	10, 12, 14, 15, 91, 154

Abbreviation	Description	Page
mP	Milli-Polarisation Units	28, 181, 184
mRNA	messenger Ribonucleic Acid	7, 9–14, 31, 70, 92, 93, 116
MSX	L-Methionine Sulfoximine	24, 25
NaBu	Sodium Butyrate	15
NS0	murine myeloma cell line	6
OTE	Off-target Effect	13–15
PBS	Phosphate Buffered Saline	27, 28, 34–37, 40, 184
PBS-T	PBS, 0.1% Tween-20	36
PCD	Peak Cell Density	21, 46, 60, 62, 69, 71, 149
PCR	Polymerase chain reaction	12
PMT	Photomultiplier Tube	34
POC	Proof of Concept	v, 20, 97, 100, 109, 151, 152
POI	Protein of Interest	59
PTM	Post Translational Modification	7
qP	Specific Productivity	v, 1, 6, 16, 74, 78–85, 87, 88, 90, 92, 93, 98, 101–107, 109–111, 126–128, 130, 145, 151, 153
r-protein	Recombinant Protein	xix, 1, 2, 6, 15, 16
RAN	Repeat-Asociated Non-ATG initiated	131
RFU	Relative Fluorescence Units	51, 109
RIPA	Radio-Immunoprecipitation Assay	35, 41

Abbreviation	Description	Page
RNA	Ribonucleic Acid	xv, xvi, 7, 10–12, 14, 20, 31–33, 41, 44, 46–49, 51, 53, 55–60, 65, 66, 69–71, 73, 74, 91, 92, 116, 131, 149, 153, 154, 158, 159
RNAi	Ribonucleic Acid Interference	xvi, 10–16, 20, 44–49, 69–72, 74, 77, 79–83, 89–92, 94, 149, 150, 153, 154
RNAseq	Ribonucleic Acid Sequencing	70, 73, 76, 77, 87, 89, 90, 159
ROS	Reactive Oxygen Species	117
scFv	Single Chain Variable Fragment	2
SDS-PAGE	Sodium Dodecyl Sulfate–Polyacrylamide Gel Electrophoresis	35
SEC	Size Exclusion Chromatography	37, 41
SEM	Standard Error of the Mean	59, 60, 82, 83, 107
shRNA	Short Hairpin Ribonucleic Acid	10, 11, 14–16, 153
siRNA	small Interfering Ribonucleic Acid	xv, 10–14, 16, 20, 31–34, 41, 49, 50, 53, 55, 58–60, 70, 79, 90–92, 150, 153, 158
SME	Small Molecule Enhancer	96
SOSC	Simultaneous Overexpression and Silencing Co-transfection	v, x, xii, 20, 43, 69, 73, 75, 89, 94, 149, 150, 153
SSC	Side Scatter	34, 50
ssRNA	Single-Stranded Ribonucleic Acid	11
StD	Standard Deviation	52, 54, 55, 57, 58, 63, 64, 67, 68, 72, 88, 99, 103–106, 121, 122, 124, 125, 134, 139, 140, 143, 183, 184

Abbreviation	Description	Page
stRNA	Small Temporal Ribonucleic Acid	12
SWP	Shallow Well Plate	xiii, 20, 25, 26, 33, 61–67, 71, 72, 78, 100, 103, 121, 142, 193, 198, 199
TAE	Tris-Acetate-EDTA	29
TBS	Tris Buffered Saline	35, 36
TCD	Total Cell Density	26, 27
TE	Tris-Ethylenediaminetetraacetic Acid	33
TMP	Trimethoprim	19
tncRNA	Tiny Non-coding Ribonucleic Acid	12
tRNA	Transfer Ribonucleic Acid	11
UPR	Unfolded Protein Response	9, 10, 17–20, 74, 76, 78, 89, 92, 93, 96, 97, 109, 114, 126, 151
UV	Ultra-Violet	33
VCD	Viable Cell Density	26, 27, 55, 58, 59, 61, 64, 67, 100, 106, 121, 122, 133, 134, 142
Vh	Heavy Chain Variable Domain	2–4
Vl	Light Chain Variable Region	4

Glossary of Genes & Proteins

This glossary contains a complete list of genes and proteins used throughout this thesis. Acronyms referring to genes are italicised in the the thesis body.

Abbreviation	**Description**	**Page**
APP	amyloid precursor protein	114, 116
ASK1	Apoptosis Signalling Kinase 1	9
ATF4	Activating Transcription Factor 4	9
ATF6	Activating Transcription Factor 6	9, 10, 18–20, 96, 97, 109, 114, 151
ATF6α	Activating Transcription Factor 6α Isoform	10
ATF6β	Activating Transcription Factor 6β Isoform	10
Bak	BCL2 Antagonist/Killer	15
Bax	Bcl-2-Associated X Protein	15
Bcl2	Shared Bcl-2 Homology Domains	15, 16
BIP	Immunoglobulin Binding Protein	9, 55, 58–60, 70, 78, 84
C9ORF72	Chromosome 9 Open Reading Frame 72	118, 131, 139, 141, 146
CALR	Calreticulin	9, 81, 87, 91
CANX	Calnexin	9, 81, 91, 92
CHOP	C/EBP Homologous Protein	9
DHFR	Dihydrofolate Reductase	5, 6, 19
DICER	Endoribonuclease Dicer	xv, 11, 12
EDEM1	ER Degradation Enhancing α-mannosidase Like Protein 1	9

Abbreviation	Description	Page
eGFP	Enhanced Green Fluorescent Protein	34, 48–51, 56–58, 69, 70, 80
eIF2α	Eukaryotic Initiation Factor 2 α	9, 10, 19
ERDJ3	Endoplasmic Reticulum DNA J Domain-Containing Protein 3	78, 81, 84, 91, 92
ERDJ4	Endoplasmic Reticulum DNA J Domain-Containing Protein 4	78, 81, 85, 87, 92, 93
ERDJ5	Endoplasmic Reticulum DNA J Domain-Containing Protein 5	73, 81, 84, 86, 87, 91, 92, 154
ERO1A	Endoplasmic Reticulum Oxidoreductase 1 Alpha	78, 86, 92
ERO1B	Endoplasmic Reticulum Oxidoreductase 1 Beta	78, 81, 84, 86, 91, 92
FKBP12	12-kDa FK506-Binding Protein	117
FOXA1	Forkhead Box Protein A1	75
FUS	RNA Binding Protein 'Fused in Sarcoma'	113, 131, 139, 146
FUT8	Fucosyltransferase 8	16
GAPDH	Glyceraldehyde 3-phosphate dehydrogenase	36
GMD	GDP-D-Mannose Dehydratase	16
GRP94	94-KDa Glucose-Regulated Protein	55, 58–60, 70, 85, 86, 92, 93
GS	Glutamine Synthetase	6, 89, 90
HSF1	Heat shock factor 1	114, 117
HSP	Heat Shock Protein	17
HSP90	Heat Shock 90-KDa Protein	117, 145, 152
HSPA1	Heat Shock 70-KDa Protein member A1	77, 90
Htt	Huntingtin protein	118, 145, 146, 152
HYOU1	Hypoxia Up-Regulated 1	81, 88, 91, 93

Abbreviation	Description	Page
IgG	Immunoglobulin G	xvii, 2–4, 16, 18, 28, 37, 38, 41, 66, 71, 78, 120, 122, 124–128, 136, 137, 139, 180–184
IRE1	Inositol Requiring Enzyme 1	9, 18, 19, 78, 96, 114
MAPK	Mitogen-Activated Protein Kinase	117, 141, 145, 146, 152
MAPK14	Mitogen-Activated Protein Kinase 14	13
mTOR	mammalian Target Of Rapamycin	113, 118, 145
NFκB	Nuclear factor kappa beta	117
P4HB	Prolyl 4-Hydroxylase Subunit Beta	9, 74, 84, 85, 87, 92
PDI	Protein Disulfide Isomerase	76
PDIA2	Protein Disulfide Isomerase Family A Member 2	77, 90
PDIA5	Protein Disulfide Isomerase Family A Member 5	55
PDIa6	rotein Disulfide Isomerase Family A Member 6	81, 84, 91, 92
PERK	PKR-like ER Kinase	9, 18, 19
PKR	Ribonucleic Acid Dependent Protein Kinase	10
PPIases	Peptidyl-Prolyl cis/trans Isomerases	117
PPIB	Peptidylprolyl Isomerase B	84, 85, 87
RIPK1	Receptor-Interacting serine/threonine-Protein Kinase 1	118
RISC	Ribonucleic Acid Induced Silencing Complex	xv, 11, 12, 14
RNAse	Ribonuclease Protein Family	18
RNase III	Ribonuclease III	11, 12
SEC22B	ER-Golgi SNARE of 24 KDa	55, 58–60, 70, 158
SOD1	Superoxide Dismutase 1	118

Abbreviation	Description	Page
SRP14	Signal Recognition Particle 14	78, 81, 84, 87, 88, 92
TDP43	Transactive response DNA-Binding Protein 43	113, 131, 139, 146
TRAF2	TNF Receptor Associated Factor 2	9
TTR	Transthyretin	18–20, 109, 114
XBP1	X-box Binding Protein 1	9, 19, 78
XBP1s	Spliced form of X-box Binding Protein 1	18, 74, 84, 87, 92, 96, 114

Chapter 1

Introduction

1.1 Introduction

Cell culture technology has considerably matured in the last 20 years, evolving to become evermore reliable and robust. There are many steps to be optimized that synergistically contribute to the successful exploitation of this technology and produce a given Recombinant Protein (r-protein) at high quantity and desired quality, while keeping production costs low.

Production yield is dependent on numerous factors due to the complexity of Monoclonal Antibody (mAb) manufacture, therefore each step requires stringent evaluation and optimisation. One major step is the upstream process, starting from the frozen vial of the producer clone and ending with the harvest of the culture broth. Critical parameters in this procedure are; (i) the time until the desired cell density is reached, determined by the specific growth rate (μ) of the cells, (ii) the duration of the production phase enabling accumulation of r-protein from a high-density and viable culture, and (iii) the obtainable product titre determined by the Specific Productivity (qP) and the overall process duration.

Synthetic host cell engineering aims to increase the duration of a fed-batch process in the bioreactor. The process improvements, which are often only empirically described, are facilitated by achievements in vector design and genetic engineering of host cell lines.

1.2 Bio-Pharmaceuticals and Recombinant Protein Development

Paul Ehrlich proposed the idea of a 'magic bullet' in the early 20th century, theorising that if a compound could be designed to specifically target a disease-causing pathogen, then a toxin could be delivered alongside the selective agent (Tansey and Catterall 1994). In 1970, it was understood that cancerous B-cells produce a single type of antibody, but it was not until 1975 that Georges Köhler and César Milstein fused myeloma cells with B-cells creating hybridomas capable of producing specific antibodies to known antigens. Riechmann et al. 1988 pioneered the process of mAb humanisation, eliminating immune reactions caused by previous attempts.

Although natural analogues were the first bio-pharmaceutical products developed, mAbs are the controlling force in the modern market (Walsh 2003). As of 2014, 47 mAbs have been approved in the US and Europe with an average approval rate of 4 products per year, and a predicted $125 billion per annum in sales by 2020 (Ecker et al. 2015). Monoclonal antibodies are homogeneous molecules, created by identical cells all derived from a single parental clone. Therefore, they have monovalent affinity to their target antigen. Theoretically, antibodies can be raised to specifically bind to almost any substance, although development of these into a production pipeline to create a U.S. Food and Drug Administration (FDA) approved drug can be problematic.

The broad umbrella of bio-pharmaceuticals covers any pharmaceutical drug that has been manufactured, synthesised, or extracted in/from a biological organism or component. These include a vast array of products including vaccines, blood components, tissues and gene therapies (Rader 2008). Of interest to my project is the production of r-proteins. These are the most common type of bio-pharmaceuticals, holding the largest market share of the industry by significant margins. r-proteins can be divided into a range of subclasses including analogues to natural proteins (for example erythropoietin), monoclonal antibodies, fusion proteins, bi-specifics, biosimilars and more.

As the r-protein industry has matured, molecules have been dissected into smaller antigen binding fragments deviating further from those found in nature, to produce mono and multivalent fragments. The driving force is that often the Constant Domain of Antibody (Fc) of an IgG can have undesired immune-activating effects (Holliger and Hudson 2005); a common failure for antibodies targeting solid tumours with physical barriers. This is due to the large Fc region limiting therapeutic effects by preventing the antibody penetration to the centre of the tumour (Christiansen and Rajasekaran 2004). Antibody fragments are often used in place of whole IgG molecules where accessibility can be a limiting factor.

Antibody fragments are typically based on the Fragment, Antigen Binding (FAB) domain or Single Chain Variable Fragment (scFv) as building blocks (Figure 1). The Antibody Variable Domain (Fv) consists of the variable domains of the heavy and light chains. Problematically, Fv domains inherently have limited stability due to domain disassociation, hence a peptide linker was introduced to create the scFv, which is a naturally monomeric multivalent fragment. Varying linker length can allow control over the degree of multimerisation (Bird et al. 1988; Holliger, Prospero, et al. 1993; Wilkinson, Hall, et al. 2009). Due to these characteristics, scFvs have become one of the primary building blocks of antibody fragments. Once single mouse Heavy Chain Variable Domains (Vhs) were shown to be functional, it was suggested they may be able to target pathogenic receptors otherwise inaccessible to intact antibodies. The Vh fragments encountered many problems including lack of affinity, solubility and aggregation (Ward et al. 1989). This was not addressed until Vh domains containing long Complementary Determining Region (CDR) loops were discovered in both camelids and the shark variable new antigen receptor domain; allowing targeting of previously inaccessible active sites (Greenberg et al. 1995; Muyldermans et al. 1994). Several companies have been founded based on these single domain antibody technologies (Wesolowski et al. 2009).

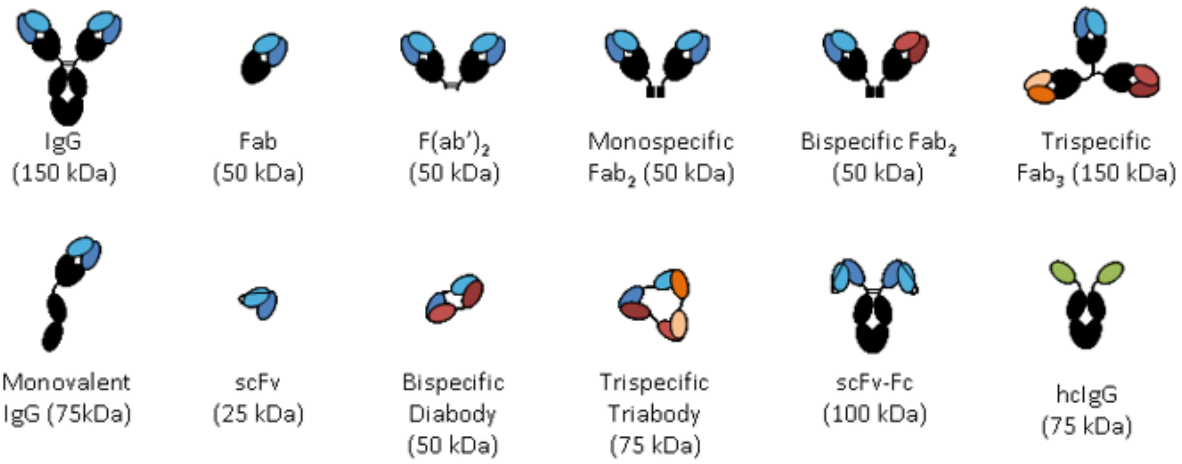

Figure 1.1: Schematic representation of different antibody formats.
Schematic representation of different antibody formats showing the classical IgG molecule, camelid heavy chain IgG (hcIgG) and shark IgNAR alongside antibody fragments generated from these. Figure taken from absoluteantibody.com on 21/11/2017.

Despite the above, a key drawback to antibody fragments is the lack of an Fc domain. Without this, Fc-mediated membrane recycling and bidirectional transcytosis of IgG across epithelial cells are prevented (Kuo and Aveson 2011). As a result, these molecules have a greatly reduced half-life. This has led to independent research efforts by many companies such as Genentech, Astrazeneca and Pfizer, in attempts to re-engineer this natural IgG property with molecules containing a single FAB arm, or monovalent IgGs (half antibody) (Ishino et al. 2013; Martens et al. 2006; Wilkinson, Fowler, et al. 2013). These engineering challenges require host production cells to produce molecules beyond the standard IgG models which are outside of their natural capacity, therefore a need exists to develop novel methodologies to supplement our existing engineering toolbox. These molecules fall under the category of Difficult to Express (DTE) mAbs, a category that includes; antibody-receptor fusions, condensed FAB regions, antibody-drug conjugates, bi-specific and FABs antibodies. Models are also expanding to tri-specifics, single Vh domains and beyond (Figure 1.1).

Bi-specifics are the largest upcoming classes of antibody and antibody-like proteins, which combine at least two specific antigen-binding elements. As these do not naturally occur, they are typically synthetically constructed. The primary advantage of binding multiple epitopes resides in the ability for one arm to bind with a molecule, marker or organism, while the other arm acts as an effector; allowing recruitment of effector cells or delivery of a payload (Gu and Ghayur 2012). Additionally, bi-specific molecules can be used to dual-target a cell type with much higher specificity than mono-specific IgGs. Some key types are quadromas, hetero-dimeric bi-specific IgGs, bi-specific fusion antibodies and multi-specific antibodies.

The first described bi-specific antibodies were created through the fusion of two hybridoma cell lines, creating a quadroma (or hybrid hybridoma) cell line capable of secreting whole IgGs with binding characteristics of both parental hybridomas (Milstein and Cuello 1983). However, due to the random pairing of 4 heterogeneous antibody chains (2 heavy and 2 light), only 12 % yield is the desired functional antibody, leading to production and purification challenges. Bi-specific

antibodies are generally understood to be hetero-dimeric molecules (with each arm targeting a different antigen). Several techniques have been developed to skew antibody formation towards the desired antibody stoichiometry. These include knobs-in- holes, amino acid substitutions by Genentech (Ridgway et al. 1996), and electrostatic steering by Amgen (Gunasekaran et al. 2010), however these only address the issue of heavy chain association. To address the final issues of light chain shuffling, two key options exist. Firstly, CrossMab (Roche) exchanges the proximal CH1 and CL domains on one arm, keeping the Vh and Light Chain Variable Region (Vl) domains constant, making heterodimer formation preferential (C. Cain 2011). Alternatively switching to an scFv-Fc model, whereby the heavy and light chains are linked together.

Bi-specific antibody fusions have been considered to avoid the manufacturing complications associated with heterodimeric bi-specific antibodies such as heterodimer formation and light chain shuffling. Direct coupling of domains in fusion molecules avoids the production of shuffled variants but results in a non-standard IgG molecule.

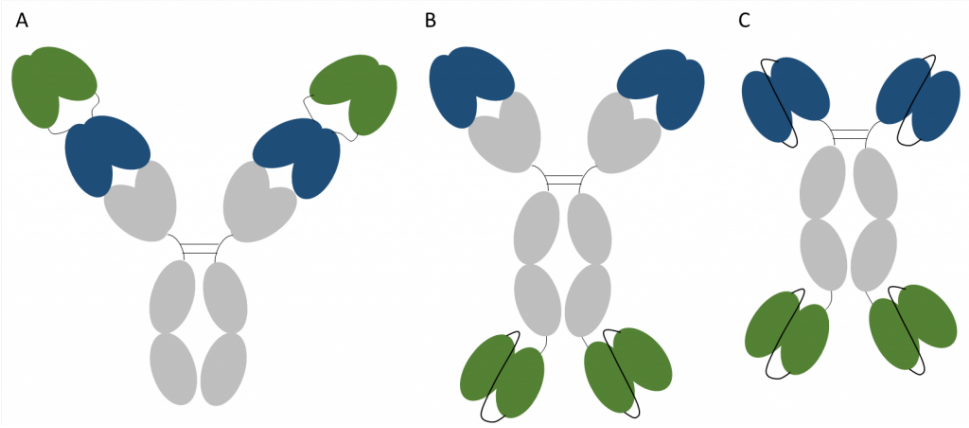

Figure 1.2: Graphical representations of antibody formats.
A) duel variable domains B) IgG-scFv and C) scFv-Fc-scFv fusion. Grey regions are non-modified from the traditional IgG model, green and blue regions represent differential specificities. Figure taken from absoluteantibody.com on 29/11/2017.

Figure 1.2 shows several different bi-specific antibody fusion modalities. The first is the Duel Variable Domain (DVD) IgG developed by Abbott where the N-terminus is elongated by addition of a second variable domain resulting in a hetero-tetramer molecule possessing 2 heavy and 2 light chains with tandem variable domains, as shown in Figure 1.2a (Gu and Ghayur 2012). Other approaches include engineering an antibody that binds one antigen at the N-terminus, and another at the C-terminus (Figure 1.2b), or an scFv-Fc-scFv format can be used where the variable domains on both aspects of the bi-specific molecule are linked (Figure 1.2c). Multi-specific antibodies can be generated by combining any of the existing technologies to create tri-, tetra- and penta-specific antibodies. Examples include AstraZenecas's reported IgG with back to back scFvs on the molecule C-terminus, and the linking of antigen binding peptides to the C and/or N terminus to allow up to 5 specificities by Zygenia (Dimasi et al. 2015; LaFleur et al. 2013).

With mAb development progressing rapidly, there are ever-increasing pressures to produce complex and un-natural molecules on a large scale, at high qualities to reach commercial viability.

Several examples of the most complex molecules are shown in Figure 1.3.

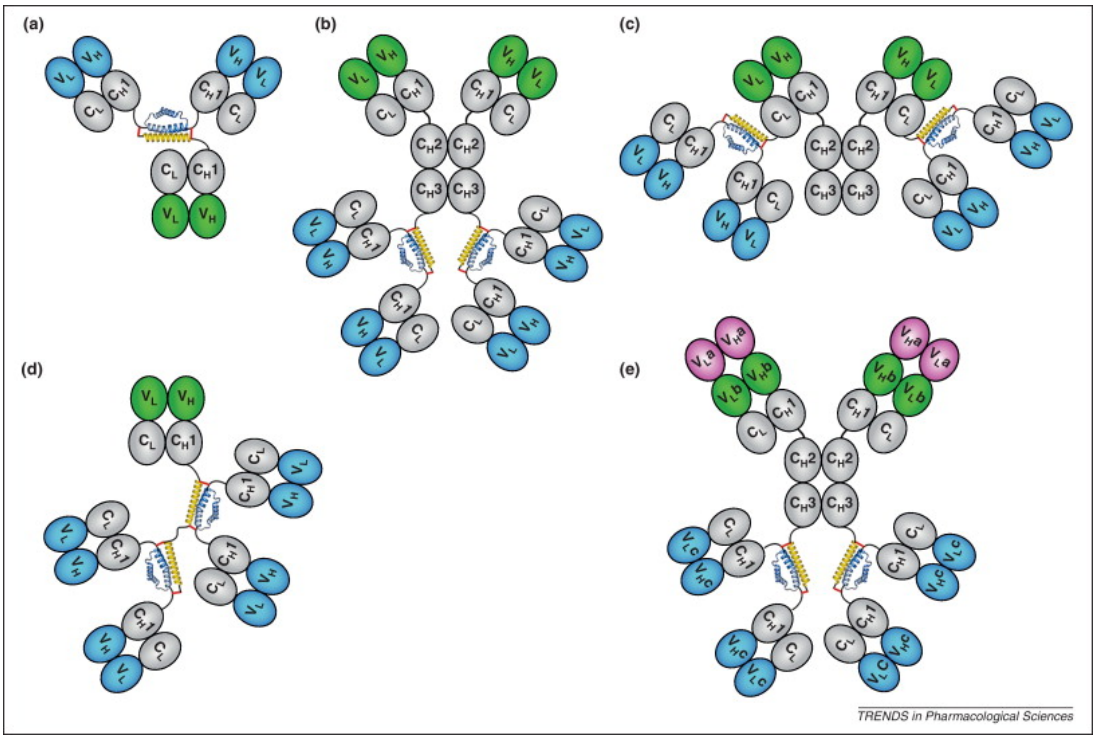

Figure 1.3: Examples of multimeric, multi-specific antibodies.
(a) bi-specific tri-Fab molecule, (b) & (c) bi-specific HexAB's, (d) Penta-Fab structure with a tandem AD2-Fab module, (e) 3 tri-specific octovalent antibody. Variable domains (V, pink, green or blue) and constant domains (C, grey) of the heavy (H) and light (L) chains respectively with locations for locking disulphide bridges as red lines.

1.3 Chinese Hamster Ovary Cells

Emerging challenges focus on successfully producing complex molecules emerging via drug discovery pathways. Production of molecules involves inserting the genetic vector for the mAb into the production cell line. Next, stringent clonal selection procedures are undertaken to isolate the best performing clone that can successfully grow and produce the product with a high abundance and quality.

Chinese Hamster Ovary (CHO) cells were originally isolated from the epithelium of a Chinese hamster in 1956, and remain the most commonly used host in the bio-pharmaceutical industry for the production of therapeutics (Wurm 2004). The most notable CHO cell developments are CHO-K1 (isolated in 1957); the first cell line used for protein production, and CHO-DG44 (created in 1983); the first cell line lacking the DHFR locus allowing antibiotic-free pressured selection of plasmid Deoxyribonucleic Acid (DNA) (Wurm & Hacker 2011; Urlaub et al. 1983).

Today many variants of the original CHO cell lines have been developed into suspension culture, with bio-pharmaceutical companies having multiple cell lines with specifically defined purposes, predisposed to best produce different antibody modalities. Advances in cell culture technology support production titres of more than 10g/L, bringing the cost of therapeutic proteins lower (J. Y. Kim et al. 2012). Many reasons exist for CHO cells remaining the popular choice for

protein production. Primarily they have been demonstrated as safe over the course of two decades, making approval for therapeutic proteins from regulatory agencies such as the FDA more straightforward. Secondly, powerful gene amplification processes exist such as *DHFR*-mediated or *GS*-mediated systems allowing high qP to be achieved (J. Y. Kim et al. 2012). CHO cells also perform efficient post-translational modifications when compared to other options (bacteria, insect cell lines and murine myeloma cell line (NS0) and Human Embryonic Kidney 293 (HEK293) cells), producing glycol-forms that are biologically active and compatible with humans (Haas et al. 2007). Lastly CHO cells have been easily adapted to serum-free suspension growth conditions; important for both regulation and use in large scale bioreactors.

Bandaranayake1 and Almo 2014 analysed cell culture technology developments, describing how 30 years ago bioprocesses were operated for 7 days in batch mode achieving cell concentrations of 3×10^6 cells.ml^{-1} and r-protein yields of up to 100 mg.l^{-1}. In 2007, modernised processes reached much higher cell densities, and mAb titres of 1–5 g/L, due to improved basal media and feed strategies. Further developments in specific feed concentrates to meet the different demands throughout cultivation phases (such as lag, exponential and stationary phase) enable even higher cell concentrations and titres beyond 10 g/L (Figure 1.4) (Kunert and Reinhart 2016). Recently, continuous strategies such as perfusion systems have begun to gain momentum led by a paradigm shift in process development from prioritising higher titres to control over product quality and improving process consistency (Kelley 2009).

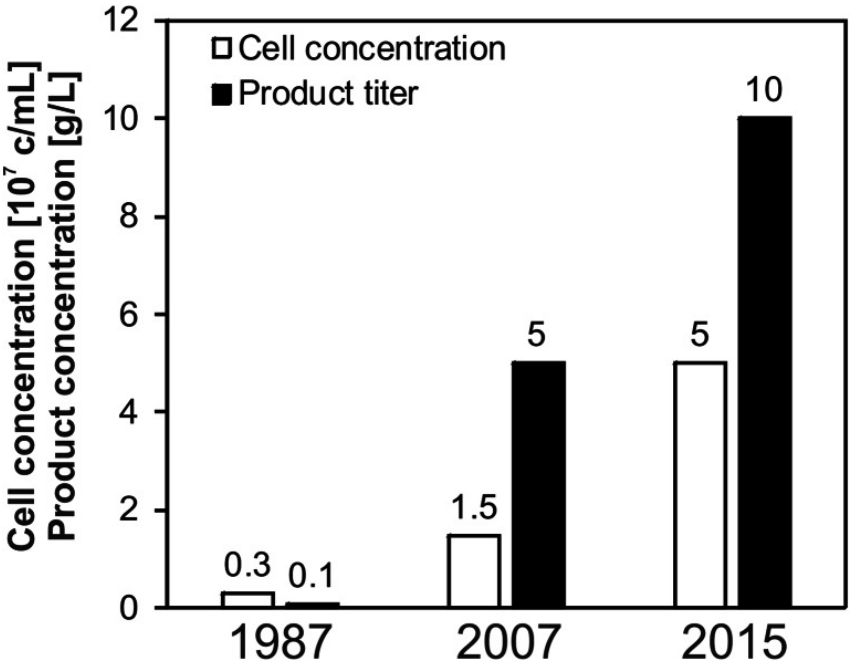

Figure 1.4: Culture density and titre trends over time.
Taken from (Kunert and Reinhart 2016) demonstrating the exponential increase in both maximum cell densities and product titres over the last 30 years.

Until 2011 CHO cell engineering was genetically limited as no CHO sequenced genomics existed. Due to this, genetic engineering approaches were based on sequenced Mouse and Human genomes, with limited success. The first ancestral CHO-K1 genomic sequence was presented by X. Xu et al. 2011 comprising of a of 2.54 Gb genomic sequence assembly, and 24,383 predicted

genes (X. Xu et al. 2011). Although full annotation of the genome is a lengthy process, with significant variability between CHO lineages, this has become a vital tool in the CHO engineering toolbox, allowing elucidation of components and characterization of poorly understood phenotypes. Another important finding identifies 99% homology to the human glycoprotein profile, with 53% actively expressed, opening up a unique opportunity for glycoprotein manipulation in CHO cells (X. Xu et al. 2011). These allow CHO engineering to be approached in an information based maner, using bioinformatic evaluation to inform our experimental decisions.

1.4 Engineering the ER and UPR

Protein secretion allows a vast array of diverse events to occur, from enzyme secretion in saprobes to hormonal signalling in multicellular organisms, and facilitates the production of r-proteins in most production hosts, making it one of the most important processes in eukaryotes (Güler-Gane et al. 2016). Protein secretion is multifaceted, utilising numerous steps spanning multiple cellular compartments. The secretory pathway has two primary functions; performing proper folding and Post Translational Modification (PTM) of proteins (for example glycosylation) and directing proteins to their intra- or extra-cellular destination. The diverse processes along the secretory pathway are handled by secretory components and protein traffic is directed by numerous regulatory and structural proteins (J. K. Liu 2014). A specific set of regulatory proteins are dedicated to elicit the correct secretory response to circumstantial factors such as cellular stress, environmental changes and nutrient availability (Kaufman 1999). Malfunctions in secretory components are often the result of human neuropathies such as Huntington's, Alzheimer's, and Parkinson's diseases. Additionally, protein specific misfolding can lead to cystic fibrosis and antitrypsin deficiency (Vembar and Brodsky 2008; Yoshida 2007).

Although major successes have been achieved, particularly with mAbs and complex antibody derivatives, increased transcriptional activity does not always enhance the amount of secreted r-proteins due to reaching a plateau. Hence, very high transgene copy number and messenger RNA (mRNA) levels may not correlate with an elevated protein yield. Furthermore, such approaches can be unsuccessful for some proteins, whereby moderate levels of secretion cannot be achieved. This is hypothesised to be linked to the cells inability to cope with the synthesis or processing of complex and DTE proteins, eliciting cellular stress responses and cell toxicity effects (Johari et al. 2015; A. A. Shukla et al. 2017).

Additional cellular bottlenecks likely include downstream cell machinery such as polypeptide processing, modification and/or secretion (Le Fourn et al. 2014). Limitations on the expression of r-proteins may reflect the cell inadequately handling the necessary post-transcriptional events to effectively keep up with the high supply of the mRNA and polypeptide. This would result in post-translational steps becoming limiting factors, in addition to yielding proteins bearing heterogeneous or variable modifications. Hence, consistent production of r-proteins at high yields requires the identification of limiting bottlenecks, as well as specific engineering strategies to modify and improve the post-translational protein processing and secretion machineries. The secretion of proteins by mammalian cells is a complex pathway involving polypeptide transloca-

tion from the cytosol into the lumen of the Endoplasmic Reticulum (ER), where they fold and assemble before being targeted to their destination (Figure 1.5).

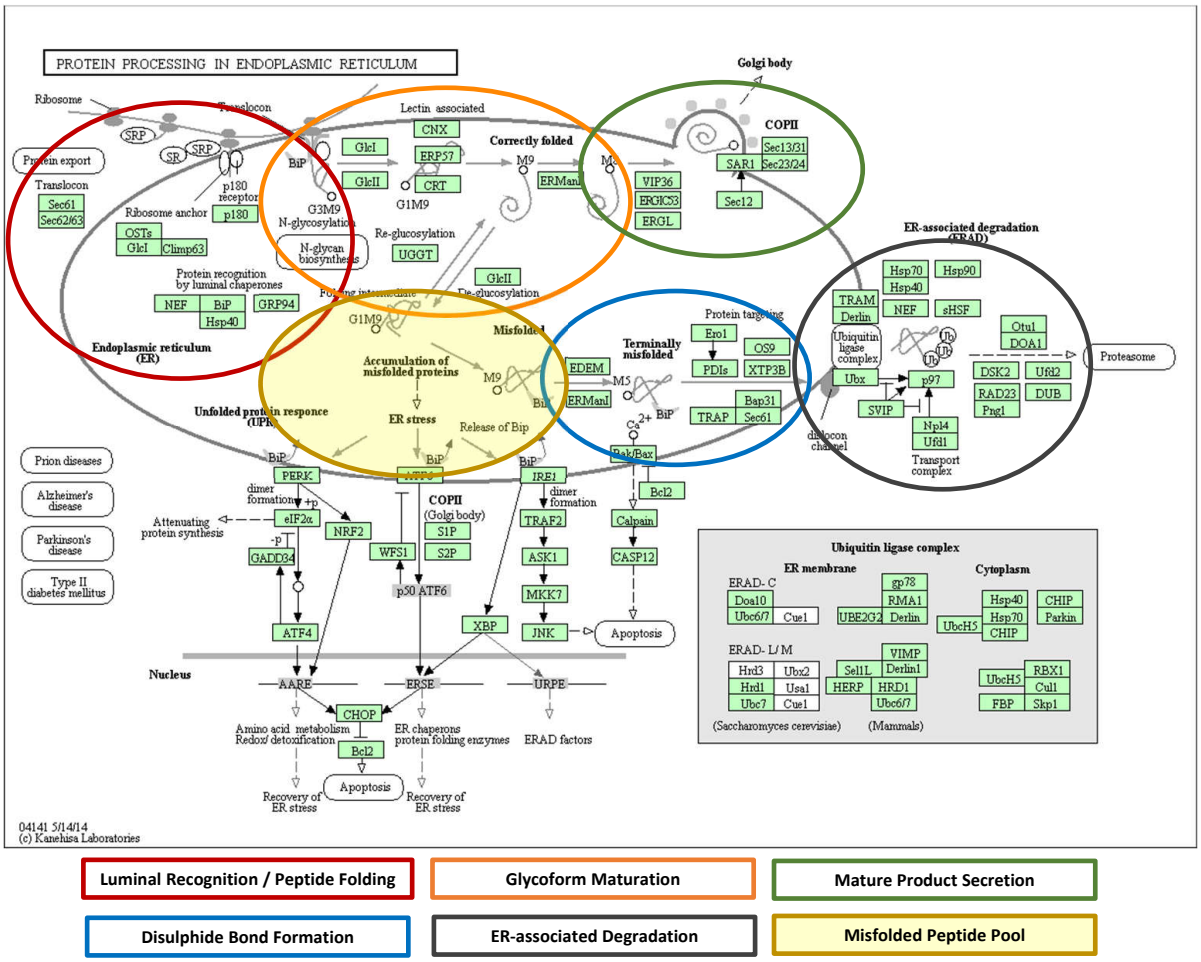

Figure 1.5: KEGG pathway: Protein processing in the endoplasmic reticulum.
The image highlights the scale of point of intervention to stimulate or disrupt protein processing to impact overall yields and product quality. Arrows show major known interactions between host endoplasmic reticulum. Although far more interactions occur, these may have less impact or need further evidence to be added. Image is taken from Kanehisa and Goto 2000 and adapted for purpose.

Many studies report that the bioengineering of host cell lines may improve the modification or secretion of heterologous proteins and other therapeutics (Baik, Gasimli, et al. 2012; Goh et al. 2010; Y. Lim et al. 2010; R.-W. Peng and Fussenegger 2009; P. Zhang et al. 2010). Functional proteins involved in the various post-translational steps of the endoplasmic reticulum, secretory pathway and of exocytosis have been studied, and could be successfully engineered to solve bottlenecks and cellular limitations (Mariati et al. 2012). It was shown that chaperones, Unfolded Protein Response (UPR), ER-Associated Protein Degradation (ERAD) components, and stress-mediated apoptosis pathway ER components can be modified and over-expressed to create novel host cell lines allowing higher production capacities. For example CHO cells have been engineered to express differing protein di-sulfide isomerases or *XBP1*; a regulatory transcription factor for secretory cell differentiation and ER maintenance, showing a decrease ER stress and increase protein titres (Borth et al. 2005; R.-W. Peng and Fussenegger 2009; Tigges and Fussenegger 2006). Other attempts included the chaperone expression such as ERp57,

CANX, *CALR* and *BIP* in CHO cells (Chung et al. 2004; S. O. Hwang et al. 2003; Morris et al. 1997). A key limiting factor in this research is the molecular mechanisms by which these ER proteins can improve protein secretion and their ability to act on various r-proteins have not been studied systematically. This is proving challenging as changes in cell performance vary greatly in a product dependent manner, reliant on the specific CHO cell line used. Increasingly trends point towards extreme specificity of production with different engineering targets, hence it is unlikely that an improved cell line can be produced to ubiquitously increase expression of r-proteins.

The UPR is a cellular response activated by ER stress that is conserved between all mammalian species, yeast and worm organisms. However, if the UPR fails to equilibrate the cellular environment to normal levels, cell dysfunction and death follows (Oslowski and Urano 2011). The UPR consists of 3 distinct branches, each initiated by a different ER-transmembrane protein: IRE1, PERK, and ATF6. Under stress-free conditions, BIP binds to these master switches inhibiting their activity (Oslowski and Urano 2011). Each of the mentioned UPR regulators have distinct functions in adaptive response, feedback control and cell fate regulation respectively, and ultimately dictate whether the cell will survive, or initiate apoptotic pathways (Oslowski and Urano 2011).

IRE1, a type I ER transmembrane kinase, senses ER stress leading to dimerisation and autophosphorylation, activating downstream signalling cascades. *IRE1* exists in two isoforms; IRE1α and IRE1β. *IRE1*α is expressed ubiquitously in all cell types. Activated IRE1α splices XBP1 mRNA, which is a transcription factor that up-regulates UPR target genes involved in ERAD and protein folding, such as EDEM1 and P4HB (Calfon et al. 2002; A.-H. Lee et al. 2003; Yoshida, Matsui, Hosokawa, et al. 2003; Yoshida, Matsui, Yamamoto, et al. 2001). Elevated levels of chronic ER-stress can cause recruitment of TRAF2 and the activation of ASK1, leading to the regulation of the BCL2 family of proteins (Nishitoh et al. 1998). IRE1β is less well documented in the relevant literature.

PERK is also a type I ER transmembrane kinase and similarly to IRE1α when ER stress removes inhibition from BIP, PERK oligomerizes, auto-phosphorylates and then directly phosphorylates eIF2α (Nishitoh et al. 1998). Once phosphorylated, eIF2α prevents the formation of ribosomal initiation complexes causing a global reduction in mRNA translation, protecting cells from ER stress-mediated apoptosis (Nishitoh et al. 1998). Meanwhile, ATF4 requires eIF2α phosphorylation for translation, resulting in regulation of several UPR target genes including CHOP (Harding et al. 2000).

The third arm of ER stress signalling is regulated by the type II ER transmembrane transcription factor ATF6, which exists in two isoforms; ATF6α and ATF6β. Only ATF6α has been extensively studied concerning ER Stress. Upon ER stress conditions, ATF6α moves into the Golgi and is cleaved by proteases. The processed form of ATF6α activates UPR genes and associates with protein folding and degradation after translocating to the nucleus (Harding et al. 2000).

Additional tools are constantly being developed to aid the ever-growing bio-pharmaceutical in-

dustry. One thought-provoking report (Lund et al. 2017) recently used literature from the Yeast, Human and Mouse secretory pathways to compile a comprehensive catalogue of characterised ER and secretory genes with functional annotations and interactions. In total 801 distinct components were mapped from Mouse literature; the most comprehensive to date. These were then applied to CHO-K1 using comparative genomic and transcriptomics data resulting in 764 validated and annotated CHO secretory components, providing a strong platform for target selection of an RNA Interference (RNAi) screen of ER and secretory pathway components in CHO cells.

1.5 RNAi

1.5.1 Overview of principles

RNAi is a naturally occurring biological process by which Ribonucleic Acid (RNA) molecules inhibit gene expression or translocation to accurately silence a gene with high potency. This is historically known as co-suppression or post-transcriptional gene silencing. Two key discoveries lead to the birth of RNAi. The discovery of the regulatory lin-4 and let-7 Micro RNAs (miRNAs) led to the discovery of RNAi by Double Stranded Ribonucleic Acid (dsRNA). RNAi was first experimentally documented when Fire et al. 1998 demonstrated that 20-25 nucleotide small interfering RNA (siRNA)s are the key effectors of RNAi in *C. elegans.*

In mammalian cells, a global non-specific mechanism for inhibition of protein synthesis was observed through exposure to dsRNAs greater than 30 bp (Tran et al. 2004). PKR, and 2', 5' oligoadenylate synthetase (2', 5'-OAS) are shown to be responsible for non-specific silencing. PKR shuts down global protein synthesis through phosphorylation of translation initiation factor eIF2α. Resultantly, RNase L is activated inducing non-specific degradation of all mRNAs in a mammalian cell (Tran et al. 2004). The non-specific interference pathways represent the mammalian cell response to viral infection or other stress (Bass 2001). Tuschl first demonstrated that RNAi could be directly mediated by siRNA mammalian cells, as siRNA does not integrate into the genome, hence the RNAi response is only transient. However, stable gene suppression can be induced through utilization of RNA Pol III promoter-driven expression of Short Hairpin Ribonucleic Acids (shRNAs) (Elbashir et al. 2001).

In nature, RNAi plays a protective role defending against parasitic nucleotide sequences from viruses and transposons, in addition to having regulatory functions during development (Saurabh et al. 2014).

The inherent RNAi pathway is found in many eukaryotes, including animals and is highlighted in Figure 1.6. It is initiated by the Dicer complex, that cleaves exogenous dsRNA (in plants), or shRNA (in humans) molecules into short fragments of 20-25bp. Short dsRNA in the cells cytoplasm initiates the RNAi process through activation of the RISC. Each siRNA is unwound into 2 Single-Stranded Ribonucleic Acid (ssRNA), known as the guide and passenger strands. The guide strand is incorporated into the RISC, while the passenger is degraded. The best studied outcome of this process is post-transcriptional gene silencing whereby this complex binds to and cleaves mRNA complementary to the guide strand, through induction of Argonaute 2

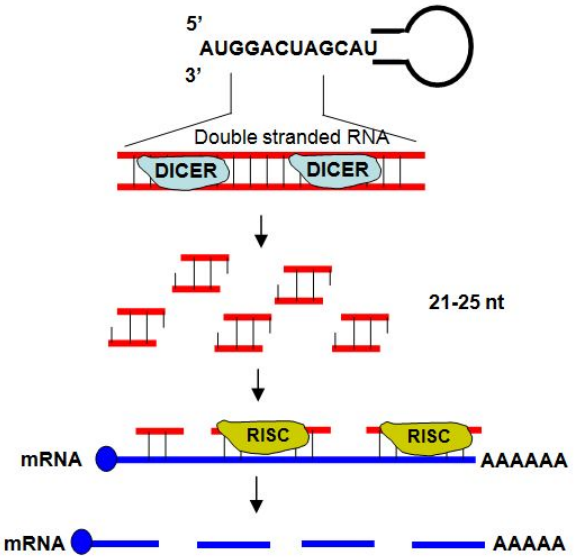

Figure 1.6: Representation of dsRNA degradation by DICER and RISC complexes. The DICER RNase III complex identifies the dsRNA and cleaves them into 21 to 25 bp siRNAs. These molecules are recognized by the RISC complex, leaving the antisense strand in the RISC, resulting in the complex activation. The activated RISC next targets and cleaves complementary mRNA to the antisense strand of the siRNA (Portilho and Almeida 2011).

(Portilho and Almeida 2011). The initiating dsRNA can also be endogenous, in the form of pre-microRNAs expressed from RNA-coding genes. Primary transcripts are first processed into the stem-loop structure in the nucleus before export from the nucleus to the cytoplasm (Bagasra and Prilliman 2004). This silencing mechanism makes RNAi an invaluable research tool, as synthetic RNA introduced into cells can selectively and consistently induce robust suppression of individual Gene of Interest (GOI). Modern applications of RNAi in cellular engineering involve large-scale high-throughput screens systematically shutting down individual genes to aid identification of components necessary for a particular cellular event (Kupferschmidt 2013).

1.5.2 RNA isoforms: siRNA, miRNA, and esiRNA

Various RNAi methods have been employed for siRNA based knock-down of specific genes in mammalian cells (G. Hu et al. 2009). DNA-vector-mediated RNAi silences genes transiently in mammalian cells, while other expression systems are used for stable silencing. The promoters of RNA polymerase II and III, U6 and H1 respectively, have been used for stable silencing (Hu et al. 2009), along with Transfer Ribonucleic Acid (tRNA) promoter-based systems. Additionally, retroviral-vector-based delivery of siRNAs has also been utilized for more efficient silencing. Interestingly, transgenic mice have been established with germline transmission of a shRNA expression cassette for silencing of genes not targeted by homologous recombination-based approaches (Tiscornia et al. 2003).

The use of RNAi is not limited to the determination of gene function, in fact having many potentials in healthcare applications, such as treatments for viral infections and cancer. Viral and human genes required for viral replication can be attacked to generate viral-resistant host cells or to treat viral infections (J. A. Smith et al. 2010). Oncogenes, which accelerate cancer growth, can also be targeted by RNAi, are important for neurovascularisation, and could prevent tumour growth (Chaika et al. 2012; S. K. Shukla et al. 2015).

An siRNA is a 20-25 nucleotide long dsRNA molecule possessing 2-3bp 3' overhangs. Normally,

siRNAs are generated by DICER cleavage and phosphorylated by kinases before entering the RISC complex (Denli et al. 2004). It is hypothesised that the hydroxylated 3' termini are essential for siRNA-primed amplification steps. Studies have shown non-priming alterations in the 3' hydroxyl group did not adversely affect RNAi-mediated silencing. They described how siRNAs operate as a guide, not the primer-RNAs for gene repression in human and Drosophila RNAi pathways (Schwarz et al. 2002). Conversely, other work demonstrates modifications to the 3' end of the siRNA anti-sense strand abolished RNAi silencing, while modifying the 3' end of the sense-strand had no negative impact on RNAi silencing (Hamada et al. 2002). When combined, these support the model that each strand of siRNAs possesses differing functions in the RNAi process, with the 3' hydroxylated end of the antisense strand likely priming amplification.

Micro RNAs are 19–25-nucleotide small RNA strands produced by cleavage of endogenous 70 nucleotide non-coding stem-loop precursors by the DICER complex. The miRNAs can either repress the target mRNA translation (mostly in mammals) or facilitate mRNA destruction (mostly in plants), allowing for minor sequence mismatches (Ambros et al. 2003). Currently, approximately 2000 different miRNAs have been identified across a spectrum of species including plants, animals and lower species. Following the most common terminology, miRNAs with well-characterized functions (lin-4 and let-7 etc.) are referred to as Small Temporal Ribonucleic Acids (stRNAs), while those with unknown functions are called miRNAs (Ambros et al. 2003). Many miRNAs have been characterized due to physiological roles in cancer and other diseases (Singh et al. 2012). Over recent years miRNA focused cell engineering has gained increasing attention (Jadhav et al. 2013). Contrastingly to single gene over-expression and knock-down strategies, miRNAs open the possibility of regulating entire signalling networks, as a single miRNA can post-transcriptionally suppress up to 100 different mRNA targets (Barron et al. 2011; Hackl et al. 2012).

Tiny Non-coding Ribonucleic Acids (tncRNAs), which are very similar to miRNAs in size, have a single-stranded structure and lack of complementation to a given mRNA. The key differentiation factors are their lack of processing from a hairpin precursor and phylogenetic non-conservation. Like miRNAs, tncRNAs are transcribed from non-coding sequences, however, the developmental role they take is not fully understood.

An endoribonuclease prepared small interfering siRNA (esiRNA) is a cocktail of siRNA oligos formed by cleavage of a longer 200+bp dsRNA by RNase III or DICER in-vitro Kittler et al. 2004 . Generally, esiRNAs are created through Complementary Deoxyribonucleic Acid (cDNA) template amplification by Polymerase chain reaction (PCR) followed by tagging with bacteriophage promoter sequences. This facilitates RNA polymerase mediated transcription of DNA. This complex mix of siRNAs is like the mixture created by in-vitro DICER RNAi, hence the nomenclature endoribonuclease prepared. The heterogeneous mixture of siRNAs targeting the same mRNA sequence led to highly specific effective silencing, greatly reducing non-target specific phenotypes. Figure 1.7 highlights the increased specificity and reduction of Off-target Effects (OTEs) offered by esiRNAs over individual siRNAs and pools of siRNAs. Buchholz suggests that within a complex mixture, each siRNA is found at a low concentration, and the on-target effect of the multiple siRNAs is additive. Although each siRNA may also have an

off-target effect, these differ for each siRNA in the mix, hence the off-target effects are diluted out (Theis and Buchholz 2011).

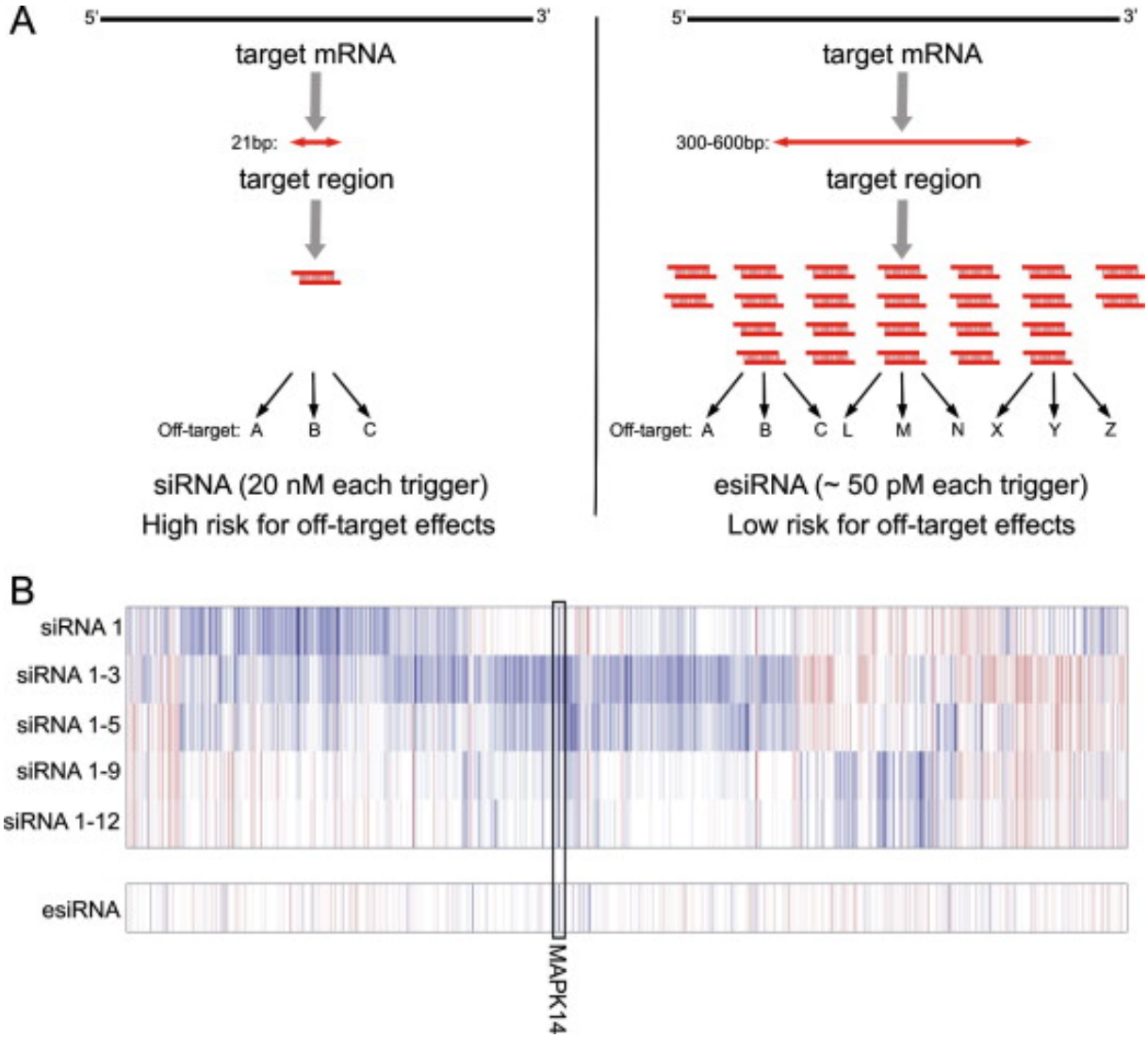

Figure 1.7: Comparison of siRNA and esiRNA as knockdown methods.
(A) Comparative overview of esiRNA and siRNA methodologies. siRNAs target a region of 19 bp to 23 bp in a transcript. esiRNAs are heterologous pools of many differing siRNAs covering a region of 300 bp to 600 bp of the target transcript. Note each siRNA within this pool has different off-target signatures (represented by letters). Hence pooling dilutes out OTEs whereas the on-target effect remains unaltered. (B) Expression array analysis of changes in transcription levels after MAPK14 depletion by both RNAi techniques. Transcripts which are significantly altered ($p < 0.01$, blue: down-regulated and red: up-regulated) are shown in clusters. Increasing numbers of pooled siRNAs (1–12 individual siRNAs) reduces the number of off-target events. show the most specific knock-down (bottom panel). Figure taken from Theis and Buchholz 2011.

1.5.3 Targeting, prediction and design rules

RNAi technology is applicable for gene silencing in many species and has been used extensively in *C. elegans* for functional genomics. High-throughput investigation of most of the 19,000 genes has been accomplished for *C. elegans* with one group producing an RNAi library, representing

86% of the genes (Singh et al. 2012). This strategy has been replicated with varying levels of success in multiple other model organisms, including some human studies (G. Hu et al. 2009).

In order to streamline screening efforts, specific siRNA design rules have been proposed and validated over several years (S.-C. Wu 2009). Original proposals by Tom Tushel suggested generating 23 nt duplexes following the motif AA(N19)TT (N; any nucleotide) containing approximately 50 % Guanine and Cytosine (GC) content. As molecule thermodynamics effect initial recognition of the siRNA-RISC complexes, a lower GC content (36 % to 52 %) and avoiding internal repeats were found to benefit stability (Reynolds et al. 2004). Additionally, the sequence-specific properties of siRNAs can influence critical siRNA-protein interactions required for mRNA cleavage. These include an A in positions 3 and 19 of the sense strand, the absence of G or C in position 19, a U at position 10 and the absence of G at position 13 of the sense strain (Mittal 2004; Reynolds et al. 2004). Other reported criteria include the absence of U at position 9, the presence of G or C but no U at 15 of the sense strands, and the 3' overhang nucleotide 2 preferentially being A and avoiding C (Bradáč et al. 2007). These rules generally only apply to synthetic siRNAs and plasmid-encoded shRNAs because the siRNA duplex is completely conserved in naturally occurring miRNAs.

Early excitement about RNAi was initially dampened by false-positive results. Like all screening approaches, RNAi has a strong association with false discovery, particularly connected with off-target effects OTEs (Echeverri et al. 2006; Sigoillot and King 2011). A large practical challenge of RNAi applications in research is the prediction and minimisation of these OTEs. As RNAi intersects with multiple pathways, often non-specific effects are triggered by the experimental introduction of siRNAs when RNAi reagents bind to RNAs other than their intended target, owing to partial complementarity. Additionally, when a mammalian cell encounters a dsRNA it may confuse this as of viral origin, initiating an immune response. Screens may be undertaken to identify engineering targets for improving various capacities of production cell lines. The issue arises when secondary genes with incomplete complementarity are silenced alongside the GOI. This may lead to incorrect conclusions over the GOIs function.

Off-target effect mitigation is continually improving with advancing technologies and can be minimised with appropriate experimental controls and powerful siRNA design algorithms. The most powerful of these is DEQOR; a web-based design tool for siRNA quality and specificity (Hendershot 2004). DEQOR utilises multiple algorithms to maximise siRNA potency including sequence length, GC content and inclusion/aversion of specific nucleotide sub-chains. Furthermore, specificity can be evaluated by a Basic Local Alignment Search Tool (BLAST) search incorporated into the program. The two predominant variables are siRNA potency and CHO cell dependent specificity, as currently the DEQOR BLAST search application does not support direct CHO or *C. griseus* inputs.

New experimental approaches and the use of novel genome-engineering systems to validate RNAi results are allowing better and faster identification of OTEs. Conversely, RNAi screening in mammalian cells has paved the way for innovation in related areas, including the use of miRNA mimics and inhibitors, the use of RNAi or mutagenesis in three-dimensional mammalian culture systems, and the development of *in-vivo* disease models in mice (S. E. Mohr et al. 2014).

1.5.4 High-throughput RNAi Screening

RNAi screening combines the power of genetic screens with the rapid time-frame of phenotypic assays — the use of which had previously been limited in cell lines to small-molecule screens. RNAi screening has made it possible to identify new genes, or gene networks, and elucidate their function in a wide variety of biological processes. This includes areas such as signal transduction, organelle or protein localization and/or function, cell and organelle morphology amongst others (Boutros and Ahringer 2008).

RNAi technology introduced functional genomic studies in human and other types of cultured and primary cells. Cell-based RNAi screening compliments established techniques, instrumentation, assays and liquid handling methods previously developed for chemical screening in cells. Overall, cell-based RNAi screens provide a rapid and accessible platform for genome-scale functional studies (Boutros and Ahringer 2008; S. Mohr et al. 2010; Neumüller and Perrimon 2011).

Typically, large screens are facilitated by emerging genome-wide RNAi libraries, developed by both academics and commercial entities. New libraries help build our understanding of the most effective strategies for design and delivery of RNAi reagents. To date, hundreds of large scale screens have been undertaken in C. elegans, D. melanogaster, mouse and human cell lines (E. Yanos et al. 2012; S. Mohr et al. 2010; Perrimon et al. 2010; Root et al. 2006). More recently, methods have been developed for screening neuronal and muscular primary Drosophila cells of embryonic origin (Bai et al. 2009). In addition, an increasing number of studies are being performed using mammalian stem cells (Zou 2010). High quality transcriptomics data for tissues, tumours and cell lines, made available by rapid advances in next-generation sequencing technologies, is constantly shifting and updating choices and interpretation of cell-based RNAi screen data (Neumüller and Perrimon 2011; Nijwening and Beijersbergen 2010; Sioud 2011).

1.5.4.1 Previous CHO applications of RNAi screening

Documentation of previous RNAi screening studies in CHO cells is limited with publication dates ranging from 2006 to 2019. Of these, S.-C. Wu 2009 is a review highlighting the prospects of RNAi in improving r-protein production in CHO cells. Synthetic RNAi silencing of host gene expression has been used in a variety of ways to improve commercial cell lines. The stable silencing of *Bax* and *Bak* of the *Bcl2* family of genes using shRNA vectors have been shown to improve both viability and yield of CHO producer cell lines (S. F. Lim et al. 2006). Additionally, duel silencing of both caspase-3 and caspase-7 simultaneously followed by Sodium Butyrate (NaBu) treatment displayed marked benefits to production cell lines (Y. H. Sung et al. 2007). Both methodologies primarily impact genetic control of the apoptotic pathway via the mitochondrial branch (Bcl2) or terminal apoptotic activators (caspases) (Arden and Betenbaugh 2004).

Klanert et al. 2019 applied a whole mouse genome siRNA library to CHO cells, identifying two hits. When evaluated in multiple cell lines producing therapeutic proteins, several product specific titre and qP improvements were observed. However, titres were low in the $30\,\mathrm{mg.l^{-1}}$ to $200\,\mathrm{mg.l^{-1}}$ range, therefore applicability to biopharmaceutical development processes is limited.

Furthermore, silencing of glycosylation associated gene expression in CHO cells has been shown to enhance product efficacy, offering great cost per dose reductions. The in-vivo circulating half-life of glycoproteins can be manipulated from minutes to hours or days. The use of stable shRNA vectors against sialidase cDNA can reduce sialidase activity, reducing the rate of sialic acid removal, improving glycoprotein production yield (Ngantung et al. 2006). Also looking at post-transcriptional modifications, the use of siRNA targeting FUT8 can result in a defucosylated IgG1 product, which in one instance had 100-fold greater antibody-dependent cell-mediated cytotoxicity (Mori et al. 2004). This effect has been further amplified by double silencing of *FUT8* and *GMD* (Imai-Nishiya et al. 2007). Lastly, an siRNA approach has been used to reduce glucose consumption rates, resulting in slowing the rate of lactate production, improving culture longevity and r-protein production (S. H. Kim and G. M. Lee 2007).

Up to 2009, several groups have investigated the promise of RNAi in production cell lines. One approach is to use genome-scale micro arrays on producing lines looking for globally down regulated genes. The 'hits' from 3 studies have been highlighted in Table 1.1.

Table 1.1: Examples of gene down-regulation correlating with increased r-protein production.
Genes highlighted from genome-scale micro-array studies, in which effector gene down-regulation is correlated with high r-protein production in CHO cells.

Author	Highlighted Targets
Wong et al. 2006	*Rpl37a, Ercc5, Pgm2, Igfpb4, Bcl10, Ptma, S100a6, BIP, Atp5, GJA1*
Yee, Gatti, et al. 2008	*Fdps, Cyp51, Sc5d, Csel1, Chek1, Ptma, Apc, Pdcd4, Dap3, Traf3, Bid, Gadd45b, Ppid, Trap1, XBP1*
Trummer et al. 2008	*Itpr3, Tuba1, Fads3, Hmgcs1, Ncam1, Tmsb4x, Spnb2, Flnb, S100a13, Vldlr, Usp34, Ntan1, Abhd6, Pdhb, Mdh1, Gstm5, Papolg, Nipbl, Cul4a, Pdhb, Mdh1, Nup155, Vdac3, Mtif2, Cct6b, Spnb2, Nup155, Vps54, Golga7, Vldlr, Papolg, Ash2l, Sertad2, Mrps31, Tm2d2*

There are several other published examples of RNAi based gene silencing in CHO cells aiding r-protein productivity. In 2012, Hamond and Lee demonstrated transient silencing of cofilin, a regulator of actin cytoskeleton dynamics, can enhance specific productivity by up to 80 % in multiple CHO cell lines. In support, replication of transient data using stable shRNA vectors resulted in a 65 % productivity improvement, suggesting cofilin modulation alongside its regulators may be a viable approach for further CHO engineering (Hammond and Kelvin H. Lee 2012).

1.6 Molecular Chaperones, Chemical Chaperones and Regulators

1.6.1 Chemical Chaperones

The use of chemicals as chaperones and regulators is not a new concept. In the field of protein synthesis and UPR, there has been a large research focus on the use of chemical chaperones in disease pathology, especially those involving protein folding such as Alzheimer's, Parkinson's, Huntington's and other prion diseases.

Molecular chaperones are proteins which interact with the none-native form of proteins assisting in folding or unfolding, and are not present in the final structure. This mechanism is the first, and strongest line of defence against protein misfolding and aggregative expansion (Muchowski and Wacker 2005). Over expression of HSPs, the prominent family of molecular chaperones in cells has been shown to have neuroprotective properties in neurodegenerative diseases. This has led to studies of HSPs as potential therapies, making them an interesting target for production cell line engineering (Muchowski and Wacker 2005).

Chemical chaperones are low molecular weight compounds that specifically bind proteins inducing refolding or structure stabilization, aiding restoration of protein function. Chemical chaperones can be divided into 2 subgroups: osmolytes and hydrophobic compounds. These have a nonspecific mode of action and often cannot bind directly to the proteins, unlike pharmacological chaperones. Frequently, they only have effect at high molar concentrations, so they have been historically neglected as therapeutic agents (Bernier et al. 2004).

Cellular osmolytes are ancient members of stress responses, playing a significant role for organisms exposed to stress conditions. The major osmolytes in eukaryotes are restricted to a few classes of low molecular weight compounds: free amino acids and their derivatives, polyols, and methyl-amines. Under denaturing environmental conditions, the intracellular environment is enriched with organic osmolytes increasing the stability of proteins without affecting their activity. Osmolytes appear to be involved in particular individual stress conditions, while polyols protect cells against extreme temperature and dehydration. Amino acids protect against high extracellular salt environments, and methylamines are present in urea-rich cells (Yancey et al. 1982). A recognised example of cellular osmolytes to bio-pharmaceuticals is Dimethyl Sulfoxide (DMSO).

Generally, hydrophobic chaperones such as sodium 4-Phenylbutyrate (4-PBA) and bile acids have a mechanism of action defined by the interaction of hydrophobic regions of the chaperone with exposed segments of the unfolded protein protecting it from aggregation. 4-PBA and bile acids reduce aggregate accumulation *in vivo* and *in vitro*, reversing ER stress. However, it has been suggested these molecules have more complex mechanisms of action with higher levels of regulation (Cuadrado-Tejedor et al. 2011). 4-PBA has potential benefits for a wide variety of diseases including cancer, cystic fibrosis, thalassemia, spinal muscular atrophy as well as protein folding diseases such as type 2 diabetes mellitus, Amyotrophic Lateral Sclerosis (ALS), Huntington's, Alzheimer's, and Parkinson's. Although 4-PBA has been classically described as

a chemical chaperone, based on its effects on ER stress and aggregate accumulation, the actual molecular mechanisms involved in its beneficial effects are not completely clear (Cortez and Sim 2014; Ozcan et al. 2006).

1.6.2 Proteostasis Regulators

Primarily, the proteome is maintained by ER localised biologic pathways. ER quality control pathways regulate secreted proteins by directing non-native conformations between folding and degradation pathways. These pathways prevent the secretion of incorrect conformations of proteins (Wiseman et al. 2007). Energetically destabilised proteins are generally targeted to degradation pathways as low stability prevents them from properly folding within the steady-state ER environment. However, stable proteins can efficiently fold in the ER, increasing their trafficking to downstream environments.

Since the components of both these pathways engage non-native protein conformations, changing the relative activities and stoichiometry's of the pathways directly influences the relative flux of polypeptides through folding or degradation pathways. For instance, increasing the activity of ER protein folding pathways via ER chaperones and folding factor over expression can reduce targeting of non-native proteins to degradation pathways, facilitating folding through iterative chaperone cycles (Wiseman et al. 2007). The extracellular aggregation of destabilized, aggregation-prone proteins such as TTR or IgG light chains are implicated in the pathogenesis of prion diseases like TTR amyloidosis and light chain amyloidosis (Plate, Cooley, et al. 2016; Ryno et al. 2013). Other protein folding diseases shown to be impacted by UPR dependent secretory pathway modulation include retinal degeneration, A1AD-associated emphysema, Gaucher disease, Fabry disease, and idiopathic epilepsy (Chiang et al. 2012; Di et al. 2016; Grandjean et al. 2020; Han et al. 2015; T.-W. Mu et al. 2008; Plate, Cooley, et al. 2016; S. E. Smith et al. 2011).

Inequalities in ER quality control threaten downstream events, impacting disease associated aggregation via the UPR. These UPR quality control mismanagements seen in aggregative diseases could be similar in methodology to UPR induced ER-stress as a response to DTE antibodies in production cell lines. Chemical biologic strategies have recently been elucidated to independently activate the ER-stress arms *IRE1*, *XBP1s* and/or ATF6 to physiologic levels. These tools have revealed unique contributions of *IRE1*, *XBP1s* and *ATF6* activation to remodelling of the ER environment.

Initially, activation of the *IRE1* branch of the UPR was achieved through chemical-genetic targeting of the kinase active site ofIRE1 protein via mutation of a gatekeeper residue, bypassing the need for IRE1 phosphorylation to activate its endoribonuclease function (DeRisi et al. 1997; Urano et al. 2000). Discovering that kinase inhibitors can induce IRE1 to activate its RNAse activity led to subsequent identification of more potent pharmacological activators (Korennykh et al. 2009). Problematically, off-target effects limit the general utility of these compounds, which can also target PERK.

Selective activation of the *PERK* pathway is achieved by fusion of the cytosolic PERK kinase domain to two modified FK506 binding domains, allowing induced dimerisation through the addition of a small-molecule ligand AP20187 (Z. P. Lin et al. 2011). Ligand-induced dimerisation induces PERK auto-phosphorylation and downstream pathway activation through eIF2α phosphorylation. Stress-independent PERK activation has defined several protective roles of the PERK pathway on ER function, in addition to anti-proliferative and pro-apoptotic function (J. H. Lin et al. 2009). This chemically induced dimerisation approach has been similarly been applied to IRE1 (H. B. Sung et al. 2006). Strategies of ATF6 pathway activation absent of ER stress involve the fusion of ATF6 to a Mutant Oestrogen Receptor Domain (MER), allowing ligand-dependent regulation with tamoxifen (Thuerauf et al. 2007).

Alternatively, the activated form of the ATF6 protein can be fused to a destabilised mutant of DHFR, causing constitutive degradation, while stabilising the entire fusion protein. Subsequently ATF6 activity is selectively activated through addition of the ligand Trimethoprim (TMP) (H. B. Sung et al. 2006). TMP dose titration allows incremental induction of ATF6 transcriptional targets to endogenous levels. Similar approaches have also been applied to regulate XBP1 activity (Shoulders et al. 2013). These tools have defined the distinct roles for IRE1, XBP1 and ATF6 in regulating ER proteostasis for many proteins that aggregate in association with diverse protein aggregation diseases.

Utilising chemical biologic strategies, it is becoming clear that activation of *IRE1*, *XBP1*, and/or *ATF6* have individually distinct roles in ER quality control regulation. This has been best demonstrated through evaluation of the impact of UPR signalling on the redirection of destabilised proteins between folding and trafficking or degradation pathways. In another example, stress-independent activation of ATF6 proteins, but not XBP1, can specifically reduce the secretion of aggregation prone TTR variants (Shoulders et al. 2013). This corresponds with increased targeting through mechanisms such as ER and autophagy (J. J. Chen et al. 2014).

1.7 Thesis Aims and Overview

High Throughput (HTP) screening platforms can be utilised to address the challenges presented by complex biotherapeutics and help to overcome limitations in host CHO cell factories. Genetic and chemical CHO engineering solutions are often highly context specific and cellular responses differ greatly between hosts and therapeutic products. The strict timelines associated with cell line development campaigns limit the applicability of employing genetic screening approaches to identify product specific engineering solutions, and although host cell engineering strategies are not limited by these constraints, solutions are less prevalent.

Genetic overexpression and chemical chaperone supplementation approaches have successfully identified non-product specific CHO host engineering solutions. These are designed to improve the yield of multiple Easy to Express (ETE) therapeutics, however this rarely translates to complex DTE, bi-specific and aggregate-prone molecules. The unique folding and assembly challenges presented by complex DTE molecules amplify the need for rapid, information rich methods for HTP screening of effector genes.

Emerging research explores the beneficial effects of chemical induced branch-dependent UPR regulation on protein aggregates, in proteopathic disease models. This may be applicable in a DTE mAb production context, providing new research avenues for CHO engineering.

This research project can be divided into three main aims:

1. Design and develop a transient screening platform capable of effector gene knock-down and overexpression in suspension CHO cells.
2. Test the functionality of the screening platform for identifying product specific and CHO host engineering strategies.
3. Investigate the applicability of compounds with anti-aggregative properties in proteopathic disease models as enhancers of product yield and quality producing CHO cells.

These aims were investigated and addressed throughout the duration of this PhD studentship, and are compiled into the thesis chapters described below.

Chapter 2 outlines the materials and methods used throughout the project to generate the data presented in subsequent chapters.

Chapter 3 describes the design, development and validation of a HTP transfection and culture platform for transient Simultaneous Overexpression and Silencing Co-transfection (SOSC) genetic screening. This starts with a detailed description of the design criteria which features chemically defined, high cell density co-transfection of DNA and RNA, for the overexpression and knock-down of effector genes. This was achieved through experimental of evaluation siRNA knock-down technologies, adapted to ensure industry applicability. The highest performing siRNA transfection method, electroporation, was then successfully optimised for plasmid DNA co-transfection as validated by flowcytometric analysis. Next the established HTP 96-Deep Well Plate (DWP) cell culture platform was evaluated, and transitioned to 24-Shallow Well Plates (SWPs), improving overall culture performance. Finally, the chapter addresses variability observed in seeding densities post HTP electroporation by automating transfection, seeding and sampling of cells on an Opentrons OT-2 liquid handler.

Chapter 4 Describes a case study, exploring the application of the designed SOSC gene screening platform to identify genetic engineering targets for producing CHO cells. Paired transcriptomics data from a CHO host and ETE producer cells was leveraged to identify a library of effector genes, whose expression was differentially regulated upon adaptation to stable mAb production. By experimentally screening stable producers of ETE and DTE mAbs derived from a common host, this chapter identifies product specific and host cell engineering targets. The inclusion of RNAi knock-downs facilitated evaluation of the difference in sensitivity of the ETE and DTE mAb producers, highlighting Integral Viable Cell Density (IVCD) variability in the ETE, and titre in the DTE model systems. This is likely a result of adaptations during the cell line selection process.

Chapter 5 investigates the application of a select group of proteostasis regulators as CHO cell culture enhancers. In literature the compounds were found to preferentially activate the ATF6 branch of the UPR in HEK293 cells and reduce pathogenic aggregates in cell models of TTR

or light-chain amyloidosis. This chapter was a Proof of Concept (POC) study, evaluating the transferability of research investigating disaggregation in neurological pathologies, into a CHO engineering context. The select proteostasis regulators were first titrated into CHO cultures producing an ETE mAb, to identify the pharmacologically active concentration ranges and evaluate their effect on cell growth and productivity. The observed growth limiting effects highlighted the need for supplementation of compounds to be delayed until cultures were approaching Peak Cell Density (PCD). Further assessment of DTE CHO models known to suffer from aggregation demonstrated product specific growth and titre improvements, supporting further investigation into the applicability of compounds which alleviate aggregation in disease models.

Primarily Chapter 6 investigates the application of a broad library of pre-clinical candidates, identified from the AstraZeneca Open Innovation compounds database, as novel tools to reduce the aggregation rate of DTE mAbs. Based on the findings from Chapter 5 a diverse library of compounds was identified from literature, AstraZeneca's phenotypic screening assays, and the current mechanistic understanding of aggregative pathologies and CHO engineering. The results presented demonstrate the applicability of the compound library on a DTE model mAb known to suffer from intracellular product aggregation caused by the formation of disulfide cross-bridges between engineered cysteine residues. Culture conditions were found to be sub-optimal due to glucose depletion between culture feeds. Hit compounds were re-evaluated following a revision of the media and feed composition by the AstraZeneca Cell Line Development team. Although incomplete, initial data validates the efficacy of identified hit compounds, and inclusion of an alternative mAb model suggests the library is non-product specific. Overall, the results substantiate the use of disaggregases from proteopathic disease research as novel CHO engineering tools, providing strong evidence for further investigation from a mechanistic biology perspective.

Chapter 2

Materials and Methods

The following chapter details the methodology used to complete the research discussed in subsequent chapters. A full equipment and materials list can be found at the end of this chapter.

Bacterial and molecular work was undertaken in a separate laboratory to mammalian cell culture to prevent cross-contamination and ensure sterility. Any materials coming into direct contact with mammalian cells were pre-sterilised, or autoclaved at 121 °C *and/or underwent* 0.22 µm *filtration. All mammalian cell culture work was carried out in a High-Efficiency Particulate Absorbing (HEPA) filtered laminar flow hood. Any material, container or lab equipment was decontaminated with* 70 % *ethanol before entering the flow hood. Materials purchased were of high quality and of cell culture grade.*

Work undertaken was either completed in the Department of Chemical and Biological Engineering, University of Sheffield and its associated facilities, or the Department of Biopharmaceutical Development, AstraZeneca, Cambridge.

2.1 CHO Cell Culture

2.1.1 Cell Lines

All the cell lines and hosts used in the scope of this work are of Chinese Hamster Ovary (CHO) linage and were provided by AstraZeneca. For all stable producing cell lines 50 μM L-Methionine Sulfoximine (MSX) selection was used to maintain product production. Details of each are below:

- MEDI-CHO - Non-producing parental host of CHO-K1 linage which has been suspension adapted. All subsequent cell lines are daughters of the MEDI-CHO host.
- CHO_{ETE} - Stable clonal producer of Monoclonal Antibody $(mAb)_{ETE}$, a model Easy to Express (ETE) IgG1 known as Nip109.
- CHO_{DTE} - Stable pool producing mAb_{DTE} a Difficult to Express (DTE) IgG1.
- $CHO_{BIS\text{-}A}$ - Stable clonal producer of $mAb_{BIS\text{-}A}$, an appended BIS-5 scFv-IgG bi-specific DTE antibody displaying highly aggregative properties.
- $CHO_{BIS\text{-}B}$ - Stable clonal producer of $mAb_{BIS\text{-}B}$, a DTE BIS-4 bi-specific antibody.
- CHO_{T2} - Non-producing clonal cell line adapted for improved transient production.

2.1.2 Cell Culture Maintenance

Cells were cultured in CD-CHO medium (Thermo Fisher Scientific, MA, USA) with the required supplementation described in Table 2.1. During routine cell maintenance cultures were grown in vented Erlenmeyer flasks (Cornering, Surrey, UK) or TPP TubeSpin Bioreactors (Thermo Fisher Scientific, MA, USA). Cultures were maintained at 37 °C and 5 %(v/v)CO_2. Erlenmeyer flasks were shaken at 140 rpm, and TPP TubeSpin Bioreactors at 200 rpm with a 25 mm throw.

Cells were sub-cultured, every 3-4 days to a density of 0.2×10^6 cells.ml^{-1} to ensure exponential growth was maintained. Cell density, viability and diameter were quantified on a Vi-Cell XR (section 2.1.4). To minimise genetic drift, cells were sub-cultured a maximum of 15 times. The number of subcultures a cell line has undergone is referred to as the 'passage' number.

When undertaking Biological replicates CHO cell cultures have undergone at least 2 further passages or have been separated at least 2 passages previously to ensure sufficient genetic variation.

2.1.3 Revival, Cryopreservation and Cell Bank Generation

Master and working cell banks of each cell line in section 2.1.1 were generated as described below:

2.1.3.1 Revival

Cells were rapidly thawed at 37 °C and slowly diluted into 40 ml of pre-warmed CD-CHO media. Cells were then pelleted by centrifugation at 200 g for 5 minutes and re-suspended into 10 ml of

Table 2.1: Cell line supplementation for routine maintenance.
Table of selection markers and growth supplements required for each cell line used, with working concentrations and supplier details.

Cell Line	Supplement	Supplier
MEDI-CHO	6 mM L-Glutamine	Thermo Fisher Scientific, MA, USA
CHO_{ETE}	50 µM MSX	Sigma Aldrich, MI, USA
CHO_{DTE}	50 µM MSX	Sigma Aldrich, MI, USA
$CHO_{BIS\text{-}A}$	50 µM MSX	Sigma Aldrich, MI, USA
$CHO_{BIS\text{-}B}$	50 µM MSX	Sigma Aldrich, MI, USA
CHO_{T2}	25 µM MSX, 100 µg.ml^{-1} Hygromycin-B	Thermo Fisher Scientific, MA, USA

pre-warmed CD-CHO media. Cells were seeded at 0.3×10^6 cells.ml^{-1} and labelled as passage 0. Cells were allowed 3 subcultures to recover post revival prior to any experimental work.

2.1.3.2 Cryopreservation and Cell Bank Generation

Cell banking was undertaken 3 passages post revival to minimise genetic ageing of the cell population. Cryopreservation media was formulated from CD-CHO media supplemented with 7.5 % Dimethyl Sulfoxide (DMSO) (Sigma Aldrich, MI, USA) to prevent the formation of ice crystals during freezing. At 3 days post subculture, cells were centrifuged at 200g for 5 minutes and re-suspended in cryopreservation media at 10×10^6 cells.ml^{-1}. Aliquots of 1 ml were placed into NUNC™cryovials (Thermo Fisher Scientific, MA, USA) and stored in a 'Mr Frosty' (Nalgene, Roskilde, Denmark) container filled with isopropanol overnight at −80 °C for a controlled freezing rate. Cryovials were then transferred into a liquid nitrogen cryostat at −196 °C for long term storage.

2.1.4 High-throughput Cell Culture

Several alternative culture formats were used throughout this project dependent on experimental scale, culture material requirements and work location. All high-throughput shaking cultures used vented lids secured with clamps (Duetz System; Enzyscreen B.V., Heemstede Netherlands). These are described in the following sections:

2.1.4.1 96 Deep Well Plates

Cells were cultivated in 96 Deep Well Plates (DWPs) (Masterblock®; Grenier Bio-One, Kremsmünster, Austria) maintained at 37 °C and 5 %(v/v)CO_2, 85 % humidity and shaken at 320 rpm (25 mm throw). Cells were seeded at variable densities from 0.2×10^6 cells.ml^{-1} to 1.0×10^6 cells.ml^{-1} at a volume of 475 ul and were cultured for 5 days unless otherwise stated.

2.1.4.2 24 Shallow Well Plates (University of Sheffield, Sheffield)

Cells were cultivated in 24 Shallow Well Plates (SWPs) (Nunc™, Nunclon Delta coated, flat bottom; Thermo Fisher Scientific, MA, USA) maintained at 37 °C and 5 %(v/v)CO_2, 85 % hu-

midity and shaken at 230 rpm (25 mm throw). Cells were seeded at variable densities from 0.5×10^6 cells.ml^{-1} to 1.5×10^6 cells.ml^{-1} at a volume of 700 µl and were cultured for 5 days unless otherwise stated.

2.1.4.3 24 Shallow Well Plates (AstraZeneca, Cambridge)

Cells were cultivated in 24 SWPs (Cornering® Costar® TC-Treated, flat bottom; Sigma Aldrich, MI, USA) maintained at 37 °C and 6 %(v/v)CO_2, 70 % humidity and shaken at 210 rpm (25 mm throw). Cells were seeded at 0.7×10^6 cells.ml^{-1} at a volume of 800 µl and were cultured for 10 days unless otherwise stated.

2.1.5 Fed-Batch Culture

When cultures were run as fed-batch, the following procedures were followed unless otherwise stated in both The University of Sheffield and AstraZeneca. At The University of Sheffield cultures were fed every third day with an equal mix of CD-CHO EfficientFeed™A and B (Thermo Fisher Scientific, MA, USA) totalling 10 % culture volume starting at day 3 post-seed. When at AstraZeneca, a proprietary in-house feed was used. The 24 shallow well plates were fed on alternate days starting at day 3 post-seed.

2.1.6 Assessment of Cell growth and Viability

2.1.6.1 Vi-Cell XR, Beckman Coulter

The Vi-Cell XR (Cell Viability Analyser; Beckman Coulter, High Wycombe, UK) assesses many aspects of a culture including Total Cell Density (TCD), Viable Cell Density (VCD), Viability and mean cell diameter via an automated Trypan Blue Dye exclusion method. The Vi-Cell XR allows simultaneous loading of 9 samples for easy cell analysis.

2.1.6.2 Presto Blue

PrestoBlue™was used as a high-throughput measure of culture performance prior to January 2018. The viable cell population of cultures can be estimated using PrestoBlue™Cell Viability Reagent (Thermo Fisher Scientific, MA, USA); a blue, non-fluorescent, resazurin based solution that is cell-permeable. Upon entering the cell, PrestoBlue™is reduced at a rate directly proportional to the metabolic activity of the cell. The resultant compound (resorufin) is red and highly fluorescent. As a result an indirect measurement of the viable cell population can be attained.

PrestoBlue™was diluted (1:1) in CD-CHO. Cell culture was diluted as required. A 100 µl culture sample was added to each well of a 96-well plate (Nunc™, Nunclon Delta coated, flat bottom; Thermo Fisher Scientific, MA, USA). A minimum of 3 blank samples (CD-CHO in place of sample) was included on each plate. A 20 µl aliquot of diluted PrestoBlue™was added to each well and pipette mixed. Following a 35 minutes incubation in a static incubator (37 °C, 85 % humidity, 5 %(v/v)CO_2), the flourescence intensity was measured using the PHERAstar Plus

(Plate Reader; BMG Labtech, Ortenberg, Germany) (excitation: 540 nm, emission: 590 nm). Raw values were converted into normalised readings shown in eq. (2.1).

$$Relative\ flourescence(RFU) = \frac{Sample\ flourescence}{Blank\ flourescence} - 1 \tag{2.1}$$

2.1.6.3 Norma HT, Iprasense

The Iprasense (Norma HT; Iprasense, Clapiers, France) was acquired in January 2018 and replaced the use of Presto Blue Assays. The device uses lens-free microscopy to measure the culture TCD, VCD, viability and mean cell diameter amongst other parameters (C. Allier et al. 2017; Cedric Allier et al. 2018). Samples were loaded onto slides containing 48 fluidic chambers with a depth of 100 µm. A point light source illuminates each sample from above. The light diffraction was captured by a sensor below creating a holographic image. A reconstruction algorithm was applied to construct the image from diffraction patterns. Viable and non-viable cells have distinct holographic signatures (derived from longitudinal and Z-profiles), hence can be distinguished.

The 100 µm counting chambers had an accurate range of 0.2×10^6 cells.ml^{-1} to 5.0×10^6 cells.ml^{-1} and a loading volume of 10 µl. For greater cell densities a 1 in 2 dilution step into CD-CHO was performed. Image reconstruction and assessment was performed using the HORUS software (Iprasense).

2.1.6.4 Trypan Staining on the Cellavista®, Synentec (AstraZeneca, Cambridge)

The Cellavista® 3 (Synentec GmbH, Elmshorn, Germany) is a high-throughput imaging system capable of many bright field and fluorescence assays. Firstly, 0.4 % trypan blue (Beckman Coulter, High Wycombe, UK) was diluted 4-fold in Phosphate Buffered Saline (PBS) to 0.1 %. A 96-well Masterlock® (Greiner Bio-One, Kremsmünster, Austria) was pre-filled with 665 µl PBS. A 96-well plate was filled with 100 µl PBS and 20 µl of 0.1 % trypan blue. A 35 µl cell culture sample was added to each matrix block well (1:20 dilution). An 80 µl aliquot of diluted sample was transferred from the matrix block to the 96-well trypan blue plate (1:2.5 dilution). The plate was centrifuged for 1 minute at 130 g and 4 °C prior to imaging on the Cellavista 3 at a final dilution of 1:50. The Synentec image processing software analysed the culture health to give TCD, VCD, viability and other metrics. When necessary an extra dilution step in PBS was performed to reach a maximum dilution on 1:200.

2.2 Recombinant Protein Quantification

2.2.1 Valita™TITER IgG Quantification Assay

Valita™TITER IgG Quantification Assay (ValitaCell, Dublin, Ireland) is a rapid, high-throughput assay that quantifies IgG-Fc interactions with a fluorescently labelled derivative of protein G via Fluorescence Polarization (FP). FP is detected through excitation of the sample wells with plane polarized light. The intensity of emitted light is measured in both the parallel (polarized proportion) and perpendicular (depolarized portion) planes to the exciting light. The FP is expressed as a normalised difference of the two intensities, typically expressed in Milli-Polarisation Units (mP). The amount of the Fc-containing molecule present is proportional to the polarisation of the well.

Cell culture supernatant was diluted to within the assay range of 2.5 mg.L^{-1} to 100 mg.L^{-1}. A 60 µl aliquot of Valita™mAb Buffer (ValitaCell) was added to the Valita™TITER plate, followed by 60 µl of diluted sample. The plate was mixed by pipetting and was incubated at room temperature in the dark for 30 minutes. Fluorescence polarisation was measured using the SpectraMax iD5 (Microplate Reader; Molecular Devices, CA, USA) with 485 nm excitation and 520 nm (parallel and perpendicular) emission wavelengths. The mP was calculated using the SoftMax Pro (Molecular Devices) software as per eq. (2.2), where $I_{vertical}$ represents fluorescence intensity measured in the vertical plane, and $I_{horizontal}$ represents fluorescence intensity in the horizontal plane. Standard curves (using IgG1 kappa standard (Sigma-Aldrich)) were used to interpolate recombinant IgG concentration.

$$mP = \frac{I_{vertical} - I_{horizontal}}{I_{vertical} + I_{horizontal}} \tag{2.2}$$

2.2.2 Octet Quantification Assay

Supernatant samples were diluted 1:20 into PBS prior to titre analysis. The analysis of product titre for cell culture work completed at AstraZeneca was outsourced to the BioProcess Analytics team. Titre was analysed on an Octet HTX System (Forte Bio, CA, USA). A molecule specific standard curve was run with each 384-well assay and was used to calculate the mAb concentration from the specific binding rate measured.

2.3 Plasmid DNA Creation, Amplification and Preparation

2.3.1 *De novo* gene Synthesis

Gene synthesis was outsourced to GeneArt (Thermo Fisher Scientific, MA, USA). Input sequences were either *C. griseus* or *H. sapiens* dependent on protein specific interactions. Each Coding DNA Sequence (CDS) was codon optimised by GeneArt's proprietary sequence optimisation tool. The full list of synthesised CDS constructs can be found in Appendix B.

2.3.2 Restriction Digest of Plasmid DNA

From 0.5 µg to 3.0 µg of plasmid Deoxyribonucleic Acid (DNA), 1x CutSmart™Buffer (New England Biolabs, MA, USA) and various High-Fidelity® Restriction Endonucleases were mixed and incubated for 2 hours at 37 °C. Digested DNA was used immediately or stored at 4 °C for up to 1 week.

2.3.3 Gel Electrophoresis and Extraction

Plasmid DNA was run on a 1.0 % agarose Tris-Acetate-EDTA (TAE) (Sigma Aldrich, MI, USA) gel with 1:10,000 SYBR™Safe DNA Gel Stain (Thermo Fisher Scientific, MA, USA) for 75 minutes with HyperLadder™1kb (Bioline, UK) at 100 V. Gels were imaged under UV light using a Biospectrum Imaging System (UVP, CA, USA).

Fragments of interest were excised using a scalpel and purified from the agarose gel using a QIAGEN Minelute gel extraction kit (QIAGEN, Manchester, UK) according to the manufacturer's protocol.

2.3.4 Plasmid Cloning

Insert and vector fragments were combined at a 6:1 molar ratio respectively as per eq. (2.3). The required mass of insert and vector was made up to 9 µl in nuclease-free water and the ligation was performed using NEB™'s Quick Ligation kit (New England Biolabs Ltd, Hitchin, England) as per the manufacturer's instructions. Ligation reactions were incubated for 15 minutes at room temperature.

$$Insert\ mass(ng) = Ratio\ excess \cdot \frac{Insert\ length(bp)}{Vector\ length(bp)} \cdot Vector\ mass(ng) \tag{2.3}$$

2.3.5 Plasmid Transformation and Amplification

Plasmid vectors for amplification were transformed into Subcloning Efficiency™DH5α *Escherichia coli* (*E. coli*) Competent Cells (Thermo Fisher Scientific, MA, USA). A 50 µl of DH5α cells were thawed on ice then incubated with 100 ng of plasmid DNA for 10 minutes on ice. Cells were heat-shocked for 40 seconds at 42 °C and incubated for a further 2 minutes on ice. Cells were added

to 1 ml LB-Broth (Thermo Fisher Scientific, MA, USA) and incubated at 37 °C and 700 rpm (5 mm throw) for 30 minutes. Cells were spread onto LB-Agar (Thermo Fisher Scientific, MA, USA) plates containing Ampicillin (Sigma Aldrich, MI, USA) at 100 µg.ml^{-1} and incubated at 37 °C overnight. A single colony was inoculated into 10 ml LB-Broth with 100 µg.ml^{-1} Ampicillin, which was incubated for 16 hours at 37 °C and shaken at 200 rpm overnight. For larger amplifications, the 10 ml culture was incubated for 8 hours, then expanded to 150 ml for 16 hours.

2.3.6 Plasmid Purification from DH5α *E.Coli*

Either QIAGEN Spin Miniprep or QIAGEN Plasmid Plus Maxi Kits (Qiagen, Manchester, UK) was used to lyse *E. coli* cells and purify the amplified plasmid DNA as per the manufacturer's protocol. In summary, provided buffers and centrifugation steps lyse (via alkaline lysis) the cells, and precipitate a large portion of cellular components including genomic DNA. The remaining supernatant was applied to an anion exchange column, binding plasmid DNA. Washing occurred prior to elution in Tris (trisaminomethane) buffer. Purified plasmid DNA was kept at −4 °C or −20 °C for short and long term storage respectively.

2.3.7 NanoDrop Quantification of DNA

A NanoDrop™One (Microvolume UV-Vis Spectrophotometer; Thermo Fisher Scientific, MA, USA) was used to determine DNA concentration and purity. The absorbance of a sample can be calculated using the Beer-Lambert Law (eq. (2.4)) where A represents the optical attenuation; ϵ the molar attenuation coefficient; L the optical path length; C the concentration of the attenuating species.

$$A = \epsilon LC \tag{2.4}$$

2.4 Design and Synthesis of esiRNA Constructs

For each design target, *C. griseus* messenger RNA (mRNA) sequences were analysed for transcript variants. Where no transcript variants existed, the full mRNA sequence was sent for endoribonuclease prepared small interfering siRNA (esiRNA) design. Where variants exist, mRNA transcripts were aligned and a partial transcript of minimum 500 bp was selected which maximises homology across all variants. Design and synthesis of esiRNAs was outsourced to Eupheria Biotech (Dresden, Germany), who analyse the selected mRNA sequences through a program called DEQOR (Henschel et al. 2004). This mimics esiRNAs by fragmenting the input sequence into pieces of 16 nt to 25 nt, whereby the sequence window is shifted along by 1 nt at each iteration step of the algorithm. DEQOR analyses sequence length, GC content and inclusion/aversion of specific nucleotide sub-chains to maximise esiRNA potency. Furthermore, specificity was ensured by Basic Local Alignment Search Tool (BLAST) analysis to minimise off-target effects.

On delivery, esiRNAs were stored at −20 °C as per the manufacturer's instructions.

2.5 Chemical Supplement Preparation and Storage

Chemical supplements tested in this study were ordered from commercial suppliers, or through the AstraZeneca Open Innovation Collaboration drug library. Powdered compounds were re-suspended in either DMSO or nuclease-free water, according to the manufacturer's instructions. If necessary compounds were filter-sterilised using a 0.22 µm filter (Cornering, Surrey, UK). Compounds were stored at −80 °C for long term storage, or 4 °C for short term storage. A full list of chemical supplements, and supplier information can be found in Appendix C.

2.6 Transient Transfection Methods

2.6.1 Lipofection and Nano-Particle Transfection Methods

DharmaFECT®2 (Horizon Discovery Group, Cambridge, UK), DharmaFECT®4 (Horizon Discovery Group, Cambridge, UK), MISSION small interfering RNA (siRNA) (Sigma Aldrich, MI, USA) and NanocinRibonucleic Acid (RNA) (Tecrea, London, UK) transfection reagents were stored according to the manufacturers instructions. Where not already available, the manufacturers protocols were adapted to reverse transfect suspension cells at a final density of 0.5×10^6 cells.ml^{-1}. The below sections describe protocols for transfections into a final volume of 200 µl at 0.3×10^6 cells.ml^{-1} incubated in static conditions.

When using 96-DWP cultures, the described methods were scaled up for a culture volume of 475 µl. Plates were incubated for 2 hours at 37 °C, 5 %(v/v)CO_2 and 85 % in a static incubator before being transferred to shaking conditions as described in section 2.1.4.1.

2.6.1.1 Dharmafect

The required volume of siRNA was diluted in 20 µl of non-supplemented media and was mixed by pipetting. Between 0.1 µl to 1.0 µl DharmaFECT®2 or DharmaFECT®4 was diluted into 20 µl of non-supplemented media into a 96-well culture plate and was mixed by pipetting. Following a 5 minute incubation at room temperature the diluted siRNA was added to the diluted DharmaFECT®reagent. The transfection mix was carefully mixed by pipetting and incubated at room temperature for 20 minutes.

The required number of cells were centrifuged at 200 rpm for 5 minutes and re-suspended into 160 µl then seeded directly onto the 40 µl transfection mix. Cells were incubated at 37 °C, 5 %(v/v)CO_2 and 85 % humidity for up to 5 days.

2.6.1.2 Mission RNAi

The required volume of siRNA was diluted in non-supplemented media to 48.5 µl in a 96-well culture plate and was mixed by pipetting. Next 1.5 µl of MISSION siRNA was added, and immediately mixed for 10 seconds by pipetting. The transfection mix was incubated for 15 minutes at room temperature.

The required number of cells were centrifuged at 200 rpm for 5 minutes and re-suspended into 50 µl then seeded directly onto the 50 µl transfection mix, the cells were mixed gently by pipetting. Cells were incubated at 37 °C, 5 %(v/v)CO_2 and 85 % humidity for 4 hours then 100 µl of non-supplemented media was added for a final culture volume of 200 µl. Transfected cells were incubated at 37 °C, 5 %(v/v)CO_2 and 85 % humidity for up to 5 days.

2.6.1.3 NanocinRNA

The required volume of siRNA was diluted in non-supplemented media to 9.2 µl in a 96-well culture plate and was mixed by pipetting. Next 0.8 µl of Nanocin RNA reagent was added, and

immediately mixed by pipetting. The transfection mix was incubated for 20 minutes at room temperature.

The required number of cells were centrifuged at 200 rpm for 5 minutes and re-suspended into 190 µl then seeded directly onto the 10 µl transfection mix. The culture was mixed by pipetting and incubated at 37 °C, 5 %(v/v)CO_2 and 85 % humidity for up to 5 days.

2.6.2 High-throughput Electroporation

The high-throughput 96-well plate electroporation process described below has been adapted from a protocol previously developed by Claire Bryant during the course of her Ph.D. and allows rapid delivery of DNA and RNA into cells.

The passage of cells prior to transfection was performed in CD-CHO media without the presence of selective markers. All successive steps were in non-supplemented CD-CHO media. A 2.0×10^6 cells aliquot was transfected in a volume of 20 µl, with 0 ng to 500 ng DNA per well, and an siRNA or esiRNA concentration of 0 nM to 2600 nM.

Experimental triplicates were pre-paired together in 50 % excess and separated when transferring to the final nucleofection plate. The DNA and/or RNA were combined with Tris-Ethylenediaminetetraacetic Acid (TE) buffer (Sigma Aldrich, MI, USA) to a final volume of 7 µl. This was added to 38 µl of nucleofection solution (prepared as per the Amaxa SG Cell Line 96-well electroporation kit (Lonza, Basal, Switzerland) instructions) in a 96-well U-bottom plate (Thermo Fisher Scientific, MA, USA). Cells were centrifuged at 200 g for 5 minutes and re-suspended in CD-CHO media at a density of 200.0×10^6 cells.ml^{-1}. A 45 µl aliquot was added to each triplicate preparation totalling 90 µl per triplicate condition. A 20 µl aliquot of each triplicate condition was transferred to 3 wells of a 96-well electroporation plate (Lonza, Basal, Switzerland). The Amaxa plate was then electroporated on the Amaxa Nucleofector 96 Shuttle System (Lonza, Basal, Switzerland) on program FF-158. Immediately post-electroporation, 80 µl of pre-warmed pre-gassed CD-CHO was added. A 40 µl or 70 µl sample of transfected cells was seeded into 96 DWPs or 24 SWPs respectively, also containing pre-warmed, pre-gassed CD-CHO media. The cultures were incubated according to conditions outlined in section 2.1.4.

2.6.2.1 Cleaning of Lonza Electroporation Plates

The following procedure was performed in a HEPA filtered laminar flow hood. The cleaning procedure was only used to transfect biological replicates.

Immediately after use plate wells were washed with 170 µl of 100 % High-Performance Liquid Chromatography (HPLC) grade iso-propanol 5 times. Wells were then incubated with 220 µl for 30 minutes. The plates were left uncovered to dry for 1 hour, followed by a further 1 hour under Ultra-Violet (UV)-light to ensure sterility. Plates were used for a second transfection the same day.

2.7 Flow Cytometry

The presence of intracellular cyan-5 Fluorescent-Tagged Small Interfering Ribonucleic Acid (ftRNA) and expression of intracellular eGFP was quantified by flow cytometry. This methodology measures the fluorescence intensity within living cells, allowing assessment of the transfection efficiency of multiple siRNA delivery methods. In addition the co-transfection of DNA and siRNA can be assessed. Initially the Photomultiplier Tube (PMT) voltages were adjusted for optimal detection of mock-transfected and CHO_{T2} cells. The cell size and granularity was adjusted for by setting Front Scatter (FSC) and Side Scatter (SSC) respectively. The detection channels for cyan-5 and eGFP was adjusted so that the Median Fluorescence Intensitys (MFIs) were 0 by adjusting the PMTs. Positive control cells for each fluorescence signal were measured on the device to adjust the PMTs to ensure the maximum fluorescence intensity was within range. Cross detection and compensation was not required as the emission spectra of the fluorescence signals do not exhibit any interference (Figure 3.1).

Table 2.2: Attune NxT flow cytometer optimised settings.
Summary of the lasers, emission filters, fluorophore channels and voltages utilised for the detection of Cyan-5 ftRNA and eGFP. These settings were applied for both single and multi-fluorescent analysis.

Laser Name	Channel Name	Excitation Wavelength (nm)	Emission Filter (nm)	Fluorophore Detected	PMT Voltage
Forward Scatter	FSC-A	N/A	N/A	N/A	1250
Side Scatter	SSC-A	N/A	N/A	N/A	2700
Red	RL1-A	633	660/20	Cyan-5	2650
Green	BL1-A	488	530/30	eGFP	750

Prior to flow cytometry analysis cells were harvested by centrifugation at 200 g for 5 minutes. Live cells were re-suspended and mixed 2 times in PBS (Thermo Fisher Scientific, MA, USA) with an equivalent centrifugation step between each wash. Cells were then re-suspended in CD-CHO to maintain cell viability. Flow cytometric analysis was performed on an Attune Acoustic Focusing Flow Cytometer (Thermo Fisher Scientific, MA, USA). The wavelength of lasers and filters, channel names and PMT voltages are shown in Table 2.2. The auto-sampler settings were as follows:

- Sample volume: 150 µl
- Maximum sample uptake volume: 150 µl
- Upper event limit: 50,000 events
- Lower event limit: 10,000 events
- Mixing cycles: 2
- Washes: 2

Data was analysed using FlowJo™ analysis software, analysis and gating strategies are described in chapter 3.

2.8 Quantification of Intracellular Proteins

Cells for western blot analysis were harvested by centrifugation at 500 g for 3 minutes and washed once in ice cold PBS (Thermo Fisher Scientific, MA, USA). Upon centrifugation and removal of PBS, pellets were immediately transferred into storage at −80 °C for sample preservation. All samples were stored on ice unless otherwise stated.

2.8.1 SDS Polyacrylamide Gel Electrophoresis

Lysis buffer was prepared by combining Radio-Immunoprecipitation Assay (RIPA) (Sigma Aldrich, MI, USA) buffer with Protease Inhibitor Cocktail Set III (50x) (Merck Millipore, Darmstadt, Germany) and Benzonase Nuclease (Merck Millipore, Darmstadt, Germany) (100 U/ml). The lysis buffer was added to cell pellets for a final concentration of 1.0×10^7 cells.ml^{-1} and incubated for 2 hours shaking at 700 rpm with 5 mm throw at 4 °C.

Protein lysate concentration was assessed on a NanoDrop™One (Microvolume UV-Vis Spectrophotometer; Thermo Fisher Scientific, MA, USA) to ensure total protein concentration of (26.0 ± 2.5) mg.ml^{-1}.

Samples were prepared for Sodium Dodecyl Sulfate–Polyacrylamide Gel Electrophoresis (SDS-PAGE) by volume as follows: 25 %(v/v) protein lysate, 25 %(v/v) NuPAGE™LDS sample buffer(4x) (Thermo Fisher Scientific, MA, USA), 10 %(v/v) NuPAGE™Sample Reducing Agent (10X) (Thermo Fisher Scientific, MA, USA) and 40 %(v/v) di−H_2O. Samples were incubated at 75 °C for 5 minutes. Chameleon® Duo Pre-stained Protein Ladder (LI-COR® Biosciences, NE, USA) was incubated at 95 °C for 2 minutes.

Either 20 µl of sample or 5 µl of ladder were loaded into NuPAGE™pre-cast 4 % to 12 % Bis-Tris Protein Gels (1.5 mm, 15-well; Thermo Fisher Scientific, MA, USA). Gels were run in NuPAGE™MOPS SDS Running Buffer (20X) (Thermo Fisher Scientific, MA, USA) made up with di−H_2O at 180 V for 90 minutes or until the loading dye ran to the end of the gel.

2.8.2 iBlot® Gel Transfer

Protein gels were transferred using the iBlot® Dry Blotting System (Invitrogen™, Thermo Fisher Scientific, MA, USA) (20 V, 23 V, 25 V for 1 minute, 4 minutes and 2 minutes respectively) onto Novex™iBlot® Nitrocellulose Transfer Stacks (Invitrogen™, Thermo Fisher Scientific, MA, USA) as per the manufacturer's instructions.

2.8.3 Western Blotting

The following blocking buffers were used dependent on the target: PBS/Tris Buffered Saline (TBS) and 5 %(v/v Bovine Serum Albumin (BSA) (Sigma Aldrich, MI, USA), or Intercept® (PBS/TBS) Blocking Buffer (LI-COR® Biosciences, NE, USA). Primary (Table 2.3) and sec-

ondary (Table 2.4) antibody solutions were made in 2 ml of blocking buffer. The wash buffer comprised of PBS/TBS with 0.2 %(v/v) TWEEN® 20 (Sigma Aldrich, MI, USA).

Unless otherwise stated, incubation steps were performed on a rocker at 18 rpm. Membranes were blocked in 20 ml of blocking buffer and incubated for 2 hours, then were washed once in 20 ml PBS, 0.1% Tween-20 (PBS-T) for 5 minutes. Membranes were heat-sealed in a plastic pouch with 2 ml primary antibody solution and incubated overnight at 4 °C rotating on a vertical axis at 12 rpm. Membranes were washed 3 times in 20 ml PBS-T for 5 minutes, then heat-sealed with 2 ml secondary antibody solution for 2 hours at room temperature rotating on a vertical axis at 12 rpm. After a further 3 washes in 20 ml PBS-T for 5 minutes, membranes were dried between 2 sheets of filter paper. Membranes were stored in the dark and imaged within 72 hours.

Western blots were imaged on the LI-COR Odyssey® Sa Infrared Imaging System (LI-COR® Biosciences, NE, USA) controlled with Image Studio™Software (LI-COR® Biosciences, NE, USA). Images were analysed on Image Studio™and the target protein was quantified relative to β-actin or GAPDH controls.

Table 2.3: Western blot primary antibodies.
Complete list of western blot primary antibodies, dilution ranges and supplier information.

Target	Host	Dilution Range	Product No.	Supplier
Sec22b	Rabbit	1:2,000 - 1:5,000	SY-186003	Synaptic Systems (Göttingen, Germany)
BIP	Rabbit	1:1,000 - 1:3,000	ab-21685	AbCam (Cambridge, UK)
HSP90B1	Rabbit	1:1,000 - 1:2,000	PA5-24824	Thermo Fisher Scientific (MA, USA)
β-actin	Mouse	1:400 - 1:200	ab-8227	AbCam (Cambridge, UK)
GAPDH	Mouse	1:750 - 1:1,000	Ab-97166	Cell Signalling (London, UK)

Table 2.4: Western blot secondary antibodies.
Complete list of western blot secondary antibodies, dilution ranges and supplier information.

Target	Marker	Dilution Range	Product No.	Supplier
Anti-Rabbit IgG (H+L)	Alexa Flour Plus 800	1:5,000 - 1:10,000	A32735	Thermo Fisher Scientific (MA, USA)
Anti-Mouse IgG (H+L)	Alexa Flour 700	1:5,000 - 1:10,000	A-21036	Thermo Fisher Scientific (MA, USA)
Anti-Mouse IgG (H+L)	DyLight® 800	1:7,000 - 1:12,000	Look Up	Thermo Fisher Scientific (MA, USA)
Anti-Rabbit IgG (H+L)	Alexa Flour 680	1:5,000 - 1:8,000	Look Up	Thermo Fisher Scientific (MA, USA)

2.9 IgG Product Quality Analysis

This method was developed by Jennifer Spooner (AstraZeneca, Cambridge, UK) and adapted for this work.

Cell culture samples were centrifuged at 1000 g, 4 °C for 5 minutes to remove cells and debris. The aspirated supernatant for IgG product quality analysis when used within 3 days samples were stored at 4 °C, otherwise samples were frozen at −80 °C immediately after harvest.

2.9.1 IgG Purification by Protein A Affinity

All incubation steps were performed at room temperature shaking at 1300 rpm and 5 mm throw and all centrifugation steps were at 1000 g for 2 minutes.

Mabselect SuRe protein A-derived resin (50 $\%_{(v/v)}$ in 20 % ethanol; GE Healthcare, IL, USA) was diluted to 10 % with 20 % ethanol and 500 µl was added to each well of a 96-well filter plate (0.45 µm polypropylene membrane, 800 µl; Agilent Technologies, CA, USA). The filter plate was centrifuged to remove the 20 % ethanol. The plate was then washed twice to equilibrate the resin by incubating with 300 µl PBS for 5 minutes and centrifuging. A 500 µl aliquot of supernatant was incubated in the filter plate for 60 minutes and centrifuged to remove the supernatant. The plate was then washed 3 times to remove contaminants by incubating with 300 µl PBS for 5 minutes and centrifuging. The filter plate was incubated with 200 µl of 0.1 M Glycine Buffer pH 2.7 for 60 minutes then centrifuged to elute the IgG into a 96-well HPLC plate (0.5 ml, round bottom; Agilent Technologies, CA, USA). Purified protein concentration was verified by UV absorbance measurement at 280 nm on a Stunner (Unchained Labs, CA, USA) HPLC and stored at 4 °C prior to further analysis.

2.9.2 High-Performance Size Exclusion Chromatography

Post-purification IgG samples were analysed for aggregate profiles on an Agilent Technologies 1260 Infinity HPLC system on a Walters BEH200 (150 mm x 4.6 mm Size Exclusion Chromatography (SEC) column (Waters Corporation, MA, USA) under the following conditions:

- Flow rate: 0.400 $ml.min^{-1}$
- Detection wavelength: 280 nm
- Injection volume: 10 µl
- Temperature: 20.00 °C
- Mobile Phase Buffer: 0.1 M Phosphate, 0.1 M Sulphate pH 6.8
- Pressure: 280 bar
- Run time: 6 minutes

Two 96-well plates of samples could be loaded onto the HPLC system at a time, and maintained at 4 ℃ prior to injection. Gel Filtration Standards (Bio-Rad Laboratories, CA, USA) and a NIP228 control IgG1 were run before and after each plate to monitor column integrity and ensure correct peak identification. Peaks were integrated by the Agilent Technologies software and peak areas used to calculate the abundance of IgG and other High Molecular Weight Species (HMWS).

2.10 Automated Liquid Handlers

2.10.1 OT-2, Opentrons

The OT-2 (Opentrons, NY, USA) is a fully customisable, fast and precise bench-top liquid handler with the flexibility to run any plate protocols. Equipped with 2 pipetting arms and 11 lab-ware positions, large protocols can be completed without intervention. This was procured in September 2019 and was used for all high-throughput cell culture in chapter 4.

Protocols were written in Python within the Opentrons API 2.0 environment. Protocols were simulated on the Opentrons Simulator run through Jupyter™Notebook prior to laboratory optimisation. Protocols were finalised after 3 successful mock runs. Examples of protocols include; plate-based electroporation (section 2.6.2), Valita™TITER IgG quantification (section 2.2.1), Iprasense slide loading (section 2.1.6.3), high-throughput culture feeding (section 2.1.5) and sample collection for western blotting (section 2.8.3). All plate-based cell culture experiments that generated the data presented in chapter 4 were completed on the Opentrons OT-2 liquid handler. The finalised Python scripts for all experiments completed on the Opentrons OT-2 liquid handler are available in Appendix D.

2.10.2 Biomek FX, Beckman Coulter

The Biomek FX Laboratory Workstation (Beckman Coulter, High Wycombe, UK) was used when available for sampling cultures, preparing trypan plates for culture assessment and harvesting cultures. Biomek FX protocols were already set up and followed the methodology described in section 2.1.6.4.

Table 2.5: List of equipment.
Alphabetical list of equipment used with supplier information.

Equipment	Supplier
Attune Acoustic Focusing Flow Cytometer	Nunclon Delta coated, round bottom; Thermo Fisher Scientific, MA, USA
Biospectrum Imaging System	UVP, CA, USA
Biomek FX automated liquid handler	Beckman Coulter, High Wycombe, UK
Cellavista®	Synentec GmbH, Elmshorn, Germany
Duetz System	Enzyscreen B.V., Heemstede, Netherlands
Erlenmeyer flasks	Cornering, Surrey, UK
iBlot® Dry Blotting System	Invitrogen™, Thermo Fisher Scientific, MA, USA)
Iprasense	Norma HT; Iprasense, Clapiers, France
LI-COR Odyssey® Sa Infrared Imaging System	LI-COR® Biosciences, NE, USA
Amaxa Nucleofector 96 Shuttle System	Lonza, Basal, Switzerland
Mr Frosty	Nalgene, Roskilde, Denmark
NanoDrop™One	Microvolume UV-Vis Spectrophotometer; Thermo Fisher Scientific, MA, USA
Octet HTX System	Forte Bio, CA, USA
OT-2 Liquid Handler	Opentrons, NY, USA
PHERAstar Plus	Plate Reader; BMG Labtech, Ortenberg, Germany
SpectraMax iD5	Microplate Reader; Molecular Devices, San Jose, USA
Vi-Cell	XR Cell Viability Analyser; Beckman Coulter, High Wycombe, UK

Table 2.6: List of materials part A.
Alphabetical list of materials used with supplier information part A.

Material	Supplier
24-well Plate	Cornering® Costar® TC-Treated, flat bottom; Sigma Aldrich, MI, USA
24 Well Plate	Nunc™, Nunclon Delta coated, flat bottom; Thermo Fisher Scientific, MA, USA
96-well Masterblock®	Greiner Bio-One, Kremsmünster, Austria
96-well electroporation plate	Lonza, Basal, Switzerland
96-well filter plates	0.45 µm polypropylene membrane, 800 µl; Agilent Technologies, CA, USA
96-well HPLC plates	0.5 ml, round bottom; Agilent Technologies, CA, USA
96-well plate	Nunc™, Nunclon Delta coated, flat bottom; Thermo Fisher Scientific, MA, USA
96-well U-bottom plate	Thermo Fisher Scientific, MA, USA
Amaxa SG Cell Line 96-well electroporation kit	Lonza, Basal, Switzerland
Ampicillin	Sigma Aldrich, MI, USA
Benzonase Nuclease	Merck Millipore, Darmstadt, Germany
Bovine Serum Albumin	Sigma Aldrich, MI, USA
CD-CHO medium	Thermo Fisher Scientific, MA, USA
CD-CHO EfficientFeed™A	Thermo Fisher Scientific, MA, USA
CD-CHO EfficientFeed™B	Thermo Fisher Scientific, MA, USA
Chameleon® Duo pre-stained protein ladder	LI-COR®, NE, USA
Cryovial NUNC™1.5 ml	Thermo Fisher Scientific, MA, USA
CutSmart® Buffer	New England Biolabs, MA, USA
DharmaFECT®2	Horizon Discovery Group, Cambridge, UK
DharmaFECT®4	Horizon Discovery Group, Cambridge, UK
Dimethyl Sulfoxide	Sigma Aldrich, MI, USA
Gel Filtration Standards	Bio-Rad Laboratories, CA, USA
Hygromycin-B 50 $mg.ml^{-1}$	Thermo Fisher Scientific, MA, USA
HyperLadder™1kb	Bioline, UK
IgG1 kappa standard	Sigma Aldrich, MI, USA
Intercept® (PBS) Blocking Buffer	LI-COR®, NE, USA
LB-Agar	Thermo Fisher Scientific, MA, USA
LB-Broth	Thermo Fisher Scientific, MA, USA

Table 2.7: List of materials part B.
Alphabetical list of materials used with supplier information part B.

Material	Supplier
L-Glutamine (200 mM)	Thermo Fisher Scientific, MA, USA
L-Methionine Sulfoximine 100 µM	Sigma Aldrich, MI, USA
Mabselect SuRe protein A-derived resin	50 %(v/v) 20 % ethanol; GE Healthcare, IL, USA
MISSION siRNA transfection reagent	Sigma Aldrich, MI, USA
Nanocin RNA	Tecrea, London, UK
NEB™'s Quick Ligation kit	New England Biolabs Ltd, Hitchin, England
Novex™iBlot® Nitrocellulose Transfer Stacks	Invitrogen™, Thermo Fisher Scientific, MA, USA
NuPAGE™4 % to 12 % Bis-Tris Protein Gels	1.5 mm, 15-well; Thermo Fisher Scientific, MA, USA
NuPAGE™LDS sample buffer (4x)	Thermo Fisher Scientific, MA, USA
NuPAGE™MOPS SDS Running Buffer (20X)	Thermo Fisher Scientific, MA, USA
NuPAGE™Sample Reducing Agent (10X)	Thermo Fisher Scientific, MA, USA
Phosphate Buffered Saline	Thermo Fisher Scientific, MA, USA
PrestoBlue™	Cell Viability Reagent; Thermo Fisher Scientific, MA, USA
Protease Inhibitor Cocktail Set III (50x)	Merck Millipore, Darmstadt, Germany
QIAGEN Minelute gel extraction kit	Qiagen, Manchester, UK
QIAGEN Spin Miniprep	Qiagen, Manchester, UK
QIAGEN Plasmid Plus Maxi Kits	Qiagen, Manchester, UK
RIPA	Sigma Aldrich, MI, USA
Subcloning Efficiency™DH5α Competent Cells	Thermo Fisher Scientific, MA, USA
Sterilising filter 0.22 µm	Cornering, Surrey, UK
SYBR™Safe DNA Gel Stain	Thermo Fisher Scientific, MA, USA
TPP TubeSpin Bioreactors	Thermo Fisher Scientific, MA, USA
Tris-acetate-EDTA buffer	Sigma Aldrich, MI, USA
Trypan blue	Beckman Coulter, High Wycombe, UK
TWEEN® 20	Sigma Aldrich, MI, USA
ValitaTITER™IgG Quantification Assay	ValitaCell, Dublin, Ireland
Walters BEH200 SEC column	Waters Corperation, MA, USA

Chapter 3

Design and Development of a Simultaneous Overexpression and Silencing Co-transfection (SOSC) Screening Platform for CHO Cell Engineering

This chapter describes the design, development and validation of a high-throughput gene screening platform for co-transfection of DNA and RNA while maintaining industrially approved mAb production conditions. A comparative assessment of RNA delivery methods was conducted in order to identify the optimal transfection methodology to transfect suspension cells at high density. The selected transfection methodology was validated with three target genes and the knock-down potency, duration and consistency were assessed through relative quantification of intracellular Host Cell Protein (HCP) abundance. A better suited high-throughput cell culture format was optimised and evaluated against the existing 96-DWP format. The performance and precision of an automated liquid handler was assessed against a human operator when completing protein quantification assays and the selected transfection method. The complete gene screening platform capable of SOSC of target proteins was then automated to run on the Opentrons OT-2 liquid handler.

3.1 Introduction

The expanding development of complex engineered Monoclonal Antibodys (mAbs) in unnatural formats has lead to increasingly complex Chinese Hamster Ovary (CHO) engineering strategies being trailed to improve host cell lines and support the cell line development processes (Fischer, Handrick, et al. 2015).

Despite the success of transient and stable gene overexpression studies aiming to improve mAb secretory capacity and cell growth characteristics (Johari et al. 2015; Ku et al. 2008; Pybus et al. 2014; Wlaschin and W. S. Hu 2007), engineering solutions are often non-transferable due to high cell line and mAb specificity. Resultantly, unique engineering solutions need to be identified for optimal development new mAbs requiring a standardised High Throughput (HTP) method of screening effector genes and evaluating changes to cell performance within a short time frame. An example of such a method is described in Cartwright et al. 2020, where a HTP overexpression gene screening platform for rapid transient screening of effector genes in CHO cells has been developed.

Stable knockout of effector genes are another engineering solution to improving the production of Difficult to Express (DTE) bio-therapeutics. The transient knock-down of effector genes by RNA Interference (RNAi) is a well established and documented process with hundreds of screens published in *C. elegans*, *D. melanogaster*, mouse and human cell lines (E. Yanos et al. 2012; S. Mohr et al. 2010; Perrimon et al. 2010; Root et al. 2006). Typically RNAi is used in HTP screens of hundreds to thousands of genes in genome-scale functional studies, aiming to identify new genes and elucidate their function in biological processes (Boutros and Ahringer 2008). However, the documented RNAi studies in CHO cells are limited with only Klanert et al. 2019 evaluating the effect of RNAi on producing CHO cells. Furthermore, the use of RNAi for transient knock-down is mostly limited to low density static cultures with little applicability to a industrial mAb production formats.

The development of a RNAi screening platform capable of evaluating the performance of producing CHO cells in culture conditions representative of bioreactor production. This could be used to screen effector genes hypothesised to improve cell performance and mAb production, broadening the toolbox of engineering targets available for the development of new mAbs. Such a platform could assess the sensitivity of cell lines to the knock-down of genes associated with mAb production (e.g. folding and assembly processes), providing insights into generic and mAb specific production bottlenecks in the CHO secretory pathway. Furthermore, the ability to transiently co-transfect Deoxyribonucleic Acid (DNA) and Ribonucleic Acid (RNA) would open a number of research opportunities such as effector gene titration and the direct comparison of cell line responses to gene up- and down-regulation, offering a greater depth of information than either strategy in isolation.

This chapter explores the design, optimisation and characterisation of a practical and scalable HTP RNAi screening platform, compatible with plasmid-DNA co-transfection as an engineering tool. This began with identification of the platform design requirements and evaluation of the available transfection methodologies ability to meet these requirements. After the optimal

transfection method was validated experimentally, the knock-down dynamics were evaluated to identify optimal RNAi concentration ranges and characterise the duration of the Gene of Interest (GOI) depletion. Next the culture conditions of the platform were optimised to maximise performance so the stationary culture phase could be reached within the five-day duration of effective RNAi knock-down. Lastly the entire platform was automated on an Opentrons OT-2 liquid handler to improve the accuracy, robustness and throughput.

3.2 Results

3.2.1 Design of a RNA and DNA Co-transfection Methodology

3.2.1.1 Identification of platform design requirements

The first step when evaluating the knock-down methodologies for CHO cell engineering was assessment of the desired characteristics and outputs. A framework was created by reviewing the literature for existing RNAi screening methods in CHO cells. The platform requirements were assessed for use in industrial biopharmaceutical production settings, identifying limitations of current methodologies. The key design characteristics are described below:

a) *Robust, accurate and consistent* - This was vital for research based cell engineering in academia and for future use as an engineering tool during cell line development campaigns in industrial settings. This was needed to allow for standardised rapid high-throughput transfection of both producing and non-producing CHO cell lines, and primarily interface with a range of small scale suspension culture formats.

b) *Simple and reproducible RNA and DNA co-transfection* - The ability to directly compare RNAi silencing to transient over-expression of target genes was essential. Therefore, the platform adopted needed to be capable of delivering both forms of nucleic-acid, either simultaneously or through successive transfections. Unlike RNA, DNA exerts a significant transcriptional burden on the cells, therefore DNA load must be standardised across all conditions within an experiment.

c) *Alignment to industrial mAb production* - This required the platform to support suspension cultures and achieve exponential and stationary growth phases seen in industry mAb production processes. RNAi silencing remains effective for up to 7 days in dividing cells, however this is likely to be reduced beyond 5 days (Bartlett and M. E. Davis 2006). Therefore an ideal solution would achieve Peak Cell Density (PCD) by 5 days post-transfection.

d) *Chemically-defined and protein-free* - These are essential characteristics for platform integration in the biopharmaceutical industry where the use of animal derived products during biotherapeutic development is not permitted by regulatory agencies (S. Mohr et al. 2010). Therefore, common supplements to RNAi methodology such as Fetal Bovine Serum (FBS) and Fetal Calf Serum (FCS) must be avoided (Pasettoa et al. 2015; Theis and Buchholz 2011).

e) *Cost efficient and scalable* - The screening platform should be as cost effective as possible while meeting the above design characteristics. The importance of this scales with the number of screening targets. A secondary objective is incorporating the design flexibility to optimise greater cost efficiency into the process in the future.

3.2.1.2 Advantage and disadvantages of selected RNA transfection methods

There are two commonly used knock-down methodologies dependent on the cell model and desired output. Lipofection is most common in RNAi screening studies offering scalability and

rapid reverse transfection protocols for large scale screening in addition to documented double knock-downs for prolonged silencing. DharmaFECT™ lipofection reagents are the gold standard within this category, however no published methodology exists for its use in suspension cultures. Additionally, electroporation offers direct instant delivery of DNA and RNA to a large number of cells, however it is only used in small scale studies due to the high cost and complexity.

Due to the limited literature of RNAi studies in suspension CHO cells, multiple transfection methods were experimentally assessed. Lipofection, electroporation and nano-particle transfection methodologies were selected and Table 3.1 highlights the advantages and disadvantages of each. Reagents were evaluated and prioritised for testing based on the likelihood of success and cost efficiency:

1. DharmaFECT™ 2 & 4 - As the gold standard for RNAi screening, two reagents from Horizon were recommended for use in CHO cells. These also served as a benchmark to compare other reagents. However, performance when transfecting cells in suspension or at high density has not been previously documented, therefore an alternative lipofection reagent was evaluated.

2. MISSION®siRNA - The key benefits listed in Table 3.1 include cost efficiency and documented transfection of suspension cells. Additionally, the manufacturer's recommended transfection density was higher then DharmaFECT™ reagents. Only 80 % transfection efficiency in suspension cultures was advertised, however only electroporation had a value for comparison. A major concern was the effectiveness without the addition of serum to improve RNA uptake and cell growth.

3. Nanocin RNA - This was the 'wild card' transfection method, advertised as a novel nanoparticle RNA delivery vehicle. Nanocin RNA had been demonstrated to be less cytotoxic than other methods permitting better culture growth, and had an existing protocol for reverse transfection of suspension cells. Additionally, the transfection cell density was similar to that of MISSION®siRNA. However, the company was relatively new, with little literature available to support the method.

4. SG Cell Line 96 Nucleofector™ Kit - The many benefits of the Lonza electroporation platform were evaluated against the higher cost per transfection. Although this method is likely to succeed, it was placed as a reserve with priority given to optimisation of a more cost effective transfection platform for improved scalability. The strength of RNAi silencing may be reduced as RNA can only enter cells during electroporation. The primary hurdles identified were increased protocol complexity and cost implications.

Table 3.1: Assessment of the advantages and disadvantages of the RNA delivery methods tested.
The table provides and an overview of the benefits and limitations of each RNA delivery reagent/method in the context of the proposed screening platform.

Reagent *(Method)*	Advantages	Disadvantages
DharmaFECT™ 2 & 4 *(Lipofection)*	• Gold standard for RNAi screening studies. • Double knock-down for prolonged silencing demonstrated in the literature.	• Validated for adherent cells only. • Low density of cells transfected. • Reagent presence stunts cell growth.
MISSION®siRNA Transfection Reagent *(Lipofection)*	• Validated for transfection of suspension cells. • Can conduct transfections at a high cell density (up to 1.5×10^6 cells.ml^{-1}). • Best cost efficiency of the proposed methods.	• Serum recommended to improve RNA uptake. • Maximum advertised silencing efficiency of 80 % in suspension cultures. • Reagent presence stunts cell growth.
Nanocin RNA *(Nano-particle Assembly)*	• Lower cytotoxicity than lipofection techniques. • Tecrea also offer Nanocin DNA for successive transfections. • Double knock-down for prolonged silencing. • Validated for transfection of suspension cultures.	• New technology with limited literature. • Validated for adherent cells only.
SG Cell Line 96 Nucleofector™Kit *(Electroporation) (Cartwright et al. 2020; Yang et al. 2015)*	• Simple adaptation of DNA transfection platform. • High cell density • Transfection efficiencies with 96% for eGFP. • Instant nucleic acid delivery • Cost reductions possible through plate reuse. • No cytotoxic reagents permits normal cell growth.	• High kit cost at £3.30 per transfection • Complex protocol with time sensitive steps. • Lower through put than other suggested methods.

3.2.2 Developing a Method to Quantitatively Assess RNA and Plasmid DNA Delivery

There was a requirement to accurately and reliably assess both the transfection efficiency and potency, primarily for small interfering RNA (siRNA) and subsequently plasmid DNA co-delivery. When compared to other RNAi screening platforms (section 1.5.4.1), one important divergence was high cell density transfection in excess of 1.0×10^6 cells.ml^{-1}. Therefore a consistent, reliable and robust method for simultaneous assessment of both RNA and DNA transfection was needed.

After reviewing available approaches, transfection of a Fluorescent-Tagged Small Interfering Ribonucleic Acid (ftRNA) and subsequent measurement by flow cytometry was selected as an effective and reliable method (Homann et al. 2017; L. Peng et al. 2017). In addition, the use of a eGFP plasmid vector would allow assessment of co-transfection capabilities.

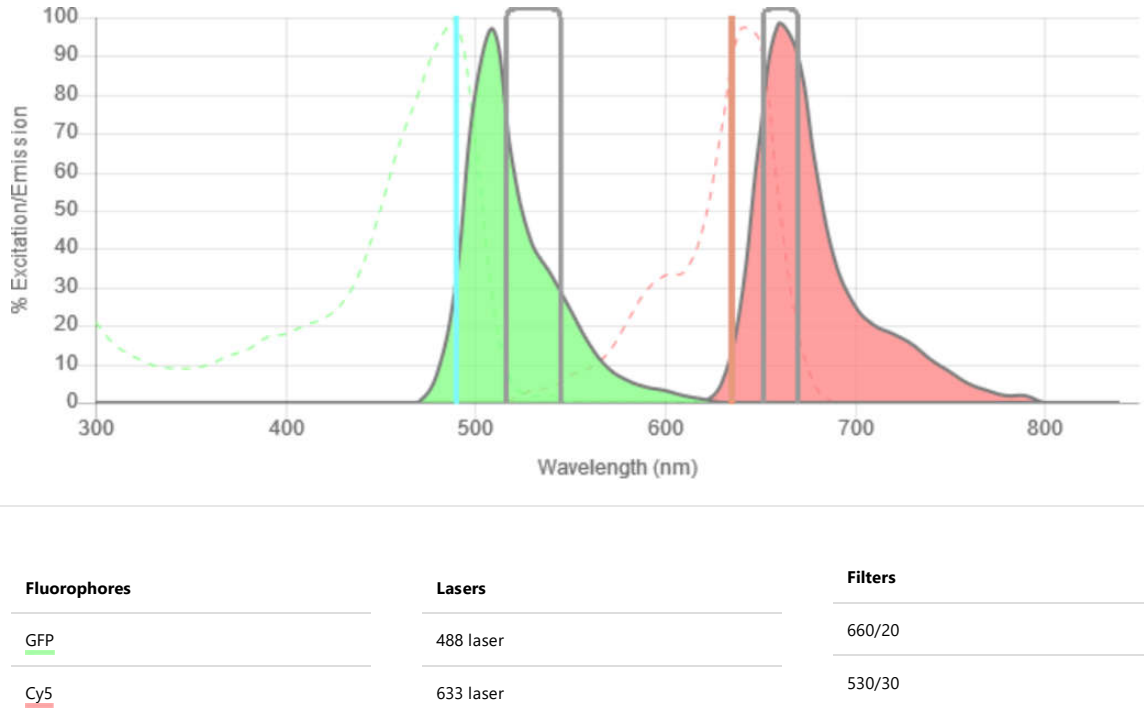

Figure 3.1: Cyan5 and eGFP excitation and emission spectra with Attune NXT flow cytometer lasers and bandpass filters.
Cyan5 and eGFP excitation and emission spectra's are displayed by dotted and solid filled lines respectively. The 633 nm and 488 nm lasers are represented by red and blue vertical lines respectively. The RL1 (660/20 nm) and BL1 (530/30 nm) bandpass filters read areas represented by the grey boxes with 95 % and 46 % filter coverage respectively.

When reviewing the commercially available negative control siRNAs, a cyan-5 ftRNAs was selected for the following reasons; Firstly, the available lasers on the Attune NxT flow cytometer allowed for efficient excitation of the fluorophore. Secondly, the emission spectra of cyan-5 and eGFP do not exhibit any cross interference when using the available lasers and bandpass filters. Figure 3.1 shows a schematic of the excitation and emission spectra of cyan-5 and eGFP when excited by 633 nm and 488 nm lasers with measurements taken by RL1 (660/20 nm) and BL1

(530/30 nm) bandpass filters. A consideration when measuring siRNA transfection efficiency with ftRNA was the requirement for a robust washing procedure. This ensures that measured fluorescence is from positively transfected cells, not ftRNA still present in the culture medium or stuck to the outer cell membrane. The washing procedure described in section 2.7 is the result of several optimisation steps and the effectiveness is demonstrated in subsequent figures.

3.2.2.1 Flow cytometer parameter optimisation

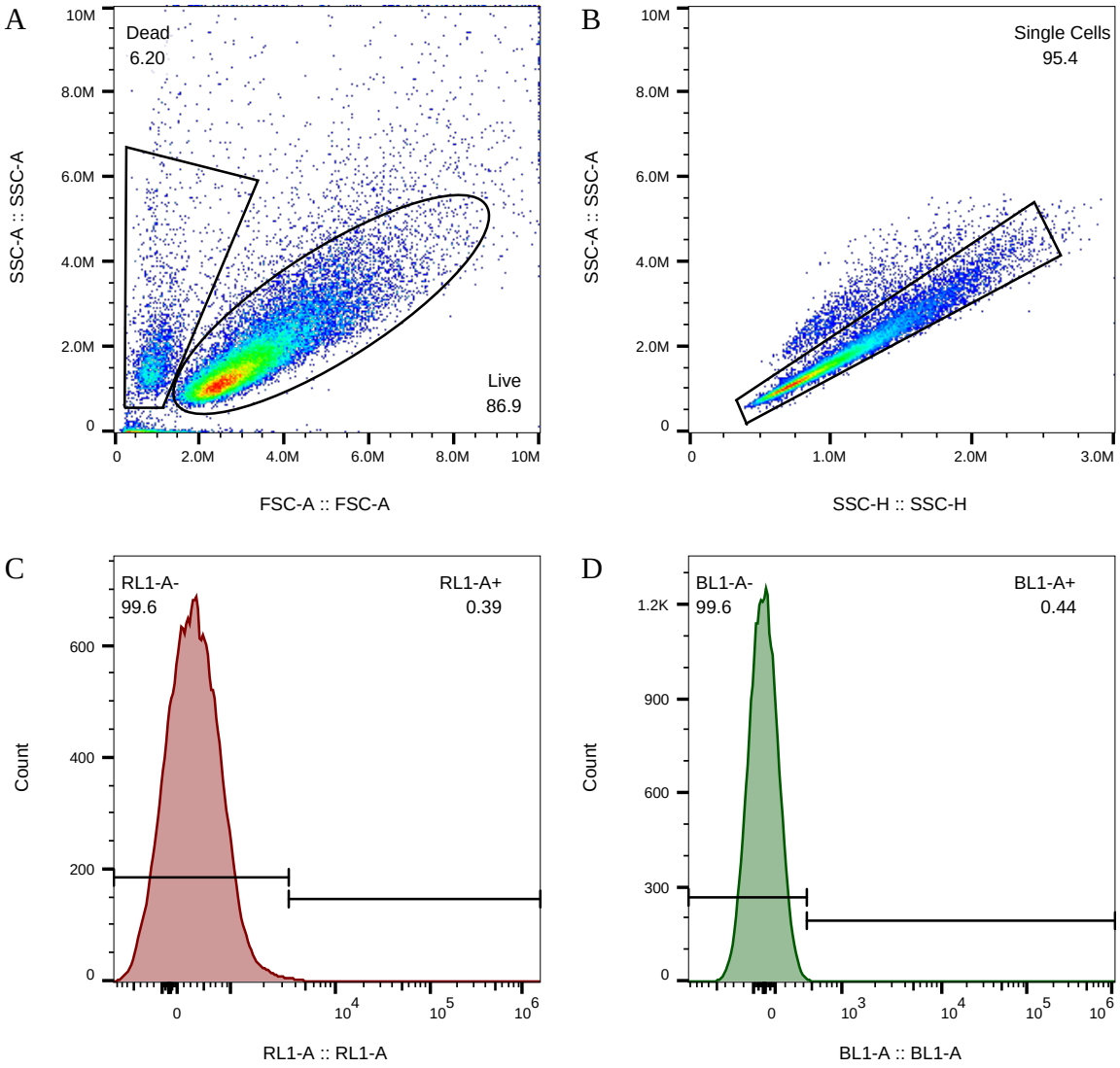

Figure 3.2: Flow cytometry gating strategy.
Figure shows the gating method employed to isolate and analyse cells transfected with Cyan5 tagged ftRNA or co-transfected with ftRNA and eGFP. The depicted example demonstrates the identification of single cell transfectants in a mock-transfected cell population. The single cell population was selected stepwise by first gating for viable and dead cell populations (**a**), next the viable cell population was gated for single cells (**b**). Finally the the threshold for cyan5 ftRNA (**c**) and eGFP (**d**) positive transfection was set so that in excess of 99.5 % of cells were negative in all mock-transfected control samples.

The first step in establishing a detection methodology was to set up the optimal voltages and gating strategies to accurately identify the viable population of single cells. The voltage selections for Front Scatter (FSC) and Side Scatter (SSC) are described in section 2.7. Figure 3.2

shows the gating strategy used to quantify transfection efficiency and potency of cyan-5 ftRNA and eGFP. Initially the viable and apoptotic cell populations were isolated (Figure 3.2a), allowing an estimation of cell viability as per eq. (3.1). Subsequently single cells were isolated, excluding doublets and larger aggregates (Figure 3.2b). Finally, the voltages on the 633 nm and 488 nm lasers were adjusted to account for autofluorescence of the parental cell line. In order to ensure the fluorescence of transfected cyan-5 ftRNA and expressed eGFP was within the detectable range, the voltages were adjusted to ensure the Median Fluorescence Intensity (MFI) on the RL1-A and BL1-A fell between 100 RFU and 1000 RFU (figures 3.2c and 3.2d). Gating was set to ensure for all replicates at least 99.5 % of measured mock transfected cells fell into the negative gate.

For measuring both ftRNA and eGFP transfections, both the MFI and the transfection efficiency (calculated per eq. (3.2)) were the primary measure of transfection method performance.

$$Estimated\,Cell\,Viability\,(\%) = \frac{Viable\,Cells}{Viable\,Cells + Apoptotic\,Cells} \cdot 100 \tag{3.1}$$

$$Transfection\,Efficiency\,(\%) = \frac{Total\,Positive\,Transfectants}{Total\,Parent\,Population} \cdot 100 \tag{3.2}$$

3.2.3 Assessment of RNA Transfection Methods

3.2.3.1 Optimising transfection reagent volumes

In order to assess the candidate transfection reagents, CHO_{T2} cells were transfected with a range of reagent and ftRNA concentrations. Cells were transfected as described in section 2.6.1 with a final seeding density of 0.5×10^6 cells.ml^{-1}. The concentrations tested for each reagent can be found in Table 3.2, with ftRNA concentration fixed at 30 nM.

Table 3.2: Reagent concentrations for assessing the performance of candidate transfection methods.
The table displays the volume added, and proportion of final culture volume of each transfection reagent during method screening. All conditions used a cyan-5 ftRNA concentration of 30 nM.

DharmaFECT™2		DharmaFECT™4		MISSION®siRNA		Nanocin RNA	
µl	*% by vol.*	µl	*% by vol.*	µl	*% by vol.*	µl	*% by vol.*
0.10	*0.05*	0.10	*0.05*	0.50	*0.25*	0.20	*0.10*
0.20	*0.10*	0.20	*0.10*	1.00	*0.50*	0.40	*0.20*
0.40	*0.20*	0.40	*0.20*	2.00	*0.10*	0.80	*0.40*
0.80	*0.40*	0.80	*0.40*	3.00	*1.50*	1.60	*0.80*

Figure 3.3e summarises the experimental controls employed. The RNA only control ensures that the Relative Fluorescence Units (RFU) value measured was respective of intracellular transfected cyan-5 ftRNA, without being skewed by non-transfected ftRNA on the outer cell membrane. Of the reagents tested, only Nanocin RNA auto-fluoresces, resulting in a 11.2 % false positive transfection rate. Although the MFI of the Nanocin RNA only control was 2.6 fold higher

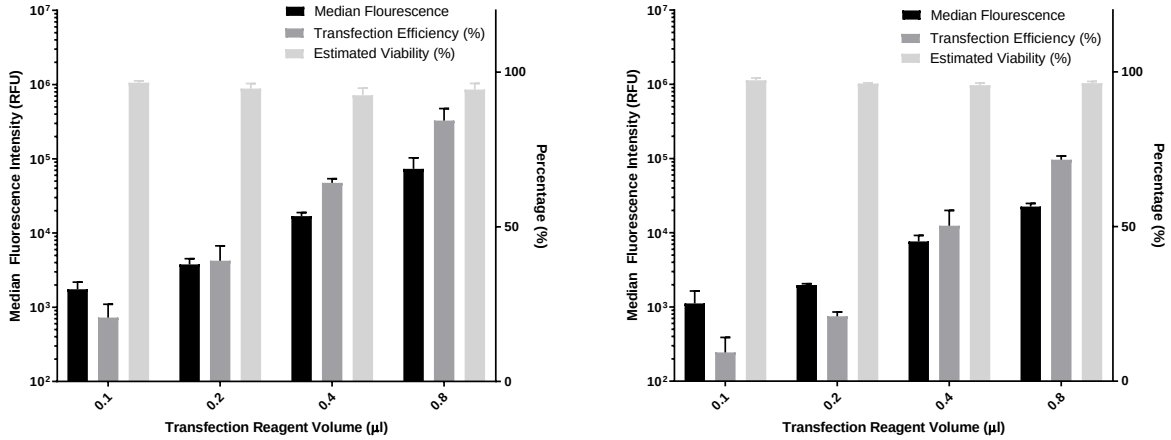

(a) DharmaFECT™2

(b) DharmaFECT™4

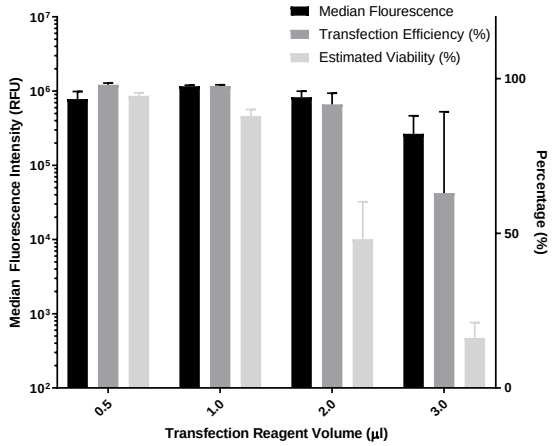

(c) MISSION siRNA

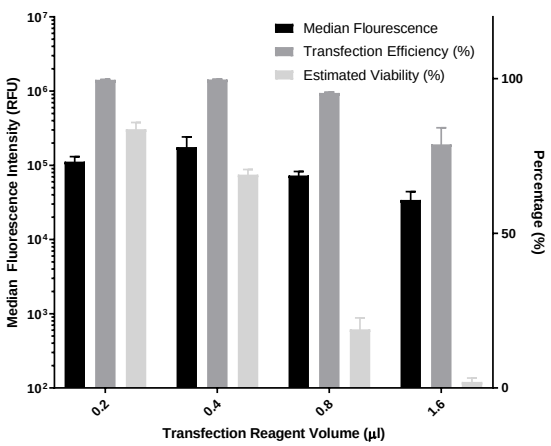

(d) Nanocin-RNA

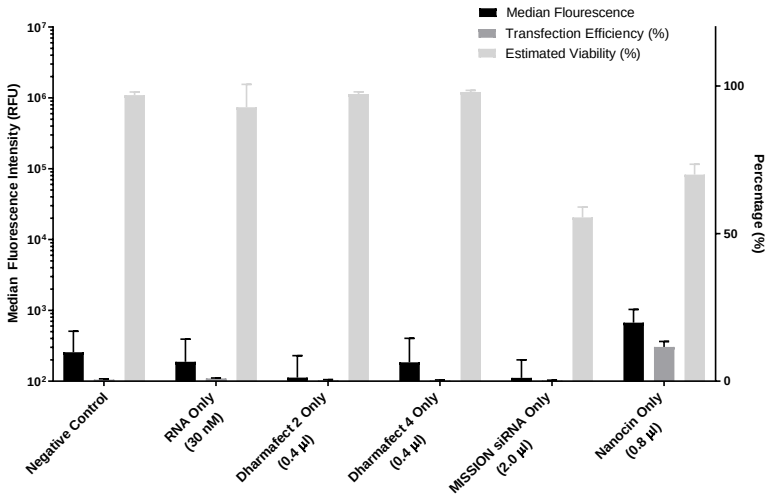

(e) Control Conditions

Figure 3.3: Titration of DharmaFECT™2, DharmaFECT™4, MISSION®siRNA and Nanocin RNA transfection reagent volumes.
Transfections were performed at a total volume of 200 µl in static 96-well plates with a final seeding density of 0.5×10^6 cells.ml^{-1}. The concentration of cyan-5 ftRNA was 30 nM for all conditions excluding the negative and reagent only controls. Cultures were incubated for 24 hours prior to assessment by flow cytometry. Results depicted are the mean and Standard Deviation (StD) from $n = 3$ replicates.

than the negative control cells, this is 100 fold lower than the MFI of ftRNA transfections (Figure 3.3d).

The results from DharmaFECT™ 2 and DharmaFECT™ 4 titration's are displayed in Figures 3.3a and 3.3b respectively. Both reagents maintained a high cell viability across the tested concentration ranges, and the MFI and transfection efficiency was positively correlated with transfection reagent concentration. The highest MFI and transfection efficiency was observed with 0.8 µl of reagent for both DharmaFECT™ reagents, despite this being 4 fold greater than the manufacturer's recommendations. Overall DharmaFECT™ 2 performed better with a maximum MFI of 7.21×10^4 RFU, 3.3 fold greater than DharmaFECT™ 4. The maximal DharmaFECT™ 2 transfection efficiency was 84.4 %, 13.2 % greater then DharmaFECT™ 4. Overall results suggest higher reagent volumes may improve both MFI and transfection efficiency, despite already greatly exceeding the manufacturer's recommendations.

When assessing the performance of MISSION®siRNA (Figure 3.3c), viability drops significantly as transfection reagent volume increases to a minimum of 16.2 %. MFI and transfection efficiency are high for the first 3 conditions, with the manufacturer's recommendation of 1.0 µl yielding an MFI of 1.16×10^6 RFU. When compared to the best condition using DharmaFECT™2 the MFI is 16 fold greater, and the transfection efficiency is 97.51 %; a 13.1 % improvement.

When tested at 0.2 µl and 0.4 µl volumes, Nanocin RNA (Figure 3.3d) had transfection efficiencies of 99.64 % and 99.75 % respectively. This came at the cost of greater cell stress, as seen through the reduced cell viabilities of 83.7 % and 69.0 %. The highest MFI observed was 1.76×10^5 RFU; 6.6 fold lower than MISSION®siRNA.

MISSION®siRNA and Nanocin RNA demonstrate significant cytotoxicity at higher concentrations, which has been shown to be a common problem with lipofection (Elshereef et al. 2019; J. Li and Z. Liu 2015; Rahimi et al. 2018). Additionally, the control conditions demonstrate this is primarily due to the reagent toxicity, although the literature suggests that nucleic acid complexing with cationic liposomes exacerbates reagent mediated cytotoxicity (Nguyen et al. 2007).

3.2.3.2 Optimising ftRNA concentration

The relationships between of cyan-5 ftRNA concentration with MFI, transfection efficiency and viability were evaluated to assess siRNA concentrations for optimal transfection dynamics. Figures 3.4a to 3.4c show the respective MFI, transfection efficiency and estimated viability of cyan-5 ftRNA transfections ranging from 0 nM to 60 nM. With the exception of Nanocin RNA, increasing ftRNA concentration had negligible impact on MFI. This suggests the maximum amount of RNA uptake had been achieved, and to effectively control target gene knock-down lower doses of ftRNA are required. Similarly, a minor increase in transfection efficiency was observed when increasing ftRNA dose from 10 nM to 60 nM. Both DharmaFECT™ 2 and DharmaFECT™4 had maximum transfection efficiencies of 66.4 % and 50.5 % respectively. The low gradient observed suggests that increasing ftRNA concentration will not further improve the positive transfection rate.

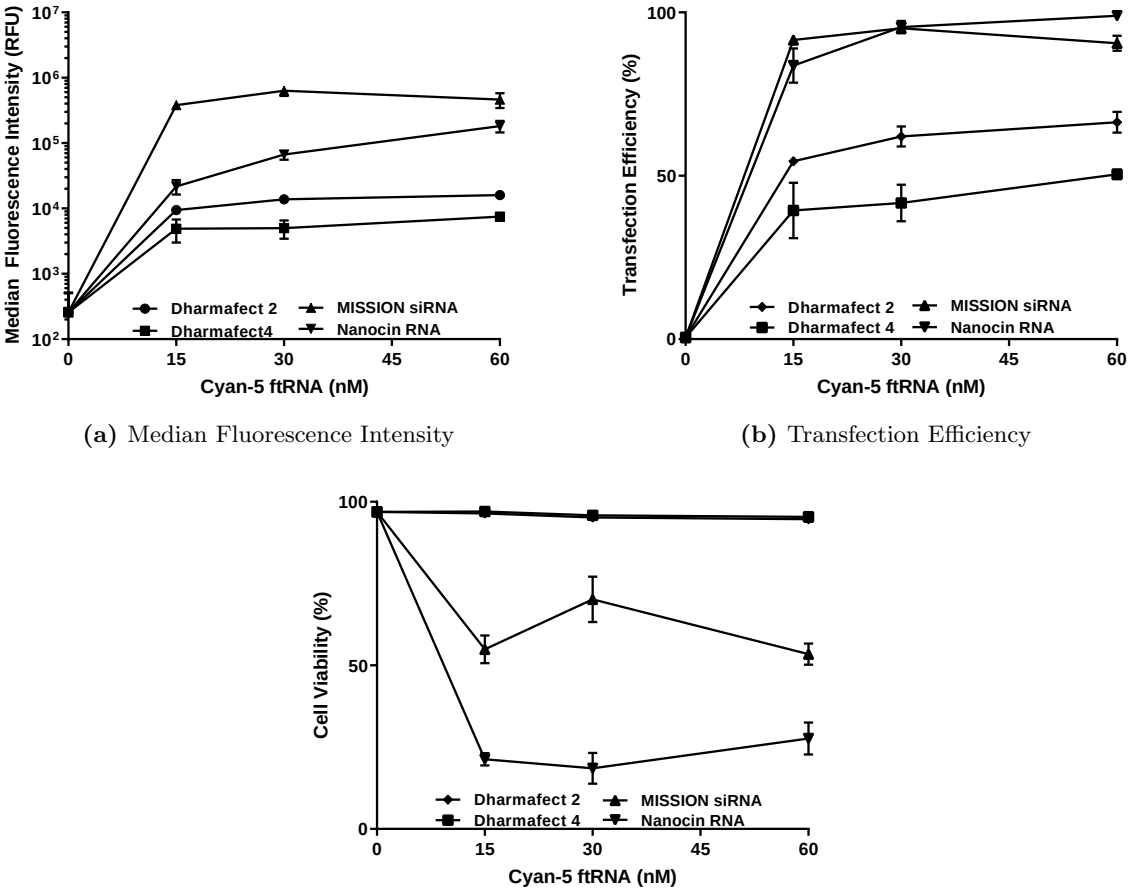

(a) Median Fluorescence Intensity

(b) Transfection Efficiency

(c) Estimated Viability

Figure 3.4: Titration of ftRNA concentration with fixed DharmaFECT™2, DharmaFECT™4, MISSION®siRNA and Nanocin RNA reagent concentrations.
All transfections were performed at a total volume of 200 µl in static 96-well plates, with a seeding density of 0.5×10^6 cells.ml^{-1}. Transfection reagent concentration was fixed at 0.4 µl, 0.4 µl, 2.0 µl, 0.8 µl for DharmaFECT™2, DharmaFECT™4, MISSION®siRNA and Nanocin RNA respectively, corresponding with row 3 of Table 3.2. Cultures grown for 24 hours prior to assessment by flow cytometry. Results depicted are the means and StDs from $n = 3$ replicates.

The transfection efficiency of MISSION®siRNA and Nanocin RNA was over 80 % across all concentrations demonstrating consistent ftRNA delivery throughout the cell populations. Lastly, ftRNA concentration had minimal impact on cell viability, which although low for MISSION®siRNA and Nanocin RNA, is a result of reagent mediated cytotoxicity as discussed in Figure 3.3.

Overall, MISSION®siRNA outperformed the other reagents in both MFI and transfection efficiency metrics. Nanocin RNA produced the highest transfection efficiency, however the result was unreliable due to an increased rate of false positive events in the reagent only control. DharmaFECT™ 2 ranked 2nd and has the potential to perform better with increased reagent concentrations. In Table 3.1, MISSION®siRNA was highlighted as being the most cost effective method and performed optimally at the manufacturer's recommended concentration. Having already been tested at 4 fold the manufacturer's recommendation, increases in DharmaFECT™2 volume would further increase the cost efficiency gap.

Upon review of the overall performance of the reagents tested, MISSION®siRNA was taken

forward as the primary candidate for method optimisation and integration into the proposed screening platform.

3.2.3.3 Assessing the effect of MISSION®siRNA transfection on culture performance

In order to perform knock-downs in a format comparable to industry mAb production conditions, cultures must undergo exponential cell division before plateauing into a stationary phase. CHO_{T2} cells were transfected with custom designed endoribonuclease prepared small interfering siRNAs (esiRNAs) targeting *SEC22B*,*BIP*, *GRP94*, and *PDIA5* and a final MISSION®siRNA concentration of 0.50 %(v/v). Cells were seeded into Deep Well Plates (DWPs) and after 5 days growth and viability were assessed. The results are displayed in Figure 3.5.

In comparison to the negative control, all transfections exhibited a 4.5 fold to 12.5 fold reduction in Viable Cell Density (VCD) 5 days post transfection. There was no change observed in culture growth in the RNA only control, indicating no negative effects occur from the presence of RNA in the culture medium. When comparing the negative control to the MISSION®siRNA only control, a 3.6 fold reduction in VCD was observed. This indicated that the presence of the MISSION®siRNA reagent was strongly inhibiting cell proliferation, and in some conditions complete growth arrest was seen. The presence of the transfection reagent alone had a lower impact than the esiRNA transfections, confirming RNA-reagent complexing exhibits a greater effect than the reagent alone. Further reduction in growth at higher esiRNA concentrations evidenced a dependency on RNA concentration.

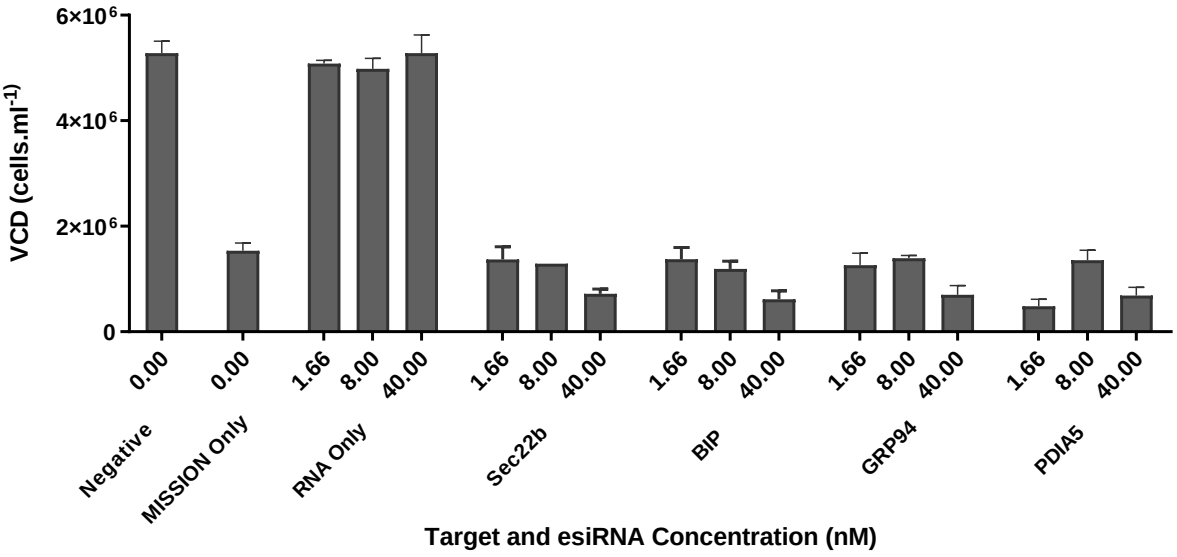

Figure 3.5: Effect of MISSION®siRNA on cell growth.
A panel of esiRNAs were transfected into cells at multiple concentrations and seeded in 96-DWPs at 0.5×10^6 cells.ml^{-1}, and after 5 days cell growth and viability was assessed. Results depicted are the means and StDs from $n = 3$ replicates. Measured cell viability was above >97.0 % in all conditions.

Measured cell viability was >97.0 % in all conditions indicating that although MISSION®siRNA prevents cell growth, it is not cytotoxic at the concentrations tested.

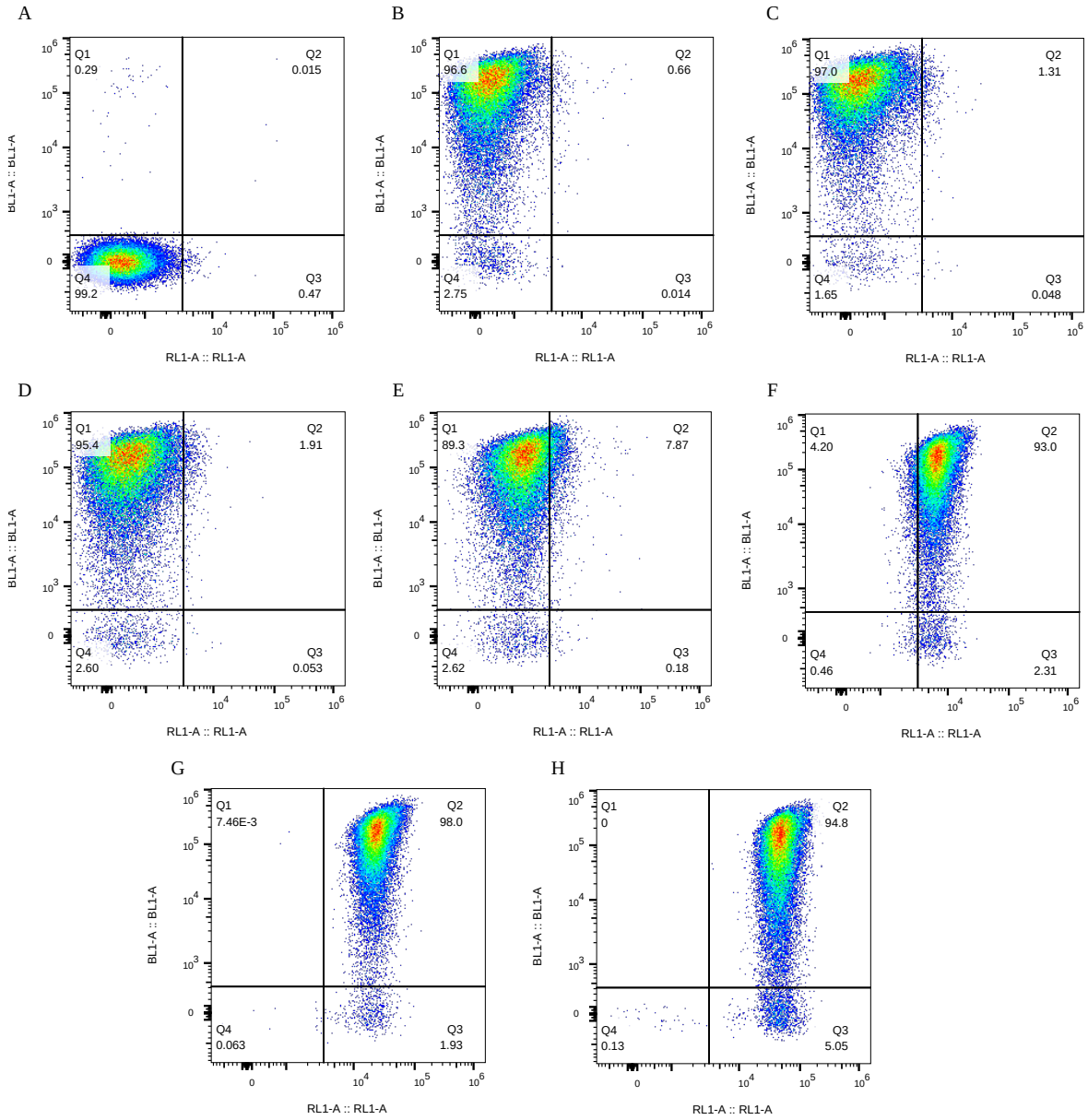

Figure 3.6: Example of the 2-dimensional gating strategy used for cyan-5 ftRNA and eGFP co-transfection with HTP electroporation platform.
Cultures were transfected with 0 nM (**a, b**), 6.50 nM (**c**), 21.6 nM (**d**), 72.0 nM (**e**), 240 nM (**f**), 800 nM (**g**), 2600 nM (**h**) of cyan-5 ftRNA alongside 500 ng empty (**a**) or *eGFP* (**b-h**) vectors. Post transfection 800 nM ftRNA was added to the RNA wash control **(b)**. Transfected cells were incubated under static conditions and analysed by flow cytometry after 24 hours. Gating limits are the same as described in Figure 3.2.

3.2.4 Evaluating High-Throughput Electroporation as an RNA Delivery Method

Due to the hurdles encountered in lipofection based transfection methods, the Lonza HTP electroporation platform was evaluated for comparison. The electroporation platform for plasmid DNA delivery was already established and validated. As a linear relationship between plasmid DNA load and eGFP fluorescence had been demonstrated, optimisation proceeded with RNA and DNA co-transfection (Cartwright et al. 2020). The manufacturer's recommended RNA concentration range for optimisation was 2 nM to 2000 nM, dependent on cell type and concentration.

Electroporation had a much greater optimisation range than previously tested methods due to a greater range of transfection densities. In the previously optimised CHO plasmid DNA electroporation platform cells were transfected at a density of 100×10^6 cells.ml^{-1} in 20 µl followed by serial dilution to the desired seeding density. Resultantly the total mass of esiRNA per cell was comparable to lipofection techniques.

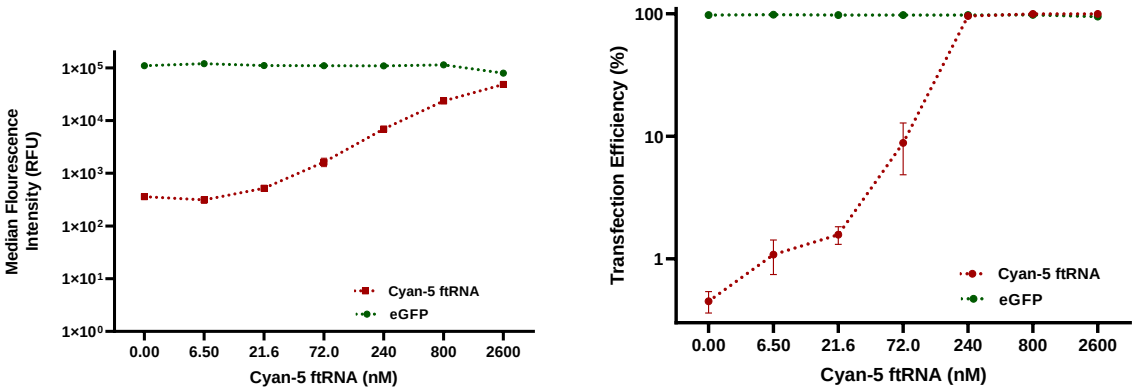

(a) Median Fluorescence Intensity

(b) Transfection Efficiency

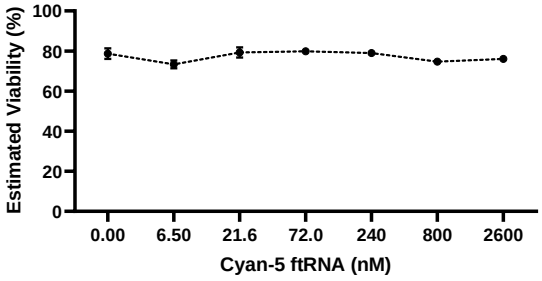

(c) Viability

Figure 3.7: Assessing HTP electroporation as a co-transfection platform.
Cyan-5 ftRNA was titrated from 0 nM to 2600 nM while being co-transfected with 500 ng eGFP vector. Transfected cells were incubated under static conditions and analysed by flow cytometry after 24 hours. Results depicted are the means and StDs from $n = 6$ replicates.

Figure 3.6 shows example heat-scatter plots of cyan-5 and eGFP fluorescence for each condition and Figure 3.7 displays the mean MFI, transfection efficiency and estimated cell viability. Minimal shift in the number of ftRNA positive transfectants was observed between the negative control (Figure 3.6a) and wash control (Figure 3.6b) panels. An average positive transfection rate of 0.66 % was observed for the wash control, an increase of 0.21 % over the mock-transfected control, confirming the RNA effectiveness of the wash procedure.

Through panels (c) to (h) of Figure 3.6, the 2-dimensional shape of the population was maintained and the RL1-A fluorescence signal increased with ftRNA concentration. In the RL1-A channel there was minimal population lag observed as the ftRNA concentration increases, demonstrating consistent RNA delivery across the population resulting in ubiquitous knockdown. Some population lag was observed in the BL1-A channel indicating greater variation within the population. Transfection efficiency remained constant at (97.60 ± 0.75) % in all eGFP positive conditions (Figure 3.7b).

Figure 3.7a showed a linear increase in MFI when cyan-5 ftRNA concentration was increased from 21.6 nM to 800 nM, defining our working dynamic range. The observed eGFP MFI is unaffected by ftRNA concentration up to 800 nM and a minor reduction was observed at 2600 nM ftRNA.

The transfection efficiency (Figure 3.7b) has been plotted on a log axis to visualise the minor increases in positive transfectants at 21.6 nM and 72.0 nM concentrations. A maximum transfection efficiency of 99.88 % was seen at 2600 nM ftRNA, and all conditions between 240 nM and 800 nM both had greater than 95.0 % transfection efficiency.

Increasing the concentration of cyan-5 ftRNA had no impact on estimated cell viability (Figure 3.7c), with all observed viabilities ranging from 72.0 % to 80.0 %.

3.2.4.1 Assessing extended culture performance of electroporated cells

To assess culture performance post-RNA transfection, CHO_{T2} cells were transfected with 21.6 nM to 800 nM of siRNA or esiRNA targeting SEC22B, BIP, GRP94 or a non-targeting control and cultured in shaking conditions for 5 days. Co-transfection of empty vector standardised DNA load to 300 ng.well^{-1}.

Unlike the lipofection techniques previously tested, transfection of esiRNAs via electroporation allowed reasonable cell growth over a 5 day period (Figure 3.8). When comparing the non- and mock-transfected controls, the electroporation process reduced the final VCD by 50.6 %.

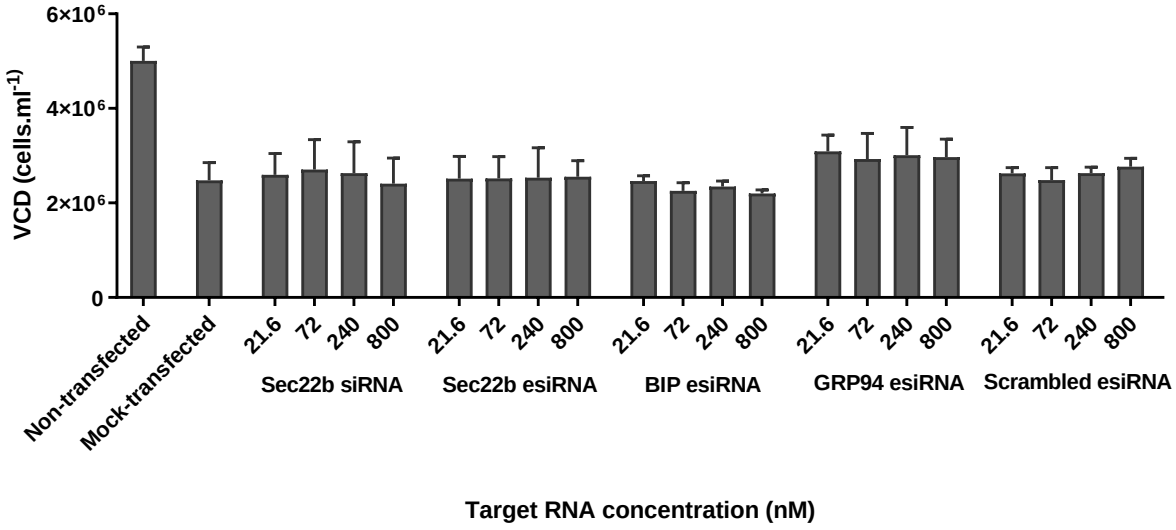

Figure 3.8: Culture growth post-electroporation.
A panel of esiRNAs were transfected into CHO_{T2} cells at multiple concentrations. Cultures were seeded at 0.5×10^6 cells/ml in 96-DWPs and incubated for 5 days. Results depicted are the means and StDs from $n = 3$ replicates. Measured cell viability was above >95.0 % in all conditions.

No change in cell growth was observed when increasing the esiRNA concentration with any of the target genes. As a non-producing cell line, CHO_{T2} is predicted to be less sensitive to changes in Endoplasmic Reticulum (ER) chaperone and secretary pathway protein levels. To ensure the knock-downs were been successful, quantification of intra-cellular levels of target proteins was

required. Importantly no change in VCD was observed between the mock-transfected control and the scrambled esiRNA transfections, suggesting no positive or negative effects were exerted on the cell population by the delivery of non-targeting esiRNA.

$$FC_{VCD} = \frac{VCD_p}{VCD_0} \tag{3.3}$$

Cell growth can be expressed as a fold change in VCD measurements between two time-points (FC_{VCD}) and can be calculated as per eq. (3.3) where, VCD_0 and VCD_p are initial and peak VCD measurements respectively. The average FC_{VCD} of the mock-transfected control was calculated to be 4.6 fold. This was significantly lower than the 10.2 fold increase of non-transfected cells, and is a significant improvement over the 3.2 fold increase observed from the previous MISSION®siRNA mock transfection. However, the results demonstrate the growth limitations found with most DNA and RNA delivery methods.

3.2.5 Quantification of RNAi Knock-Down Dynamics

It was important to demonstrate that successful delivery of RNA into cells translated to a reduction in intracellular concentration of the target protein. An siRNA targetting SEC22B was used as a positive control due to its previous validation in CHO cells (Dickens et al. 2016). In addition, this allowed a comparison of the reliability, potency and consistency of esiRNAs in relation to siRNAs.

Western blots were selected to provide accurate relative quantification of the target intracellular HCP abundance. Each western blot was multiplexed with the protein of interest and β-actin, a constitutively expressed housekeeping control, being measured simultaneously in different fluorescent channels. For each sample the fluorescence intensity of the Protein of Interest (POI) was normalised against the β-actin control to calculate the relative HCP abundance in relation to the mock-transfected control. Example western blots for SEC22B siRNA, SEC22B esiRNA can be seen in Appendix A Figures A.1a and A.1b respectively.

Figures 3.9a and 3.9b show the relative change in intracellular SEC22B protein in response to knock-down by the positive control siRNA and designed esiRNA. The esiRNA produced a stronger knock-down across all concentrations and time points. At the lowest concentration tested (21.6 nM) the *SEC22B* esiRNA had an average HCP abundance of 31.4 % across the 3 time points. Comparatively, the siRNA had an average abundance of 72.2 %, suggesting increased potency from the esiRNA. When reviewing the effect of increasing the *SEC22B* esiRNA concentration, only marginal improvements are seen. Conversely, the 72 nM siRNA knock-down of *SEC22B* reduced the HCP abundance to 38.6 % 2 days post transfection.

Evaluation of the variation between replicates for each condition revealed an average Standard Error of the Mean (SEM) of 7.41 % for the *SEC22B* esiRNA, whereas the *SEC22B* siRNA average SEM was 2-fold greater at 15.50 %. Overall the *SEC22B* esiRNA produced a stronger and more consistent knock-down, with the strongest knock-down of 88.7 % being recorded 2 days post-transfection with 800 nM esiRNA. Similar observations of variation for *BIP* and *GRP94* esiRNA

knock-downs in Figures 3.9c and 3.9d, where 12.97 % and 10.91 % variation in protein abundance was measured respectively, further demonstrating the superior consistency of esiRNAs.

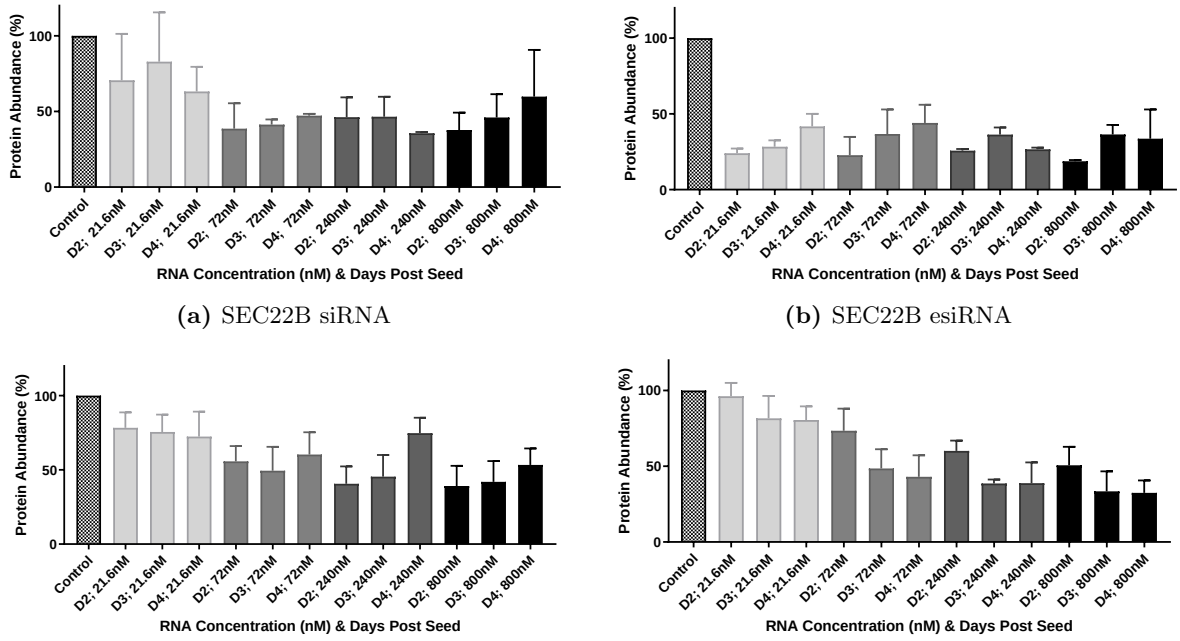

(a) SEC22B siRNA

(b) SEC22B esiRNA

(c) BIP esiRNA

(d) GRP94 esiRNA

Figure 3.9: Quantification of RNAi knock-down efficiency by western blot.
Figure shows the calculated intracellular target protein abundance below for SEC22B siRNA (**a**), and SEC22B (**b**), BIP (**c**) and GRP94 (**d**) esiRNAs. CHO_{T2} cells were electroporated with 0 nM to 800 nM of RNA and seeded at 0.5×10^6 cells.ml^{-1} in 96-DWPs. Samples were taken 2, 3, and 4 days post-transfection and triplicates pooled for western blot analysis. Protein abundance was normalised against the β-actin house keeping control. Figure A.1 shows example western blots for SEC22B siRNA (**a**) and SEC22B esiRNA (**b**). Graphs display the mean and SEM of $n = 3$ biological replicates normalised to the mock-transfected control.

Unlike SEC22B, both BIP (Figure 3.9c) and GRP94 (Figure 3.9d) knock-downs demonstrated a strong correlation between esiRNA concentration and HCP abundance. BIP was the least effective esiRNA tested, with a maximum of 60.9 % reduction in HCP observed 2 days post-transfection with 800 nM esiRNA. BIP was the only target where every increase in esiRNA concentration notably increased the knock-down amplitude. When knocking down GRP94, the intracellular protein concentration on day 2 reduces with every increase in esiRNA concentration. Lastly when observing the change in concentration over time the levels of HCP began to rise by day 4 post-transfection for most SEC22B and BIP knock-down conditions. When knocking down GRP94 the strongest knock-down is observed 4 days post transfection.

3.2.6 Improving High Throughput Culture Performance

During the course of optimising transfection conditions, it was noticed that cells were not growing as effectively as expected over 5 days in the 96-DWP culture platform, highlighted by low cell densities and high cell doubling times for non-transfected cells. This is especially evident when observing non-transfected CHO_{ETE} and CHO_{T2} cells growing optimally as in Figure 3.10 reaching a PCD of 1.2×10^7 cells.ml^{-1} and 9.3×10^6 cells.ml^{-1} respectively on day 6 of culture.

It was hypothesised that inefficient cell mixing during shaking incubation at 320 rpm resulted in cells settling in the plate, limiting the growth rate. In order to best align performance with bioreactor conditions good cell growth is essential.

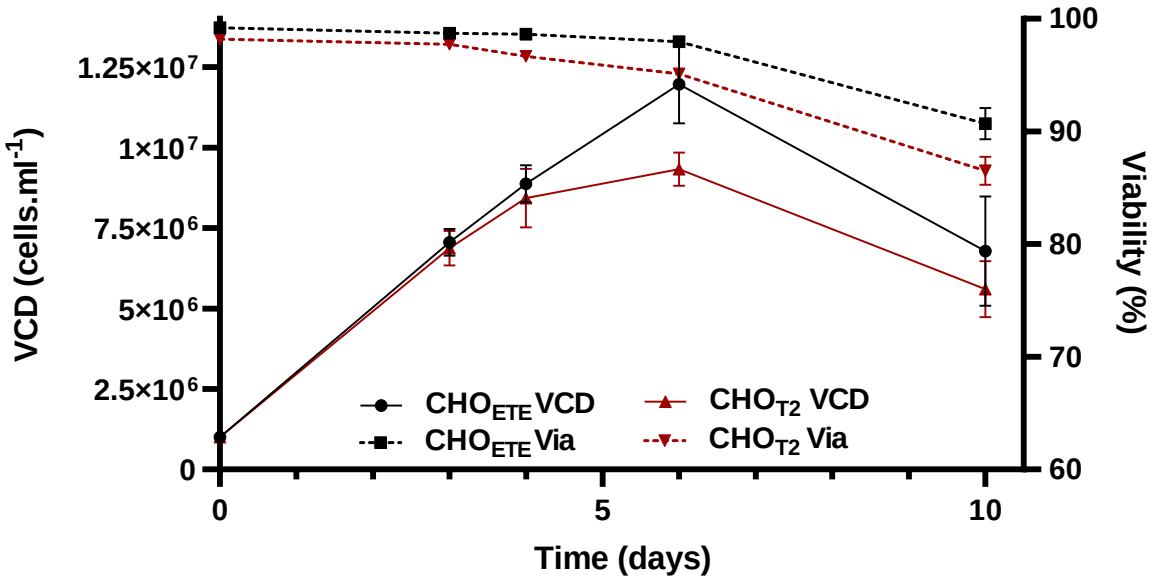

Figure 3.10: CHO_{ETE} and CHO_{T2} culture growth in Erlenmeyer flasks.
CHO_{ETE} (black) and CHO_{T2} (red) cells were seeded at 1.0×10^6 cells.ml^{-1} in 125 ml Erlenmeyer fed-batch cultures and VCD (solid line) and viability (dashed line) was measured on days 3, 4, 6 and 10 of culture. Error bars represent the standard deviation of $n = 8$ and $n = 5$ replicates for CHO_{ETE} and CHO_{T2} respectively.

Volume sensitivity was another known limitation of the 96-DWP culture format. During previous set-up and parameter optimisation by colleges a working range of 465 µl to 485 µl was established between which cell growth, viability and productivity are consistent. This poses an additional challenge as mid-culture sampling was required to quantify the target HCP abundance.

Due to these limitations, a 24-Shallow Well Plate (SWP) culture platform was tested and optimised aiming to provide improved growth characteristics and a reduced volume sensitivity. For simplicity the same Duetz system of Sandwich Cover plate lids and clamps made by EnzyScreen were used. Enzyscreen offered 3 different lid types compatible with Nunc 24-SWPs, each with varying properties as described in Table 3.3. The CR1524 model was immediately eliminated as an evaporation rate of 30 µl/day would result in a significant loss of culture volume.

Table 3.3: Specifications of plate lids for Nunc 24-SWPs from EnzyScreen.
Stated evaporation rates are correct for 30 °C and 50 % humidity.

Lid Type	Hole Diameter (mm)	Gas Exchange Rate (ml.min^{-1})	Evaporation Rate (µl.day^{-1})
CR1324a	1.20	0.70	16.0
CR1524	1.00	1.10	30.0
CR1524a	0.20	0.25	6.0

CR1324a and CR1524a plate lids were assessed with electroporated CHO_{ETE} and CHO_{T2} cells and the results are displayed in Figure 3.11. CHO_{ETE} and CHO_{T2} were transiently transfected with empty vector or mAb_{ETE} and cuvettes were pooled before seeding between the different plate formats. Plate performance was assessed in batch and fed-batch culture modes with cells seeded in 24-SWPs at 0.5×10^6 cells.ml^{-1} and cultured for 13 days.

Overall the CR1324a plate lid (Figure 3.11a) had a more consistent and reproducible growth profile than the CR1524a (Figure 3.11b), and demonstrated increased consistency between replicates. Both lids permitted good cell growth with PCDs being recorded on day 7 in batch and fed-batch modes. Cell viability was also more consistent with the CR1324a plate lid (Figure 3.11c) when compared to the CR1524a model (Figure 3.11d), with reduced variability across all cultures.

Upon closer inspection, the CR1524a sandwich cover did not sit on the plate as tightly as the CR1324a model, posing a contamination risk. Additionally, it was hypothesised that the smaller diameter holes provided insufficient gas exchange, explaining the inconsistent growth observed. Resultantly only the CR1324a sandwich cover was taken forward for further assessment.

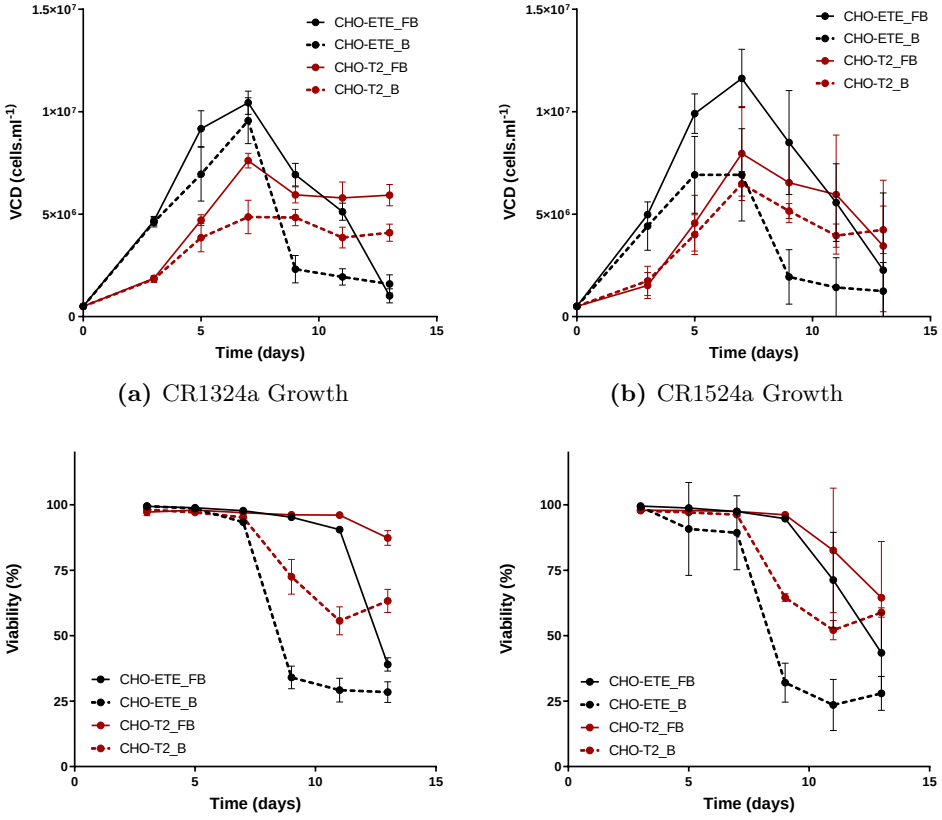

(a) CR1324a Growth

(b) CR1524a Growth

(c) CR1324a Cell Viability

(d) CR1524a Cell Viability

Figure 3.11: Batch and fed-batch culture performance in 24-SWP with CR1324a and CR1524a plate lids.
Both lid formats were assessed with a stable cell line (CHO_{ETE}) and CHO_{T2} cells electroporated with 500 ng.well^{-1} of empty vector or mAb_{ETE} plasmid respectively. Here the growth (**a,b**) and cell viability (**c,d**) results are shown for the CR1324a and CR1524a lids respectively. A stably expressing (black) and transiently transfected (red) cell lines were grown in both batch (dashed line) and fed-batch (solid line) modes. Results are the means and StDs of $n = 6$ replicates.

3.2.6.1 Identifying 24-SWP working range and evaporation

After several rounds of optimisation a working volume range of the 24-SWP culture format was established. When seeded at volumes ranging from 650 µl to 750 µl there was no impact on cell growth (Figure 3.12a) or viability (Figure 3.12b) observed. This provided the working range required to allow culture feeding and sampling with no negative effect on culture performance.

In order to run longer fed-batch experiments it was important to assess the evaporation rate of the CR1324a plate lid. CHO_{ETE} cells and CD-CHO was seeded into 24-SWPs and after 7 days incubation without intervention and the volume in each well was measured by reverse pipetting. The mean evaporation rate of the CR1324a plate was 1.26 µl.day^{-1} and 1.04 µl.day^{-1} when incubated with CHO_{ETE} and CD-CHO media respectively (Figure 3.12c), resulting in negligible changes to culture volume over the duration of batch or fed-batch studies. The difference in evaporation rate between the CHO_{T2} culture and CD-CHO media was not statistically significant (Welches t-test: $P = 0.06$), and was attributed to the build up of cell sediment around the walls of plate wells.

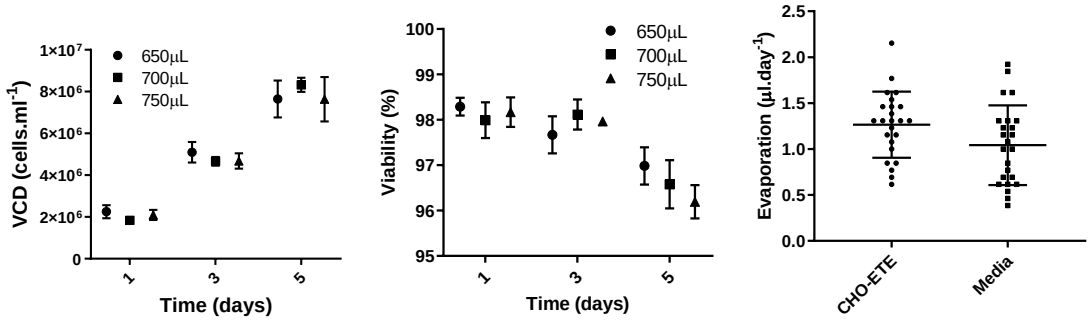

(a) VCD **(b)** Cell Viability **(c)** Evaporation Rate

Figure 3.12: Assessing the working parameters of 24-SWPs.
CHO_{ETE} cells were seeded at 650 µl, 700 µl or 750 µl in 24-SWPs and incubated for 5 days. On days 1, 3 and 5 VCD (**a**) and viability (**b**) was measured on a Norma-HT with points and error bars representing the mean and StD of $n = 8$ replicates. Panel (**c**) depicts an independent assessment of the evaporation rate from 24-SWPs. CHO_{ETE} cells or CD-CHO was incubated for 7 days with no intervention. Error bars represent the mean and StD of $n = 24$ replicates.

3.2.6.2 Comparison of the 24-SWP and 96-DWP culture platforms

Following parameter optimisation, the growth rate of transfected cells in the 24-SWPs was directly compared to the existing 96-DWP culture format. CHO_{ETE} growth rate increased by 1.51 fold over in the 24-SWPs and the average culture viability was 4.0 % higher after 5 days (Figure 3.13a). Similarly the CHO_{T2} growth rate increased by 1.48 fold and culture viability increased by 3.9 % (Figure 3.13b). Near identical improvements in both cell lines support the hypothesis that 96-DWPs provide sub-optimal conditions and limit cell growth.

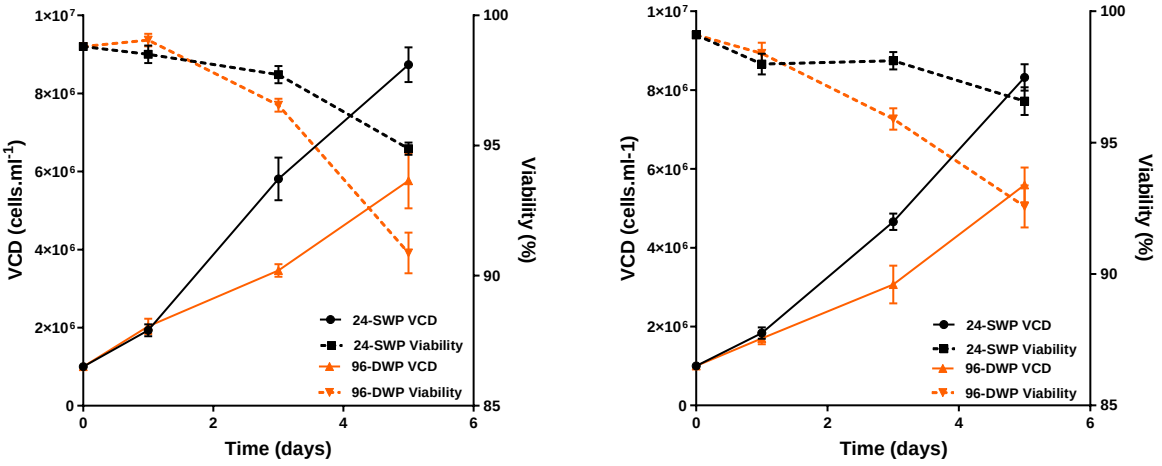

(a) CHO_{ETE} **(b)** CHO_{T2}

Figure 3.13: Comparison of culture performance in 24-SWP and 96-DWP formats.
Figure depicts culture performance of CHO_{ETE} (**a**) and CHO_{T2} (**b**) transfected with empty vector and mAb_{ete} vector respectively. Transfected populations were pooled and cultured in 24-SWPs (orange) and 96-DWPs (black) for 5 days. On days 1, 3 and 5 VCD and viability was measured on a Norma-HT, represented by the solid and dashed lines respectively. Points and bars are the means and StDs of $n = 12$ replicates.

The calculated 5 day FC_{VCD} of CHO_{ETE} and CHO_{T2} cells in 96-DWPs was 5.9 fold and 5.1 fold respectively, consistent with previous experiments in section 3.2.4.1. Cell growth rate was significantly improved in the 24-SWPs with respective 5 day FC_{VCD} of 8.6 fold and 8.3 fold for CHO_{ETE} and CHO_{T2} cells.

The data demonstrated that 24-SWPs are a significant improvement over the existing cell culture platform, offering improved growth characteristics for transfected cells and negligible rates of evaporation. However, implementation of the 24-SWP format reduced incubator throughput by 25 % as three 24-SWPs could be stacked in place of a single 96-DWP.

3.2.7 Assessing the Technical Reproducibility of the Opentrons OT-2 Liquid Handler

3.2.7.1 Identifying the high throughput transfection platform constraints

HTP nucleofection is a complex laboratory process with many repetitive mixing and low volume transfer steps required. Occasional user errors when handling a large number of culture plates had led to unexpected results requiring repeat experiments. Additionally, inaccuracies in culture seeding densities were often seen. It was hypothesised that rapid cell settling was the primary cause, resulting in a cell density gradient between wells emerging during the electroporation process. Extensive mixing of cells had helped alleviate this, however the subjectiveness of mixing regimes between wells, experiments and users was evident.

Outlined below are some key issues encountered when completing the HTP transfection protocol by hand, and why it was hypothesised a liquid handling robot could alleviate these:

- *Inefficient and inconsistent mixing of cell suspensions* - During the set-up of a nucleofection plate, cells are re-suspended at a density of 200×10^6 cells.ml^{-1} then diluted to 100×10^6 cells.ml^{-1} for electroporation. At both the resuspension and electroporation densities, cell settling was visible within 20 seconds. Manually mixing by pipetting is a subjective process, often with the number, speed and location of mixes within each well varying. A liquid handler will treat every well identically and can eliminate this inconsistency.
- *Interface between mixing and transfers* - Unfortunately low volume electronic pipettes were not available, and when using a manual pipette (single or multichannel) you are limited to a single volume. When transferring the transfection mix (cells + DNA/RNA + buffer) into the Lonza nucleofection plate, 20 µl is transferred 3 times from a 90 µl stock. The OT-2 could be programmed to mix a larger volume and subsequently transfer 20 µl without any delay in changing pipette settings. Additionally, the mixing volume can be reduced for each subsequent transfer to match the volume available.
- *Air bubbles in the nucleofection plate* - Air bubbles cause an arc discharge errors during the electroporation process. Removal requires bursting with a sterile hypodermic needle, significantly increasing the time cells are kept at a high cell density in suboptimal buffer conditions. These are difficult to avoid with a manual pipette, however a liquid handler can

aspirate excess cell suspension and only dispense the required volume without introducing any air into the system.

- *Pipetting reliability and consistency* - When performing many repetitive plate based pipetting actions by hand there is an increased probability of human error, which may go unnoticed impacting experimental results. Unnoticed errors will be eliminated with a liquid handler, as any mistakes would be easily traceable.

3.2.7.2 Benchmarking the Opentrons OT-2 against a human operator

Before assessing the performance of the OT-2 with the high-throughput transfection platform, it was important to ensure the robot could perform standard laboratory assays with the same or greater accuracy than a human operator. The Opentrons OT2's reproducibility was assessed when running the Valita®TITER and Valita®TITER Plus IgG quantification assays. The performance was then compared directly against an experienced human operator, defined as a scientist that has completed the assay at least 20 times.

This work was completed in collaboration with Valitacell and Opentrons, and has been published as an AppNote on the respective companies web pages (*Opentrons* 2020; *Valitacell* 2020). The article titled *'Automated, Rapid & Reproducible Measurement of Immunoglobulin G using Opentrons OT-2 liquid handling robot and Valita® TITER and Valita® TITER Plus'* has been reproduced in Appendix D with the permission of all contributors. The lab work in this article was completed solely be myself. Hannah Byrne, Head of Science at Valitacell provided input into the planning, data analysis and writing of the article. Laurie Vazquez, Content marketing Manager at Opentrons was brought in once a draft was available to ensure proper representation of the OT-2 and to obtain company approval.

3.2.7.3 Assessing the consistency of the Opentrons OT-2 liquid handler with the HTP electroporation platform

After confirming that the OT-2 could match or outperform a human operator with the straight forward laboratory assays, the protocols required to automate the electroporation platform were developed. Below is a simplified version of the HTP electroporation protocols identifying the steps completed by the OT-2 or the user:

1. **User:** Prepares DNA/RNA mix in master plates.
2. **OT-2:** Fills 24SWPs with media.
3. **OT-2:** Transfers electroporation buffer and DNA/RNA mix to set-up plate.
4. **User:** Re-suspends cells to 200×10^6 cells.ml^{-1} and add to robot trough.
5. **OT-2:** Mixes and transfers cells to each column of set-up plate to complete the transfection mix.
6. **OT-2:** Transfers transfection mix into electroporation plate in triplicates.

7. **User:** Removes electroporation plate, performs the electroporation then returns it to the OT-2.
8. **OT-2:** Adds 80 µl of media to each well of electroporation plate.
9. **OT-2:** Mixes each well thoroughly and seeds cells into 24-SWPs.

In order to evaluate the OT-2 a small scale electroporation experiment was performed manually and by the OT-2, with 24 replicates and biological duplicates for a total of n=48 transfections by each method. CHO_{ETE} cells were transfected with 300 ng.well^{-1} of empty vector, seeded into 24SWPs and evaluated immediately. Figure 3.14 shows the results with each biological repetition plotted independently.

When calculated, the theoretical seeding density would 1.60×10^6 cells.ml^{-1} under the assumptions of: perfect cell homogeneity throughout the protocol, optimal cell pelleting and re-suspension and 100 % cell viability post electroporation. Manual and automated electroporation had equal impact on cell viability with calculated means of 90.58 % and 91.31 % respectively. Assuming a 91.00 % viability the theoretical target seeding density was 1.46×10^6 cells.ml^{-1}. The difference between theoretical and observed seeding densities was a result of the following variabilities:

- Over-dilution resulting from imperfect media removal from pelleted cells.
- Variability from cell pelleting and re-suspension at very high densities of 200×10^6 cells.ml^{-1}.
- Cell settling resulting from inefficient mixing before cell transfer steps.

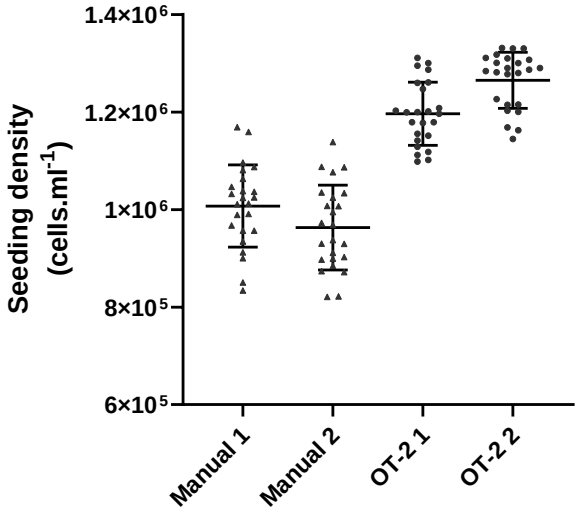

Figure 3.14: Evaluation of the consistancy of the HTP electroporation platform completed manually and by the Opentrons OT-2.
Identical independent nucleofection experiments were conducted manually and with OT-2. Cells were transfected with various esiRNAs and seeded in 24-SWPs. VCD measurements were taken immediately after seeding. Experiments 1 and 2 are independent experiments. The mean and StD of each population are displayed.

Cell pelleting, media removal and re-suspension would be a contributing factor to the difference between theoretical and observed seeding densities. However, as it was performed manually

in both methodologies it did not contribute to the difference between manual and automated electroporation platforms. This variation would also be a major contributing factor to the difference in mean seeding density between biological replicates. It was hypothesised that the dominant factor affecting the difference in seeding density between the manual and automated electroporation methods was the efficiency of mixing procedures.

A 25.4 % increase in average seeding density by the OT-2 was observed, highlighting the severity of cell loss due to inefficient mixing and cell settling during manual completion of the protocol. Table 3.4 shows a summary of the statistical analysis of Figure 3.14. When assessing the whole populations, robotic operation had a lower StD and Coefficient of Variation (CV) in both replicates. When compared to manual completion, the OT-2 average seeding density StD was 28.6 % lower. This translated to a 42.8 % reduction in CV demonstrating the improvements in consistency offered by the OT-2's.

Table 3.4: Statistical summary of Figure 3.14.
.

Experiment	Mean (cells.ml^{-1})	StD (cells.ml^{-1})	CV (%
Manual 1	1.01×10^6	8.27×10^4	8.21
Manual 2	0.96×10^6	8.50×10^4	8.83
OT-2 1	1.20×10^6	6.35×10^4	5.31
OT-2 2	1.27×10^6	5.62×10^4	4.44

The variation in average seeding densities seen between biological replicates for both manual and automated experiments was 5.1 % and 5.6 % respectively. The cell pelleting and re-suspension of cells to 200×10^6 cells.ml^{-1} prior to electroporation is a major source of variation in the protocol. Small variations when removing excess media from the pellet are unavoidable during both manual and automated variations of the procedure. As a result comparisons made between electroporation plates should be normalised through internal plate controls.

3.3 Discussion

This chapter describes the individual methods designed, optimised and validated to form a SOSC gene screening platform for CHO cell engineering. The aim of this work was to develop an RNAi platform capable of plasmid DNA co-transfection at cell densities high enough to reach PCD within 5 days.

The first step was identification of the design requirements and key characteristics to ensure the platform met the project needs. Key requirements were outlined based on the available literature on RNAi in CHO cells and more generically, with a focus on applicability to both academic and industrial research work flows. The following list of characteristics were identified: robust, accurate and consistent; simple and reproducible RNA and DNA co-transfection; alignment to industrial mAb production; chemically defined and protein free; cost-efficient and scalable.

Next the best method(s) of delivering RNA and DNA into the target cells needed to be identified. Examples of RNAi screening in the literature are generally in adherent cultures and focus on phenotypic screening. A wide range of RNA delivery methods were selected for testing to find the optimal method to meet the design requirements. The identified RNA delivery methods were ranked based on individual properties and alignment with the proposed platform characteristics. The Lonza SG Cell Line 96 Nucleofector™Kit remained as a reserve option as the complexity and high cost would limit scale and scope of future RNAi screening.

Accurate evaluation of RNA and DNA delivery required a quantitative assessment of transfection potency and efficiency. Flow cytometry would allow accurate quantification on a cell-by-cell basis, with the benefit of multiple fluorophores allowing simultaneous measurement of RNA and DNA delivery. Cyan-5 ftRNA was selected as a reporter to characterise RNA delivery based on its emission spectra relative to that of eGFP, a common reporter for plasmid DNA delivery.

From initial experiments with a range of lipofection and nano-particle based delivery systems, MISSION®siRNA transfection reagent was identified as the best candidate. It offered superior transfection efficiency, potency and had minimal effect on cell viability when used at the manufacturer's recommended concentration. DharmaFECT™ 2 outperformed DharmaFECT™ 4, and increasing the concentration beyond 0.4 %(v/v) could produce transfection potencies and efficiencies comparable to MISSION®siRNA. However, as MISSION®siRNA Transfection Reagent had the baseline best cost efficiency, DharmaFECT™ 2 concentration was not increased beyond 4 fold the manufacturer's recommendations. MISSION®siRNA was taken forward for further method optimisation.

The performance of MISSION®siRNA transfection reagent over a longer culture duration was investigated. Results demonstrated a significant reduction in cell proliferation after addition of the reagent. Control conditions confirmed near complete growth arrest was caused by the MISSION®siRNA reagent, with a minor amplification upon RNA-reagent complexing. This documented effect is commonly overcome by the addition of FBS, FCS or other growth factors to the culture medium to stimulate cell growth (Ovcharenko et al. 2005; Rahimi et al. 2018). Achieving PCD within the 5 day time frame of RNAi knock-down, would require increasing

transfection densities and improving the cell growth rate in the presence of MISSION®siRNA.

Published literature demonstrated that electroporation as a DNA delivery method avoids the inhibition of cell growth seen with lipofection (Maurisse et al. 2010; Tabar et al. 2015). Although initially stressful on the cells, electroporation is a very fast transfection process, with the full DNA or RNA load being delivered into the cells immediately. In comparison, internalisation of cationic lipid-DNA complexes take 1-2 hours (Elouahabi and Ruysschaert 2005).

Upon reviewing the limitations of the available transfection methods against the platform criteria and available literature, the reliability of the Lonza SG Cell Line 96 Nucleofector™ Kit was assessed as an RNA delivery method. As this transfection methodology was utilised in Cartwright et al. 2020 for plasmid DNA delivery over a prolonged culture period, identical conditions were employed as a starting point for development RNA delivery parameter optimisation.

The concentrations of RNA tested at the point of transfection were from 6.50 nM to 2600 nM; significantly higher than with the lipofection and nano-particle methods. The cell density at the point of electroporation is 100×10^6 cells.ml^{-1}; more than 100 times greater than lipofection techniques. Resultantly the RNA per cell is comparable between electroporation and lipofection delivery methods.

Co-transfection results demonstrated that electroporation was a good method of ftRNA delivery in CHO cells, with >97.0 % transfection efficiency when more than 240 nM cyan-5 ftRNA is transfected. The maximum observed MFI of 4.8×10^4 RFU was significantly lower than MISSION®siRNA transfections, however the consistency between replicates was improved. Interestingly the concentration of ftRNA had no measurable impact on eGFP expression within the working range of 21.6 nM to 800 nM, demonstrating the co-transfection robustness of this method.

Quantification demonstrated successful knock-down of SEC22B, BIP and GRP94 to varying extents. When directly compared, the SEC22B esiRNA produced a stronger knock-down than the equivalent siRNA, and demonstrated higher reliability. Furthermore, all esiRNAs displayed lower variability between replicates than the model siRNA.

When ranking the maximal knock-down achieved for each target, SEC22B was strongest followed by GRP94 and BIP with 81.2 %, 67.5 % and 60.9 % reductions in intracellular target protein respectively. It is evident from the data described that the degree of knock-down is target specific. The working hypothesis was that messenger RNA (mRNA) abundance is a key factor impacting knock-down strength. As no mRNA data was available for the CHO_{T2} cell line used, RNA Sequencing (RNAseq) data from the MEDI-CHO parental host was reviewed (Geoghegan et al. 2018). The mean Fragments per Kilo-base of Transcript per Million mapped readss (FPKMs) of SEC22B, BIP, and GRP94 were 44.5, 855.2 and 524.6 respectively, supporting the above hypothesis. Results also suggested higher esiRNA concentrations are required to achieve a similar knock-down of more abundant mRNA transcripts.

Lastly results demonstrated that the rate and duration of RNAi knock-down was target specific. As a result the optimal point to measure the knock-down strength differs for each target. From the data presented and the available literature, day 3 post-transfection was selected to

assess target HCP abundance in future screening experiments (Bartlett and M. E. Davis 2006; Distefano 2019; W. Wu 2004).

When put together, the Lonza SG Cell Line 96 Nucleofector™ Kit is a robust and accurate method for high-throughput, high-density co-transfection of RNA and DNA for parallel RNAi and over-expression screening. Although the high cost initially ranked the method poorly, alternative methods severely inhibited cell growth or encountered unforeseen cost amplifications. Though there was a large improvement over lipofection methods, the growth rate of was still compromised when culturing electroporated cells in 96-DWPs. As the observed doubling time of 47 hours to 49 hours was significantly higher than the expected rate 22 hours to 28 hours during exponential growth, further optimisation of the HTP platform was required (Baik and Kelvin H. Lee 2018; Takagi et al. 2017).

It was hypothesised that the sub-optimal cell growth in the 96-DWP platform was a result of inefficient cell mixing within the wells. Additionally, the narrow 20 µl working range left little room for mid-culture sampling. After reviewing the available options and observing the high-throughput culture platform utilised by AstraZeneca, several 24-SWP formats were evaluated.

After initial assessments, the CR1324a sandwich cover lid performed best with transfected CHO_{T2} cells reaching a PCD of 7.61×10^6 cells.ml^{-1} in fed-batch cultures. Upon further characterisation, a working range from 650 µl to 750 µl was demonstrated to have no impact on culture growth or cell viability without the culture making contact with the plate lid when shaking. Lastly the measured evaporation rate through the lids was under 1.5 µl.day^{-1}, and would have negligible impact on culture performance over applicable longer culture durations. A direct performance comparison demonstrated 24-SWPs reduced cell doubling times of transfected CHO_{T2} and CHO_{ETE} cells by 18.8 % and 19.2 % respectively.

The scale of the planned gene-screening experiments in addition to the high complexity of the HTP nucleofection platform and associated sampling led the procurement of an automated liquid handler. It was hypothesised that through automation of high-throughput cell culture screening, the well-to-well variability could be reduced leading to increased reliability. This was a particular concern with the Lonza electroporation platform as transfection occurred at very high cell densities, therefore maintaining a homogeneous cell suspension for pipetting steps was an ongoing challenge.

It was important to benchmark the Opentrons OT-2 liquid handler's accuracy and reproducibility before designing and testing the complex electroporation platform protocols. As the most common IgG titre assay utilised by the research group, the Valita®TITER assay was the logical choice to assess the liquid handler's performance.

The sample-to-sample variability when generating a full plate standard curve with the Valita®TITER and Valita®TITER Plus IgG quantification assays was assessed when performed by the liquid handler and a human operator. In total 24 independent standard curves were generated for each assay by the robot and the human operator. The data demonstrated the OT-2 performed the Valita®TITER assay with the same consistency and precision as the human operator. Addi-

tionally, the OT-2 outperformed the human operator when performing the Valita®TITER Plus assay with reduced StD and CV values for 80 % data points along the standard curve.

Lastly the Opentrons OT-2 was shown to perform the liquid handling steps with greater precision than a human, with a average reduction in Percentage Coefficient of Variation (%CV) in seeding density of 42.8 %. As a positive correlation between inefficient mixing and cell settling is expected, the reduced seeding density variation supports attributing the difference in seeding density between methods to inefficient mixing. Furthermore, flexibility of the robotic pipettes to mix, aspirate and dispense variable volumes reduced the protocol duration by ≈30 %, increasing the potential throughput of the gene-screening platform.

Following the successful validation of the OT-2 with the Lonza HTP electroporation protocol, the remaining plate-based protocols and assays within RNAi screening platform were automated. In addition to transfection, this included sampling from 24-SWPs, feeding cultures, loading samples onto the Iprasense HTP cell counter and running Valita®TITER assays at variable dilutions. The Python scripts for the protocols used here, and designed for use in chapter 4 are available in Appendix E.

Chapter 4

Evaluating the Sensitivity of ER Folding and Assembly Machinery Through Simultaneous Overexpression and Silencing Co-transfection (SOSC) Effector Gene Titration

The results described in this chapter aim to demonstrate the applicability of the SOSC gene screening platform developed and validated in Chapter 3, as a tool to rapidly identify Chinese Hamster Ovary (CHO) host and cell line specific genetic engineering targets. Furthermore, the use of paired host and producer transcriptomics data was investigated as a method for identifying effector genes for High Throughput (HTP) screening experiments.

Effector genes were selected by leveraging Gene Ontology (GO) annotations, and RNA Sequencing (RNAseq) transcriptomics data in the host producer. A list of 46 genes which were differentially expressed and associated with Endoplasmic Reticulum (ER) folding and assembly processes was identified. A subset of this list was experimentally assessed using the SOSC gene screening platform to transiently overexpress and knock-down effector genes in two cell lines expressing an Easy to Express (ETE) and Difficult to Express (DTE) Monoclonal Antibody (mAb) respectively.

From six engineering targets found to improve productivity in the DTE model, only overexpression of ERDJ5 also improved productivity in the ETE model system, suggesting generic applicability to the CHO host genetic background. Despite derivation from a common host, in the ETE mAb model Integral Viable Cell Density (IVCD) varied most in response to gene titration, whereas titre variation was prevalent in the DTE model, highlighting product specific changes to cell factory characteristics.

4.1 Introduction

In a mAb production context, transient overexpression studies have identified a range of approaches and targets for the engineering of host CHO cell lines. It has become a key tool, as complex therapeutics push the limits of biological factories. A well known trait of genetic engineering solutions is the highly context specific nature of cellular responses limiting their applicability to individual therapeutic protein products and host cell backgrounds.

Given the complexity of mAb folding and assembly, and the vast number of genes whose expression could be modulated to improve production, a significant number of engineering approaches have focused on transcription factors as diverse regulators of gene expression (Gulis et al. 2014). *XBP1s* is a transcription factor activated upon ER stress, and is one of the most prominent CHO engineering targets with demonstrated applicability to mAb production (K. Cain et al. 2013; Cartwright et al. 2020; Gulis et al. 2014; Tigges and Fussenegger 2006) and other therapeutic proteins (Hansen, Nilsson, et al. 2015; Johari et al. 2015; Ku et al. 2008; Tigges and Fussenegger 2006), however contradictory results have also been demonstrated (Ku et al. 2008; Rahimpour et al. 2013).

A further exemplification of this is seen when reviewing published studies on the effect of ectopic *P4HB* expression on therapeutic protein productivity in CHO cells (Borth et al. 2005; Cartwright et al. 2020; R. Davis et al. 2000; Hansen, Nilsson, et al. 2015; Hayes et al. 2010; Johari et al. 2015; Mohan et al. 2007; Nishimiya et al. 2013; Pybus et al. 2014). The ER resident enzyme P4HB confers disulphide isomerase activity. It plays a key role in oxidation and reduction of disulphide bonds in nascent polypeptides, and functions as a chaperone inhibiting the aggregation of folding intermediates (Appenzeller-Herzog and Ellgaard 2008; Hatahet and Ruddock 2009). The reported effects of *P4HB* overexpression on titre and Specific Productivity (qP) vary from a 50 % decrease, through negligible effects, and up to a 40 % increase. This inconsistency can, to some extent, be explained by product specificity, as several different recombinant proteins have been used as models in examples such as Pybus et al. 2014. However, many context specific cellular and experimental factors are at play when examining how an effector gene effects productivity, thus the inconsistency in P4HBs on therapeutic protein production is likely more complex than product specificity alone.

The majority of published examples addressing product specificity focus on transient mAb production systems, which apply the associated ER and Unfolded Protein Response (UPR) stress in an acute manner (Becker et al. 2008; K. Cain et al. 2013; Hansen, Pristovšek, et al. 2017; Johari et al. 2015; Pybus et al. 2014). The cells UPR pathways to chronic and acute stresses differ, with long term stress inducing wider reaching transcriptome regulation and chromatin remodelling (DuRose et al. 2006; Merquiol et al. 2011; K. T. Smith and Workman 2012). This limits the transferability of findings from transient mAb to stable production cell lines, hence screening of effector genes on stable producers is more appropriate to inform industry processes.

The use of RNA Interference (RNAi) screening has also become common when studying the pathology of disease, allowing for rapid screening of genome scale libraries in cell models. However, due to limitations raised and addressed in chapter 3, RNAi previously had limited appli-

cability to the optimisation of biopharmaceutical production pipelines. Incorporation of knock-down methods help facilitate the evaluation of cell line sensitivity to effector gene knock-down and could help identify genetic redundancy in mAb folding and assembly pathways. This chapter is a case study aiming to demonstrate the application of the SOSC gene screening platform designed in chapter 3 as an engineering tool to identify targets for CHO cell engineering.

By exploring the response of two cell lines of the same host linage, expressing ETE and DTE model mAbs, the aim was to gain an insight into the product and context specificity of commonly employed genetic engineering approaches. Any differential responses observed between these cell lines may improve our understanding of production bottlenecks introduced by complex biotherapeutics. Genes able to improve the stable production of different mAbs would be examples of engineering targets that are not product specific, with wider applicability in the CHO host.

Cell line and host specific transcriptomics data were utilised to identify effector genes which undergo a change in expression during the cells adaption to stable mAb production. A similar approach was employed by Berger et al. 2020, who experimentally identified five engineering targets from a library of 32 genes which were bioinformatically predicted to improve production of ETE therapeutics. One of these genes (FOXA1) was found to also improve the production of a DTE mAbs. This study aims to further assess whether the use of host and cell line specific transcriptomics data can increase the likelihood of successfully identifying genetic engineering targets.

4.2 Results

4.2.1 Bioinformatic Identification of Effector Genes

Target genes were selected by data and hypothesis driven approaches, leveraging published literature, bioinformatic analysis and CHO_{ETE} specific RNAseq data. This was used to identify a subset of target genes associated with mAb folding and assembly, in which CHO_{ETE} is predicted to be sensitive to up- or down-regulation.

4.2.1.1 Identification of genes associated with key mAb folding and assembly processes

By reviewing the current understanding of mAb folding and assembly mechanisms in the ER (section 1.4) a set of four GO terms associated with key mAb folding and assembly processes were selected. The GO terms cover aspects of; peptide targeting and recognition, protein folding, quaternary structure assembly, quality control mechanisms, UPR components and regulators. These are described below according to Madeira et al. 2019:

- *GO: ER-UPR (0030968)* - A series of proteins differentially transcribed or translated in response to an increase in unfolded proteins in the ER or increased ER stress.
- *GO: Unfolded Protein Binding (0051082)* - A collection of proteins, commonly named chaperones, which selectively and non-covalently interact with unfolded proteins.
- *GO: PDI-activity (0003756)* - A group of proteins that catalyse the creation and rearrangement of disulfide bonds in proteins.
- *GO: Protein-targeting-to-ER (0045047)* - The process of directing proteins to the ER using self-contained signals; commonly a 16-30 amino acid signal sequence on the protein N-terminus.

Using Ensembl's BioMart tool (Yates et al. 2020) a comprehensive list of genes associated with each GO term was extracted from the *Cricetulus griseus* CHOK1GSHDV1 genome yielding 332 unique results.

4.2.1.2 Gene list mapping to a CHO_{ETE} transcriptomics dataset

The extracted gene list was mapped to an RNAseq dataset from (Geoghegan et al. 2018) to identify and interrogate genes showing differential regulation between host and daughter cell lines at different culture stages. The dataset, generated by Geoghegan et al. 2018, contained data from duplicate CHO_{ETE} (producer) or MEDI-CHO_{GSKO} (GSKO control) cultures in early (day 4) and late (day 8) culture phases. Transcript abundance is given in Fragments per Kilo-base of Transcript per Million mapped reads (FPKM), accounting for sequence depth and gene length. Previous mapping of the dataset identified 20,020 of 25,072 annotated genes, covering 79.8 % of the predicted *Cricetulus griseus* CHO-K1 genome. Following alignment with the CHO_{ETE} RNAseq data the gene list was reduced to 219 genes, of which 212 were unique. Table 4.1

displays the number of genes associated with each GO term mapped to the CHO_{ETE} RNAseq dataset, and the number remaining at each subsequent stage of analysis.

Genes with a mean transcript abundance ≤5 FPKM in the producer or control cell lines were removed, eliminating 28.7 % of the identified genes. This maintained the validity of differential expression analysis, eliminating artefacts and ensuring sufficient transcript abundance for effective RNAi knock-down. To evaluate the limitations of this step, the 61 eliminated genes were manually interrogated to identify any genes commonly associated with mAb folding and assembly. Two genes were identified; firstly *PDIA2* with an abundance of 0.000 FPKM and 0.001 FPKM for the producer and GSKO cells respectively, and secondly *HSPA1* with an abundance of 0.650 FPKM and 1.245 FPKM.

Table 4.1: Bioinformatic overview of effector gene library identification.
The selected GO terms and identifiers are displayed with the number of genes associated in the *Cricetulus griseus* CHOK1GSHDV1 genome identified through Ensembl's BioMart tool (Yates et al. 2020). Subsequent columns show the number of genes remaining after each of the following bioinformatic steps: mapping to CHO_{ETE} RNAseq dataset (Geoghegan et al. 2018), mean transcript abundance ≤5 FPKM, and differentially expressed relative to the control dataset.

GO Term (Identifier)	CHOK1GS Total	Mapped to RNAseq	Expression ≤ 5 FPKM	Differentially expressed
ER UPR (GO:0030968)	64	52	42	12
Unfolded protein binding (GO:0051082)	220	137	91	33
PDI activity (GO:0003756)	13	11	9	6
Protein targeting to the ER (GO:0045047)	32	19	16	3
Total GO term appearances	329	219	158	51
Unique genes	322	212	151	46

4.2.1.3 Identification of differentially expressed genes

The conditions for differential expression were defined as a positive or negative fold change ≥1.66, equated to a 66.66 % increase or 40.00 % decrease in the producer cells when compared to the GSKO control. Equations (4.1) to (4.3) define the three fold-change (FC) statistics utilised, as described below:

- Fold change in the mean transcript abundance in early stage culture.
- Fold change in the mean transcript abundance in late stage culture.
- Change in up- or down-regulation between early and late stage culture.

$$FC_{Early} = \frac{Producer_{Day4}}{Control_{Day4}} \tag{4.1}$$

$$FC_{Late} = \frac{Producer_{Day8}}{Control_{Day8}} \tag{4.2}$$

$$FC_{Regulation} = \frac{Producer_{Day8}}{Producer_{Day4}} \div \frac{Control_{Day8}}{Control_{Day4}} \tag{4.3}$$

From the described analysis, 46 unique genes were identified as potential screening targets, having met at least one of the differential expression conditions (Appendix A Table A.1). A hypothesis driven methodology was employed to identify a screening library of 15 genes. To inform effector gene selection previous CHO engineering studies (Carlage et al. 2012; Cartwright et al. 2020; Harreither et al. 2015; Yee, Gerdtzen, et al. 2009) and literature surrounding the ER localised DNA-J homologue (ERDJ) family of co-chaperones which were relatively understudied in a mAb production context (Cunnea et al. 2003; Plate and Wiseman 2017; Shen et al. 2002).

Two genes, *ERO1A* and *ERDJ4*, were not found in the bioinformatically identified list of differentially regulated genes. *ERO1A* was included as a constitutively expressed functional homologue of *ERO1B*, which exhibits tissue and cell type specific expression levels and more rapidly induced in response to UPR activation (Dias-Gunasekara et al. 2005; Tavender and Bulleid 2010). *ERDJ4* is a co-chaperone for *BIP*, and is thought to play a key role in IRE1 mediated UPR induction upon ER stress signal cascade activation(Shen et al. 2002). Furthermore, Kampinga and Craig 2010 discovered that ERDJ3 is responsible for delivering misfolded substrates to BIP stimulating the chaperones activity, and Genereux et al. 2015 identified that ERDJ3 is secreted in response to UPR stress, promoting extracellular proteostasis.

XBP1 and *SRP14* were added to the final effector gene selection as pseudo-positive controls creating a library of 17 genes. *XBP1* overexpression has been demonstrated to improve mAb production in CHO cells in multiple publications (K. Cain et al. 2013; Cartwright et al. 2020; Ku et al. 2008; Tigges and Fussenegger 2006). *SRP14* was one of the most successful genes for improving mAb production in stable pools generated from a MEDI-CHO host background in Cartwright et al. 2020. The mean transcript abundance and metrics of differential regulation identified from transcriptomics data and calculated from genetic titration for the final library of 17 genes can be found in Appendix A Table A.2.

4.2.2 Setting Experimental Screening Parameters

CHO_{ETE} and $CHO_{BIS\text{-}A}$ were selected to evaluate the differential responses and sensitivities to molecular titration, as the former is a standard ETE IgG1 and the latter a complex DTE bi-specific. Transfected cells were cultured for five days with a 10 % feed on day 3. Growth and viability measurements were taken on day three and at harvest using the Iprasense NormaHT. Product titre was evaluated using the ValitaTITER assay at harvest with independent standard curves created for each mAb.

When compiling and analysing the data, all metrics were normalised to the empty-vector-only controls within each 24-Shallow Well Plate (SWP) and expressed as a fold change. In order to minimise the chance of confounding variables, all the screening conditions for each Gene of Interest (GOI) were represented in triplicate in a single 24-SWP. Importantly, this layout allowed the response in IVCD, titre and qP of each condition to be expressed as a fold-change relative to the controls within each 24-SWP. Including the empty vector control, this allowed for 8 genetic titration points per target. Due to the large variability in efficacious endoribonuclease prepared

small interfering siRNA (esiRNA) concentrations between target genes, four knock-down and three overexpression conditions were screened.

Based on the characterisation of knock-down dynamics in section 3.2.5 a maximum esiRNA concentration of 600 nM was selected. After evaluation of the stable and transient gene screening results in Cartwright et al. 2020 a maximal plasmid Deoxyribonucleic Acid (DNA) load of 200 ng.well^{-1} was also selected. A 2.5 fold decrease was used between each titration point and all conditions were made up to 200 ng.well^{-1} with empty vector to normalise for the effects of DNA toxicity resulting in the screening parameters described in Table 4.2. As discussed in chapter 3, the effect of increasing esiRNA concentration was negligible, and did not require normalisation.

Table 4.2: Over-expression and RNAi conditions for the titration of ER chaperones.
Each target gene was screened at each of the conditions described below with all wells were made up to 200 ng.well^{-1} of plasmid DNA load with empty vector.

Titration Point	RNA (nM)	Target DNA (ng.well^{-1})	Empty DNA (ng.well^{-1})
3	0.0	200.0	0.0
2	0.0	80.0	120.0
1	0.0	32.0	168.0
0	0.0	0.0	200.0
−1	38.4	0.0	200.0
−2	96.0	0.0	200.0
−3	240.0	0.0	200.0
−4	600.0	0.0	200.0

4.2.3 Normalisation of the cell response to RNAi

Upon evaluation, it was evident that esiRNA transfection resulted in a small but measurable increase in growth rate and titre in both CHO_{ETE} and $CHO_{BIS\text{-}A}$. This can be seen in Figure 4.1 depicting the titration of the scrambled-esiRNA control for CHO_{ETE} (**a**) and $CHO_{BIS\text{-}A}$ (**b**).

In CHO_{ETE} the increase in IVCD was significant at two titration points, whereas only one was significant in $CHO_{BIS\text{-}A}$. The increase in titre in response to RNAi was significant to $P < 0.01$ at all titration points in both CHO_{ETE} and $CHO_{BIS\text{-}A}$. A reduction in response to RNAi at titration points -3 and -4 in qP was observed in CHO_{ETE}, whereas in $CHO_{BIS\text{-}A}$ a qP increase was seen. However, no changes in qP were statistically significant in either cell line.

It was evident from the scrambled esiRNA results that the empty-vector control (titration point 0 in Table 4.2) was not the appropriate negative control for the RNAi conditions. Normalisation of the RNAi conditions against the scrambled control was required to directly compare the effect of knock-down and over-expression of the effector genes. Theoretically normalisation of each knock-down titration point against the correlating scrambled control condition would be the most appropriate method.

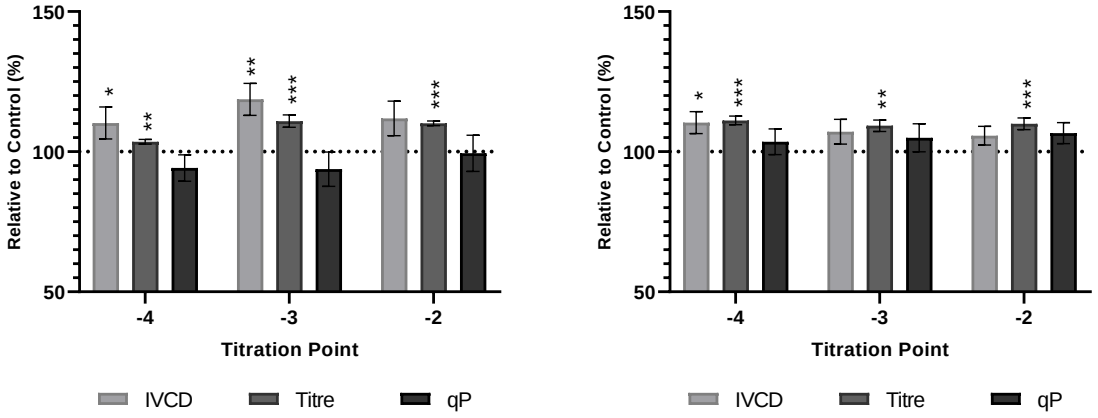

(a) $\mathrm{CHO_{ETE}}$ **(b)** $\mathrm{CHO_{BIS\text{-}A}}$

Figure 4.1: RNAi data normalisation: Scrambled esiRNA control performance evaluation. The results from the scrambled esiRNA control targetting eGFP are shown for $\mathrm{CHO_{ETE}}$ (**a**) and $\mathrm{CHO_{BIS\text{-}A}}$ (**b**), expressed as a relative fold change of the empty-vector control (dotted line). Error bars are SEMs of $n = 6$ replicates comprised of technical triplicates of biological duplicates. Significance, represented by $*(P < 0.05)$, $**(P < 0.01)$, or $***(P < 0.001)$ was calculated by unpaired t-test.

When considering the variation seen this would have placed a high weighting on each titration point of the scrambled control. The scrambled esiRNA was not evaluated at the -1 titration point due to practical restrictions in the experimental design. Subsequently, a more conservative approach was taken by performing a linear regression on the scrambled control results, as depicted in Figure 4.2. This captured the overall trend in response to RNAi and was extrapolated to objectively normalise titration point -1. The linear regression formulae for IVCD, titre and qP are shown below by eqs. (4.4) to (4.6) and eqs. (4.7) to (4.9) for $\mathrm{CHO_{ETE}}$ and $\mathrm{CHO_{BIS\text{-}A}}$ respectively:

$$CHO_{ETE}:$$

$$IVCD: \quad y = -6.616 \times 10^{-3}x + 115.3 \tag{4.4}$$

$$Titre: \quad y = -1.415 \times 10^{-2}x + 112.5 \tag{4.5}$$

$$qP: \quad y = -8.695 \times 10^{-3}x + 986.1 \tag{4.6}$$

$$CHO_{BIS-A}:$$

$$IVCD: \quad y = \ \ 9.268 \times 10^{-3}x + 104.8 \tag{4.7}$$

$$Titre: \quad y = \ \ 2.902 \times 10^{-3}x + 109.2 \tag{4.8}$$

$$qP: \quad y = -5.743 \times 10^{-5}x + 106.8 \tag{4.9}$$

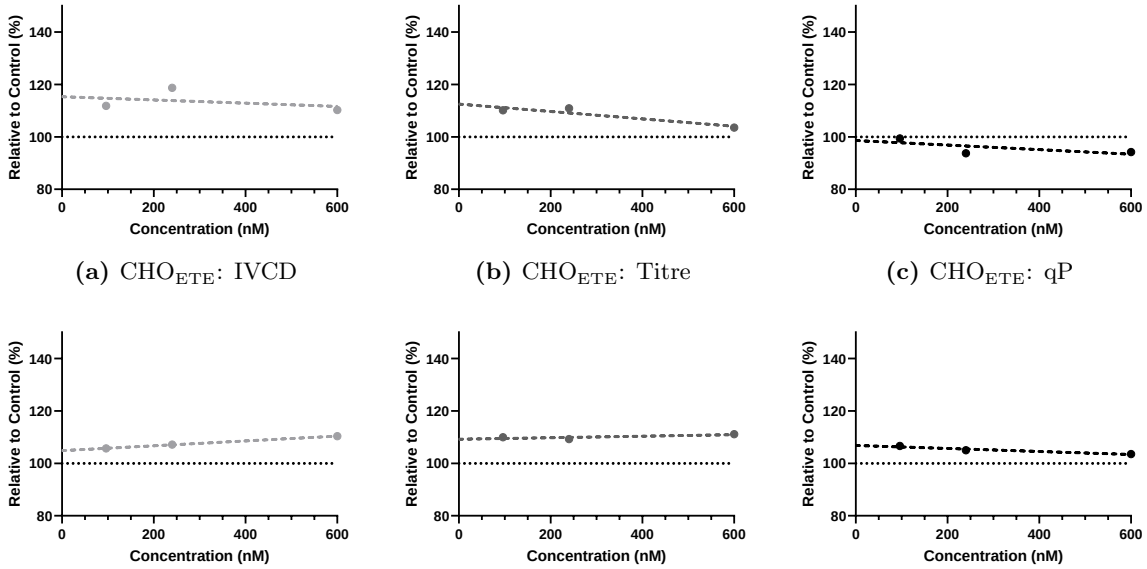

(a) CHO_{ETE}: IVCD **(b)** CHO_{ETE}: Titre **(c)** CHO_{ETE}: qP

(d) $CHO_{BIS\text{-}A}$: IVCD **(e)** $CHO_{BIS\text{-}A}$: Titre **(f)** $CHO_{BIS\text{-}A}$: qP

Figure 4.2: RNAi data normalisation: Scrambled esiRNA control linear regressions. The figures show the liner regressions (dashed lines) of the scrambled esiRNA RNAi control relative to the empty-vector control (dotted lines at $y = 1$) with the mean of each titration point CHO_{ETE} (**a-c**) and $CHO_{BIS\text{-}A}$ (**d-f**) respectively for IVCD, titre and qP overlaid. The equations for each regression in (**a**) to (**e**) are displayed in eqs. (4.4) to (4.9).

4.2.4 Response of CHO_{ETE} and $CHO_{BIS\text{-}A}$ to Molecular Titration of ER Folding and Assembly Machinery

The response to genetic titration of the effector gene library was plotted for CHO_{ETE} and $CHO_{BIS\text{-}A}$ in Figures 4.3 and 4.4 respectively with graphs (a), (b) and (c) displaying the change in IVCD, titre and qP. Data is displayed as a percentage relative to the empty vector control (red, titration point 0).

The knock-down of most effector genes negatively or negligibly impacted CHO_{ETE} IVCD (Figure 4.3a). *ERDJ3*, *ERDJ4* and *ERDJ5* produced a significant IVCD reduction at $\geq$75 % of titration points with little correlation between fold-decrease and RNAi concentration. The exception was *ERO1B*, for which knock-down and over-expression increased IVCD, resulting in a U-shaped trend with titration point -1 at the base. Ten conditions produced a significant IVCD increase in CHO_{ETE} with overexpression of *CALR* and *HYOU1* having the greatest magnitude. Other than *SRP14*, the over-expression of the effector genes did not negatively impact IVCD, although increases are modest.

$CHO_{BIS\text{-}A}$ IVCD (Figure 4.4a) was less sensitive than CHO_{ETE} to knock-down and overexpression of effector genes with seven conditions identified as a significant change from the control performance. Gene titration positively correlated with IVCD for a number of genes, most evidently the titration of *CANX* and *ERDJ3*, whereas in CHO_{ETE} this was less abundant. Again *ERO1B* was the only knock-down which increased IVCD, although to a lesser extent than in CHO_{ETE}. *PDIa6* demonstrated the most consistent growth increase from effector gene over-expression in $CHO_{BIS\text{-}A}$ with *CALR*, *CANX*, *ERO1B* and *HYOU1* displaying moderate benefits.

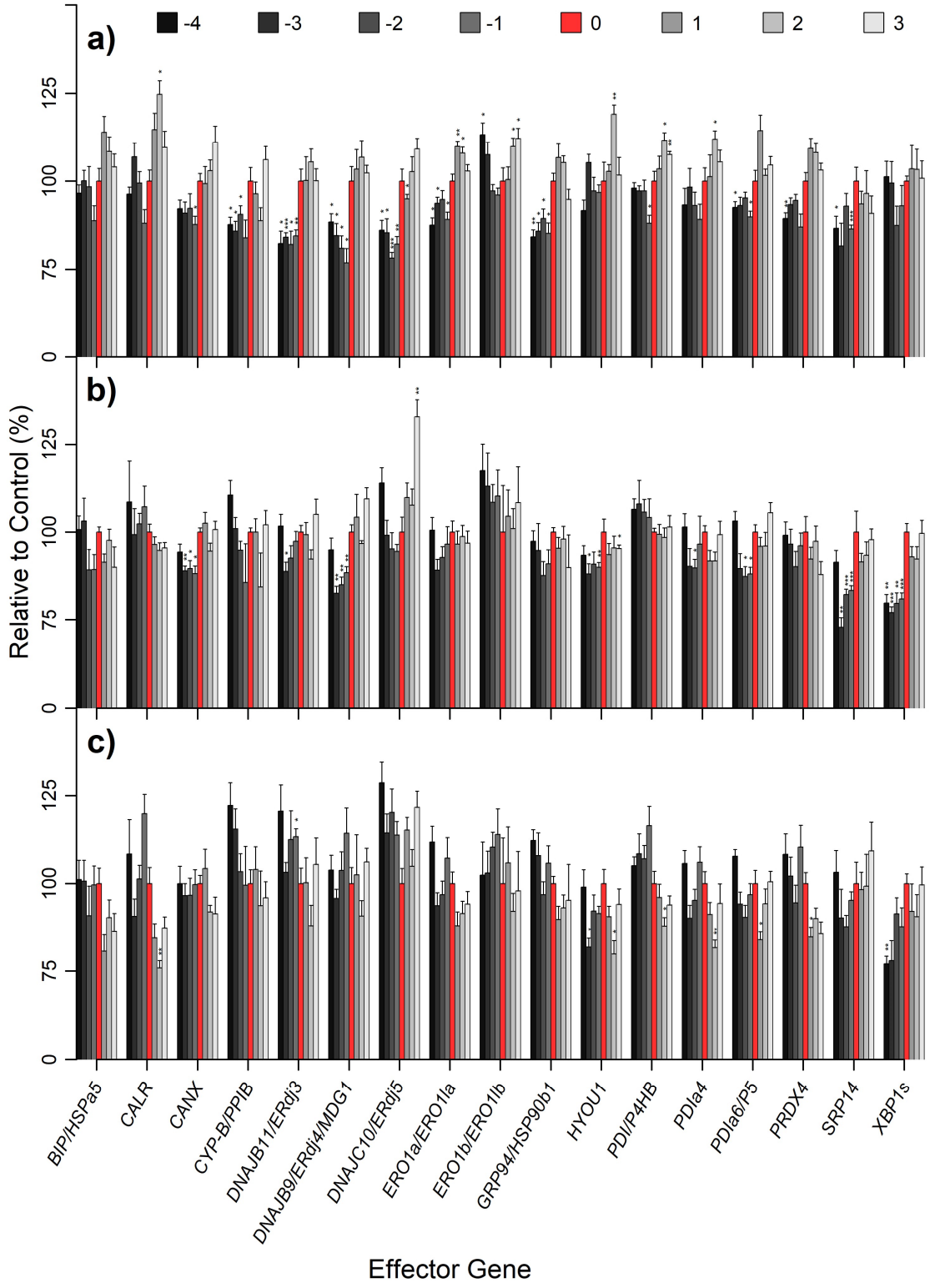

Figure 4.3: Titration of ER folding and assembly effector genes in CHO_{ETE} cells.
A total of 17 genes were transiently knocked-down or over-expressed in CHO_{ETE} creating an 8-point titration as shown in Table 4.2 with total DNA mass normalised to 200 ng.well^{-1} with empty-vector. Culture IVCD (**a**), titre (**b**) and qP (**c**) were calculated after 5 days. Results are depicted as a percentage fold change relative to the empty vector control (titration point 0) with knock-down conditions further normalised against a scrambled RNAi control as described in section 4.2.3. The data displayed is the mean and Standard Error of the Mean (SEM) of $n = 6$ replicates comprised of technical triplicates of biological duplicates. Significance, represented by *($P < 0.05$), **($P < 0.01$), or ***($P < 0.001$), was calculated by t-test followed by a Benjamini Hochberg adjustment to allow for multiple comparisons.

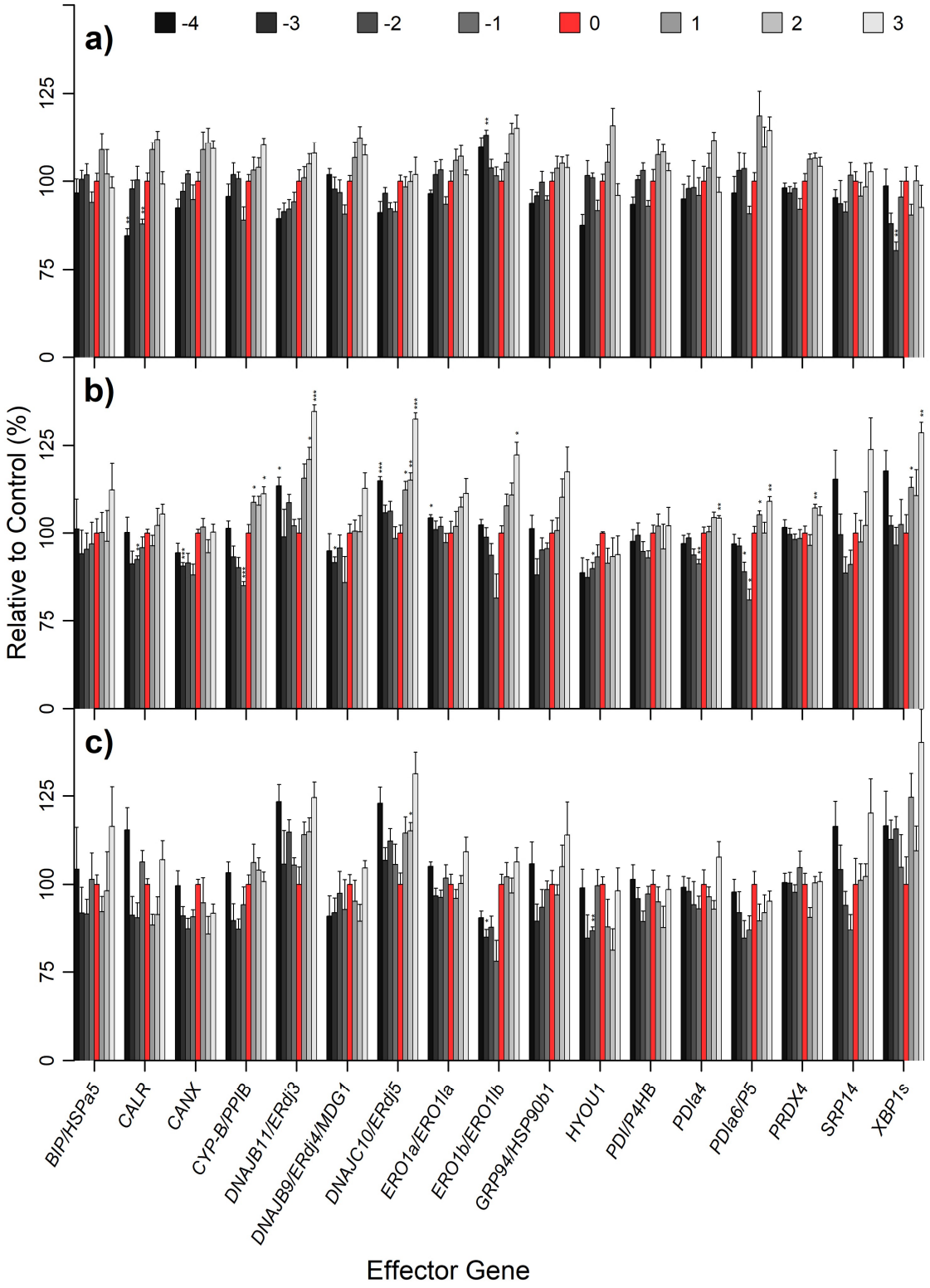

Figure 4.4: Titration of ER folding and assembly effector genes in $CHO_{BIS\text{-}A}$ cells. A total of 17 genes were transiently knocked-down or over-expressed in $CHO_{BIS\text{-}A}$ creating an 8-point titration as shown in Table 4.2 with total DNA mass normalised to 200 ng.well^{-1} with empty-vector. Culture IVCD (**a**), titre (**b**) and qP (**c**) were calculated after 5 days. Results are depicted as a percentage relative to the empty vector control (titration point 0) with knock-down conditions further normalised against a scrambled RNAi control as described in section 4.2.3. The data displayed is the mean and SEM of $n = 6$ replicates comprised of technical triplicates of biological duplicates. Significance, represented by *($P < 0.05$), **($P < 0.01$), or ***($P < 0.001$), was calculated by t-test followed by a Benjamini Hochberg adjustment to allow for multiple comparisons.

When observing CHO_{ETE} titre responses (Figure 4.3b), overexpression of *ERDJ5* resulted in a 29 % titre increase at titration point 3, however knock-down also improved mAb_{ETE} titre resulting in a U-shaped correlation. Although the results are non-significant, all *ERO1B* and *P4HB* knock-down conditions improved mAb-ETE titre while over-expression had minimal effect. Lastly mAb_{ETE} titre was very sensitive to *SRP14* and *XBP1s* knock-down with no benefit to overexpression.

Overall $mAb_{BIS\text{-}A}$ (Figure 4.4b) titre was more responsive to over-expression than mAb_{ETE}. A $\geq$20 % increase in titre was observed from the overexpression of six genes, of which *ERDJ3*, *ERDJ5*, *ERO1B* and *XBP1s* were identified as statistically significant. When compared to CHO_{ETE}, $CHO_{BIS\text{-}A}$ titre was on average less sensitive to the knock-down of effector genes with sensitivity observed from *PPIB*, *ERO1B* and *PDIa6*. Four of the effector genes screened improved $mAb_{BIS\text{-}A}$ titre when overexpressed and knocked-down.

The qP trends observed in CHO_{ETE} (Figure 4.3c) and $CHO_{BIS\text{-}A}$ (Figure 4.4c) in response to effector gene titration are less apparent than IVCD and titre with highly differing responses between adjacent titration points. Most qP increases in CHO-ETE were in response to effector gene knock-down, and effector gene overexpression generally reduced production rate in mAb_{ETE}. The qP of $mAb_{BIS\text{-}A}$ was increased by the overexpression or knock-down of *BIP*, *ERDJ3*, *ERDJ5*, *SRP14* and *XBP1s*, although none of these results were statistically significant.

4.2.5 Evaluating the sensitivity of CHO_{ETE} and $CHO_{BIS\text{-}A}$

4.2.5.1 Elimination of numerical bias through a log_2 data transformation

When mathematically comparing the magnitude of increases and decreases relative to a control value, data expression as a percentage- or fold-change is numerically biased. As shown in Figure 4.5a fold-change is biased towards fold-increases leading to a discrepancy in the magnitude of results for equivalent fold-increases and fold-decreases.

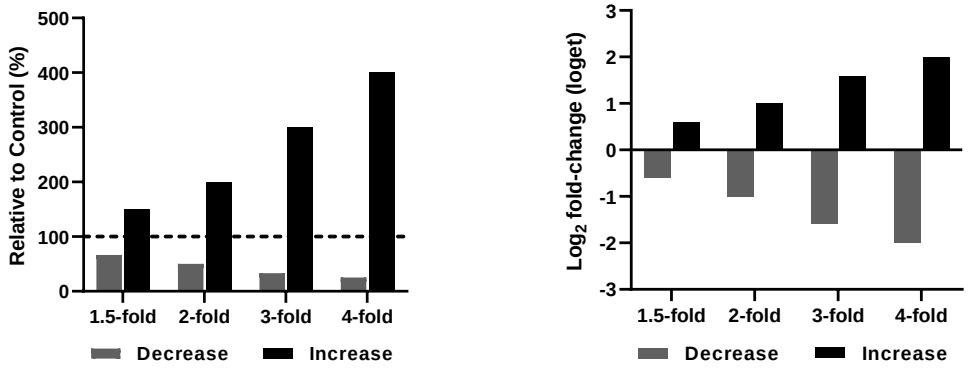

(a) Expressed as FC **(b)** Expressed as log_2FC

Figure 4.5: Graphical representation of relative fold-change data.
Relative data can be plotted as a fold change (**a**) representing the absolute changes seen. Making a log_2 transformation of relative fold-change data (**b**) normalises the magnitude of fold-increases and fold-decreases and has the units 'loget' (Pacholewska 2017). Data in this figure is artificially constructed for for representative purposes.

This can be corrected by making a log_2 data transformation, equalizing the magnitude of fold-increases and fold-decreases to allow for non-biased data evaluation and aid interpretation of graphically displayed results (Figure 4.5b). The term 'loget' was defined by Pacholewska 2017 to simplify the description of a 'log_2 fold change' in prose.

The raw data was transformed to loget as per equation eq. (4.10) below:

$$loget = log_2(\frac{test\ value}{refereance\ value}) \tag{4.10}$$

4.2.5.2 Deriving a measurement of sensitivity to effector gene titration

This sensitivity score was designed to compare the responsiveness of CHO_{ETE} and $CHO_{BIS\text{-}A}$ to changes in the abundance of each effector gene, inclusive of overexpression and knock-down. To achieve this the population variance (σ^2) for IVCD, titre and qP were calculated from the mean of the loget values at each titration point, disregarding the variability in experimental replicates.

Equation (4.11) shows the equation for variance (σ^2) where N is the population size, the x_i are data points and u is the mean of population x:

$$\sigma^2 = \frac{1}{N}\sum_{i=1}^{N}(x_i - u_x)^2 \tag{4.11}$$

When applied to the effector gene titration data to calculate the variance in IVCD, titre or qP, each variable in eq. (4.11) is as follows:

- N is the number of titration points (8).
- i is the titration point with the range -4 to 3.
- x is the mean loget of experimental replicates at titration point i; x is substituted for the calculation of σ^2_{IVCD}, σ^2_{Titre} or σ^2_{qP}.
- u is the mean of x_{-4} to x_3.

Specific productivity was excluded from the calculation of the sensitivity score as it is not primary metric due to the nature of its derivation. The sensitivity score for each gene in each cell line is then calculated as shown in eq. (4.12):

$$Sensitivity\ score = \sigma^2_{IVCD} + \sigma^2_{Titre} \tag{4.12}$$

4.2.5.3 Comparing the of CHO_{ETE} and $CHO_{BIS\text{-}A}$ sensitivity to each effector gene

Figure 4.6 shows the calculated sensitivity score for each effector gene in CHO_{ETE} and $CHO_{BIS\text{-}A}$ with numerical data points listed in Appendix A Table A.2.

The mean sensitivity score across the effector gene library from CHO_{ETE} was 0.0237, compared to 0.0189 with $CHO_{BIS\text{-}A}$ suggesting increased responsiveness to effector gene titration. Exceptions to this are ERDJ4, GRP94, P4HB and PPIB, where $CHO_{BIS\text{-}A}$ demonstrated greater sensitivity

to genetic titration than CHO_{ETE}. The greatest difference was seen in response to the titration of GRP94 where the sensitivity score was more than two times greater.

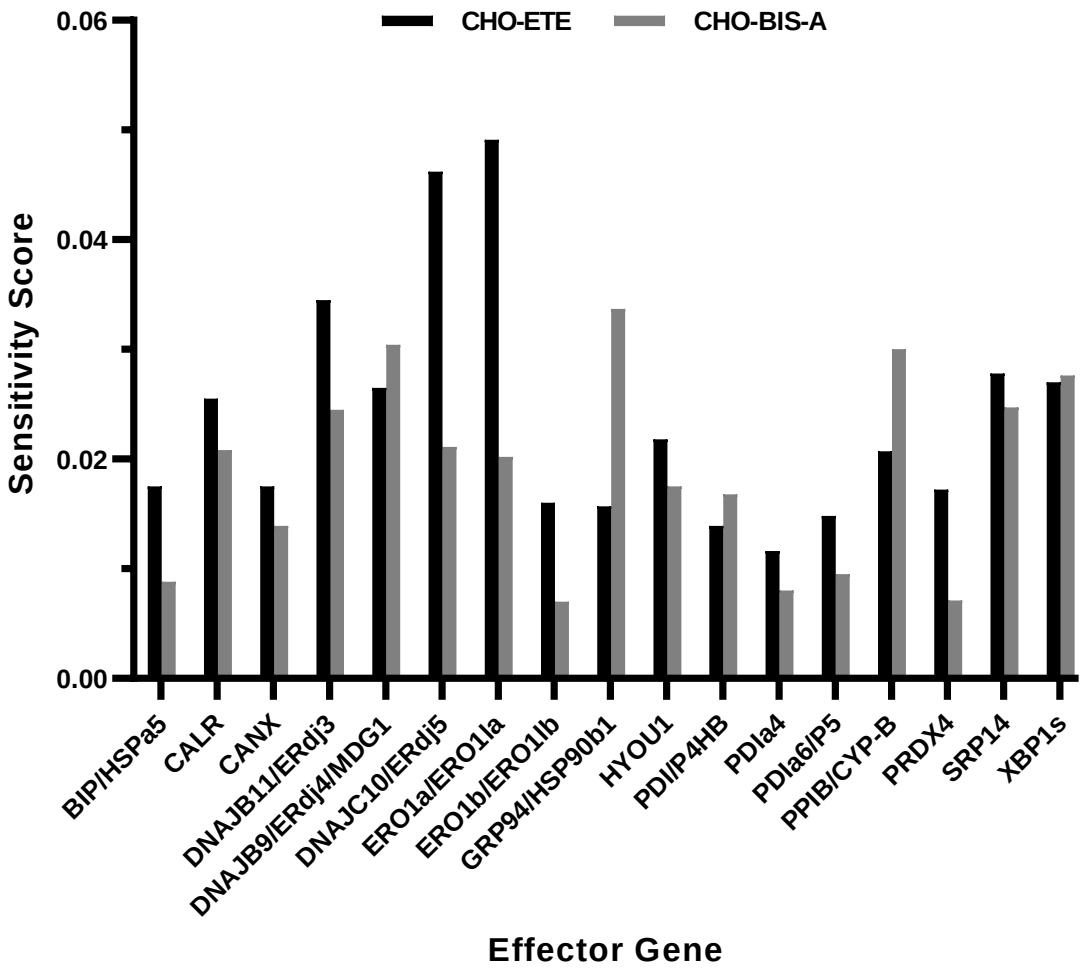

Figure 4.6: Sensitivity of CHO_{ETE} and $CHO_{BIS\text{-}A}$ to effector gene titration.
The sensitivity of each effector gene in CHO_{ETE} (black) and $CHO_{BIS\text{-}A}$ (grey) is described by the 'sensitivity score', derived from the sum of σ^2_{IVCD} and σ^2_{Titre} in response to effector gene titration.

CHO_{ETE} was most sensitive to the titration of ERDJ5 and ERO1A, however this was not true for $CHO_{BIS\text{-}A}$, with a sensitivity score >2 fold lower in response to these effector genes. A similar difference in sensitivity was also observed in response to titration of ERO1As paralog, ERO1B although the sensitivity score of both was low.

The six genes demonstrating the highest sensitivity in CHO_{ETE} (CALR, ERDJ4, ERDJ5, SRP14, XBP1s) all had a mean transcript abundance ≤110 FPKM in the RNAseq dataset from Geoghegan et al. 2018. A linear regression was performed on Figure 4.7, showing the mean transcript abundance and sensitivity score for each effector gene in CHO_{ETE}. An R^2 of 0.217 indicated a very weak correlation in the total dataset. Comparison of the relationship between mean transcript abundance and σ^2_{IVCD} or σ^2_{Titre} (the two components of the sensitivity score) returned respective R^2's of 0.032 and 0.263 Appendix A Figure A.2. Lastly evaluation of the relationships between metrics of differential expression (as calculated from Geoghegan et al. 2018 in section 4.2.1.3) and the CHO_{ETE} sensitivity score for each effector gene resulted in an R^2 ≤0.02 in all cases (Appendix A Figure A.3).

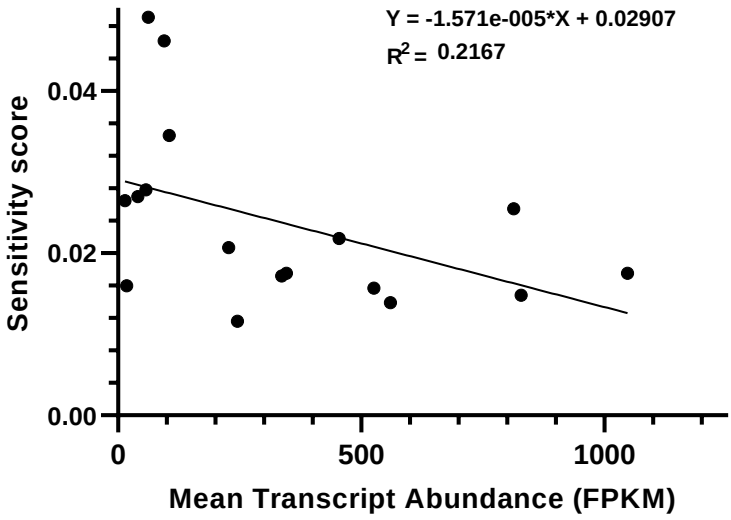

Figure 4.7: Scatter plot of mean transcript abundance against sensitivity score in CHO_{ETE}. The scatter plot shows the relationship between mean transcript abundance (calculated from Geoghegan et al. 2018) and the calculated sensitivity score in CHO_{ETE} for each effector gene. A linear regression was performed (black line) returning an R^2 of 0.217.

4.2.5.4 Differential sensitivity between CHO_{ETE} and $CHO_{BIS\text{-}A}$

Differential sensitivity was calculated by subtracting the respective σ^2_{IVCD}'s, σ^2_{Titre}'s and σ^2_{qP}'s in CHO_{ETE} from $CHO_{BIS\text{-}A}$ independently for each effector gene. Differential sensitivity was plotted in Figure 4.8 for IVCD (a), titre (b) and qP (c) with negative values (left protruding bars) indicating higher sensitivity in CHO_{ETE}, and positive values (right protruding bars) indicating higher sensitivity in $CHO_{BIS\text{-}A}$.

CHO_{ETE} demonstrated higher IVCD sensitivity than $CHO_{BIS\text{-}A}$ in response to 14 of 17 effector genes titrated suggesting a higher susceptibility to changes in growth rate. The magnitude of the differential sensitivity was low (<0.04) in the 3 genes (P4HB, PPIB and XBP1s) demonstrating higher growth sensitivity in $CHO_{BIS\text{-}A}$ relative to genes exhibiting greater sensitivity in CHO_{ETE}.

Of the five genes showing the greatest difference in titre sensitivity between cell lines, four are more sensitive in $CHO_{BIS\text{-}A}$ than CHO_{ETE}. Overall $CHO_{BIS\text{-}A}$ titre is more sensitive to effector gene titration, evidenced by a mean differential sensitivity of all 17 genes of 0.0018. Compet-

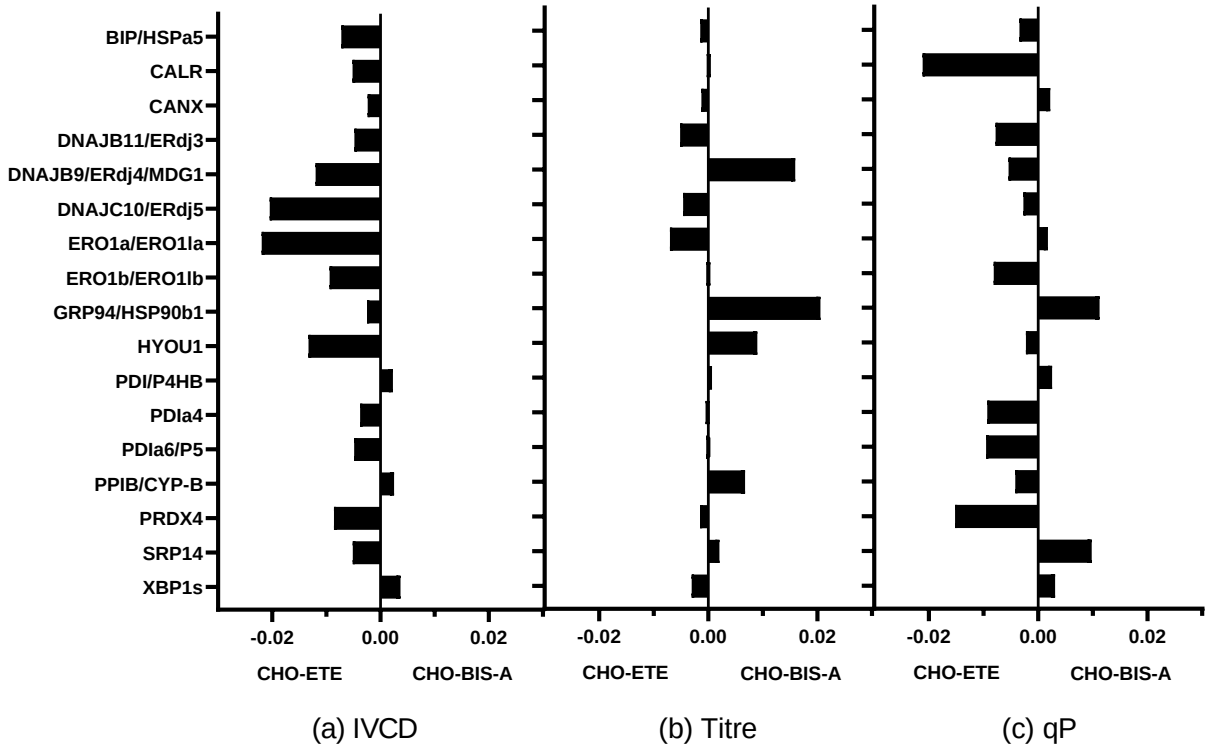

Figure 4.8: Assessing the differential sensitivity breakdown between $\mathbf{CHO_{ETE}}$ and $\mathbf{CHO_{BIS\text{-}A}}$ in response to effector gene titration.
Figure shows the difference in sensitivity to effector gene titration between CHO_{ETE} and $CHO_{BIS\text{-}A}$ for IVCD (**a**), titre (**b**) and qP (**c**). Differential sensitivity was calculated by subtracting Standard Deviation (StD) of the mean $\log_2$ fold changes at each titration point in CHO_{ETE} from $CHO_{BIS\text{-}A}$.

itively the mean differential sensitivity measured by IVCD was -0.0066 indicating CHO_{ETE} growth is more varied in response to effector gene titration.

When evaluating qP the mean difference in sensitivity was -0.0034, suggesting greater variation in mAb_{ETE} production rate in response to effector gene titration. Most effector genes (11 of 17) demonstrated greater qP variance in CHO_{ETE}, and a substantial skew towards $CHO_{BIS\text{-}A}$ was only seen in response to the titration of HYOU1 and SRP14.

4.3 Discussion

In a mAb production context, transient overexpression studies have identified a range of approaches and targets for the engineering of host CHO cell lines. It has become a key tool, as complex therapeutics push the limits of biological factories. The use of RNAi screening has also become common when studying the pathology of disease, allowing for rapid screening of genome scale libraries in cell models. However, due to restrictions discussed in chapter 3 RNAi previously had limited applicability to the optimisation of biopharmaceutical production pipelines. Therefore, this chapter is a case study exploring the applicability of the transient SOSC gene screening platform developed in chapter 3 as a tool to identify targets for host cell engineering.

The screening platform was applied to two clonal cell lines derived form the MEDI-CHO host, both producing mAbs of a differing modalities and production difficulties. The selection of CHO_{ETE} and $CHO_{BIS\text{-}A}$ were ideal candidates, predicted to experience different production bottlenecks and require differing engineering solutions. The DTE nature of $mAb_{BIS\text{-}A}$ aggregation had been characterised in Cao et al. 2018, providing a valuable resource to explain the effects of gene titration on $CHO_{BIS\text{-}A}$.

By screening two clonal production cell lines derived from a common host, an evaluation of the differential responses aimed to identify product specific reactions that could improve understanding of host cell adaption to different levels of chronic UPR stress. Shared responses and trends are likely the result of underlying characteristics and limitations in the common parental host. This chapter examines the shared and differential responses of CHO_{ETE} and $CHO_{BIS\text{-}A}$ to effector gene titration in order to identify generic host cell and mAb specific engineering targets in the MEDI-CHO genetic background.

4.3.1 Bioinformatic Effector Gene Library Identification

Step one in this study was to identify a library of effector genes for screening. Although numerous CHO overexpression studies with positive outcomes were available to compile a screening library, relevant CHO RNAi studies were sparse. However, with genetic engineering solutions being highly mAb and host cell specific, selecting successful effector genes from literature was unlikely to be fruitful.

An alternative approach was to bioinformatically select a library of effector genes. Although vast CHO bioinformatic resources are available with multiple genomes and expression datasets published, the high level of context specificity in CHO engineering solutions was still a concern. Fortunately an RNAseq transcriptomics dataset of cell lines derived from the MEDI-CHO background was generated by Geoghegan et al. 2018. Specifically the transcriptomes of CHO_{ETE} and MEDI-CHO *GS-NULL* cell lines were quantified during early (exponential) and late (stationary) phases of culture. By selecting effector genes based on the transcriptome changes observed in the MEDI-CHO host when challenged with stable mAb production, effector genes specific to the MEDI-CHO genetic background could be identified. Target identification from a context specific dataset allowed the results to be related back to the original transcriptome adaptations

during the cell selection process. This method still had limitations however, as when mapped, the RNAseq dataset only identified ∼80 % of the annotated CHOK1-GSKO genome leaving a reasonable chance that potent effector genes are absent.

The effector gene library scale was limited as the nature of genetic titration required many experimental conditions per gene, further exacerbated by the inclusion of two cell production models in the study. To maximize the probability that CHO_{ETE} and $CHO_{BIS\text{-}A}$ were responsive to each effector gene, a hypothesis driven approach was employed to identify a subset of the CHOK1GS genome closely associated with mAb production. A set of GO terms incorporating biological processes and molecular functions necessary for mAb production was selected in order to extract a list of genes associated with each term. These genes were aligned with the CHO-ETE RNAseq datset, resulting in identification of a subset of genes with a high probability of effecting mAb production when up- or down-regulated, which were known to be expressed in CHO-ETE.

The genome subset was then further reduced by identifying genes which were up- or down-regulated in the host cell line when presented with the challenge of stable mAb_{ETE} production. It was hypothesised that during the cell selection process genes were naturally up-regulated to overcome bottlenecks in production, therefore synthetic overexpression may increase mAb production capacity. Additionally, sensitivity to the knock-down of naturally up-regulated genes was predicted in response to the reimposition of such bottlenecks. Logically this hypothesis may hold true in reverse, with the knock-down of naturally down-regulated genes beneficially impacting production, with overexpression having detrimental effects.

Evaluation of the transcriptomics data revealed differential gene regulation between the producer and GS knockout control over time as culture conditions became detrimental. This suggests that the mAb producing cells have adapted their response to stresses that occur in late stage culture such as nutrient depletion, hypoxia and acidosis. Such genes that are also associated with mAb folding and assembly processes are also promising engineering targets.

The described hypotheses were translated into objective bioinformatic statements to extract genes from the genome subset. Prior to this, genes with low transcript abundances were removed. Low abundance genes risked skewing the data as small changes in transcript abundance translated to large fold-changes, especially as values approached zero. Manual evaluation identified two eliminated genes (*PDIA2* and *HSPA1*), which were commonly associated with mAb folding and assembly processes, further highlighting the limitations of a using a single context specific transcriptomics dataset.

4.3.2 Response of mAb Producing CHO Cells to RNAi

The data in this chapter suggested a generic IVCD increase in response to RNAi in both cell lines screened. In CHO_{ETE}, titre increased to a lesser extent resulting in a qP reduction, however in $CHO_{BIS\text{-}A}$ the qP was also higher.

These observations contradict the findings in Daga et al. 2018 which analysed the effect of small

interfering RNA (siRNA) transfection in whole-genome RNAi screens, who determined that the growth restricting effects observed were the result of off-target binding and hybridization-independent competition. The described findings from Daga et al. 2018 were limited to results from Hela cells, and no other studies to date have investigated the generic effect of RNAi on cell proliferation in more relevant cell models. The lack of literature suggests that the effects of RNAi on cell proliferation may be cell model specific, varying in effect and magnitude.

Competition between transfected siRNA and endogenous Micro RNAs (miRNAs) for RNAi machinery was also suggested by an examination of genome-wide transcript levels from 150 published experiments, finding that siRNA transfection led to increased expression of common miRNA targets (Khan et al. 2009). Exportin-5, responsible for nuclear-to-cytoplasmic transport of Double Stranded Ribonucleic Acid (dsRNA), has been identified by several studies as the probable competitive bottleneck post-siRNA transfection, causing inhibition of miRNA activity (Hutvágner et al. 2004; Yi et al. 2005). Additionally, the co-transfection of multiple siRNAs reduced the efficiencies of individual sequences, suggesting competition for RNAi silencing machinery (Castanotto et al. 2007).

All studied eukaryotic cells utilise miRNAs to regulate basic cellular functions including proliferation, differentiation, and apoptosis (H. W. Hwang and Mendell 2006). More than half of miRNAs are located at genomic sites frequently amplified, deleted, or rearranged in cancer, suggesting that miRNA abnormalities play a broad role in proliferation control and cancer pathogenesis (Calin et al. 2004). Therefore, it is likely that a generic reduction in miRNA activity will lead to altered proliferation rates, with effects specific to the cells genetic background.

Although reduced miRNA activity is hypothesised to be the dominant factor increasing CHO_{ETE} and $CHO_{BIS\text{-}A}$ growth rate after esiRNA transfection, this may not be exclusive. Introduction of dsRNA can lead to RNAi induced intracellular innate immune response impacting the cell transcriptome (Meng and Lu 2017). Additionally, it is possible that induction of RNAi machinery could be buffering the effects plasmid DNA induced toxicity associated with electroporation (Lesueur et al. 2016). As the non-sequence specific effects of DNA and dsRNA co-transfection have not been documented the probability or significance of such an effect occurring is unknown.

4.3.3 Generic Responses for Host Cell Engineering

A key objective for this work was to provide a case study to demonstrate the applicability of the HTP gene screening platform as a tool to identify generic engineering targets to increase cell growth and product yield in the MEDI-CHO host genetic background. Indeed, targets such as CALR, CANX, ERO1B, HYOU1 and PDIa6 improved the IVCD in both production cell lines. The extent and significance of this was more evident in CHO_{ETE} due generically higher growth sensitivity. ERDJ5 significantly increased mAb titre in both cell models, representing a novel CHO engineering target with no previous evidence supporting improved mAb production.

Uniquely from other CHO engineering studies, the incorporation of knock-down conditions provides information on the sensitivity of mAb production models to a reduction in effector gene expression. A common reduction in IVCD was most evident in response to ERDJ3 and

ERDJ5 knock-down, and ERDJ4 was the only effector gene to reduce titre in both CHO_{ETE} and $CHO_{BIS\text{-}A}$ in response to knock-down. This highlights the importance of the ERDJ family of proteins in generic mAb folding and assembly mechanisms, identifying them as very promising novel host cell engineering targets.

Despite data normalisation to account for the beneficial cell response to activation of RNAi pathways, performance improvements in both cell models were seen in response to overexpression and knock-down of ERO1B (IVCD) and ERDJ5 (titre and qP). These are most probably esiRNA sequence specific effects on the RNAi response in the MEDI-CHO genetic background, which by definition is difficult to account for. These findings are supported by Daga et al. 2018 which identified and modelled nucleotide composition dependent RNAi responses in mammalian cells. These were found to be independent of siRNA specific off target effects, and were unique to each cell model. Despite the use of esiRNAs reducing off-target silencing by an order of magnitude (Theis and Buchholz 2011) , the abundance of each nucleotide in the esiRNA cocktail is a function of the target messenger RNA (mRNA) sequence and will vary for each gene.

4.3.4 Product Specific Responses

Despite the common host background, the cell response to overexpression of some effector genes was very different, and in some cases even divergent. An abundance of effector genes were identified which, when overexpressed improved product titre and qP in $CHO_{BIS\text{-}A}$ and had negligible (ERDJ3, SRP14, XBP1s) or detrimental (GRP94) responses in CHO_{ETE} demonstrates increased engineerability in the DTE model system. This is further supported by the lack of positive effects on mAb_{ETE} production in response to overexpression. That is not to say transient effector gene overexpression is ineffective, in-fact ERO1A and P4HB improve IVCD only in CHO_{ETE}.

Detrimental CHO_{ETE} specific growth responses to knock-down were observed after the transfection of 6 effector genes (CANX, ERDJ4, ERO1A, GRP94, PDIa6 and SRP14), with no cell line specific decreases in IVCD seen in $CHO_{BIS\text{-}A}$. The absence of any effector gene manipulations having the greater a effect on $CHO_{BIS\text{-}A}$ IVCD provides further evidence of susceptibility to growth rate variation in the ETE model, and titre variability in the ETE model.

Titre reductions specific to mAb_{ETE} was seen in response to the knock-down of SRP14 and XBP1s. It was interesting that neither of these are directly involved with protein folding and assembly, and instead play roles in mRNA targeting and UPR regulation. It is unsurprising that the two genes in which mAb_{ETE} production was specifically more sensitive to knock-down (P4HB and ERO1B) both play key roles in disulphide bond formation, after Cao et al. 2018 identified size variants and antibody dimers forming as a result of incorrect cellular processing of the engineered disulfide bond.

4.3.5 Differential Sensitivity Between CHO_{ETE} and $CHO_{BIS\text{-}A}$

The relative magnitude of the responsiveness to manipulation of each effector gene (inclusive of overexpression and knock-down) in CHO_{ETE} and $CHO_{BIS\text{-}A}$ was determined through the calculation of sensitivity scores, to simplify comparisons. In general CHO_{ETE} tended to display greater growth rate fluctuations in response to the manipulation of effector genes, whereas $CHO_{BIS\text{-}A}$ growth was comparatively stable, and instead large variations in product titre were observed.

The higher mean sensitivity score in CHO_{ETE} appears to be the result of its high growth sensitivity exceeding the magnitude of the higher titre sensitivity displayed by $CHO_{BIS\text{-}A}$. When the differential sensitivity was broken down, the degree to which CHO_{ETE} is more sensitive to growth relative to $CHO_{BIS\text{-}A}$'s higher titre sensitivity became evident. Infact, titration of only 50 % of genes caused a higher σ_{titre} in $CHO_{BIS\text{-}A}$ and the mean σ_{titre} can be attributed to high variation seen in response to ERDJ4, GRP94, HYOU1. In comparison, 82.3 % of genes resulted in a greater σ_{IVCD} in CHO_{ETE} suggesting the growth sensitivity bias was more generic.

As both CHO_{ETE} and $CHO_{BIS\text{-}A}$ are derived from a common host, it is probable that differential responses and sensitivities seen are the effect of mAb specific traits such as sequence composition, folding and assembly pathways and the extent of UPR induction invoked. When considering the ETE nature of mAb_{ETE}, it is unsurprising that fewer ER engineering targets are able to improve titre or qP. Cellular bottlenecks are more likely to occur in gene transcription and subsequent mRNA processing than translation and protein folding. The susceptibility of $mAb_{BIS\text{-}A}$ production to such engineering targets is similarly unsurprising, with its DTE and aggregative nature arising from disulphide scrambling being a specific folding and assembly challenge.

Furthermore, the chronic ER, UPR and oxidative stresses associated with production of such a mAb may also explain the difference in magnitude of the growth responses. In order to survive and thrive under these conditions, $CHO_{BIS\text{-}A}$ most likely has dysregulated its stress response system to allow rapid cell proliferation in the presence of challenging ER conditions and an abundance protein aggregates in the secretory and ER-Associated Protein Degradation (ERAD) pathways. Therefore, any changes in growth rate arising from effector gene manipulation on level of ER, UPR or oxidative stress are likely to be buffered by the dysregulation of stress response pathways, reducing the magnitude of changes. Although dysregulation of stress response pathways is also likely in CHO_{ETE} relative to the MEDI-CHO host, the extent will be reflective of the significantly lower burden of an ETE mAb.

4.3.6 Identification of Engineering Targets from Host and Producer Transcriptomics Data

Transient gene overexpression or suppression is a common tool with broad applications in scientific and engineering contexts, and has been utilised to reveal mechanisms of biological processes, improve our understanding of disease pathology and solve a range of cell engineering challenges. From the varying approaches available to identify engineering targets for transient expression studies, a focus was placed on bioinformatic analysis of existing cell-line specific transcriptomics

data for this work. Although in the results described a significant number of generic and mAb specific engineering targets have been identified, it was not possible to identify a correlation between the experiential results and the bioinformatic analysis employed for effector gene selection.

The lack of a substantial correlation between CHO_{ETE} transcript abundance and the responsiveness to genetic manipulation of effector genes was unexpected. For genes known to be important in ER folding and assembly processes, it was hypothesised that genes of low abundance would be more responsive to overexpression due to larger fractional increases in transcript number relative to highly abundant targets. Similarly, the knock-down of low abundance transcripts should produce more efficient gene silencing and probability of the natural abundance being superfluous would be reduced. The absence of data supporting this hypothesis is not sufficient evidence to conclude that selecting genetic engineering targets based on differential regulation between cell hosts and daughter producers is ineffective, due to the scale and complexity of transcriptome changes during host cell adaption to stable mAb production.

4.3.7 Summary

The abundance of engineering targets identified relative to the modest effector gene library size demonstrates the success of a host-specific bioinformatic basis for effector gene selection, despite the lack of a statistical correlation back to the transcriptomics data. The described results demonstrate the added value and applicability of transient SOSC gene screening for CHO host and production cell line engineering. The additional dimension of information added through inclusion of effector gene knock-down identified positive responses to a reduction in transcript abundance, and revealed the sensitivity of CHO model systems to a reduced effector gene expression levels. However, several added complexities were encountered when employing RNAi alongside traditional overexpression methods, which would benefit from further characterisation.

Chapter 5

Investigating Proteostasis Regulators as Cell Culture Enhancers

This chapter explores the use of proteostasis regulators, identified from Plate, Cooley, et al. 2016, as Chinese Hamster Ovary (CHO) cell culture enhancers in Easy to Express (ETE) and aggregate prone Difficult to Express (DTE) Monoclonal Antibody (mAb) models. The chapter aims to evaluate the use of protein disaggregases in proteopathic disease models as CHO cell engineering tools. Evidence is provided for a broader evaluation of the hypothesis, justifying the incorporation of compounds associated with a diverse range of human diseases.

Initial evaluations in an ETE mAb model identified strong pharmacological responses when supplemented with two compounds, and demonstrated non-toxic growth arrest across the compound library. Further assessment in aggregate prone models found one compound was responsive with context specific growth and productivity enhancements identified. The second model was unresponsive to the supplementation of proteostasis regulators. Additionally, results suggested reduced effectiveness upon delayed supplementation, hypothesised to be a result of active compound internalisation. This was confirmed through further evaluation in the ETE producing CHO model system, where titre and productivity were increased by 1.2 fold and 1.6 fold respectively.

The data presented supports the use of proteostasis regulators as cell culture enhancers during the stationary phase of culture, and provides strong justification for the further exploration of proteopathic disaggregases as CHO engineering tools.

5.1 Introduction

Steadily improving CHO cell factories for the production of therapeutic proteins remains a key challenge to meet increasing demands for the biopharmaceutical sector (Barnes and Dickson 2006; Butler and Meneses-Acosta 2012).

Therefore, development and implementation of novel engineering tools are required to enable cost-effective and efficient generation of high-yielding CHO cell factories. Methods employed to increase bio-therapeutics production and counteract the limitations of mammalian cell factorie include; engineering the host cell (Budge et al. 2020; Fischer and Otte 2019; N. Lin et al. 2015) or expression vector (Bayat et al. 2018; Brown and James 2016; Jazayeri et al. 2018; Patel 2018; Wang and X. Guo 2020), optimization of culture medium and feeding strategies (C. Altamirano et al. 2004; Gifford et al. 2005; Ritacco et al. 2018), culturing the cells at low temperature (C. Altamirano et al. 2004; Gifford et al. 2005; Kumar et al. 2008; Ritacco et al. 2018; J. Xu et al. 2019), and the addition of Small Molecule Enhancers (SMEs) (Camire et al. 2017; Chang et al. 2020; Kalsi 2018; Mortazavi et al. 2019).

From the engineering approaches described, genetic engineering and SMEs are the most applicable to improving the production of problematic biotherapheutics. In comparison to genetic engineering approaches, the screening of compound libraries to identify SMEs is faster, cheaper and more practical to scale-out to additional CHO host and producer cell lines. Additionally, SMEs can be supplemented at any point in the cell culture process, allowing indirect regulation of cell culture characteristics. Although inducible transgene expression systems such as Tet-On (Das et al. 2016), lentiviral-induction (Shuen et al. 2015) and a cumate gene-switch (Mullick et al. 2006) have been developed for mammalian cells, none have been used in the production of biologics approved for use in humans (Kallunki et al. 2019; Weber and Fussenegger 2004).

Examples of SMEs improving the production of therapheutic proteins in CHO cells include S. J. Hwang et al. 2011; Johari et al. 2015; Mortazavi et al. 2019; Rahimpour 2017, yet studies focusing on aggregate prone molecules are limited. Chemical biologic strategies have recently been utilised to identify compounds which can independently activate the *IRE1*, *XBP1s* or ATF6 branches of the Unfolded Protein Response (UPR) to physiologic levels in cell models of proteopathic disease (Grandjean et al. 2020; Plate, Cooley, et al. 2016). Termed proteostasis regulators, these compounds have revealed unique contributions of *IRE1*, *XBP1s* and *ATF6* activation to remodelling of the Endoplasmic Reticulum (ER) environment.

Emerging information is demonstrating the anti-aggregative properties of proteostasis regulators in branch-dependent UPR regulation in disease models (Plate and Wiseman 2017). It may be possible that some of these effects are equally beneficial in production of complex mAbs, where unnatural products cause elevated levels of intracellular stresses. It was hypothesised that similar mechanisms underpin the management of prion mediated aggregates, and the intracellular aggregation of engineered mAbs.

In this chapter a group of compounds identified in Plate, Cooley, et al. 2016 are assessed in ETE and DTE mAb producing CHO cell lines to investigate their efficacy as cell culture enhancers.

5.2 Results

5.2.1 Proof of Concept Assessment of Proteostasis Regulators Effect on ETE mAb production

The compounds shown in Table 5.1 are seven of the top eight proteostasis regulators identified by Plate, Cooley, et al. 2016 which were selected for screening in mAb producing CHO cells. This Proof of Concept (POC) study aimed to justify the time and resources required for evaluation in aggregative DTE CHO production sytstems, whose use was restricted to AstraZeneca facilities at the time.

Table 5.1: Compounds selected from Plate, Cooley, et al. 2016 for use as CHO cell culture enhancers.
Compound indexes displayed have been assigned for this work alongside the IUPAC name of each proteostasis regulator. The ERSE-FLuc reporter assay measures activation of the ATF6 arm of the UPR, and XBP1-RLuc general UPR induction, both expressed as %relative to UPR stress induced by 6.8 μM Thapsigargin. Further information on the source, CAS-NO and molecular weight of each compound can be found in Appendix C.

Index	IUPAC Name	%ERSE-FLuc*	%XBP1-RLuc*
C1	4-bromo-N'-butylbenzohydrazide	60.9 ± 6.0	9.1 ± 0.7
C2	1-(4-fluorophenyl)-3-[(2-hydroxy-5-methylphenyl)amino]-2-propen-1-one	140.1 ± 17.4	10.3 ± 7.9
C3	N-(2-hydroxy-5-methylphenyl)-5-propylisoxazole-3-carboxamide	83.4 ± 6.3	24.5 ± 4.7
C4	N-(2-hydroxy-5-methylphenyl)-3-phenylpropanamide	63.2 ± 0.6	17.5 ± 1.9
C5	N-(2-hydroxy-5-methylphenyl)-2-((5-methyl-4-nitro-1H-pyrazol-3-yl)thio)acetamide	52.5 ± 14.3	16.6 ± 2.4
C6	3-(3-chlorophenyl)-5-(4-hydroxybenzylidene)-2,4-imidazolidinedione	68.2 ± 5.7	61.1 ± 1.5
C7	2-hydroxybenzaldehyde-(4-nitrophenyl)hydrazone	20.7 ± 2.3	2.4 ± 1.0

The POC screen was performed in an ETE mAb model to determine the active concentrations of each compound and evaluate their effects in an optimised and well characterised production system. This aimed to ensure that the tested chemicals did not induce excess cytotoxicity or negatively impact the production of mAb_{ETE}. It was hypothesised that proteostasis regulators which can alleviate antibody aggregation would have minimal impact on expression of ETE mAbs. These lack any of the protein folding and assembly bottlenecks associated with DTE mAbs, and do not suffer from chronic UPR stress induced by protein aggregates.

The effects of the proteostasis regulators on cell growth and mAb_{ETE} titre were evaluated experimentally by performing a 6 or 7 point titration at concentrations ranging from 0.63 μM to 40 μM. Cells were seeded at a density of 0.4×10^6 cells.ml^{-1}, and chemical supplements were added immediately. Cultures were incubated for 5 days in shaken 96-Deep Well Plates (DWPs) with a total culture volume of 475 µl. The resultant growth was measured by PrestoBlue assay

and mAb_{ETE} titre was assessed using the ValitaTITER assay with results shown in (Figure 5.1). The cell viability of specific conditions of interest were measured on day 5 by ViCell to assess the cytotoxicity of the compounds.

Dimethyl Sulfoxide (DMSO) was the solvent used for compound storage, therefore DMSO control conditions were set up to evaluate the excipient effects on culture performance. These included $0.2\,\%_{(v/v)}$ DMSO, equivalent to the maximum volume added when screening at $40\,\mu M$, and $0.68\,\%_{(v/v)}$ DMSO replicating the control concentration employed by Plate, Cooley, et al. 2016. These can be seen to the left of each graph in Figure 5.1. The negative DMSO control results are included in each panel (a-g) for subjective comparison to the experimental conditions. Due to practical limitations at the time of this work, a full 7 point DMSO titration was not completed, limiting the statistical evaluations possible. The minimal changes to growth and titre between the 0.0 % (negative) and 0.2 % (equivalent to $40\,\mu M$) DMSO controls were negligible relative to the response to proteostasis regulator supplementation. Therefore, it was not necessary to account for the impact of DMSO on culture performance when interpreting the proteostasis regulator titrations.

Increasing concentrations of C1 (Figure 5.1a) in CHO_{ETE} resulted in dis-linkage between the relative cell growth and mAb_{ETE} titre, most likely resulting in an increased Specific Productivity (qP). This was most evident at concentrations ranging from $5.00\,\mu M$ to $20\,\mu M$. The mean cell viability measured on day 5 was 96.4 % in $10\,\mu M$ and 71.4 % in $40\,\mu M$ C1 supplemented cultures, indicating that cytotoxicity was minimal despite the reduced growth rate.

Titration of C2 demonstrated a sharp decline in growth and titre between $5.00\,\mu M$ and $10.00\,\mu M$. Cell growth relative to titre was unchanged throughout the titration, suggesting that C2 does not impact qP. The mean day 5 cell viability of cultures supplemented with $10\,\mu M$ C2 was 83.2 % suggesting a non-toxic inhibition of cell growth, whereas $40\,\mu M$ C2 supplemented culture cell viability was 24.0 % indicating a high level of cytotoxicity. In comparison to C2, C5 shows a linear reduction in both cell growth and titre at comparable rates, although at concentrations $\geq 5.00\,\mu M$ titre is slightly reduced relative to growth, and the mean day 5 cell viability of $40.00\,\mu M$ C5 supplemented cultures was 96.9 %.

C6 and C7 notably reduced CHO_{ETE} growth and titre as compound concentrations were increased. Despite cell growth or mAb_{ETE} production from cultures supplemented with $40\,\mu M$ C6, cell viability remained high at 91.8 %. Comparatively, viability was reduced to 28.9 % in $40\,\mu M$ C7 cultures. Lastly no notable trends were observed in response to titration of C3 or C4 and cell viability remained ≥ 90.0 % at the highest concentration tested.

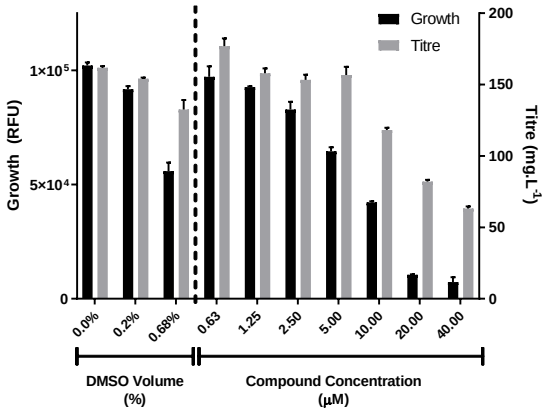

(a) C1

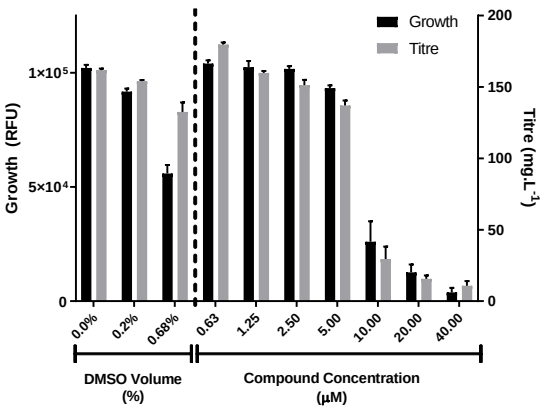

(b) C2

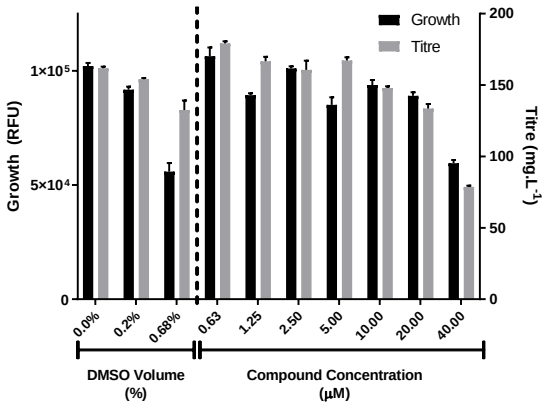

(c) C3

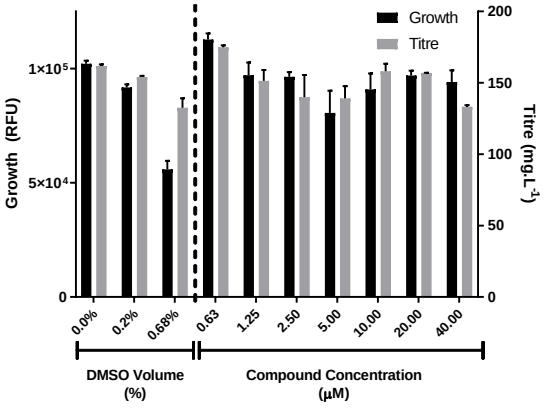

(d) C4

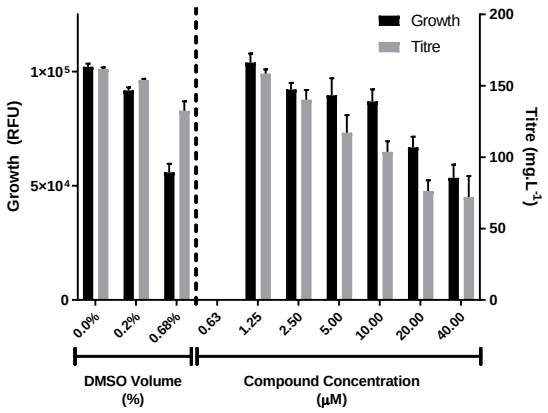

(e) C5

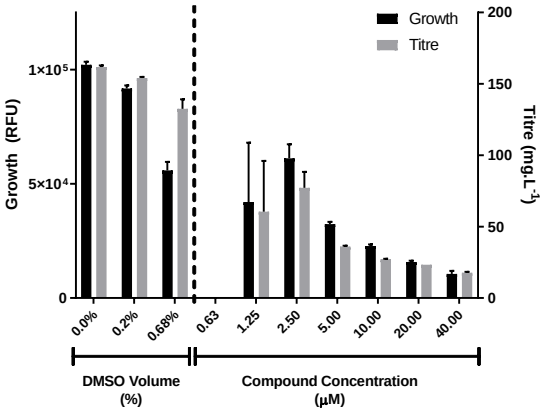

(f) C6

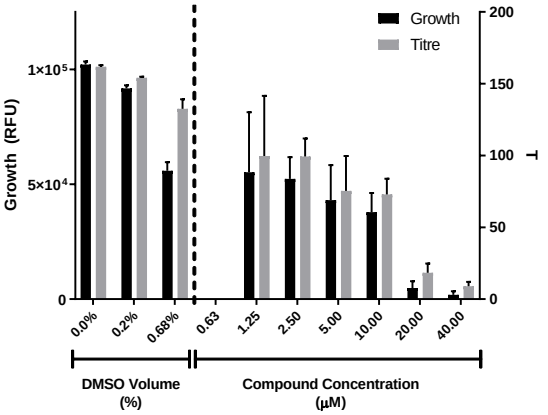

(g) C7

Figure 5.1: Preliminary assessment of proteostasis regulators in $\mathbf{CHO_{ETE}}$.
Cells were incubated for 5 days with 0.625 μM to 40 μM of the proteostasis regulators C1 to C7 (**a** to **g**) identified from Plate, Cooley, et al. 2016 to evaluate their effect on growth (black) and mAb titre (grey) in an ETE production model. Further details on the compounds are highlighted in Table 5.1. The 0.2 $\%_{(v/v)}$ DMSO control, of equal volume to 40.00 μM compound supplementation, is included depicting the maximal effect of the solvent relative to the compounds. A 0.68 $\%_{(v/v)}$ DMSO control was used in Plate, Cooley, et al. 2016 and has been included for reference. Data shows the mean and Standard Deviation (StD) of $n = 3$ technical replicates.

At the concentrations in which proteostasis regulators C1 and C2 greatly reduced cell growth rate, viability was uncompromised. Additionally, cell viability was unaffected at the highest concentrations of C5, C6 and C7 tested where growth was greatly inhibited. From these results it was hypothesised that the proteostasis regulators would be better utilised if supplemented later in the culture period, during the late-exponential or stationary phases of culture. Delayed supplementation could increase the rate of mAb production directly, or indirectly by arresting cell growth before the stationary phase is naturally reached, redirecting cellular resources.

The results described in Figure 5.1 demonstrated a complex pharmacological response in CHO_{ETE} upon titration of C1 and C2. Furthermore, titration C5, C6 and C7 resulted in a visible dose response curve. Together these provided sufficient evidence to justify further time and resource allocation, for evaluation of the seven proteostasis regulators in DTE cell models with aggregative characteristics.

5.2.2 Evaluating the Effect of Proteostasis Regulators on Bi-specific mAb Production

5.2.2.1 Identification of experimental parameters

Following the successful POC screen in CHO_{ETE}, which evaluated proteostasis regulators identified by Plate, Cooley, et al. 2016, a further evaluation was conducted in two DTE mAb producing cell lines known to suffer from product aggregation. From previous results described in section 5.2.1, three tailored screening concentrations were selected for each proteostasis regulator so the 'middle' concentration resulted in $\geq$50 % cell growth relative to the control in CHO_{ETE}. The reduced number of compound concentrations allowed for three compound supplementation time-points to be evaluated simultaneously, to investigate the concluding hypotheses from section 5.2.1.

The proteostasis regulators were evaluated experimentally on $CHO_{BIS\text{-}A}$ and $CHO_{BIS\text{-}B}$ in 13 day fed-batch overgrows in shaken 24-Shallow Well Plates (SWPs) on-site at AstraZeneca. Cells were seeded at 0.7×10^6 cells.ml^{-1} and feed was added every other day starting on day three. Proteostasis regulators were supplemented on days 0, 5 or 9 post seed, and the concentrations are described in Table 5.2. The Viable Cell Density (VCD) and viability of cultures were assessed by trypan staining measured on the Cellavista. Samples were sent for titre analysis by Octet on day seven and at culture harvest.

Table 5.2: Screening concentrations of compounds in 5.1 in bispecific cell lines.
Concentrations have been selected based on data presented in 5.1 to give optimal responses.

Index	High (μM)	Med (μM)	Low (μM)
C1	10.00	5.00	1.5
C2	10.00	5.00	2.50
C3	40.00	10.00	5.00
C4	40.00	10.00	2.50
C5	10.00	5.00	1.25
C6	2.50	1.00	0.50
C7	2.50	1.00	0.50
DMSO	$0.20\%_{(v/v)}$	$0.05\%_{(v/v)}$	$0.00\%_{(v/v)}$

5.2.2.2 Investigating and control for the effects of DMSO as a solvent for proteostasis regulators

Results described in section 5.2.1 demonstrated that $0.20\,\%_{(v/v)}$ DMSO had minimal impact on CHO_{ETE} growth or mAb_{ETE} titre. It was important to ensure that this was true in $CHO_{BIS\text{-}A}$ and $CHO_{BIS\text{-}B}$, and employ the correct data normalisation if required. This was most relevant for compounds C1, C2 and C5 where $40.00\,\mu$M concentrations were to be evaluated, equating to $0.20\,\%_{(v/v)}$ DMSO in the cultures.

As highlighted in Table 5.2, three control conditions were selected with DMSO concentrations ranging from $0.0\,\%_{(v/v)}$ to $0.20\,\%_{(v/v)}$, and were replicated for each time-point of proteostasis regulator supplementation. The effects of DMSO on $CHO_{BIS\text{-}A}$ and $CHO_{BIS\text{-}B}$ Integral Viable Cell Density (IVCD), titre and qP are shown in Figure 5.2.

A Dunnett's corrected multiple comparisons test was performed comparing the effect of $0.05\,\%_{(v/v)}$ and $0.20\,\%_{(v/v)}$ DMSO to the $0.00\,\%_{(v/v)}$ negative control. This was run independently for IVCD, titre and qP, at each supplementation time point. The described analysis did not identify any statistically significant effects of $0.05\,\%_{(v/v)}$ and $0.20\,\%_{(v/v)}$ DMSO on the performance of either $CHO_{BIS\text{-}A}$ or $CHO_{BIS\text{-}A}$. Differences observed in the negative control performance from day 0, 5 and 9 which were treated identically are the result of plate-to-plate variability, highlighting the limitations of High Throughput (HTP) culture platforms.

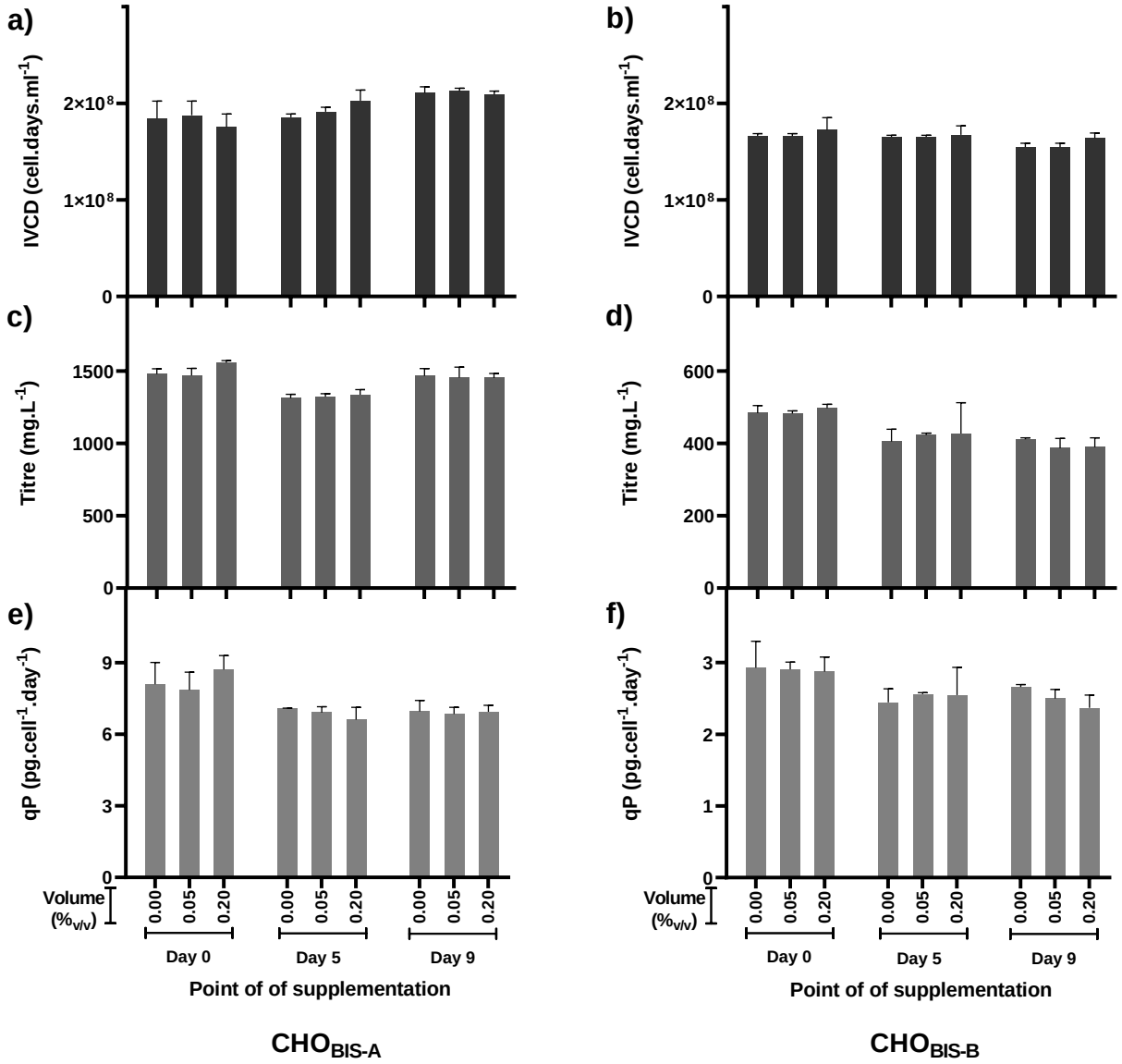

Figure 5.2: Effect of DMSO on $CHO_{BIS\text{-}A}$ and $CHO_{BIS\text{-}B}$ growth and productivity. Cultures were supplemented with DMSO 0, 5 or 9 days post seeding. Culture IVCD (**a**+**b**), titre (**c**+**d**) and qP (**e**+**f**) were calculated after 13 days for $CHO_{BIS\text{-}A}$ and $CHO_{BIS\text{-}A}$. The highest DMSO concentration ($0.2\,\%_{v/v}$) is equal in volume to the maximum supplemented compound concentration ($40\,\mu M$). A Dunnett's test was performed on the DMSO controls relative to the negative control at each addition point. No statistically significant effects on IVCD, titre or qP were identified in either $CHO_{BIS\text{-}A}$ or $CHO_{BIS\text{-}A}$.

5.2.2.3 Performance of proteostasis regulators as enhancers of DTE mAb production

The results from proteostasis regulator screening are displayed in Figures 5.3 and 5.4 for $CHO_{BIS\text{-}A}$ and $CHO_{BIS\text{-}B}$ respectively. It was not possible for triplicates of all the experimental (3 concentrations, 3 addition points) and negative control conditions to be compared on the same 24-SWP. Therefore, the results are plotted as absolute IVCD (Figure 5.3a + Figure 5.4a), titre (Figure 5.3b + Figure 5.4b) and qP (Figure 5.3c + Figure 5.4c). No effects as a result of the DMSO solvent were identified in section 5.2.2.2, therefore the negative and DMSO controls were analysed as a single population, represented by the dashed and dotted lines which are the mean and StD of 54 cultures.

A statistically significant improvement in $CHO_{BIS\text{-}A}$ IVCD was observed upon supplementation of proteostasis regulators C2, C6 and C7, with the former two being the most substantial. None of these conditions increased titre above the control mean resulting in a net reduction in qP for these conditions. No significant increases in $CHO_{BIS\text{-}A}$ titre were identified from the addition of any proteostasis regulators at any of the three supplementation time-points tested. Two conditions significantly improved $CHO_{BIS\text{-}A}$ qP relative to the controls; these were 5.00 μM C1 and 40.00 μM C4 when supplemented on day 0 of culture. Both of these are a result of significantly reduced IVCD with the change in titre being negligible or of lower magnitude.

Based on the data described, the proteostasis regulators were ineffective $CHO_{BIS\text{-}A}$ engineering tools, and the only net positive effects identified were improved IVCD in response to highly specific C2, C6 or C7 supplementation. In comparison, $CHO_{BIS\text{-}B}$ was more responsive to supplementation of proteostasis regulators, and a greater number of performance improvements and impairments were observed.

$CHO_{BIS\text{-}B}$ IVCD was significantly increased by supplementation of C1, C2, C4, C5 and C6 at one or more concentrations or time-points. Although 4 of 12 conditions identified significantly reduced qP, no significant titre reductions were seen relative to the control population. The only condition which significantly increased $CHO_{BIS\text{-}B}$ titre was supplementation of 40.00 μM C3 on day 5. This did not reduce IVCD resulting in a 1.6 fold increase in qP. Although non-significant, 10.00 μM of C3 produced the second largest titre increase, increasing qP to a similar extent.

It was evident from both $CHO_{BIS\text{-}A}$ and $CHO_{BIS\text{-}B}$ datasets that the compound effect was reduced when added later in culture, with results trending towards to the control population mean. This occurred for both increases or decreases in IVCD, titre and qP. It was hypothesised that cultures were responding based on the compound 'dose-per-cell', rather than the absolute concentration in the culture. This suggested that the compounds were being actively transported into the cells, as passive diffusion across the cell membrane would be largely unaffected by changes in cell number. Therefore, screening compounds at a higher concentration when supplementation is delayed may be more efficacious.

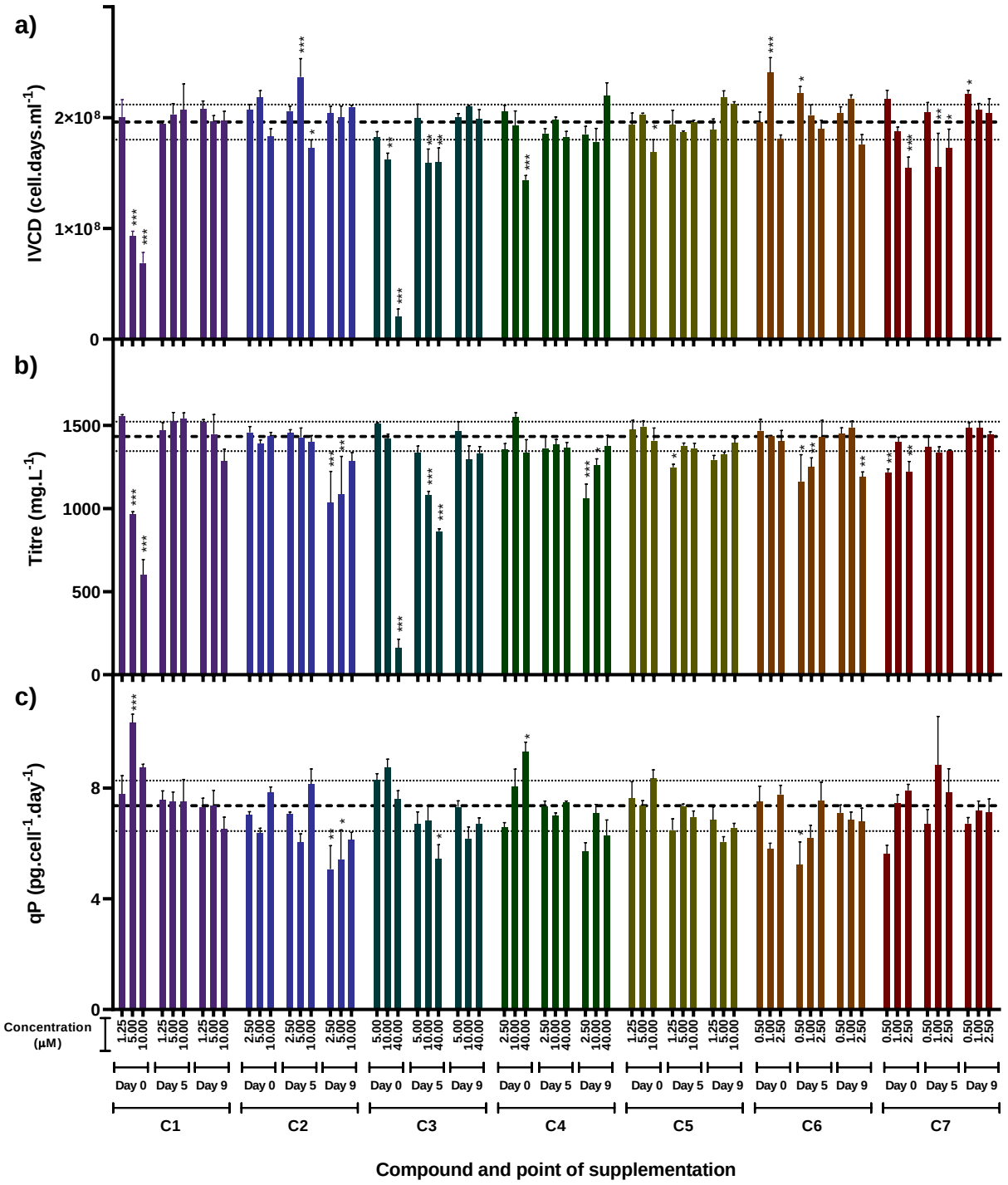

Figure 5.3: Effect of proteostasis regulators on $CHO_{BIS\text{-}A}$ growth and productivity. The seven proteostasis regulators were evaluated in $CHO_{BIS\text{-}A}$ at three concentrations when supplemented at three different time points. Compounds were supplemented either 0, 5 or 9 days post seeding and culture IVCD (**a**), titre (**b**) and qP (**c**) were calculated after 13 days. The concentrations screened for each compound were informed by the previous results in an ETE mAb model and can be found in Table 5.2. The dashed and dotted lines represent the mean and StD of $n = 54$ control cultures. The data displayed is the mean and StD of $n = 3$ technical triplicates. Significance, represented by $*(P < 0.05)$, $**(P < 0.01)$, or $***(P < 0.001)$, was calculated by t-test followed by a Holm-Sidak adjustment to allow for multiple comparisons.

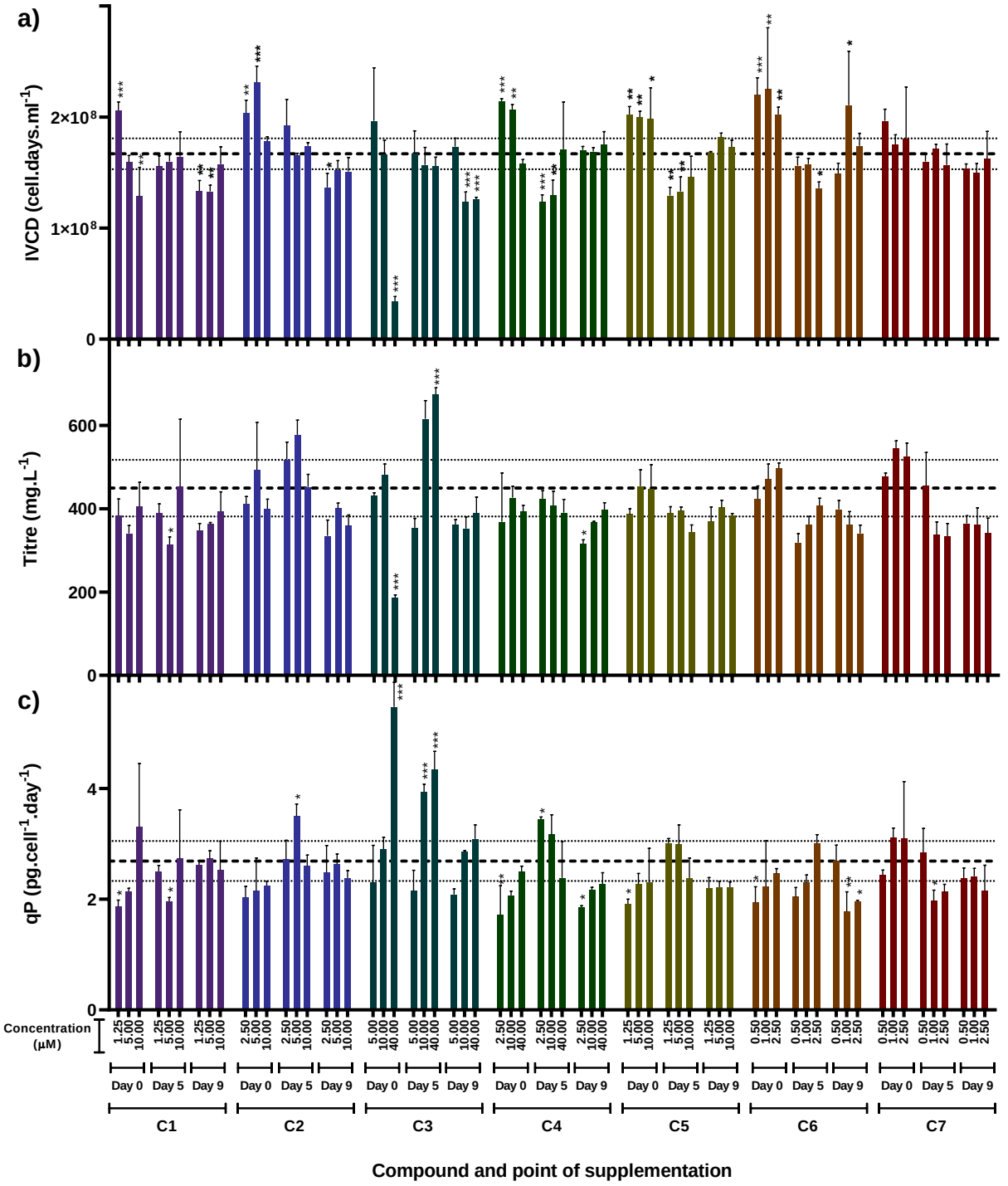

Figure 5.4: Effect of proteostasis regulators on $CHO_{BIS\text{-}B}$ growth and productivity. The seven proteostasis regulators were evaluated in $CHO_{BIS\text{-}V}$ at three concentrations when supplemented at three different time points. Compounds were supplemented either 0, 5 or 9 days post seeding and culture IVCD (**a**), titre (**b**) and qP (**c**) were calculated after 13 days. The concentrations screened for each compound were informed by the previous results in an ETE mAb model and can be found in Table 5.2. The dashed and dotted lines represent the mean and StD of $n = 54$ control cultures. The data displayed is the mean and StD of $n = 3$ technical triplicates. Significance, represented by $*(P < 0.05)$, $**(P < 0.01)$, or $***(P < 0.001)$, was calculated by t-test followed by a Holm-Sidak adjustment to allow for multiple comparisons.

Select $CHO_{BIS\text{-}A}$ supernatant samples were sent for aggregate analysis by AstraZeneca's Bio-Process Analytics team, to evaluate any changes to the rate of mAb aggregation. $CHO_{BIS\text{-}B}$ samples could not be assessed due to the minimum titre requirements not being met at the time. Figure 5.5 shows the $mAb_{BIS\text{-}A}$ monomer abundance for the control and experimental populations. No measurable or statistically significant change in aggregation rate was observed upon titration of any proteostasis regulators.

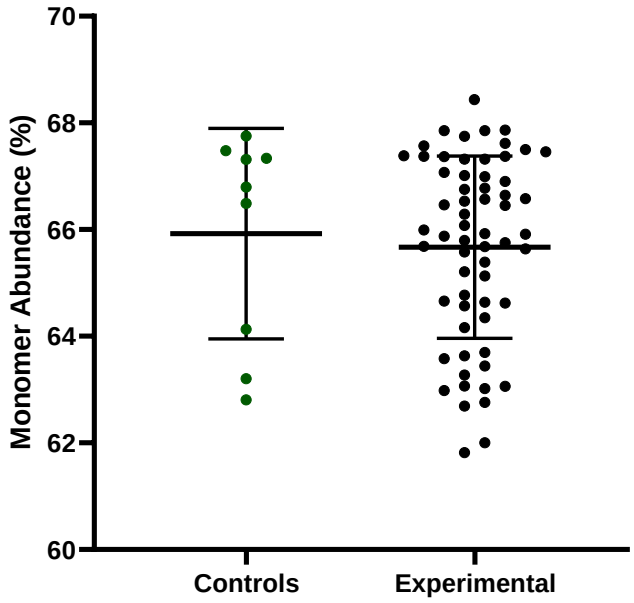

Figure 5.5: Overview of the proteostasis regulators effect on $CHO_{BIS\text{-}A}$ aggregation. Monomer abundance, expressed as a percentage of total mAb, is shown for control (green) and experimental conditions (black) inclusive of all supplementation time points. Controls include both negative and DMSO conditions. The experimental group includes representative samples from all seven proteostasis regulators. Error bars show the population mean and StD.

5.2.3 Increasing Compound Concentration in a 'Dose Per Cell' Dependent Manner

CHO_{ETE} was selected to evaluate whether delaying supplementation required higher compound concentrations, due to a 'dose-per-cell' effect. If this hypothesis was correct, the data from Figure 5.1a suggested that delayed addition of C1 at a suitable concentration would increase titre and qP. By allowing the cells to reach late exponential phase before supplementation the growth limiting effects of C1 would be negated.

Delayed addition of C1 in CHO_{ETE} was scaled up to 125 ml Erlenmeyer flasks offering better cell culture conditions than the HTP screening platform at the time, which was in 96-DWPs. Cells were seeded at 1.0×10^6 cells.ml^{-1} at a volume of 30 ml and were fed every third day starting from day 3. Concentrations ranging from 20 μM to 160 μM of the proteostasis regulator C1 were supplemented on day 5 of culture. VCD and cell viability was measured daily from the point of chemical supplementation, and mAb_{ETE} titre was assessed by ValitaTITER assay at harvest on day 10. A mock experiment was completed in parallel supplementing only 0.1 $\%_{(v/v)}$ to 0.8 $\%_{(v/v)}$

DMSO. Figure 5.6 depicts the results with IVCD, titre and qP expressed as a fold-change of the paired DMSO controls.

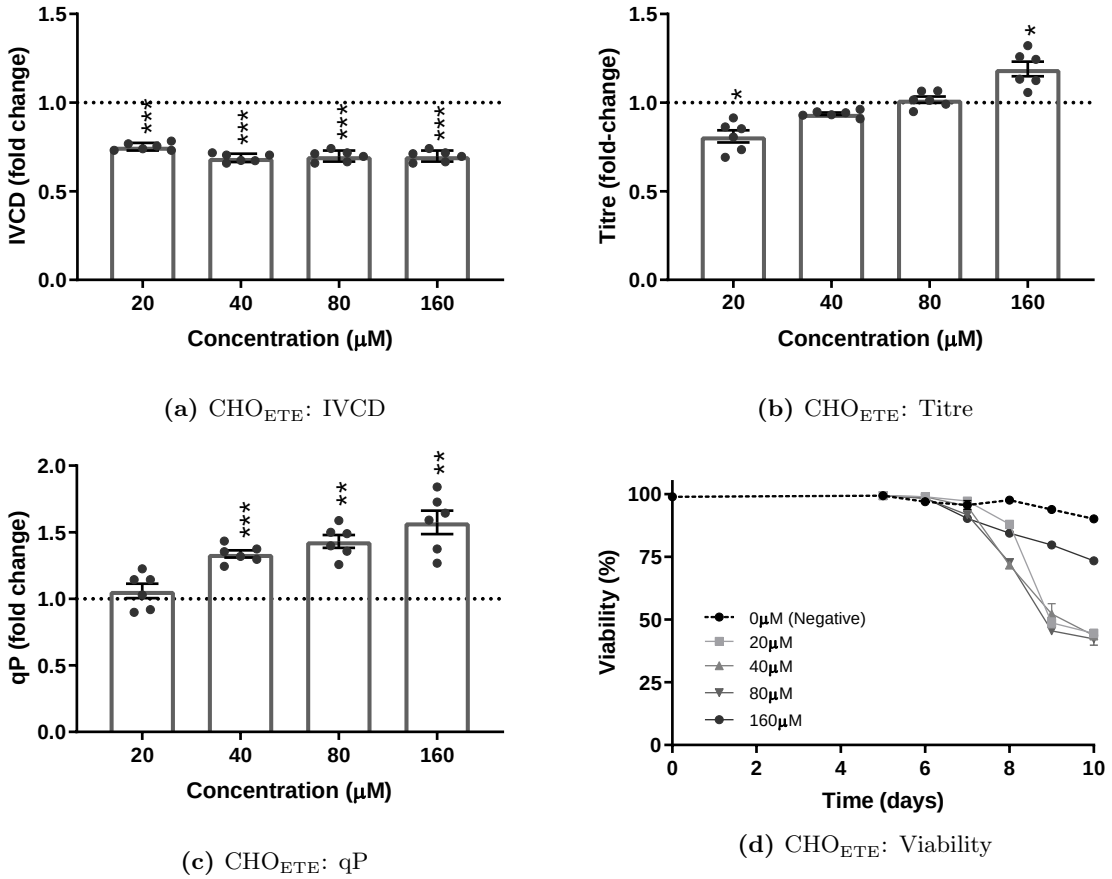

(a) CHO_{ETE}: IVCD

(b) CHO_{ETE}: Titre

(c) CHO_{ETE}: qP

(d) CHO_{ETE}: Viability

Figure 5.6: Scaled up evaluation of the proteostasis regulator C1 mid-culture in CHO_{ETE}. The proteostasis regulator C1 was supplemented at concentrations ranging from 20 μM to 160 μM on day 5 of 10-day fed-batch CHO_{ETE} cultures in Erlenmeyer flasks. Culture IVCD (**a**), titre (**b**) and qP (**c**) are expressed as a fold-change of 0.1 $\%_{(v/v)}$ to 0.8 $\%_{(v/v)}$ DMSO controls run in triplicate. Cell viabilities (**d**) are plotted as absolute values for comparison against the negative control. The data displayed is the mean and Standard Error of the Mean (SEM) of $n = 6$ replicates, comprising of technical triplicates of biological duplicates. Significance, represented by *($P < 0.05$), **($P < 0.01$), or ***($P < 0.001$), was calculated by unpaired students t-test between the matched experimental and DMSO control conditions.

The proteostasis regulator C1 significantly reduced the IVCD of CHO_{ETE} relative to the matched DMSO control at the four concentrations evaluated (Figure 5.6a). The mean IVCD was consistently reduced to between 0.68 fold and 0.70 fold of the DMSO controls when C1 was supplemented at 40 μM to 160 μM concentrations.

A decrease in mAb_{ETE} titre was observed upon supplemetation of 20 μM C1, whereas supplementation of 160 μM C1 increased mAb_{ETE} titre (Figure 5.6b). This resulted in no significant change in qP when C1 was supplemented at 20 μM and increases from 1.3 fold to 1.6 fold at concentrations $\geq$40 μM (Figure 5.6c).

The results in Figure 5.6 demonstrate that when the C1 is supplemented late in culture, higher concentrations are required to achieve pharmacological activity. This is most likely due to active internalisation of C1 by CHO cells, resulting in a lower dose-per-cell when C1 is added late in

culture relative to early culture.

5.3 Discussion

This chapter describes an investigation into the use of disaggregases in models of proteopathic disease as CHO cell culture enhancers. It was hypothesised that the mechanisms underlying aggregation in human neurological disease are similar to those seen in engineered mAbs. A group of compounds identified by Plate, Cooley, et al. 2016 were evaluated as a POC investigation, aiming to test the hypothesis and justify evaluation in a broader context. The seven proteostasis regulators had been shown to selectively activate the *ATF6* arm of the UPR in Human Embryonic Kidney 293 (HEK293) calls, and reduce TTR and light-chain aggregates in cell models of disease.

5.3.1 Initial evaluation in an ETE mAb model

The first step was to evaluate the proteostasis regulators in an ETE mAb producing cell model, in order to identify their pharmacologically active range and assess their impact on growth and titre. Initial screening in CHO_{ETE} identified a 50 % reduction in cell growth upon supplementation between 2.5 μM and 40 μM for six of the seven compounds. Minimal changes were observed between the negative and 0.2 % DMSO controls, demonstrating the excipient had minimal effects on culture performance at the proteostasis regulator concentrations supplemented, and subsequent data normalisation was not required.

As cell growth was not measured throughout culture, IVCD calculated from only day 0 and day 5 measurements would be unreliable estimations of a CHO cell culture sigmoid growth curve. It is more accurate to describe the reduction of PrestoBlue as a measure of cumulated cell metabolic activity. The PrestoBlue assay is an indirect measurement of viable cell number under the assumption that cellular metabolic rate is constant across experimental conditions. By definition, proteostasis regulators alter the turnover and composition of the ER proteostasis network, and are likely to change the cellular metabolic rate (T. W. Mu et al. 2008). For these reasons cell growth was expressed in Relative Fluorescence Units (RFU) taken directly from the PrestoBlue assay, and qP was not calculated. Resultantly, the rate of mAb_{ETE} production can only be inferred for the initial proteostasis regulator evaluations.

The dis-linking of titre and growth in response to C1 titration suggested a direct impact on the rate of mAb_{ETE} production, however neither growth nor titre increased above the control, highlighting the growth limiting effects of the compound. Defined pharmacological dose response curves were also observed upon titration of C2, in which a strong activation threshold reduced growth and titre by >3 fold between adjacent titration points. Although a negative correlation between compound concentration and growth was observed upon titration of C5, C6 and C7, no other unique pharmacologic effects were observed.

A strong inhibition of cell growth without a reduction in cell viability was observed throughout the dataset. Despite efforts to increase CHO growth rate and qP through media optimisation and nutrient supplementation (Claudia Altamirano et al. 2006; Graham et al. 2019; Pan et al. 2017; Pérez-Rodriguez et al. 2020), additional biomass generation can have negative consequences. This can complicate downstream product purification steps and increase lactate levels,

negatively impacting mAb quality (Freund and Croughan 2018; L. Zhang et al. 2019). Therefore, a balance between biomass generation and mAb production is needed to maximise overall yield in a resource limited system such as a bioreactor (Pérez-Rodriguez et al. 2020). It was hypothesised that the compounds would be better utilised when supplementation was delayed until the late exponential phase of culture, facilitating an early resource allocation shift towards mAb production, improving overall product yield.

5.3.2 Variable time of addition in DTE mAb models

It was initially hypothesised that disaggregases in human disease models would be efficacious in alleviating the aggregation in CHO cells producing DTE mAbs. Therefore, a more detailed experimental evaluation of the proteostasis regulators identified from Plate, Cooley, et al. 2016 was conducted in $CHO_{BIS\text{-}A}$ and $CHO_{BIS\text{-}B}$. Both bi-specific models suffer from significant product aggregation, and $CHO_{BIS\text{-}B}$ aggregates have been attributed to disulfide cross-bridge formation between engineered cysteine residues, leading to stable head-to-tail dimerisation (Cao et al. 2018).

The proteostasis regulators performed poorly as $CHO_{BIS\text{-}A}$ culture performance enhancers, with few significant improvements to IVCD or titre observed. C1 and C3 were found to significantly increase qP under specific conditions, however this was a consequence of growth limitation exceeding the magnitude of titre reductions in both cases. This is particularly prominent upon supplementation of C1, where the same dis-linkage between growth and titre observed in CHO_{ETE} was replicated. Several significant IVCD increases were seen, however titre did not increase relative to the controls reducing overall productivity.

In $CHO_{BIS\text{-}B}$, the library of proteostasis regulators was more fruitful, and most compounds significantly increased IVCD under the correct conditions. Delayed C3 supplementation increased titre by 1.4 fold relative to the control at two concentrations, with no negative effect of culture IVCD resulting in similar qP improvements.

Subsequent aggregate analysis of selected supernatant samples revealed that $CHO_{BIS\text{-}A}$ aggregation was unaffected by the supplementation of proteostasis regulators. When considered with the growth and titre data presented, it is evident that the library of proteostasis regulators are ineffective modulators of $mAb_{BIS\text{-}A}$ production. A minimum titre of $500\,mg.l^{-1}$ was required for the AstraZeneca Bioprocess Analytics team to measure mAb aggregation at the time this work was completed. Unfortunately, the $CHO_{BIS\text{-}B}$ control population did not meet this threshold, therefore it was not possible to evaluate the effect on aggregation in this model. In particular the effects of C3 on $mAb_{BIS\text{-}B}$ aggregation would be especially insightful.

Based on findings from the initial characterisation, compound supplementation was evaluated at three time-points post culture seeding. When reviewing results from each compound added on day five or nine of culture, it is evident the effects are reduced relative to supplementation at seed. The most prominent examples are seen in $CHO_{BIS\text{-}A}$'s response to C1 and C3 supplementation (Figure 5.3) where the IVCD and titre seen on day zero is reduced or negligible when supplementation is delayed. From these results it was hypothesised that cultures were

responding in a 'dose-per-cell' dependent manner, most likely a result of active internalisation or break down the proteostasis regulators by the cells.

5.3.3 Delayed C1 Supplementation in Scaled-Up CHO_{ETE} Cultures

Following mixed results in DTE mAb models, a final assessment of C1 in CHO_{ETE} was conducted. To account for a 'dose-per-cell' response, delayed supplementation with higher compound concentrations was hypothesised to translate the dis-linkage between growth and titre (observed in the initial evaluation) into titre and qP improvements in extended duration fed-batch conditions. The culture format was also scaled up into 125 ml Erlenmeyer flasks as a more applicable model to industry processes.

As increasing compound concentrations simultaneously increased the concentration of DMSO in the culture, each experimental condition was normalised against a matched DMSO control, with data expressed as a fold-change. Initially the experiment was performed in triplicate, however upon data evaluation a subsequent biological replication was performed resulting in $n = 6$ total replicates. When supplemented at the mid-point of a 10-day fed-batch process, C1 consistently reduced CHO_{ETE} IVCD with a significance of $p \geq 0.001$ at all concentrations. However, titre was reduced at low, and increased at high, C1 concentrations relative the matched DMSO controls. These results confirm that C1 is non-toxic at high concentrations, and its supplementation increases CHO_{ETE} productivity. Although all four concentrations reduced cell viability relative to the negative control cultures, this was least prominent at the highest concentration tested. This result was unexpected and therefore was the primary reason for the completion of additional replicates, which further supported the observation. There is currently no preferred working hypothesis, however feasible explanations include effects on cellular metabolic rate or lactate buffering.

5.3.4 Summary

The data presented in this chapter demonstrates a pharmacological response in CHO cells when supplemented with proteostasis regulators, however the library had no impact on mAb aggregation in $CHO_{BIS\text{-}A}$. Furthermore, C3 was identified as a cell culture enhancer for $CHO_{BIS\text{-}B}$, but not $CHO_{BIS\text{-}A}$, and delayed C1 supplementation was found to significantly increase CHO_{ETE} titre and qP.

These findings provided strong evidence to support the use of disaggregases in proteopathic disease models as CHO cell productivity enhancers in a context specific manner. Unfortunately, it was not possible to evaluate product aggregation in $CHO_{BIS\text{-}B}$, and analysis of select $CHO_{BIS\text{-}A}$ samples did not identify any effect on product aggregation. Therefore, these proteostasis regulators were not evaluated any further. Instead, the lessons learnt surrounding scaling up concentrations upon delayed supplementation were taken forward to evaluate a more diverse population of proteopathic disaggregases.

Chapter 6

Identification of Preclinical Neurological Compounds as CHO Engineering Tools

This chapter explores the use of compounds found to prevent or disperse aggregates in cell models of neurological proteopathy as cell culture enhancers to improve the titre and quality of Difficult to Express (DTE) Monoclonal Antibodys (mAbs). It was hypothesised that the intracellular aggregation of DTE mAbs in Chinese Hamster Ovary (CHO) cells may share a common mechanism with proteopathic disease pathology.

Preliminary evaluation narrowed down a compound library identified through the AstraZeneca Open Innovation Initiative to a subset of hit compounds, representing 27.6 % *of the compound library. A more detailed assessemnt conducted in the secondary screen identified 11 compounds which increased* $mAb_{BIS\text{-}A}$ *titre by at least* 50 % *while also reducing the rate of product aggregation. Almost a third of compounds in the secondary screen doubled mAb titre, with the most prevalent compounds associated with mTOR activation or the rescue of toxic TDP43 or FUS phenotypes. Compounds rescuing FUS toxicity in cell models were also the most promising compounds for reducing* $mAb_{BIS\text{-}A}$ *aggregation, alongside compounds shown to inhibit aggregation in models of Amyotrophic Lateral Sclerosis (ALS) and Huntington's disease. As cell viability was compromised in the preliminary and secondary screening rounds, further evaluation of hit compounds was necessary. Although, initial results demonstrate a revision of the cell media and feed composition overcame the cell culture limitations, in-person working restrictions led to postponement of product quality analyses.*

The data presented suggests a common mechanism of aggregation in proteopathic disease and CHO cell factories. It provides strong justification for evaluation of similar preclinical compound libraries, and identifies a number of engineering solutions for the $CHO_{BIS\text{-}A}$ *model system.*

6.1 Introduction

Recent developments in non-standard antibody modalities have introduced a range of new challenges for the upstream development of biotherapeutics. Product aggregation poses a significant hurdle in the production of un-natural antibody formats and can impact therapeutic properties causing immunogenic reactions (Vázquez-Rey and Lang 2011). Furthermore, aggregation can greatly increase the cost and complexity of downstream processing, resulting in pharmacologically effective molecules failing to progress to market.

Aggregation can occur intra- or extra-cellularly, and can be classified as: covalent/non-covalent, soluble/insoluble, reversible/non-reversible and native/denatured (Cromwell et al. 2006). Aggregates can exist as small dimers or fragments and can catalyse the formation of larger structures, such as sub-visible or visible particles (Kiese et al. 2008). Covalent aggregation is the chemical binding or linking between more than two monomers or partially unfolded molecules, and is most commonly a result of disulphide bond formation between previously unpaired free thiols (Andya et al. 2003). Non-covalent aggregation arises through exposed hydrophobic regions of molecules sticking together.

Previous studies have attempted to screen vast compound libraries for molecules that reprogram ER proteostasis environments through directed activation of *ATF6* (Plate, Cooley, et al. 2016), and *HSF1* (Calamini et al. 2012) in proteopathic disease models. Screening of compounds identified from Plate, Cooley, et al. 2016 in stable CHO producers in Chapter 5 has shown beneficial effects on titre and specific productivity in standard monoclonal antibodies and aggregate prone molecules in a product specific manner.

A subsequent review by Lars Plate into the regulation of secretory proteostasis describes the importance of Unfolded Protein Response (UPR) signalling regulating Endoplasmic Reticulum (ER) protein folding load and quality control capacity (Plate and Wiseman 2017). Stress-independent activation of preferential UPR pathways can have distinct effects on disease associated aggregates. This was demonstrated by Plate, Cooley, et al. 2016 where stress-independent activation of *ATF6*, but not *XBP1s*, selectively reduced secretion of aggregation prone TTR variants in TTR amyloidosis.

In neurodegenerative pathologies the effects of targeted stress-independent UPR activation are disease specific, requiring induction of different UPR branches. In contrast to TTR, the ER proteostasis of destabilised APP variants can be improved through IRE1-induced UPR remodelling, reducing aggregate associated mitochondrial toxicity in cell models of Alzheimer's and Parkinson's diseases (Grandjean et al. 2020). Context specificity in respect to MEDI-CHO genetic engineering solutions was discussed in Chapter 4, and it is expected that chemical engineering approaches will encounter similar challenges.

It was hypothesised that re-purposing pre-clinical compounds able to prevent or disperse aggregates in cell models of neurological proteopathy would be efficacious in reducing the aggregation of problematic mAbs. Medicinal compounds may exhibit positive results during in-vitro screening, and fail to progress through animal studies or clinical trials. It was further hypothesised that

directed screening of such compounds, with evidence supporting positive effects on aggregative pathologies, would exhibit higher incidences of positive hits than randomised High Throughput (HTP) screening of compound libraries.

This chapter explores the application of a compound library, identified collaboratively with the AstraZeneca Open Innovation Initiative, as cell culture enhancers for improving the production of aggregating DTE mAbs. The identification of individual compounds will provide novel CHO engineering tools for cell line development processes. Moreover, the identification of groups of efficacious compounds effecting aggregative proteopathies by a similar mechanism would suggest mechanistic commonality between disease proteopathies and engineered antibodies, opening new lines of research in both fields.

6.2 Results

6.2.1 Compound Library Identification

A research proposal was written to the AstraZeneca Open Innovation to interrogate their database of 250,000 compounds. Based on the research proposal and further input from Emma Kelsall, a library of 192 compounds was identified by Dean Brown, project leader of the neuroscience portfolio for the AstraZeneca Open Innovation programme. The basis for selection was through a combination of published literature and in-house data suggesting the compounds fell into at least one of the following categories:

a) *Reduce or fully disperse protein aggregates in cell models of neurological disease.*

b) *Inhibit or slow the formation of protein aggregates in cell models of neurological disease.*

c) *Directly interact with protein aggregates in cell models of neurological disease.*

d) *Activate, inhibit or modulate molecular chaperones or regulators of molecular chaperones which are therapeutic targets for alleviating aggregation in neurological diseases.*

e) *Rescue aggregative toxicities in models of neurological disease.*

f) *Analogues of compounds that meet the identified criteria.*

Due to intellectual property restrictions surrounding the use of the AstraZeneca compound database, the compound information in this thesis has been limited to prevent identification. In order to logically interrogate the identified library, compounds were sorted into 14 categories with a common mechanism of action or binding target. The information supporting the inclusion of 103 compounds was the result of phenotypic assays previously completed by AstraZeneca, of which the details were initially restricted. Upon completion of preliminary screening experiments, further details on successful candidates were released. Table 6.1 lists the categories of compounds and highlights their links to human neurological disease and the mechanism by which protein aggregation is alleviated.

The distribution of the 192 compound library was divided into the 14 categories is depicted in Figure 6.1. The limited information described is evidenced by the presence of 53.6 % of the library in the 'phenotypic hit' category. These compounds have been shown to rescue one or more specific aggregative toxicities in cell models, with specific toxicity models made available for compounds identified as hits in the preliminary screening allowing subdivision of the 'phenotypic hit' category in section 6.2.3. From the remaining 13 categories 'β-amyloid binders' and 'disaggregases of stress granules' are the most populous. β-amyloid is a misfolded peptide of a transmembrane protein called APP, and readily interacts with a wide range of other proteins and chemicals (G. F. Chen et al. 2017). Stress granules are composed of a heterogeneous mix of messenger RNAs (mRNAs) stalled in translation and associated mRNA binding proteins, as a result they have the ability to bind a wide range of intracellular epitopes.

Table 6.1: Categorisation of compounds identified from the AstraZeneca Open Innovation compound library.
The table lists the compound categories defined by interactions with key components of neurological proteopathic pathologies, or modulation of linked regulatory pathways. For each category the commonly associated diseases, therapeutic background and disaggregation mechanisms have been highlighted.

Group	Disease Links	Background / Mechanism of Action
β-amyloid binders	Alzheimer's, CJD, Huntington's and Parkinson's	β-amyloid is the main component of amyloid plaques containing a diverse set of proteins, and is found in Alzheimer's and other disease pathologies (Young et al. 2017). Several natural compounds such as tetracyclines and polyphenols are effective anti-amyloid agents. These are generally non-specific and can interfere with the aggregation of multiple unrelated proteins (Giorgetti et al. 2018).
Curcumin	Alzheimer's and Parkinson's disease	Curcumin is historically used in traditional medicine for the prevention of neurological diseases. The therapeutic benefits appear to be multi-factorial, through the regulation of $NF\kappa B$ activity. Curcumin has been shown to alleviate αSynuclein-induced toxicity, reduce ROS levels, protect cells against apoptosis and prevent the formation of higher molecular weight aggregates in disease models (W.-H. Lee et al. 2013).
Cyclophilin inhibitors	Alzheimer's	β-amyloid has been shown to interact with Cyclophilin D, potentiating neuronal stress in Alzheimer's disease pathology. Inhibition of Cyclophilin D can reduce ROS and it's absence can prevent β-amyloid and oxidative stress induced apoptosis (Du, L. Guo, et al. 2008; Du and Yan 2010).
Disaggregases of stress granules	ALS, Alzheimer's, FTD and Huntington's	Stress granules are dense protein aggregations in the cytosol which can accelerate neuro-degeneration and share many components with neuronal granules (L. Chen and B. Liu 2017; Mahboubi and Stochaj 2017). Persistent stress granules as a result of chronic stress act as a catalyst for aggregation of disease related proteins (Wolozin and Ivanov 2019).
FKBP12 inhibitors	Alzheimer's, Parkinson's	Linked to immunosuppressant activity, FKBP12 and other PPIases regulate Tau biology impacting pathogenesis (Blair et al. 2015). *FKBP12* inhibition has been linked to reduced aggregation of α-synuclein and Parkinson's like pathologies (Caraveo et al. 2017).
HSF1 activators	ALS, Alzheimer's, Huntington's and Parkinson's	As a regulator of molecular chaperone expression, pharmacological activation of *HSF1* delays neuro-degenerative disease progression in cell models (Neef et al. 2012).
HSP90 modulators	ALS, Alzheimer's and Parkinson's	Molecular chaperones are among the most potent suppressors of neuro-degeneration known for animal models of human disease (Muchowski and Wacker 2005). Modulating HSP90 function has great potential to become a new molecular-targeted therapy against a wide range of neuro-degenerative diseases (Waza et al. 2006).
p38 MAPK inhibitors	Alzheimer's, Parkinson's	A possible therapeutic target for autoimmune disorders (Cuenda and Rousseau 2007). Phosphorylates Parkin in Parkinson's disease models leading to cell death (J. Chen et al. 2018). Inhibition considered a promising treatment strategy for Alzheimer's disease (J. K. Lee and N. J. Kim 2017).

Group	Disease Links	Background / Mechanism of Action
Rapamycin (& analogue)	Alzheimer's, Huntington's and Parkinson's	As an inhibitor of mTOR, Rapamycin has been shown to attenuate nigrostriatal degeneration in Parkinson's models and protect against neuro-degeneration caused by mutant Htt aggregates. Rapamycin has been shown to restore *mTOR* activity in Alzheimer's and Huntington's disease models (Bové et al. 2011; Sarkar et al. 2008), and has been linked to improved production of therapeutic proteins in CHO cells (Dadehbeigi and Dickson 2015; Lalonde and Durocher 2017; Y. Li et al. 2019).
RIPK1 modulators	Alzheimer's and ALS	Evidence has linked the dysregulation of RIPK1 to the pathogenesis of ALS as well as other inflammatory and neuro-degenerative diseases.
Adapalene & O-des methyl	Alzheimer's, CJD, Huntington's and Parkinson's	Compounds are described in Young et al. 2017, and demonstrate repress amyloid formation and inhibit the accumulation of misfolded protein aggregates in cell models.
HTT. aggregation inhibitors	Huntington's	A group of compounds identified in Todd and J. Lim 2013 which have been found to alleviate poly-glutamate aggregation in cell models of Huntington's disease (Rinderspacher et al. 2009). Poly-glutamate aggregates arise from the expansion of an unstable CAG triplet repeat leading to aggregate induced toxicity (Todd and J. Lim 2013).
ALS aggregation inhibitors	ALS	A compound identified by Richard Silverman which reduces SOD1 aggregates in cell models of ALS (Y. Zhang et al. 2012).
Phenotypic Hit	n/a	Compound has rescued at least one toxic aggregative phenotype linked in human neuro-degenerative disease. The assays include the rescue of TDP43, FUS and C9ORF72-PR50 toxicities.

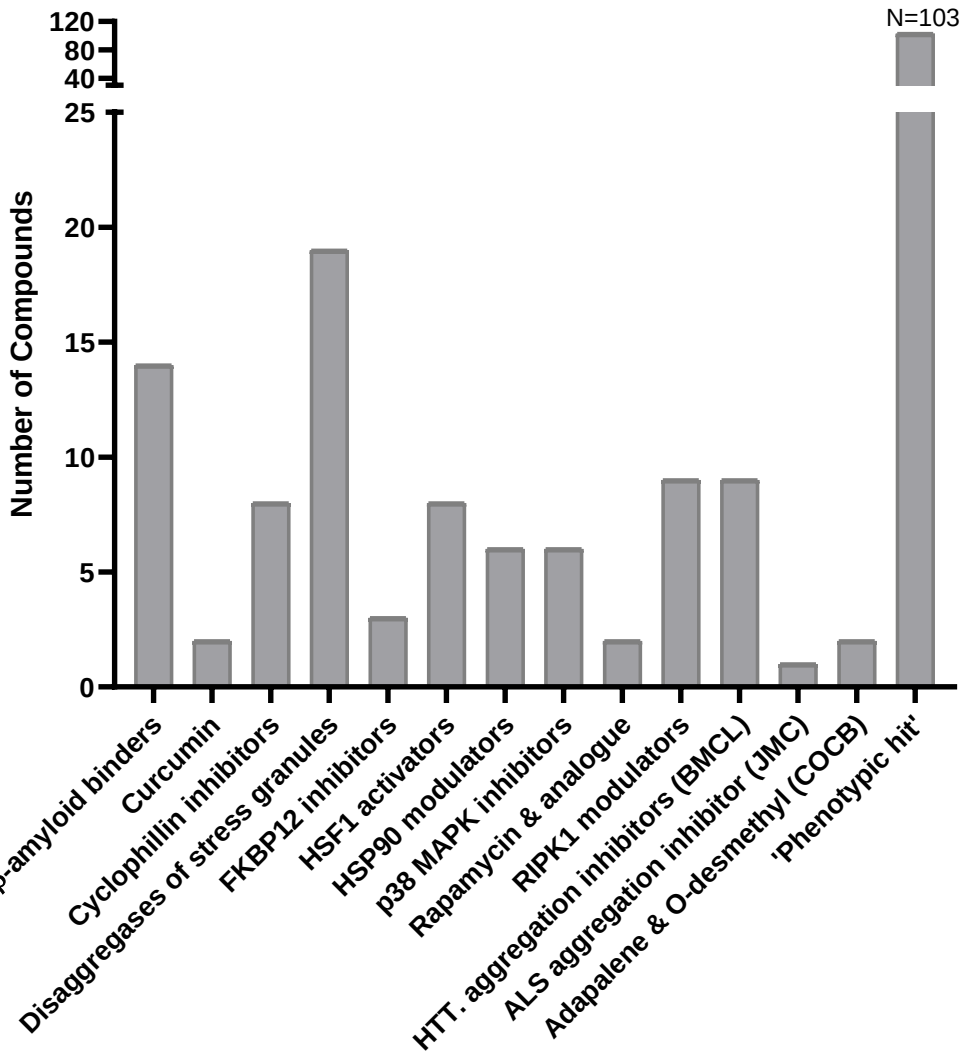

Figure 6.1: Distribution of compounds between mechanistic categories.
The library of $n = 192$ compounds have been placed into 14 categories based on interactions with, or regulation of, key components of aggregative pathologies and their regulatory pathways.

6.2.2 Preliminary Compound Screen: Library Refinement

6.2.2.1 Determining optimal screening parameters

The preliminary screen aimed to assess the compounds' ability to increase the product quality, measured as the percentage of IgG monomer produced relative to the total range of IgG species, in a model system. Secondarily, any improvements to IgG titre, specific productivity or a shift towards smaller sized aggregates would provide further evidence of performance benefits, supporting the initial hypothesis.

$CHO_{BIS\text{-}A}$ was identified as a well characterised clonal cell line with a known, internal mechanism of aggregation as described in Cao et al. 2018. Structural characterization identified a range of slight size variants resulting from the engineered disulfide bond at Cys442 and Cys640. Instead of forming an intra-chain disulphide bond, the engineered cystines were cysteinylated or glutathionylated leading to monomer variants. Additionally, stable head to tail dimers formed as a result of intra-molecular disulphide bonds between these residues (Cao et al. 2018). Additionally, $CHO_{BIS\text{-}A}$ was previously utilised as a model system in chapter 5 for the screening of proteostasis regulators for improvements in growth and titre characteristics, therefore performance should be predicable.

During preliminary High Throughput Screening (HTP) experiments, selecting appropriate compound concentrations was crucial to maximise the likelihood of experimental hits. The number of concentrations evaluated, interval between them and the library size must be balanced to achieve the maximal information from the available resources. It was initially recommended by researchers from the AstraZeneca Open Initiative that compounds be tested at concentrations ranging from $1\,\mu$M to $10\,\mu$M. Although specific evidence was not provided, literature examples of compound screens in cell models of disease suggest concentrations ranging from $0.5\,\mu$M to $100\,\mu$M (Calamini et al. 2012; Hughes et al. 2011; Plate, Cooley, et al. 2016). In chapter 5 it was demonstrated that absolute concentration is often not transferable between screening models, particularly if compounds are internalised where the number of cells present plays an important factor. Mechanistically the aggregation of BIS-A occurs in the ER, therefore it was predicted that compounds successfully reducing the aggregation rate must be internalised. Furthermore, screening methods in disease models occur at significantly lower cell densities than fed-batch CHO cultures, therefore a higher concentration would be required to maximise the chances of therapeutic efficacy in high density $CHO_{BIS\text{-}A}$ cultures.

By selecting a 10 fold interval between the two concentrations, the changes of either concentrations falling within the effective pharmacological range of the compounds would be maximised. It would be difficult to draw any conclusions from differential results between the concentrations with this interval, therefore, the effects of each concentration would need to be analysed independently. In order to characterise the full compound library at two screening concentrations with the available time and resources, each condition was screened with $n = 1$ replicates. Resultantly the preliminary screening concentrations of $5\,\mu$M and $50\,\mu$M were selected to balance efficacy and toxicity. Compounds were supplemented on day five of culture after results discussed in chapter 5 demonstrated that compounds improving productivity are likely to reduce growth

rate.

The compound library was assessed on-site at AstraZeneca, utilising proprietary media and feeds in an 11 day fed-batch overgrow in 24-Shallow Well Plates (SWPs). Cells were seeded at 0.710×10^6 cells.ml^{-1} and feed was added every other day starting on day three. The Viable Cell Density (VCD) and viability of cultures was assessed by trypan staining measured on the Cellavista and samples taken for titre analysis by Octet on day seven and at culture harvest. Supernatants were collected at culture harvest for protein-A purification and subsequent aggregate analysis by High-Performance Liquid Size Exclusion Chromatography (HPL-SEC) on an Agilent Technologies 1260 Infinity system with a Walters BEH200 column. As compounds were suspended in Dimethyl Sulfoxide (DMSO), a range of DMSO control were included with up to four times the maximal experimental DMSO concentration. Additionally, at least two negative control wells were included on each 24-SWP.

6.2.2.2 Assessing culture performance

When performing HTP experiments to assess drug candidates *in vitro*, compatibility with cell survival is the first consideration (Hughes et al. 2011). This is also true in a mAb production context, where screen specific parameters such as product titre and quality are assessed secondarily to cell survival.

Figure 6.2 shows the growth characteristics of the control cultures (green) laid over the experimental cultures (black and red). The day 7 cell viability measurements, taken 48 hours after the chemical supplementation, were deemed most relevant in highlighting compound induced cytotoxic effects. A high degree of variation was observed for the control population with Coefficient of Variations (CVs) for Integral Viable Cell Density (IVCD) and cell viability of 23.0 % and 34.8 % respectively.

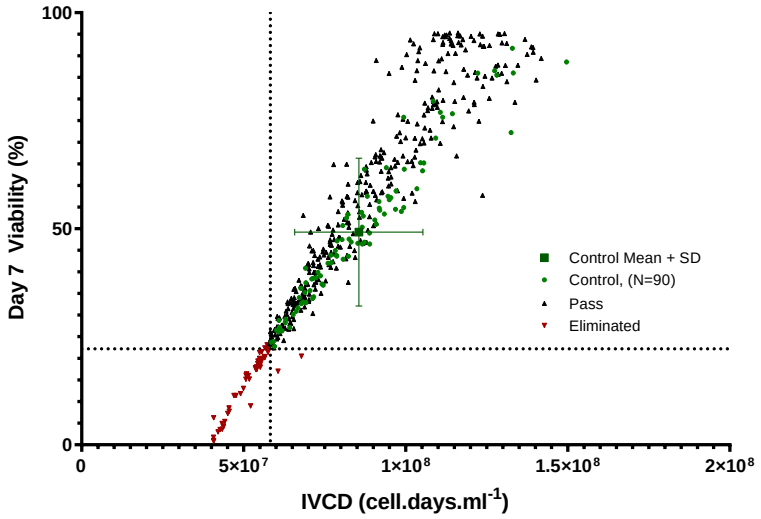

Figure 6.2: Primary screen: Elimination of poor performing cultures.
The mean and Standard Deviation (StD) of negative control cultures (green) was plotted as a reference point. The dotted lines described by eqs. (6.1) and (6.2) define the minimum accepted performance for experimental cultures to progress. IVCD was calculated from VCD measurements on days 0, 7 and 11.

The measured mean cell viability of control population was 49.2 % indicating the control cultures were not growing optimally, resulting in a mean IVCD of 8.55×10^7 cells.days.ml^{-1}. However, the mean VCD on day 7 or 11 was 15.2×10^6 cells.ml^{-1}, demonstrating that the majority of cultures had large live populations despite variable viability, validating further data analysis.

In the context of identifying compounds that improve product quality, a high cell growth rate was not a priority. However, a reduction in IVCD or cell viability relative to the control population is an indication of drug induced cytotoxicity. Therefore, boundaries were created to eliminate experimental conditions that failed to match or exceed the lowest performing control cultures. These are defined by eqs. (6.1) and (6.2) and visualised by the plotted lines in Figure 6.2:

$$\begin{aligned} x &= IVCD_{Min} \\ &= 5.82 \times 10^7 \; cell.days.ml^{-}1 \end{aligned} \tag{6.1}$$

$$\begin{aligned} y &= Viability_{Min} \\ &= 22.27 \; \% \end{aligned} \tag{6.2}$$

The minimum IVCD and viability requirements eliminated 52 conditions which were non-compatible with cell growth and survival from further analysis, leaving 332 to be interrogated. Although these conditions were detrimental, this did not rule out beneficial effects as the screened concentrations may be greater than the pharmacological range. Where both compound conditions were eliminated due to chemical induced cytotoxicity, further assessment at lower doses was considered as this may yield positive results.

6.2.2.3 Quantification of $mAb_{BIS\text{-}A}$ titre

After eliminating conditions which negatively effected culture performance, the impact on product titre and aggregation were assessed. Upon review, the product titre in the majority measured by the Octet decreased between day 7 and culture harvest on day 11, highlighted by abundance of cultures falling below the plotted line in Figure 6.3a. The assessment of health in Figure 6.2 demonstrated a mean control culture viability of 49.2 %, and an average experimental culture viability of 51.9 % on day 7 post seeding, therefore it was highly unlikely that further IgG production was negligible from this point.

To validate these findings, supernatant samples which were protein-A purified for aggregate analysis were quantified by UV absorbance measurement on a Stunner. Simultaneous purification of a NIP228 control of known concentration controlled for method consistency and was used to calculate a purification yield of 82 ± 2 % (mean + StD of $n = 8$ samples), ensuring accuracy in the alternative calculation of the mAb titre. When comparing the Stunner and Octet titre measured on day 11 (Figure 6.3b), substantially more $mAb_{BIS\text{-}A}$ was detected by quantification of the purified product.

Purification quality is a concern when quantifying mAb by UV-absorbance as the method non-specifically measures the sample total protein content. HPL-SEC analysis of the day 11 control culture supernatants post Protein-A purification identified peaks for $CHO_{BIS\text{-}A}$ monomers,

dimers and a small number of higher molecular weight aggregates as shown in Figure 6.4. This confirmed the Protein-A purification method was highly specific and $mAb_{BIS\text{-}A}$ molecules were still intact, ruling out titre elevation from the presence of cell culture debris or antibody fragments. Species identification was validated by comparison to a NIP228 control and a Bio-Rad Gel Filtration Standard, with example traces displayed in Appendix A Figure A.4. Therefore, the low titre measured by the Octet is likely due to the low cell viability at culture harvest. Product degradation or interference by supernatant debris could interfere with antibody binding to the capture molecule, resulting in a low measurement.

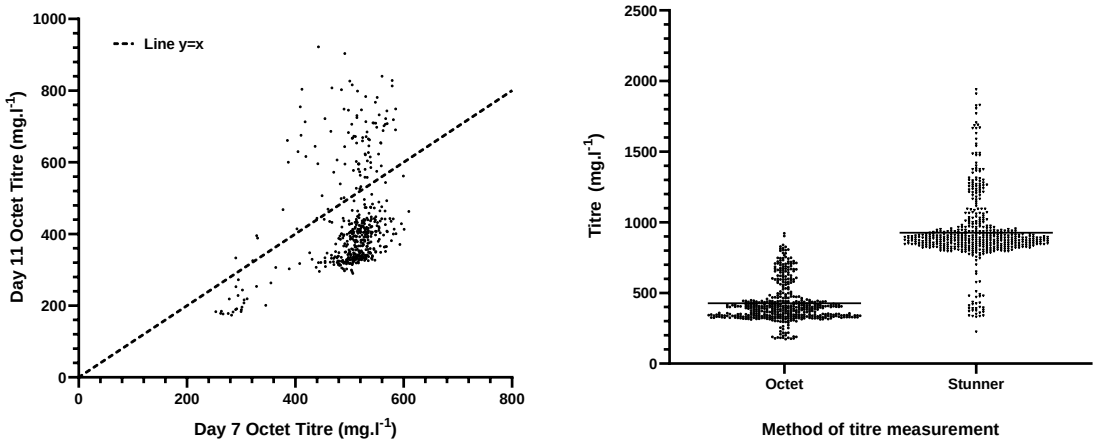

(a) Measured day 11 titre **(b)** Calculated day 11 titre

Figure 6.3: Preliminary Screen: Evaluating methods for measuring product titre.
(**a**) Titre on day 11 measured by the Octet in relation to the day 7 Octet titre measurement with the plotted line at $x = y$ represents an equal titre at the respective time points. (**b**) Comparison of the titre on day 11 measured by Octet and Stunner with bars representing the mean of 480 purifications.

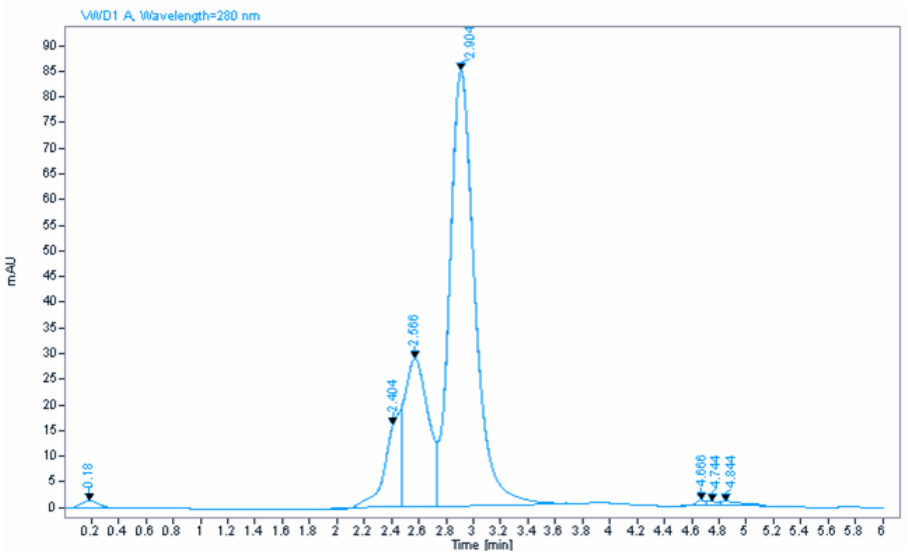

Figure 6.4: Preliminary screen: Representative HPL-SEC trace of protein-A purified $CHO_{BIS\text{-}A}$ supernatant.
The representative trace showing the peaks identified from the Protein-A purified supernatant from negative control culture harvested on day 11. The peaks at 2.90 minutes and 2.56 minutes are $mAb_{BIS\text{-}A}$ monomer and dimer respectively.

6.2.2.4 Hit identification: Evaluating product quality and titre

In order to accurately and objectively identify efficacious conditions from the general population, the desired outcomes were reviewed. The primary aim was to identify compounds that reduced the frequency of aggregate production, therefore monomer abundance was the most important metric measured. If the product titre is also increased this is an additional benefit, and would indicate that reducing aggregate induced cellular stresses can increase production capacity. Compounds that improve product titre with no observable impact on aggregation would be useful as broad engineering tools.

From these criteria 3 groups were identified with the following attributes:

- Hit group 1: Improved aggregation profile, with no negative impact on product titre.
- Hit group 2: Increased product titre, irrespective of aggregation profile.
- Hit group 3: Improved aggregation and increased product titre.

To statistically define the boundaries of each group, multiples of the control population's product titre and monomer abundance StD were added or subtracted from the mean. Equation (6.3) defined the minimum acceptable product quality for groups 1 and 3, equating to 2 StDs above the control mean. This accounted for the expected variability resulting from a lack of experimental replicates of each condition. The minimum titre for groups 2 and 3 was defined by eq. (6.4), and was similarly set at 2 StDs above the mean. The lower titre boundary for group 1 was set at 1 StD below the mean as defined by eq. (6.5), and the upper boundary was 2 StDs above the control mean:

$$\begin{aligned} y &= Monomer_{Mean} + 2 \cdot Monomer_{StD} \\ &= 64.18\ \% \end{aligned} \tag{6.3}$$

$$\begin{aligned} x &= Titre_{Mean} + 2 \cdot Titre_{StD} \\ &= 1157.5\ mg.ml^{-1} \end{aligned} \tag{6.4}$$

$$\begin{aligned} x &= Titre_{Mean} - Titre_{StD} \\ &= 743.3\ mg.ml^{-1} \end{aligned} \tag{6.5}$$

Figure 6.5 shows the relationship between product titre and IgG monomer abundance of the remaining experimental conditions in relation to the control population. The selection boundaries were plotted from the equations above relative to the control population, and coloured boxes overlaid to identify group 1 (orange), group 2 (purple) and group 3 (blue). The population distribution (green) and mean (dark green) of the controls demonstrates consistent titre and product quality despite the large variation in culture performance. The control population CV was 15.6 % and 2.22 % for titre and IgG monomer abundance respectively. This demonstrated

a consistent overall titre and minimal change in product quality between replicates, despite the variability observed in growth and viability.

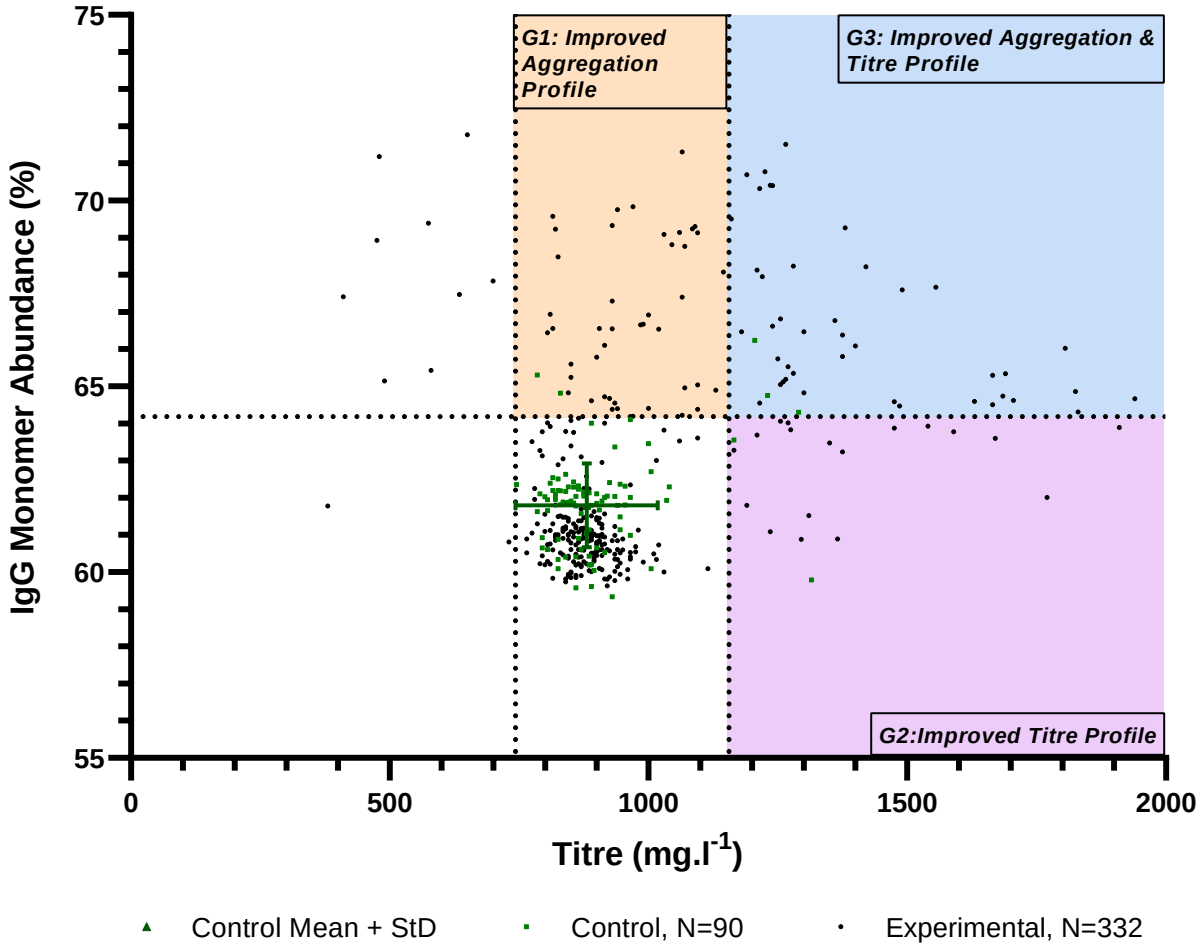

Figure 6.5: Preliminary screen: Evaluation of product titre and aggregation.
Graph shows the titre and IgG monomer abundance of the experimental conditions (black) tested in relation to the controls (green). The boundaries of each group were calculated using multiples of the control population StD as per eqs. (6.3) to (6.5).

Of the 322 conditions brought forward, 240 fell within one StD of the control population titre, indicating that a large proportion had minimal impact. The majority of these fell within a large cluster with a mean 1.12 % below the control population mean monomer abundance of 61.86 %, and contained 186 conditions. It was hypothesised that this population represented the conditions that had no measurable impact on the production of BIS-A. It was unlikely that such a large number of conditions had a minor negative pharmacological effect on the cells reducing IgG monomer abundance without impacting titre. Therefore, it was reasonable to assume that the presence of these compounds had a negative effect on IgG stability post secretion from the cell which may need accounting for in later analysis.

Groups 1, 2 and 3 pulled out 43, 18 and 44 hits respectively, totalling 27.5 % of the original 382 conditions screened. When accounting for the 28 compounds which appear twice, 77 hit compounds were identified equating to 40.1 % of the starting library. This represented an unusually high hit rate in comparison to random HTP screening experiments, strongly supporting

the initial hypothesis that compounds linked to disaggregation in models of proteopathy would be similarly efficacious in aggregate prone mAb systems.

6.2.2.5 Hit refinement: Evaluating specific productivity

Due to the high number of hit compounds identified, a further round of eliminations was required to identify a manageable number of for further experimental assessment. Instead of increasing the stringency of the existing selection criteria, the impact on Specific Productivity (qP) was evaluated in relation to the product quality to eliminate the least effective compounds.

The qP was plotted against IgG monomer abundance to assess the relationship between the rate and quality of the product produced (Figure A.5). The experimental conditions are categorised into their respective compound hit groups with the control and the eliminated population displayed. When observing the previously eliminated conditions from this perspective, the identified cluster with a mean monomer abundance of 61.86 % had a 2.1 fold broader distribution stretching 4.2 StDs. This indicated that the variance in IVCD of this population was significantly greater than the variation in titre.

When the potential elimination criteria described by eqs. (6.3), (A.1) and (A.2) were plotted, it was evident that the using a similar set of criteria would not be effective. The variation in qP of the experimental conditions relative to the control population is much lower, therefore the stringencies would have to be significantly reduced. Additionally, the overlapping triangular distribution of groups 1 and 3 indicated that varying the qP boundary would have the same effect as increasing the titre stringency, ultimately not adding any depth to the analysis. Therefore, an alternative metric was required to identify the best compounds for further experimental analysis.

The process of producing a mAb is an energy intensive process for the cell, and for DTE mAbs in particular, production exerts a significant amount of stress on the system. The measured qP of a culture is defined by the rate of product production normalised for the cumulative cell production time, and therefore will be proportional to the amount of stress exerted on the cells within the culture to produce the DTE mAb. In summary, the qP is an indirect measurement of the burden placed on the cells as a result of mAb production. At the simplest level, there are 2 ways for compound addition to increase qP beyond the control population capacity. Firstly the cell burden associated with mAb production can be reduced by relieving an intracellular bottle neck in production. Secondly, increasing the maximum burden the cell can tolerate would allow a higher mAb production rate.

Theoretically the probability of a mAb being incorrectly assembled in the control population is fixed, therefore the number of misfolded mAbs triggering a UPR will be highly consistent. This is supported by the calculated CV of 2.03 % in IgG monomer abundance in the control population. Therefore, any change in the ratio of monomer-aggregate species upon chemical supplementation indicates a change in these probabilities, increasing the cell burden by one of the following mechanisms:

- Increasing the number of misfolded species that are identified and corrected, representing an increased UPR stress and requiring more cell resources.

- Increasing the number of misfolded species sent for ER-Associated Protein Degradation (ERAD), resulting in the associated burden of degradation and the loss of resources used for initial synthesis.
- Decreasing the initial probability of incorrect folding would require a reduced folding and assembly rate, increasing the assembly time of each molecule.

As both qP and IgG monomer abundance exhibit a positive correlation with cell burden, increasing either metric requires either increasing the cells capacity or reducing the cost of production. This allows the mathematical weighting of both qP and monomer abundance to create a non-linear selection criteria to identify the best performing experimental conditions.

In Figure 6.6, qP was plotted against IgG monomer abundance with the control conditions in green and the minimum accepted cell burden depicted by the black line. The line was modelled by taking the arc running from 0° to 90° of the ellipse defined by eq. (6.6). The curve was completed by extrapolating the arc to meet the graph axis. The ellipse centre point was offset from the control population mean by 1 StD to give an increased weighting to product quality over qP. Due to the difference in control population variance between monomer abundance and qP, the monomer abundance weighting was increased by 2.25 fold as seen in the respective radii R_y and R_x.

$$\textit{Equation of cellular burden ellipse}:$$

$$\frac{x^2}{{R_x}^2} + \frac{y^2}{{R_y}^2} = 1 \tag{6.6}$$

$$\textit{with radii}:$$

$$\begin{aligned} R_x &= 2 \cdot qP_{StD} \\ &= 2.352\ pg.cell^{-1}.day^{-1} \end{aligned}$$

$$\begin{aligned} R_y &= 4.5 \cdot Monomer_{StD} \\ &= 5.98\ \% \end{aligned}$$

$$\textit{from centre point}:$$

$$\begin{aligned} &(qP_{Mean} - qP_{StD},\ Monomer_{Mean}) \\ &= (8.438,\ 61.80) \end{aligned}$$

$$\textit{with } Monomer_{Max} \textit{ and } qP_{Max} \textit{ tangents}:$$

$$\begin{aligned} y &= Monomer_{Mean} + 4.5 \cdot Monomer_{StD} \\ &= 67.52\ \% \end{aligned} \tag{6.7}$$

$$\begin{aligned} x &= qP_{Mean} + qP_{StD} \\ &= 15.49\ pg.cell^{-1}.day^{-1} \end{aligned} \tag{6.8}$$

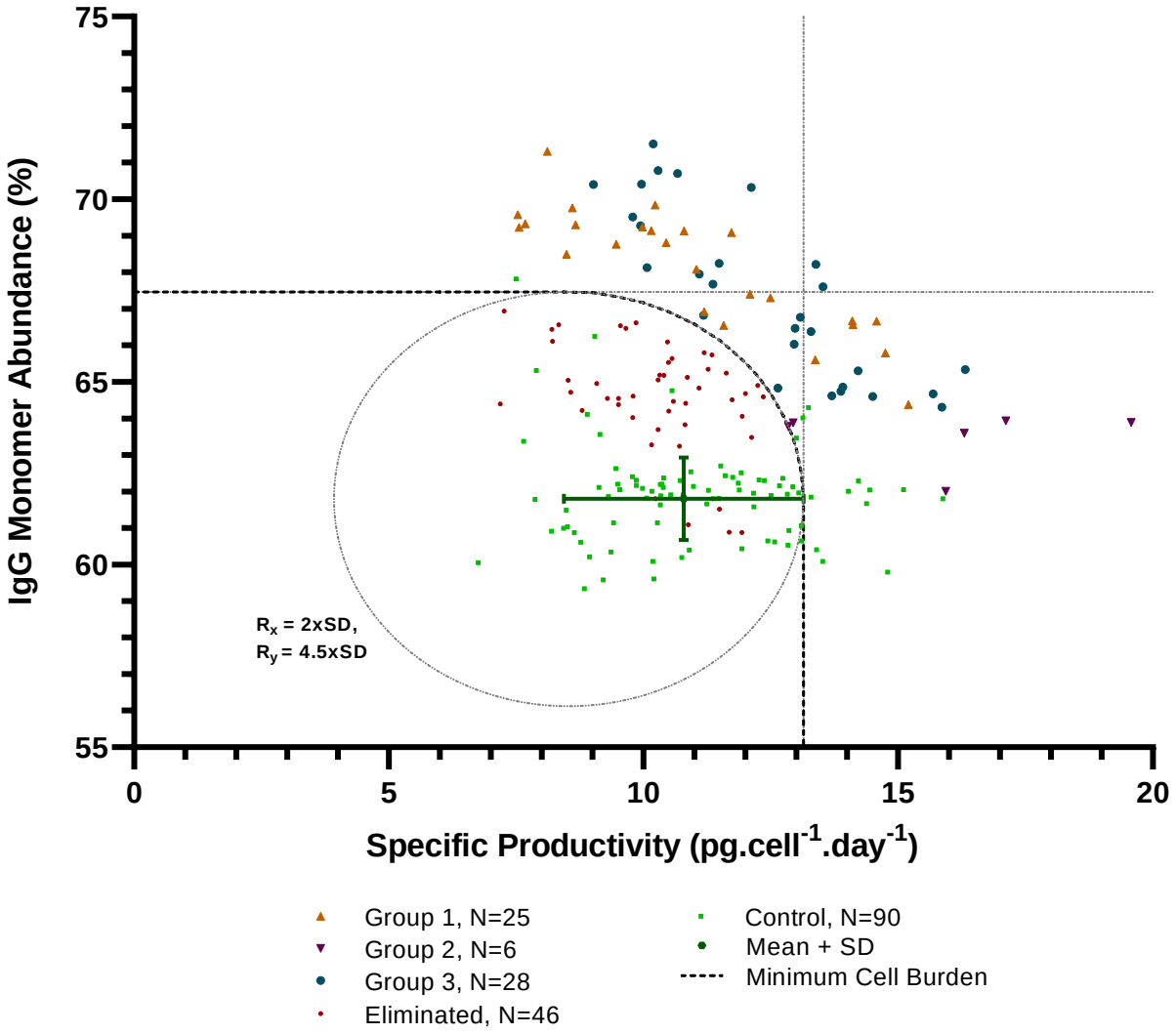

Figure 6.6: Preliminary screen: Refinement of compounds by estimated cell burden. Graph shows further refinement of the number of conditions in each group based on the estimated cellular burden. The cellular burden is depicted by the dotted line and defined by extrapolating a 90° arc of the ellipse described by eq. (6.6), resulting in maximal thresholds defined by eqs. (6.7) and (6.8) respectively.

In Figure 6.6 the experimental conditions are displayed in their respective hit groups identified in section 6.2.2.4, with conditions not meeting the minimum cell burden requirement removed (red). The creation of cell burden as a non-linear function has provided the flexibility to fairly value conditions influencing both product quality and qP simultaneously.

The dashed grey lines represent the highest IgG monomer abundance and qP requirements along the minimum cell burden curve, and were defined by eqs. (6.7) and (6.8). The area enclosed by these lines and the 90° arc of the cell burden curve highlight the conditions that would be lost by employing linear stringencies.

After the elimination of 46 conditions that did not meet the defined minimum cell burden, the total number of hits was reduced to 25 in group 1, 6 in group 2 and 28 in group 3. This resulted in an overall hit rate of 15.3 % of conditions.

6.2.2.6 Review of Identified Hit Compounds

In the 59 identified hit conditions there were 6 instances where a compound appeared twice; once in group 3, and again in group 1 or 2. As group 3 represented an improvement in both product quality and quantity, replicate appearances in groups 1 and 2 were removed. After accounting for the replicate appearances the final number of hit compounds identified in the preliminary screen was 53, representing 27.6 % of the library. Figure 6.7 shows titre and product quality of the final compound selection relative to the control population.

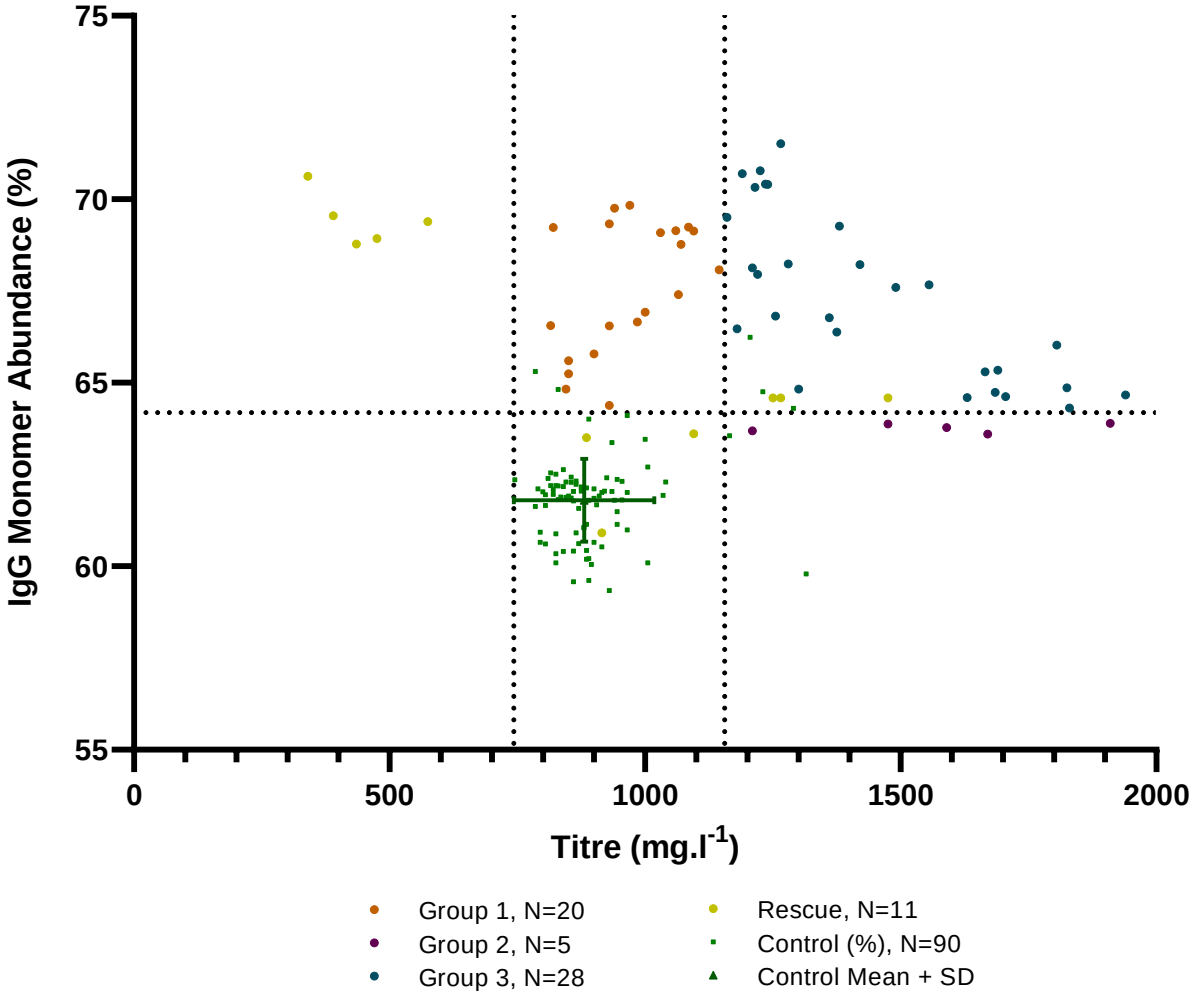

Figure 6.7: Preliminary: Overview of the compounds selected for further investigation. Where both concentrations tested appeared, only the best performing condition is shown. The boundaries of each group are shown by the dotted lines and defined by eqs. (6.3) to (6.5).

Upon manual interrogation of the data there were instances where it was deemed the screening conditions or analytical methods were not sufficient to accurately exclude a compound. An additional group was created containing compounds that had been manually 'rescued' for further investigation if capacity was available in future experimental screens. The 11 candidate compounds identified were overlaid in yellow (Figure 6.7) and were selected based on the following criteria:

- *Top left cluster* ($n = 5$) - Both compound conditions were eliminated based on culture

performance in section 6.2.2.2. This indicates that the concentrations screened were highly toxic, however these compounds may be efficacious at lower doses.

- *Control centred cluster* ($n = 2$) - Both compound conditions fell within or very close to the control population distribution for all metrics measured. This indicates the pharmacologically active concentration was not achieved and a higher concentration may be efficacious.
- *Other* ($n = 4$) With each of these compounds, one condition met the minimum product quality and titre criteria with the other meeting the minimum cell burden criteria but neither met both. In this scenario both concentrations demonstrated a degree of efficacy, and the limitations in concentrations and replicates may have resulted in a false negative result.

Upon evaluation of the compound groups for the identified hits in Figure 6.8, 52.8 % of positive results fall into the 'phenotypic hit' category, demonstrating a need for information to support further analysis. Of the 3 ineffective categories, β-amyloid binders were of particular interest initially due to the high number of compounds. One compound was identified leading to a 7.1 % hit rate, demonstrating that despite evidence suggesting they can act non-specifically on unrelated aggregates they provide no benefit in this context. Furthermore, although the measured product quality of 69.2 % monomer was a significant improvement on the control population abundance of 61.9 %, there was no improvement in titre or qP.

Due to the limitations associated with an $n = 1$ experimental study it is difficult to draw any concrete conclusions from the results observed. However the high abundance of positive hits supports the hypothesis that mechanisms of proteopathies and antibody aggregation may overlap, and provides strong evidence to further interrogate the identified hit compounds in greater detail.

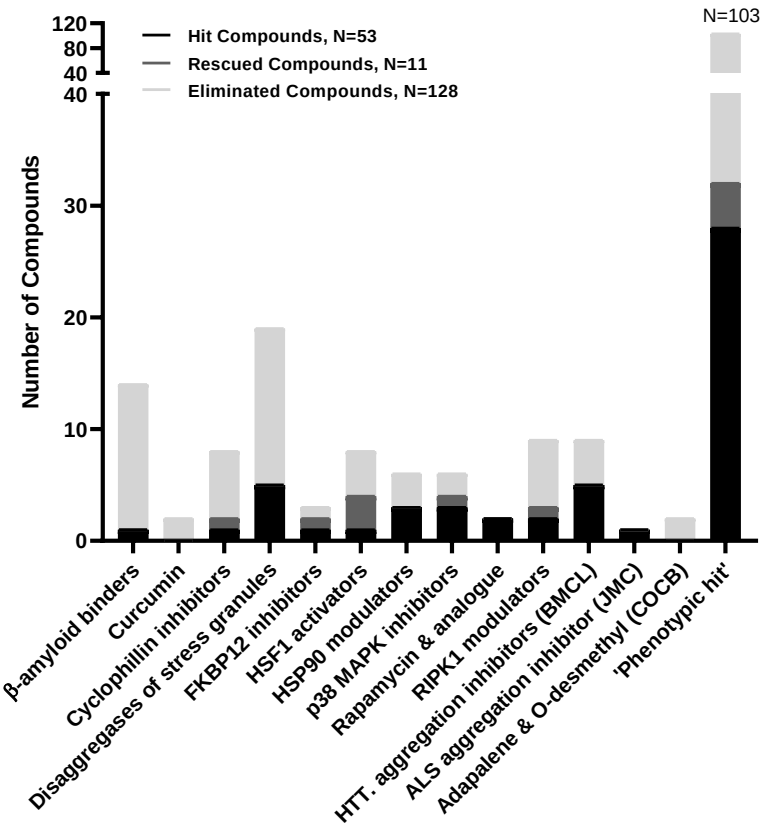

Figure 6.8: Preliminary screen: Distribution of compound library mechanistic groups overlaid with the number of successful compounds.
.

6.2.3 Secondary Screen: Interrogating 'Hit' Compounds

6.2.3.1 Overview

Following the success of the preliminary screen, additional information on the interesting compounds in the 'Phenotypic hit' category from the AstraZeneca Open Innovation database has been included. Each of these were able to rescue one or more of the following toxic proteopathies in cell models:

- FUS - FUS is an Ribonucleic Acid (RNA) binding protein associated with ALS and FTD. Toxicity is a result of a toxic gain of function of cytoplasmic FUS-containing aggregates, and the resultant reduction of nuclear FUS (Scekic-Zahirovic et al. 2016).
- TDP43 - TDP43 form cytoplasmic aggregates with FUS and is considered a hallmark of ALS pathology (Hergesheimer et al. 2019). Additionally TDP43 aggregates are able to self propagate between cells in a prion like manner and induces toxicity by binding and preventing endocytosis function (G. Liu et al. 2017).
- C9ORF72-PR50 - A key common mutation in C9ORF72 associated with ALS and FTD leads to aggregate induced toxicity and death in neuronal cell models (Hergesheimer et al. 2019; Wen et al. 2014a). Expansion of the G_4C_2 hexanucleotide repeats in C9ORF72 leads to unconventional Repeat-Asociated Non-ATG initiated (RAN) translation generat-

ing toxic dipeptide repeat proteins (Kyung Ha Lee et al. 2016). Proline-Argentine dipeptide repeat proteins form toxic nuclear aggregates leading to neuronal cell death (Wen et al. 2014b). Although the mechanisms are unclear, the remodelling of folding and assembly mechanisms leading to alleviation of PR50 aggregates may be generically applicable in CHO cell engineering.

Despite the lack of interaction or mechanistic information on these compounds the ability to rescue a aggregate induced toxicity in proteopathic models indirectly fits the library identification criteria outlined in section 6.2.1. The 'Phenotypic hit' category of compounds was subdivided based on the specific toxicities rescued resulting in a better distribution of compounds between categories Figure 6.9. As the information on compounds eliminated in the preliminary screen remains restricted it is not possible to compare the relative hit rate of the phenotypic hit subdivisions.

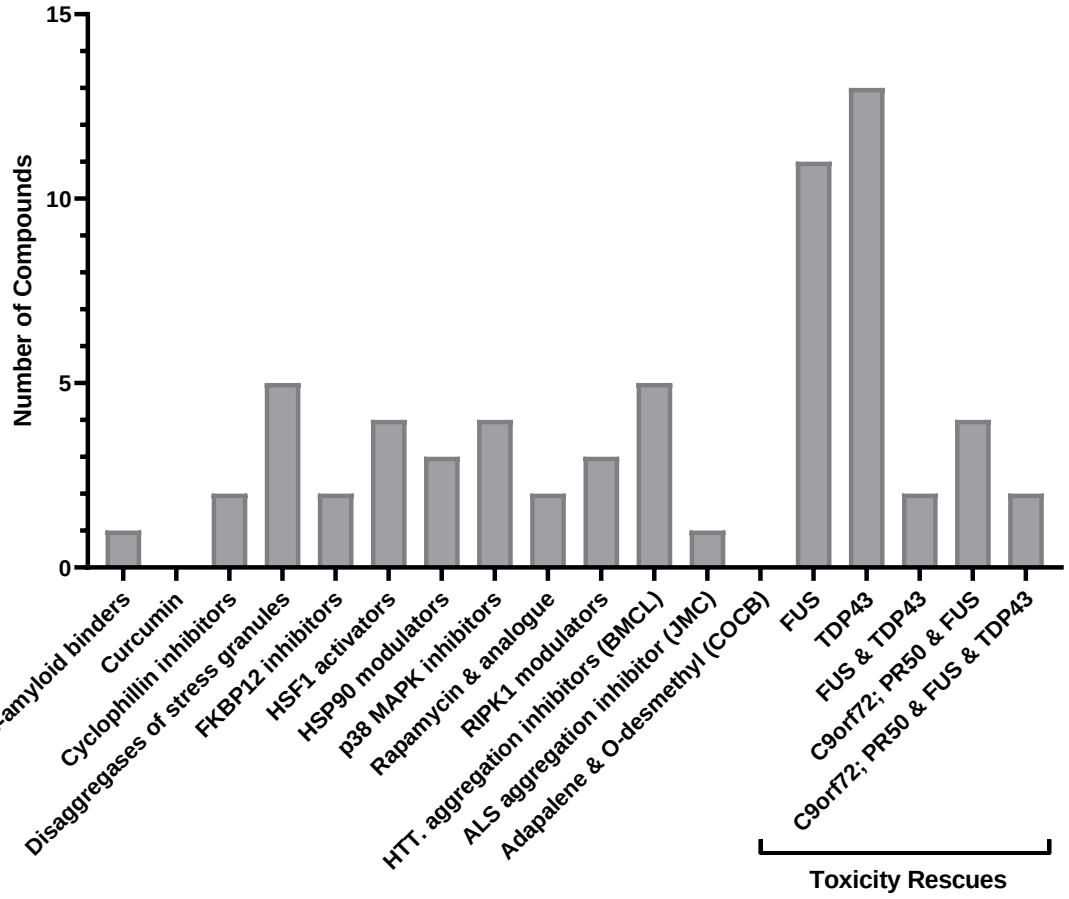

Figure 6.9: Screen 2: Distribution of compound library between mechanistic groups.
The 'Phenotypic Hit' group from the primary screen has been split into individual toxicity rescue assays.

The library scale and limited capacity of the preliminary screening required assessment of all compounds as the same concentrations. The increased resource allocation after the success of the preliminary study permitted the screening of each compound in the reduced library to be assessed at 3 concentrations in an $n = 3$ study. This would improve reliability and provide validation for additional analytical and scale-up experiments. Furthermore the information gained from the

preliminary assessment allowed the screening concentrations to be adjusted based on previous compound performance. Compounds were divided into high, medium and low groups based on a subjective analysis of whether they would benefit from an increased (6.25 μM to 100 μM), similar (3.13 μM to 50 μM) or decreased (0.38 μM to 6.13 μM) range of doses. Table C.2 lists screening concentrations of each compound alongside an internal referencing index, category and approximate molecular weight.

Minor adjustments were made to the experimental work flow from section 6.2.2 based on the previous performance of the control population. Firstly the overall culture duration was reduced from 11 days to 10 days as the mean control at harvest was 21.3 %. Secondly the point of supplementation was brought forward to day 4 so the compounds were present for the same duration as the preliminary screen.

6.2.3.2 Cell growth, viability and titre measurements

A similar data analysis pipeline as described in the preliminary screen was followed starting with evaluation of the control population growth and viability. Figure 6.10a displays the distribution of the control population when IVCD was plotted against the cell viability as measured on day 7. The mean viability was 14.2 % lower than seen in the preliminary screen (Section 6.2.2.2), suggesting a change in the control culture characteristics.

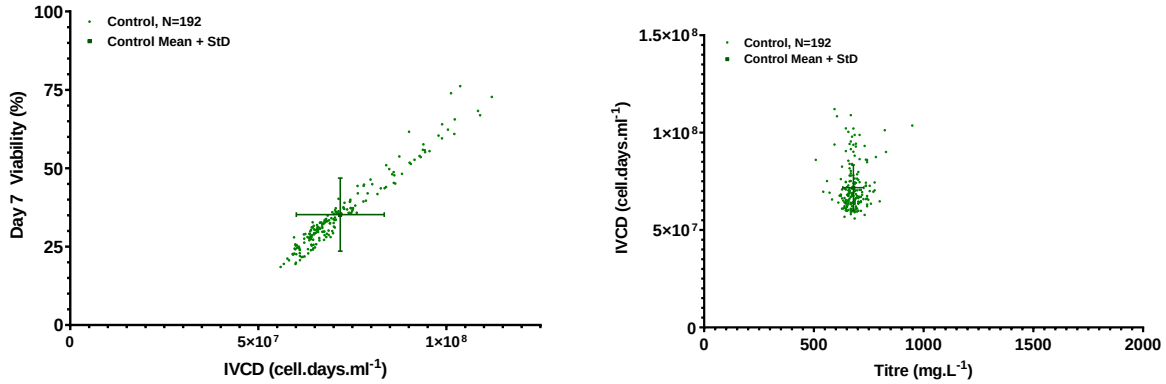

Figure 6.10: Secondary screen: Variation in the control population performance.
(**a**) Scatter plot of the control population 10 day IVCD against the day 7 viability. (**b**) Scatter plot of the control population day 10 titre against 10 day IVCD. e performance of each compound category and sub-category in the secondary screen. .

Additional Vi-CELL assessment of 24 control population wells on day 4 demonstrated consistent exponential cell growth, with an average VCD of 12.54×10^6 cells.ml^{-1} and CV of 7.24 % being observed. Additionally, the average cell viability on day 4 was high, measured at 98.34 % and a CV of 1.20 %. This demonstrated that between days 4 and 7 the conditions became unfavourable, stagnating growth and reducing the control population]viability. Furthermore, the reduced day 7 performance between the preliminary and secondary screening suggests an ongoing systemic issue with increasing consequences. Surprisingly the variation in growth characteristics did not translate to a similar variation in IgG titre as demonstrated in Figure 6.10b, suggesting a systematic error in the measurement of cell growth and viability may be significant factor.

The control population VCD and viability measured on the Cellavista was compared to independent control cultures assessed using a Vi-CELL (Appendix A, Figure A.6). The Vi-CELL measured the mean cell viability 10.6 % higher than the Cellavista, and the calculated mean VCD on day 7 was 1.56 fold higher. Additionally, a reduction in CV of 21.0 % and 34.84 % was observed for viability and VCD respectively, suggesting the Cellavista was under-counting the viable and overall population. However, this confirmed that the control populations were not performing well and did not explain the reduced performance between the preliminary and secondary screens.

Further statistical evaluation of the control population summarised in Table 6.2 revealed little variation in the Integral Total Cell Density (ITCD) or aggregate abundance. The mean ITCD was 2.1 fold greater than the IVCD, yet the range and StD was lower, suggesting resource depletion was limiting cell growth.

A review of the AZ-proprietary media composition between the $CHO_{BIS\text{-}A}$ fed-batch experiments in chapter 5 and preliminary and secondary screens described here suggested the addition of a proprietary supplement to the media composition had improved cell growth rates and allowed higher density cultures. It was hypothesised this increased the culture glucose consumption, resulting in depletion and subsequent cell apoptosis before the culture period concluded.

Table 6.2: Secondary screen: Statistical evaluation of the control population.
The mean, range, StD and CV is displayed for the control population metrics. All metrics are measured at harvest with the exception of viability, which was measured on day 7.

Statistic	Viability (%)	IVCD (cell.days.ml^{-1})	ITCD (cell.days.ml^{-1})	Titre (mg.l^{-1})	Monomer (%)	HMWS (%)
Mean	25.22	7.12×10^7	1.53×10^8	680.04	63.39	36.61
Range	57.65	6.61×10^7	4.23×10^7	440.11	9.79	9.79
StD	11.65	1.17×10^7	9.12×10^6	48.06	1.43	1.43
CV (%)	46.20	12.28	5.93	7.07	2.26	3.92

Due to the limitations identified the secondary screening would need repeating with an updated media and feed composition containing sufficient glucose. However as the titre and aggregate data demonstrated reduced variability, these could provide insights into the performance of compounds relative to the preliminary screening round, and further refine the correct pharmacological concentrations.

A comparison of the titre measured by Octet and quantified post purification demonstrated the same complications as discussed in section 6.2.2.4. Appendix A, Figure A.7a shows the titre reduced during the last 3 days of culture for the majority of data points when measured by Octet. Alternatively when the BIS-A was quantified post Protein A purification the titre had increased from the day 7 octet measurement (Appendix A Figure A.7b), and similarly to the preliminary screen, offered a more reliable measure of product titre.

6.2.3.3 Global data trends

The overall dataset was analysed irrespective of compound, concentration or controls to identify any underlying trends that may improve our understating of $mAb_{BIS\text{-}A}$ production. The relationship between titre and product quality shown in Figure 6.11a suggests that BIS-A aggregates in a concentration dependent manner with an R^2 of 0.30. A stronger negative correlation was seen between specific productivity and product quality in Figure 6.11b where the R^2 was 0.47, indicating that a high production rate may contribute to increased aggregation. Increasing the specific productivity requires an increase in the rate molecules pass through the ER resulting in less time for incorrectly folded molecules to be identified. This supports the findings in Cao et al. 2018 where intermolecular disulphide bonds between the engineered variable regions lead to head-to-tail dimers forming.

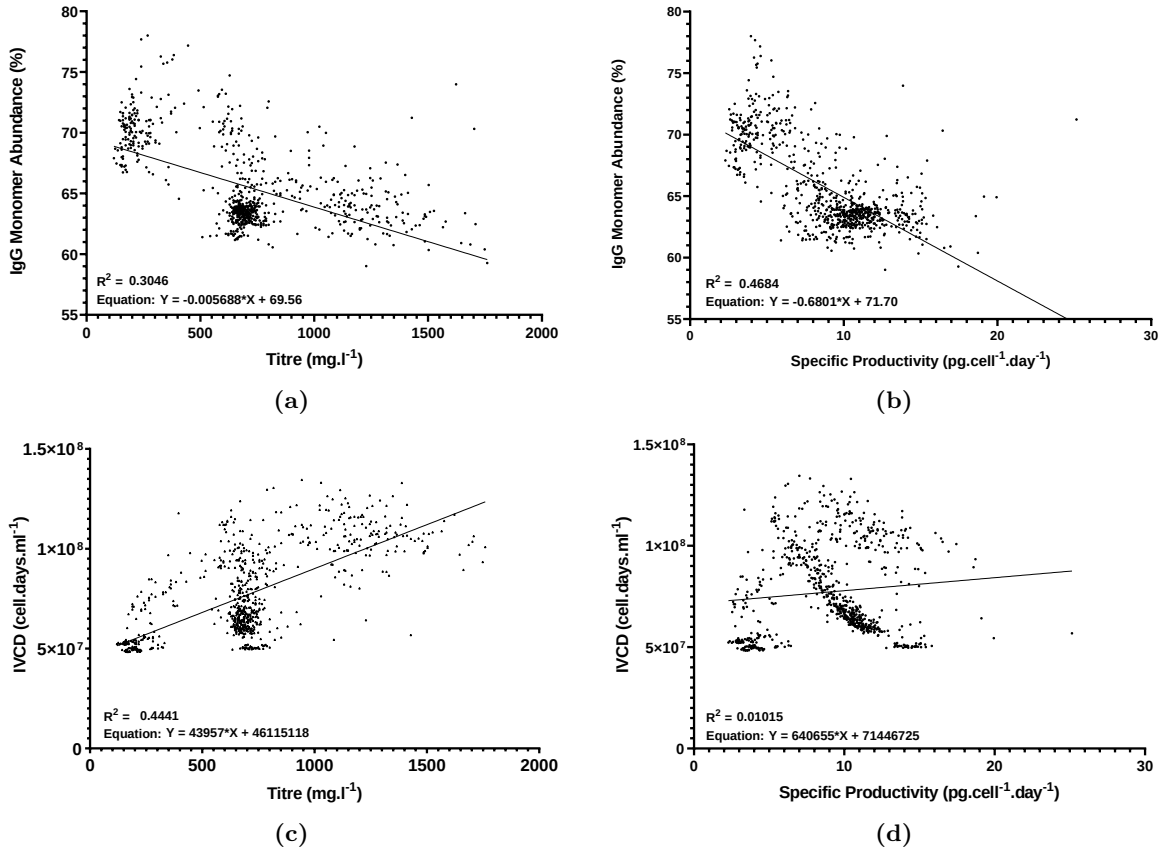

Figure 6.11: Secondary screen: Analysis of global dataset trends.
The global dataset, including controls and all experimental conditions, were plotted to identify underlying trends as follows; titre – IgG monomer abundance (**a**), titre – specific productivity (**b**), titre – IVCD (**c**) and specific productivity – IVCD (**d**). Graphs show a linear regression overlaid to look demonstrate trends.

The positive correlation between titre and IVCD displayed in Figure 6.11c is as expected. However, the R^2 indicates that only 44.4 % of the variation in product titre is a result IVCD, demonstrating the supplemented compounds were having a large impact on production rate in addition to quality. Lastly the R^2 between specific productivity and IVCD was 0.01, suggesting that the production rate was not affected by the number of cells in culture and therefore is unrelated to cell growth.

6.2.3.4 Compound performance relative to the preliminary screen

Due to the high variability in growth and reduction in viability observed by in control population it was not possible to evaluate impact of the compound library using these metrics.As the control population BIS-A monomer abundance and titre were very consistent, compound performance was assessed using these metrics to provide further information on active pharmacological concentrations and evaluate the trends within each compounds category. Due to the culture growth and viability limitations, the secondary screen needed repeating limitations on cell growth and viability had been resolved to objectively and definitively assess the hits from the preliminary screen and progress to scale-up and further analytical investigations.

Figure 6.12 demonstrates the experimental triplicates relative to the control population. The impaired performance resulted in a 22.8 % reduction in control population titre mean in the secondary screen. Additionally, the mean product quality increased by 1.53 % as a result of the negative correlation between product quality and titre identified in section 6.2.3.3. The resultant increase in the equivalent product quality criteria of 2.08 % shifted data points in the secondary screen shifting data points from the upper to lower right quadrant. Only 3.1 % ($n = 6$) conditions appear in the upper-right quadrant representing the group 3 criteria, however, 28.1 % ($n = 54$) fall into the lower-right quadrant representing group 1.

Figure 6.13 illustrates the distribution of the best performing concentration of each compound, categorised by the hit groups in section 6.2.2.4. The dotted lines highlight selection criteria equivalent to the preliminary screen, calculated from the control population distribution as per eqs. (6.3) to (6.5).

The increased mean IgG monomer abundance in the control population has significantly reduced the number of compounds appearing in the upper right quadrant representing group 3 in the preliminary screen. This resulted the 32 of 53 compounds falling into the lower right quadrant representing an increase in titre without a significant increase to IgG monomer abundance.

In the preliminary screen, hit compounds were identified by four groups: Group 1 improved product quality, group 2 improved product titre, group 3 improved both product quality and titre while the final group contained rescued compounds. As highlighted in Table 6.3, a greater proportion of compounds appear in group 2 with groups 1 and 3 reducing in relative population in the secondary screen.

The 'Rescue' group identified in the preliminary screen contained 11 compounds which were selected for further analysis, despite not meeting the criteria. They were included as it was predicted that the concentrations screened were not within the pharmacological range, so the performance of the compounds were not effectively evaluated. In Figure 6.13 four of the rescued compounds have greatly exceeded the equivalent preliminary screen criteria, although one is borderline. This confirmed that the preliminary screen parameters were not able to effectively assess the entire library, and an unknown number of false negatives will have been missed.

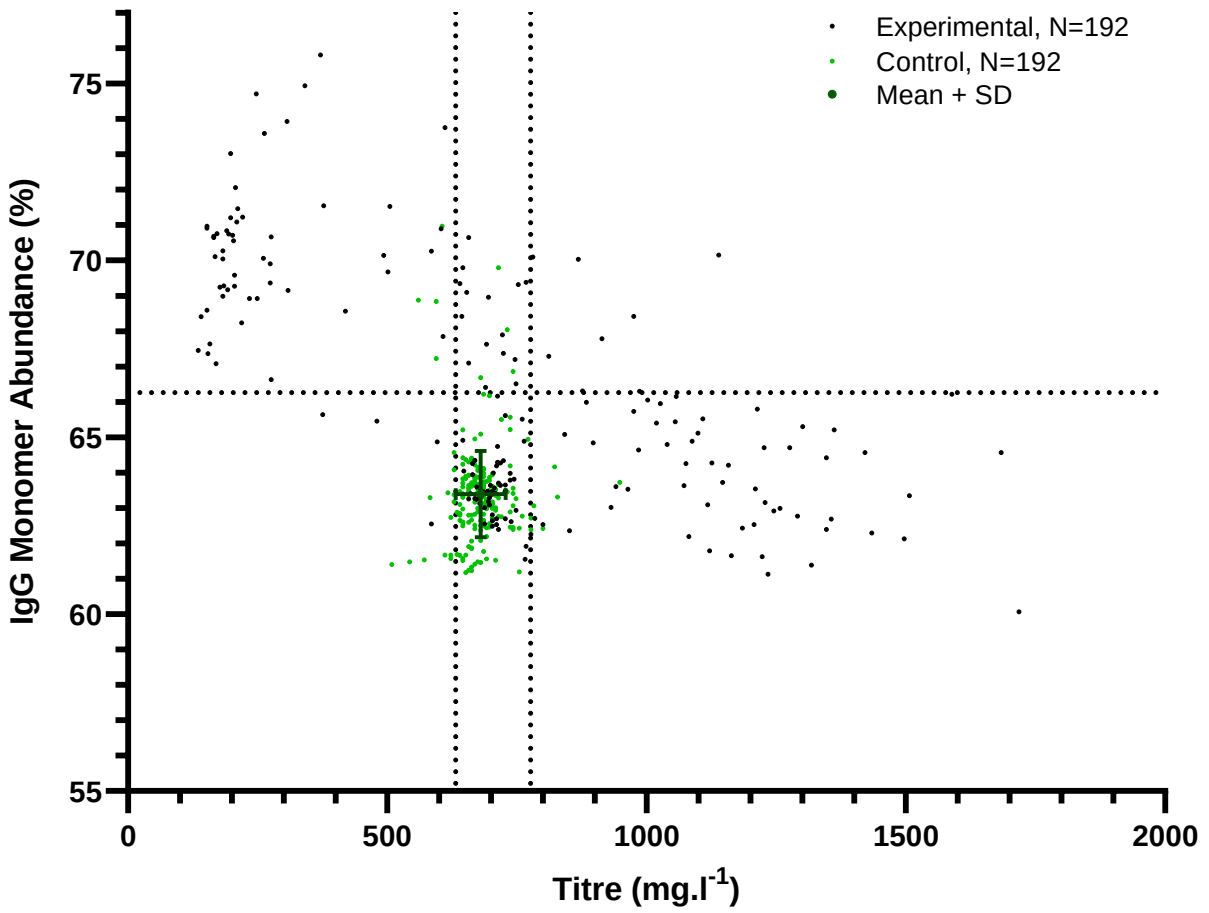

Figure 6.12: Secondary screen: Distribution of experimental triplicates on a titre vs IgG monomer abundance scatter plot.
Graph shows the titre and IgG monomer abundance of the experimental conditions tested relative to the control population (green). Data points represent the mean of $n = 3$ replicates and error bars have been excluded for clarity. Dotted lines at $y = 66.26\%$, $x = 776.1\ mg.ml^{-1}$ and $x = 631.9\ mg.ml^{-1}$ demonstrate the criteria used to eliminate conditions in the preliminary screen, defined by eqs. (6.3) to (6.5).

Table 6.3: Comparison of the group distribution between the primary and secondary screen.
The distribution of the 53 hit compounds identified in section 6.2.2.6 between the three hit groups in the primary and secondary screens between the three hit groups defined in section 6.2.2.4. The 11 'rescued' compounds from the primary screen have been excluded from these values.

Hit Group	Group Criteria	Hit Compound Distribution	
		Preliminary Screen (%)	Secondary Screen (%)
Group 1	Aggregation	37.8	11.3
Group 2	Titre	9.4	60.1
Group 3	Aggregation + Titre	52.8	13.2
None	N/A	N/A	15.4

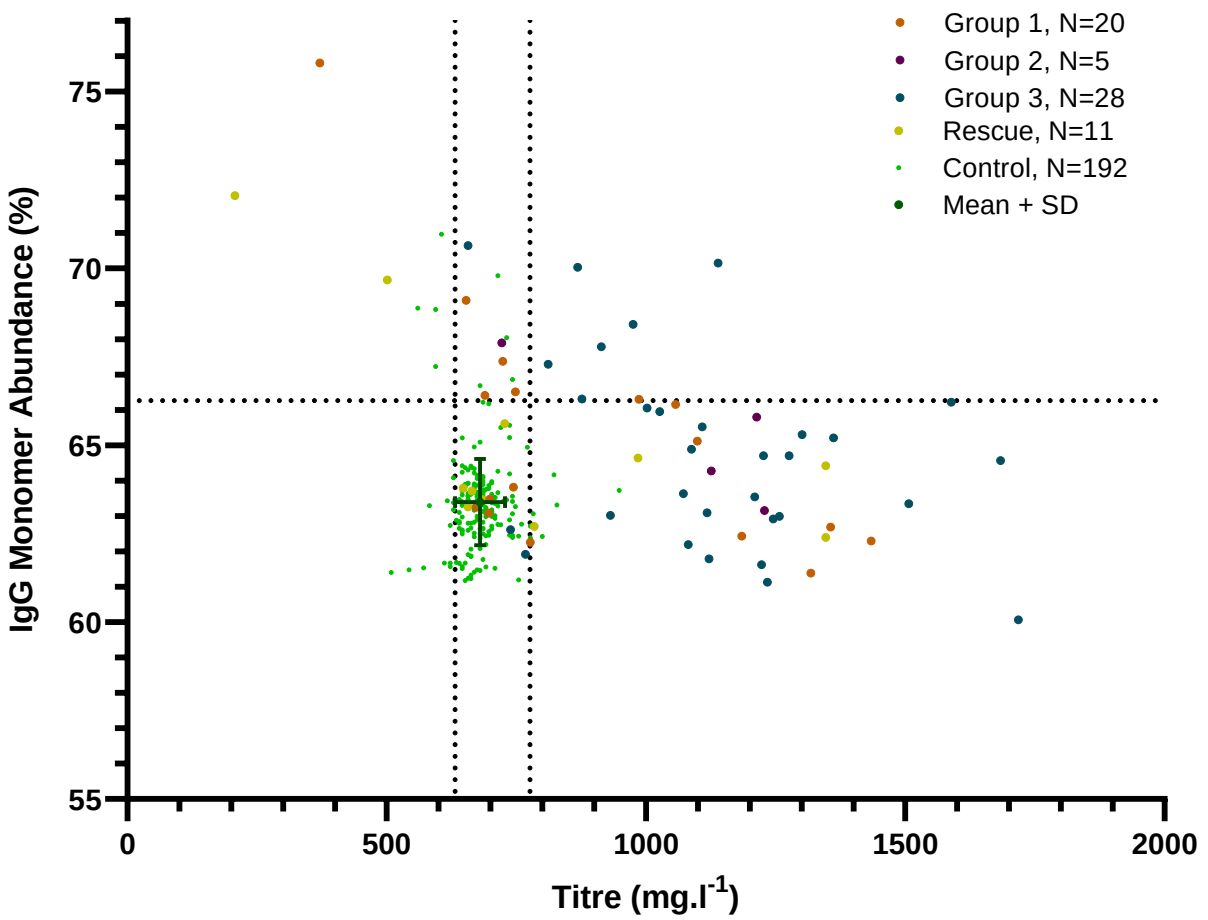

Figure 6.13: Secondary screen: Reviewing the performance of groups identified in the preliminary screen.
The graph shows the titre and IgG monomer abundance of the best concentration of each compound relative to the control population (green). Data points are colour coded into hit groups as identified in section 6.2.2.4 and represent the mean of $n = 3$ replicates with error bars excluded for clarity. Dotted lines at $y = 66.26\%$, $x = 776.1\ mg.ml^{-1}$ and $x = 631.9\ mg.ml^{-1}$ demonstrate the criteria used to eliminate conditions in the preliminary screen, defined by eqs. (6.3) to (6.5).

6.2.3.5 Reviewing the performance of compound categories

The best condition for each compound from Figure 6.13 was labelled according to the category and sub-category to evaluate their distribution relative to the control population. The category of each compound in this section can be found in Appendix C Table C.2. In order improve the clarity when adding the error bars and labels the compound library was separated into 'categories' and the 'sub-categories of the phenotypic hit group', described in sections 6.2.1 and 6.2.3.1, were separated into Figures 6.14a and 6.14b respectively.

Considering $mAb_{BIS\text{-}A}$ quality and titre together, M33 stands out as the best performing compound increasing the monomer abundance by 6.9 % relative to the control population while improving the titre by 1.7 fold. When excluding results where the mean titre is less than the lower bound of the control population StD, M1 was the most beneficial to product quality with a mean BIS-A abundance of 70.8 % and was the outlier of the C9ORF72-PR50 & FUS sub-category. M37 in the TDP43 toxicity rescue sub-category increased the titre by 2.52 fold over the control mean, the largest titre increase of any compound tested. However M37 was also highly detrimental to detriment of product quality resulting in the lowest BIS-A monomer abundance.

Table 6.4 shows a summary of the performance of each category and subcategory by highlighting the compounds that improve titre, IgG monomer abundance or both. The minimum improvements for inclusion in the table are outlined below with compounds reducing the titre below the control mean minus StD removed:

- Titre increase of $\geq$ 1.8-fold.
- IgG monomer increase of $\geq$ 3%.
- Titre increase of $\geq$ 1.5-fold and IgG monomer increase of $\geq$ 2%.

Despite the large improvements to BIS-A titre and quality identified, systemic resource depletion restricting the control population performance highlight the need for further validation of results.

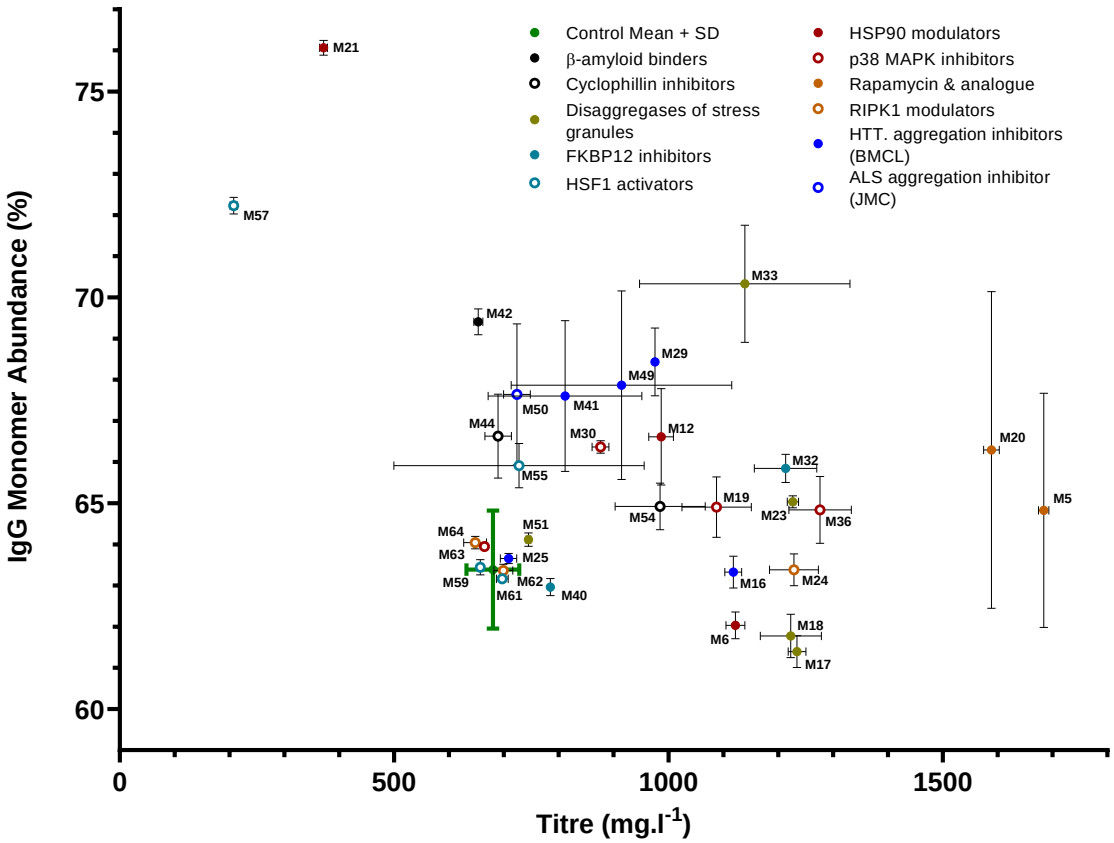

(a) Compound categories excluding 'Phenotypic hit'

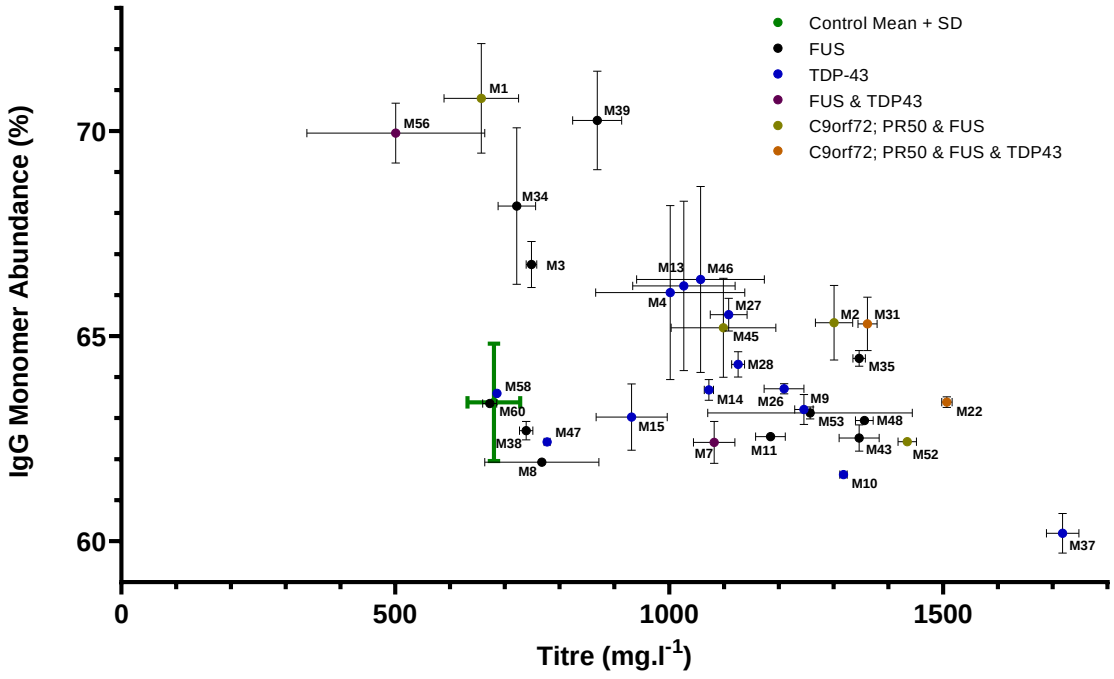

(b) Phenotypic hit sub-categories

Figure 6.14: Secondary screen: Performance evaluation of mechanistic categories. Depiction of the best performing concentration for each compound, identified by the mechanistic categories (**a**) or phenotypic hit subcategories (**b**), as defined in Table 6.1 relative to the control population. Each compound is labelled with an ID with further information on each available in Appendix C, Table C.2. Points and error bars represent the mean and StD of $n = 3$ replicates.

Table 6.4: Secondary Screen: Performance summery of the compound categories and sub-categories.
Table provides and overview of of the compounds from each category and subcategory that improve titre, product quality or both. For each the compounds that meet the criteria and percentage of the total number of compounds in the category is displayed.

Category or Subcategory	Titre FC $\geq$ 2.0		Monomer increase $\geq$ 3%		Titre FC $\geq$ 1.5 & monomer $\geq$ 2%	
(Category Size)	Compounds	Freq.	Compounds	Freq.	Compounds	Freq.
β-amyloid binders ($n = 1$)	-	0 %	M42	100 %	-	0 %
Cyclophilin inhibitors ($n = 2$)	-	0 %	M44	50 %	-	0 %
DisAgg. stress granules ($n = 5$)	M17, M18, M23 M33	80 %	M33	20 %	M33	20 %
FKBP12 inhibitors ($n = 2$)	-	0 %	-	0 %	M32	50 %
HSF1 activators ($n = 4$)	-	0 %	-	0 %	-	0 %
HSP90 modulators ($n = 3$)	-	0 %	-	0 %	M12	33 %
p38 MAPK inhibitors ($n = 4$)	M36	25 %	M30	25 %	M19	25 %
Rapamycin Analogue ($n = 2$)	M5, M20	100 %	-	0 %	M20	50 %
RIPK1 modulators ($n = 3$)	M24	33 %	-	0 %	-	0 %
HTT aggregation (BMCL) ($n = 5$)	-	0 %	M29, M41, M49	60 %	M29	20 %
ALS aggregation inhib. (JMC) ($n = 1$)	-	0 %	M50	100 %	-	0 %
FUS ($n = 11$)	M35, M43, M48, M53	36 %	M3, M34, M39	27 %	-	0 %
TDP43 ($n = 13$)	M9, M10, M26, M37	31 %	-	0 %	M4, M13, M46	23 %
TDP43 & FUS ($n = 2$)	-	0 %	-	0 %	-	0 %
C9ORF72-PR50 & FUS ($n = 4$)	M2, M52	50 %	M1	50 %	M2	25 %
TDP43 , C9ORF72-PR50 & FUS ($n = 2$)	M22, M31	100 %	-	0 %	M31	50 %

6.2.4 Tertiary Screen: Improving cell growth characteristics and investigating mAb specificity

6.2.4.1 In person working restrictions due to the COVID-19 pandemic

The tertiary screen was postponed on the 24th of March 2020 due to unforeseen in person working restrictions as a result of the COVID-19 pandemic. Culture supernatants were placed in long term storage ready for Protein-A purifications and subsequent aggregate analyses at a later date. At the time of writing it was not yet possible for the project to be resumed. As the tertiary screen is incomplete, the chapter discussion focuses heavily on the results of the secondary screen despite the cell culture performance concerns described in sections 6.2.2.2 and 6.2.3.2. Despite the aggregate analysis not being complete, initial results from the tertiary screen were included, as the data obtained was deemed important to the chapter outcomes and thesis future works.

6.2.4.2 Overview

Negative control cultures exhibited substantial variability in IVCD and cell viability in the preliminary section 6.2.2.2 and secondary screens section 6.2.3.2 limiting the conclusions which could be drawn from the previous screening rounds. A review of the HTP 24-SWP culture platform by the cell line development team at AstraZeneca identified glucose depletion was leading to reduced cell growth and viability. This was alleviated by revision of glucose concentrations in the proprietary media and feed regime.

The results from the secondary screen required replication using the revised protocol to confidently state that compounds, or categories of compounds benefit $mAb_{BIS\text{-}A}$ production. The results from the secondary screen were interrogated to further refine the compound concentrations which are listed in Appendix C Table C.2.

Previous examples throughout this thesis have highlighted the specificity of genetic and chemical engineering solutions in CHO cells. $CHO_{BIS\text{-}B}$ was selected as an additional cell line to provide initial insights into the applicability of the hit compounds as broad CHO engineering tools.

The experimental workflow employed was identical to the secondary screen. $CHO_{BIS\text{-}A}$ and $CHO_{BIS\text{-}B}$ cells were seeded at 0.710×10^6 cells.ml^{-1} and feed was added every other day starting on day three. Culture VCD and viability was assessed by trypan staining measured on the Cellavista and samples were taken for titre analysis by Octet on day seven and at culture harvest. Supernatants were collected at culture harvest and stored at $-80\,°C$ for protein-A purification and subsequent aggregate analysis by HPL-SEC.

6.2.4.3 $CHO_{BIS\text{-}A}$ and $CHO_{BIS\text{-}B}$ culture performance and mAb titre

Figure 6.15a depicts the growth characteristics of experimental conditions in black, with the negative control cultures overlaid in green. At culture harvest on day 10 the mean IVCD of the $CHO_{BIS\text{-}A}$ negative control population was 1.53×10^8 cell.days.ml^{-1}, and the mean cell viability was 60.5 %. This demonstrated a significant improvement in culture conditions as a result of the updated media composition and feed regime.

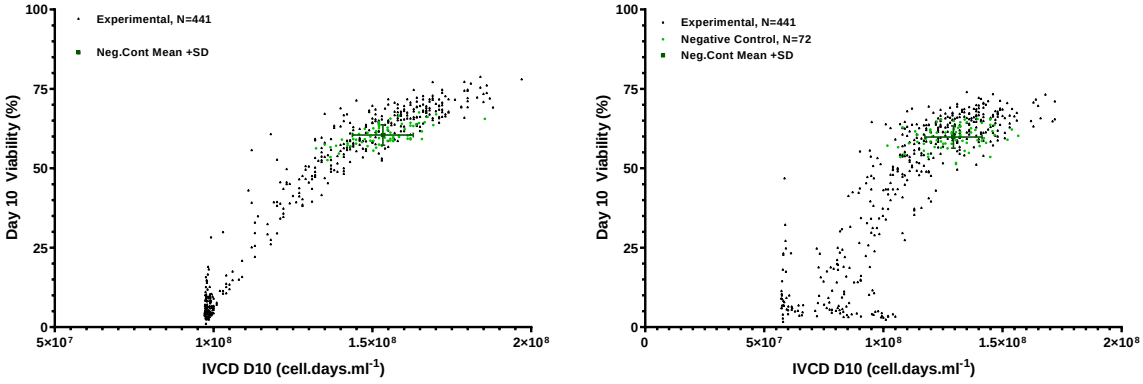

(a) $\mathrm{CHO}_{\text{BIS-A}}$ **(b)** $\mathrm{CHO}_{\text{BIS-B}}$

Figure 6.15: Tertiary Screen: Revised feed regime improved culture IVCD and viability. Plots show the distribution of experimental and control cultures when IVCD is plotted against cell viability on day 10 for $\mathrm{CHO}_{\text{BIS-A}}$ (**a**) and $\mathrm{CHO}_{\text{BIS-B}}$ (**b**). The mean and StD (dark green) of $n = 72$ negative control cultures was plotted for reference.

The mean cell viability of the $\mathrm{CHO}_{\text{BIS-B}}$ control population at harvest on day 10 was 59.8 %, and the mean IVCD was calculated to be 1.29×10^8 cell.days.ml^{-1} as shown in Figure 6.15b. This confirmed the additional cell line was also performing well with the revised media and feed compositions.

Titre, measured on day 7 and day 10 by Octet, is displayed in Figures 6.16a and 6.16b for $\mathrm{CHO}_{\text{BIS-A}}$ and $\mathrm{CHO}_{\text{BIS-B}}$ respectively. In contrast to previous experiments, the $\mathrm{mAb}_{\text{BIS-A}}$ titre was higher on day 10 than day 7 in all cultures. This was also true for the majority of $\mathrm{CHO}_{\text{BIS-A}}$ cultures. In $\mathrm{CHO}_{\text{BIS-A}}$, 24.3 % of 441 experimental cultures had a day 10 titre greater than the negative control population mean plus StD. Similarly, 30.6 % of $\mathrm{CHO}_{\text{BIS-A}}$ culture titres were more than a StD above the negative control mean.

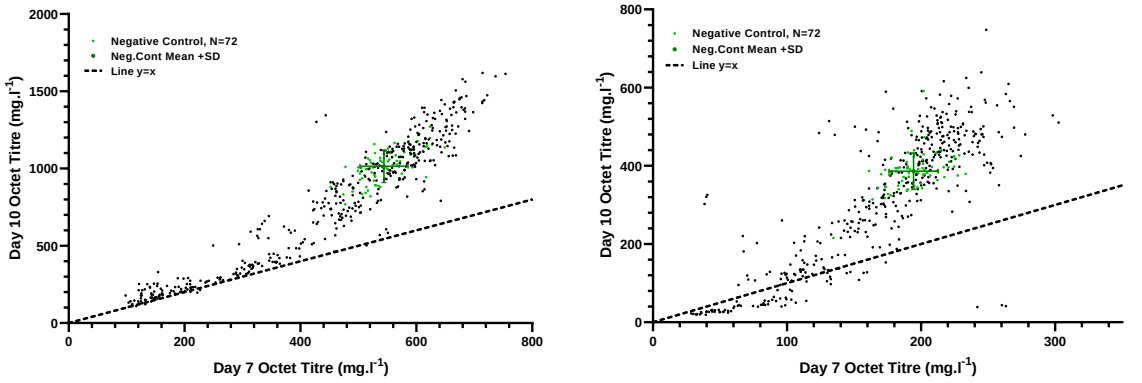

(a) $\mathrm{CHO}_{\text{BIS-A}}$ **(b)** $\mathrm{CHO}_{\text{BIS-B}}$

Figure 6.16: Tertiary Screen: Revised feed regime improved Octet product quantification. Scatter plots of $\mathrm{CHO}_{\text{BIS-A}}$ (**a**) and $\mathrm{CHO}_{\text{BIS-B}}$ (**b**) titre measured on day 7 and day 10 by Octet. The plotted line at $x = y$ represents an equal titre at the respective time points. The mean and StD (dark green) of $n = 72$ negative control cultures was plotted for reference.

The initial results from the tertiary screen demonstrate the revised media and feed compositions have overcome the culture performance hurdles encountered previously. This also alleviated the apparent loss of mAb titre between day 7 and culture harvest when measured by Octet.

6.3 Discussion

The discovery of new compounds to improve mAb production in CHO cells could help overcome a multitude of hurdles in the cell line development process, offering increased flexibility and reduced specificity than genetic engineering approaches. Furthermore, demonstrating a mechanistic commonality to a well documented class of compounds in human pathology could also improve our understanding and reveal a wide range of CHO cell engineering candidates. This chapter identifies and evaluates a library of compounds, evidenced to alleviate or prevent aggregation in models of proteopathic neurological disease as engineering tools.

Due to the vast amount of research into treating neurological disease, the first step was to identify a practically sized and representative compound library which could achieve the following two objectives:

1. Improve the production of a model problematic aggregate prone mAb as a case study.
2. Cover a wide range of mechanisms and disease models to evaluate the chemical diversity of successful compounds.

This was achieved through collaborative interrogation of the AstraZeneca Open Innovation initiatives database of 250,000 compounds. This looked sought those with mechanisms which alleviate aggregation or rescue aggregative toxicities in cell models of human proteopathies. Despite the limitations surrounding intellectual property protection, a diverse library of 192 compounds was identified with 14 distinct categories based on the mechanism of action or literature source. Over half of the compound library was placed in the phenotypic hit category. Compounds in this category have been demonstrated to rescue aggregative toxicities in models of neurological disease during drug discovery screens by AstraZeneca. As the full potential of these compounds was unknown, further information of the specific toxicities rescued was restricted to compounds of interest after the preliminary screen.

In order to evaluate the compound library, $CHO_{BIS\text{-}A}$ was selected as an optimal model system. The aggregation of BIS-A has been characterised as covalent head-to-tail dimer formation by Cao et al. 2018, making it an ideal candidate. Additionally, $CHO_{BIS\text{-}}$A was previously utilised in section 5.2.2, therefore cell growth characteristics and expected titre in a high throughput fed-batch context was known.

6.3.1 Preliminary Screen: Proof of Concept and Library Refinement

The preliminary screening round aimed to rapidly assess the initial library of 192 compounds identified by the AstraZeneca Open Innovation group. The results described in Chapter 5 provided initial evidence supporting the underlying hypothesis; compounds able to alleviate aggregation in disease models present useful CHO engineering tools. Most compounds in the pre-clinical library were relatively undocumented in comparison to the proteostasis regulators from Plate, Cooley, et al. 2016 screened in Chapter 5. Despite further evidence presented by Grandjean et al. 2020; Plate and Wiseman 2017 describing the mechanism by which proteostasis

regulators confer ER reprogramming, it was possible that none of the identified compounds would be efficacious. Therefore it was vital to evaluate the library efficiently, and narrow down the number of compounds to a practical scale for further investigation.

In the preliminary screen ≥50 % of HSP90 modulators, p38 MAPK inhibitors and Htt aggregation inhibitors were identified as hits. The success of modulating broad acting MAPK stress response pathways and HSP90 chaperones points towards efficacy in general ER stress pathway regulation as a successful engineering route. However, this success was matched by the Htt aggregation inhibitors with a specific mechanism of alleviating aggregation (Rinderspacher et al. 2009). Rapamycin, an analogue of rapamycin and the ALS aggregation inhibitor were all identified as hits, and as these categories contained two or fewer compounds these groups had a ≥100 % 'hit rate'.

Three of five categories with a ≥50 % 'hit rate' in the preliminary screens had been identified from published literature into models of prion diseases. These were the ALS aggregation inhibitor (Y. Zhang et al. 2012), Htt aggregation inhibitors (Todd and J. Lim 2013) and rapamycin (+ analogue) (Bové et al. 2011; Sarkar et al. 2008). In addition to evidence suggesting *mTOR* activation (by rapamycin or similar compounds) can reduce protein aggregates in Alzheimer's and Huntington's disease models, several studies have reported that Rapamycin improved the production of therapeutic proteins in CHO cells (Dadehbeigi and Dickson 2015; Lalonde and Durocher 2017; Y. Li et al. 2019).

6.3.2 Secondary Screening of Hit Compounds

Promising preliminary results suggested a significant proportion of the compound library had a positive effect on the quantity and quality of $mAb_{BIS\text{-}A}$ production, providing strong justification for further evaluation. By limiting the secondary screen to a third of the initial compound library, evaluation at three concentrations in triplicate. It was anticipated that results from the secondary screen would be used to identify a smaller subset of compounds for scale-up, scale-out and further analytics.

A meta-analysis was performed on the secondary screening results to search for any overarching trends between culture IVCD, titre and productivity. The aim of this analysis was to identify any characteristics or limitations of the $CHO_{BIS\text{-}A}$ cell factory, therefore all control and experimental cultures were treated as a single population. the presence or concentrations of compound was disregarded. A moderate negative correlation ($R^2 = 0.46$) was observed when qP was plotted against product quality and a similar analysis revealed a weak ($R^2 = 0.30$) correlation between $mAb_{BIS\text{-}A}$ titre and quality. This provided confirmation that compound selection based on the 'estimated cell burden' in the preliminary screen (section 6.2.2.5) was well-informed, and suggests that improving the production quality of a DTE mAb comes at the expense of quantity. Although the data described demonstrates a negative correlation between $mAb_{BIS\text{-}A}$ production rate and quality, the hypothesised cause is not conclusive. The inverse correlation could be an artefact of the experimental methods employed, threrfore there is a need to explore the

possibility of concentration dependent $mAb_{BIS\text{-}A}$ aggregation in the culture media or during sample purification.

In the secondary screen the three largest titre improvements were observed upon supplementation of rapamycin, a rapamycin analogue and a compound from the TDP43 toxicity rescue subcategory. The >2 fold increase in response to supplementation of both rapamycin-like compounds corroborates the effects seen in the preliminary screening results and CHO cell engineering literature (Dadehbeigi and Dickson 2015; Lalonde and Durocher 2017; Y. Li et al. 2019).

The distribution of Htt aggregation and p38 MAPK inhibitors was very similar, with the majority of compounds improving both titre and product quality. Htt aggregation inhibitors were identified as having a high hit rate in the preliminary screen. In the secondary screen 60 % of compounds evaluated in this category significantly improved product quality, and one of these also increased $mAb_{BIS\text{-}A}$ titre. The results suggest mAb aggregation in $CHO_{BIS\text{-}A}$ and Htt protein in Huntington's disease may share a common mechanism. Further research from a mechanistic biology perspective would therefore be greatly insightful. Upon evaluation 75 % of the p38 MAPK inhibitors increased the titre or monomer abundance of $mAb_{BIS\text{-}A}$. The single ALS aggregation inhibitor increased the monomer abundance by 4.3 % in the secondary screen. All of these compound categories were fruitful in both screening rounds, validating to the library refinement methodology employed.

Additional information from the AstraZeneca Open Innovation programme facilitated division of the 32 hit compounds in the phenotypic hit category during the preliminary screen into five subcategories. The compounds were shown to rescue one or more toxic cell phenotypes as a result of FUS, TDP43 or C9ORF72-PR50 aggregates. Overall, compounds that rescued TDP43 toxicity had a much greater effect on titre than aggregation rate, with 10 of 13 compounds found to increase $mAb_{BIS\text{-}A}$ titre by >1.5 fold. Whilst 4 of these also increased the monomer abundance in $CHO_{BIS\text{-}A}$, none did so exclusively.

In ALS and Alzheimer's diseases, TDP43 and FUS are found together in protein aggregates, therefore a similar response to both compound groups would be expected. Instead, the effects seen from compounds that rescued FUS toxicity were highly selective towards either mAb titre or quality, with no compounds effecting both.

All five compounds that rescued C9ORF72-PR50 toxicity also rescued toxic FUS and/or TDP43 phenotypes. These are of particular interest as all 6 compounds were found to be beneficial in $CHO_{BIS\text{-}A}$. Although the majority had a greater impact on product titre than quality, M1 improved $mAb_{BIS\text{-}A}$ monomer abundance by 7 %. When excluding compounds that were detrimental to $mAb_{BIS\text{-}A}$ this was biggest improvement in product quality observed.

6.3.3 Overcomming Compromised Cell Viability and Titre Measurements in the Tertiary Screen

In the preliminary screen the IVCD and viability of the control population was significantly lower than expected. Seven days post seed the mean control population viability was 43.8 %

lower than in previous work, and the IVCD was 2.3 fold lower.

A further reduction in the control population mean cell viability during the secondary screen was a more significant concern, confirming a systemic problem in the cell culture platform with increasing severity. Interestingly the mean control IVCD in the secondary screen was similar to the preliminary screen, suggesting that the culture conditions were good initially and became unfavourable over time. It was thought that the depletion of an essential nutrient was resulting in cell death, and the presence of viable cells at harvest suggested this must be present in the feed, but at insufficient levels.

Evaluating the composition of AstraZeneca's production media and feed was difficult as both were proprietary with regularly updated recipes. Fortunately, retrospective analysis of these changes identified that a proprietary nutrient, supplement X, which was added to the media composition between the work conducted in Chapter 5 and this study. The addition of supplement X helped to control lactate levels in the culture, improving culture performance in Erlenmeyer flasks and Amber bioreactors. However, it had not been evaluated in the HTP screening platform. In both Erlenmeyer and AMBR systems, cultures are monitored more precisely and data generated by the Cell Line Development team indicated that glucose consumption had increased as a result of supplement X. It was hypothesised that the low cell viability seen in the preliminary and secondary screens was most likely the result of glucose depletion. This was confirmed when the supplementation of extra glucose to the media and feed alleviated the systemic low culture viability in the tertiary screen.

In the preliminary and secondary screens the titre measured by Octet at harvest was lower than the titre measured from samples taken on day seven of culture. Sample purification and quantification demonstrated that the Octet was not effectively measuring $mAb_{BIS\text{-}A}$ titre at the point of culture harvest. In the preliminary screen, the total protein content of purified samples was greater than the mAb titre measured by the Octet. This discrepancy was amplified when taking product loss during purification into account. HPL-SEC analysis confirmed the sample purity, eliminating the possibility of inefficient purification falsely elevating $mAb_{BIS\text{-}A}$ when quantified by this method.

The initial results from the tertiary screen showed that the Octet measured $mAb_{BIS\text{-}A}$ titre was as expected when cell viability is not compromised, and increased between day seven and ten of culture. It is hypothesised that the low cell viability led to degradation or modification of $mAb_{BIS\text{-}A}$ such that the Octet assay measurement was disrupted, without effecting protein-A binding. Alternatively cell debris would be prevalent in cultures with a very low cell viability. The binding of these debris to $mAb_{BIS\text{-}A}$ may have led to steric hindrance during the Octet assay, resulting in reduced titre measurements.

It is hypothesised that in the tertiary screen, where the viability of all $CHO_{BIS\text{-}A}$ negative control cultures was $\geq$50 %, the titre discrepancy between the two quantification methods would be greatly reduced. Unfortunately purification, quantification by UV absorbance and aggregate analysis of samples from the tertiary screen was not possible due to external restrictions. If completed, a comparison between the Octet and protein-A purified titre measurements would

validate titre quantifications in previous screens where Octet measurements were compromised.

Chapter 7

Conclusions and Future Work

7.1 Conclusions

The results presented throughout this thesis have firstly led to the design and development of a High Throughput (HTP) Simultaneous Overexpression and Silencing Co-transfection (SOSC) gene screening platform for Chinese Hamster Ovary (CHO) cell engineering. Secondly, the results demonstrated the applicability of combining transient overexpression and knock-down to identify product specific and CHO host engineering targets. Thirdly, the use of proteostasis regulators identified from proteopathic disease research as CHO culture performance enhancers has been demonstrated. Finally, the broader applicability of proteopathic disease disaggregases as engineering tools to reduce aggregation and improve the production of Difficult to Express (DTE) Monoclonal Antibodys (mAbs) has been demonstrated. The conclusions drawn from each of the project outcomes are explored further in this section.

7.1.1 Design and Development of a SOSC Gene Screening Platform for CHO Cell Engineering

Following extensive development and optimisation steps, a transient SOSC gene screening platform was developed as a CHO cell engineering tool. The platform is chemically defined, protein free, and incorporates high cell density transfection, ensuring functionality and applicability to industry processes. Although initially avoided, instant delivery of Deoxyribonucleic Acid (DNA) and Ribonucleic Acid (RNA) at high cell density (achieved using the Lonza Nucleofection platform) facilitates immediate dilution post transfection. The result limits extended toxicity and supports exponential growth, achieving Peak Cell Density (PCD) within the effective time frame of RNA Interference (RNAi). Co-transfection validation by flow cytometric analysis ensured consistant and efficient nucleotide delivery, minimising the dilutent effects of non-transfected cells on overall culture performance.

If successfully optimised, alternative RNA transfection methods would have scaled better than the Lonza Nucleofection platform, however the complexity of optimising these for DNA co-transfection was not evaluated. This would require sequential delivery of DNA and RNA, ex-

acerbating the discussed effects of transfection. Alternatively, overexpression and knock-down conditions could be transfected and evaluated independently. Although this would simplify the protocol, identifying the correct experimental controls would be highly complex and directly comparing effector gene overexpression and knock-down may not be possible.

Further technology developments and process optimisations made to the established HTP culture platform improved performance, reduced replicate variability and increased the platform throughput. Once transitioned, culture growth rate of transfected cells was significantly improved, and non-transfected cells were comparable to Erlnmyer flasks, increasing the applicability to scaled up culture formats. In our research group, well-to-well variability had been an ongoing challenge when conducting HTP genetic engineering experiments. Cell settling during high density mixing steps was the most supported working hypothesis, leading to variability in the number of cells seeded. Following initial evaluations, the HTP electroporation protocol was automated on an Opentrons OT-2 liquid handler, significantly reducing the well-to-well variability seen when completed manually. Further development of automated cell counting, culture sampling and titre assays increased the feasible throughput of the SOSC gene screening platform.

7.1.2 Application of Transient SOSC Gene Screening Identify CHO Engineering Targets

To evaluate the screening platform's applicability as a tool to identify product specific and host CHO engineering targets, an extensive case study was performed, generating multiple parallel research outcomes.

A bioinformatic approach was employed to identify a list of gene screening targets which were up- or down-regulated during adaptation to stable mAb production, using matched host and producer transcriptomics datasets. This aimed to evaluate the usefulness of transcriptomics datasets to identify genetic engineering targets specific to the host cell genetic background. While successful in identifying a host cell and multiple product specific engineering targets, retrospective analyses comparing the experiential findings to the transcriptomics data was unsuccessful. Attempts to relate transcript abundance or differential regulation in the dataset with the transient screening results did not identify any substantial correlations. Despite this, the number of engineering targets identified from a narrow library supports the use of host specific transcriptome analysis for effector gene library identification.

Contrary to the effects seen during platform development, analysis of the scrambled endoribonuclease prepared small interfering siRNA (esiRNA) controls identified consistent, cell line specific responses to the presence of Double Stranded Ribonucleic Acid (dsRNA) within the cell. Growth and titre increased post scrambled esiRNA transfection in both mAb models, and the magnitude was greater in the Easy to Express (ETE) model. It is hypothesised that this was masked by lower cell growth rates in the 96-Deep Well Plate (DWP) culture system during platform development, however the differential magnitude of effects seen between cell lines would make any experimental compensation imperfect. Following normalisation of the RNAi effect,

overexpression and knock-down conditions could be compared. It was evident that the normalisation method could be improved, and although several plausible mechanisms were discussed in Section 4.3.2, the response of producing CHO cells to foreign dsRNA response is relatively uncharacterised, presenting an interesting research avenue.

Comparison of paired producers from a common host cell facilitated the evaluation of differences in host adaption to ETE and DTE mAb production. A sensitivity analysis revealed greater growth variation in the ETE producer. When considering the natural cell selection process, the factor limiting ETE mAb production is likely to be associated with transcription and translation rather than Endoplasmic Reticulum (ER) folding and assembly processes. The rate of mAb production is linked to the rate of glutamine synthesis by a common integration site, and transcriptional activity at the integration site will only be sufficient for glutamine to not limit cell growth. Conversely, in a DTE model mAb, associated ER and Unfolded Protein Response (UPR) stresses are likely to limit production. The screening results support this, and the DTE mAb producer was found to have greater titre sensitivity in response to effector gene titration.

7.1.3 Chemical Chaperones and Proteostasis Regulators as Cell Culture Enhancers

A library of seven compounds identified by Plate, Cooley, et al. 2016 as *ATF6*-specific UPR activators were evaluated as CHO engineering tools. This was a contained Proof of Concept (POC) feasibility study evaluating the application of proteopathic disaggregases, ahead of large scale screening of compounds to be identified from a broader context.

Initial compound characterisation in CHO cells producing an ETE mAb identified strong pharmacological responses upon titration of two of seven compounds. The most promising compound, C1, demonstrated a dis-linkage between growth and titre, increasing productivity. Across the library, a non-toxic inhibition of cell growth was observed. Although this reduced overall product titre, growth arrest during the late exponential phase of CHO culture can be beneficial to the overall development pipeline, reducing lactate accumulation and biomass associated purification complications (Pérez-Rodriguez et al. 2020). Additionally, delaying supplementation until the end of the growth phase can help shift cellular resources towards mAb production.

Further evaluation of the proteostasis regulators in DTE mAb models identified context specific cell culture improvements, demonstrating their viability as engineering tools. Delaying supplementation was effective in limiting the effects of growth inhibition, however changes to product titre and Specific Productivity (qP) were diluted relative to equivalent conditions added at the start of culture. The dilution of effects was hypothesised to be a consequence of active compound internalisation, resulting in the intracellular concentration being dependent on cell density.

The 'dose-per-cell' effect was demonstrated in CHO_{ETE} upon supplementation of high concentrations of C1 at the mid-point of extended fed batch cultures. In addition to reducing the growth limiting effects of C1, the qP increase observed in the initial evaluations was maintained,

increasing product titre relative to the matched Dimethyl Sulfoxide (DMSO) control. From the lack of existing available literature, this would be an interesting area of future research.

7.1.4 Re-purposing Preclinical Neurological Compounds to Alleviate Intracellular Aggregation of Bi-specific mAbs

Following the POC evaluation of proteostasis regulators as cell culture enhancers, a diverse library of compounds associated with disaggregation in proteopathies were evaluated as CHO engineering tools, demonstrating anti-aggregative and titre improvements in a DTE mAb producer known to aggregate.

A library of 192 compounds was collaboratively identified from literature and in-house data from the AstraZeneca neuroscience compound portfolio. Rapid assessment in an $n = 1$ preliminary screen validated the approach employed for library identification, assessed the efficacy of compounds and began to identify the active pharmacological concentrations. The preliminary screen identified 53 hits which improved titre and/or reduced aggregation of a model bi-specific DTE mAb. Although conclusions from the preliminary screen are limited by the lack of replicates, compounds associated with broad ER stress regulation and inhibitors of Huntington's disease associated aggregation appear most in the list of hit compounds.

Subsequent secondary evaluation identified 38 compounds significantly benefiting the production of the model mAb, representing 20 % of the initial compound library. Similar to the preliminary screen, a high percentage of Htt aggregation inhibitors were identified, whereas p38-MAPK inhibitors and HSP90 modulators which broadly regulate ER stress had limited impact.

A number of complications associated with cell growth and viability were of concern, and questioned the validity of the preliminary and secondary screening data. A final HTP screen aimed to address these after the media and feed composition was updated to improve culture performance. Despite COVID-19 associated restrictions preventing aggregate analysis, initial product titre data confirms the efficacy of the compound library, supporting confident interpretation of findings from the previous screens. Furthermore, the prominent titre improvements observed upon supplementation of rapamycin and a rapamycin analogue support previous CHO engineereing studies investigating the positive effects of rapamycin supplementation on therapeutic proteins.

Overall the results presented strongly advocate the use of compounds alleviating aggregation in proteopathic disease to solve CHO engineering challenges. This presents an exciting tool in an industry context, providing a rapid solution to extract the required performance from problematic stable CHO producers when the timelines associated with genetic engineering approaches are of concern.

7.2 Future Work

This section explores the future work required to further interrogate and validate the findings discussed within this thesis, and examines further research avenues which could be undertaken.

These include improvements to the SOSC gene screening platform, characterisation of the generic CHO cell responses to RNAi and investigating the stable expression of the genetic engineering targets identified. Other investigative avenues would be to evaluate the applicability of proteopathic disease disaggregases in alternative antibody modalities and cell hosts, explore scalability into bioreactor conditions and examine overall impact on other product quality characteristics. Lastly the implications of creating of a standardised screening tool from a library of proteopathic disease disaggregases is explored.

7.2.1 Improving the HTP SOSC gene screening platform to improve functionality and applicability

The transient screening platform developed during this PhD accurately captured the effects on the exponential and stationary phases of culture to maintain applicability to industry cell line development processes. RNAi knock-down duration was a key limitation in the design and optimisation process, requiring high density cell seeding. Despite this the platform is limited to batch culture conditions, and an alternative knock-down methodology would be required to evaluate the effect of RNAi mediated knock-down on extended duration fed-batch cultures.

The most straightforward modification to improve knock-down duration would be to utilise Short Hairpin Ribonucleic Acids (shRNAs) encoded within a plasmid vector in place of direct small interfering RNA (siRNA) or esiRNA transfection. In addition to facilitating knock-down durations comparable with transient overexpression, shRNA encoding DNA allows stable integration for long term knock-down of identified cell engineering targets (Moore et al. 2010).

As previously discussed, a key advantage of esiRNA mediated RNAi is the dilution of off-target effects facilitated by a heterogeneous pool of siRNAs targeting the Gene of Interest (GOI). Several studies have demonstrated the efficacy of multiple shRNAs encoded on a single polycystronic cassette, allowing knock-down of up to five targets simultaneously (Mcintyre et al. 2011; Weng et al. 2017; Xia et al. 2006). Studies demonstrated a negative correlation between knock-down potency and the number of shRNAs encoded, however when encoding multiple variants targeting the same GOI this would not be of concern. Therefore, the primary limitation on the number of shRNAs which could be encoded in a polycystronic cassette would be vector size. Based on insert sizes of 220 bp to 250 bp described by Weng et al. 2017 Brake et al. 2008, 10+ shRNAs targeting a single GOI would be possible. This would provide similar advantages to esiRNA mediated knock-down, which can be further improved by synthetic biology approaches.

7.2.2 Investigation into the generic CHO cell responses to foreign dsRNA

A generic increase in performance was observed in response to RNAi transfection in both mAb producer models assessed in the application of the SOSC gene screening platform. Evaluation of the scrambled esiRNA control identified increased Integral Viable Cell Density (IVCD) and titre in both models, although the differing magnitudes resulted in a net qP decrease in the ETE, and increase in the DTE producing cell lines, contradicting findings by Daga et al. 2018 in HeLa cells.

It is hypothesised that introduced dsRNA competes with endogenous Micro RNAs (miRNAs), as both utilise the same RNAi machinery, however no CHO cell specific literature is available to interrogate this. Directly comparing the impact of effector gene overexpression and knockdown is challenging as currently generic, and on-target effects of RNAi in CHO cells are difficult to decipher, leading to sub-optimal normalisation of experimental data. Therefore, performing experiments to accurately model the relationship between the transfection of non-targeting dsRNA and cell performance would enable accurate normalisation of CHO RNAi screening experiments. Subsequently, this would improve our understanding of responses to gene expression level manipulations in CHO cells.

7.2.3 Improving production CHO cell lines through stable overexpression of transiently beneficial effector genes

The transient effector gene screening described in Chapter 4 identified *ERDJ5* as a generic engineering target for the MEDI-CHO host, benefiting the production of ETE and DTE model mAbs, and identified several product specific engineering targets for $CHO_{BIS\text{-}A}$.

The applicability of the genetic engineering targets identified to industry processes is highly dependent on their efficacy upon stable expression. One confirmatory approach is to perform stable transfection of the identified effector genes, individually or in combination, in $CHO_{BIS\text{-}A}$ under an alternative selection marker. These experiments would be the most direct application of the transient data into a stable production environment.

Previous studies have seen varying success in translating transient benefits to stable production systems (Cartwright et al. 2020; Gulis et al. 2014). More recently, unpublished data generated by Dr. Joe Cartwright has demonstrated limited success when transiently beneficial effector genes are stably overexpressed in existing CHO producers.

As an alternative approach, stable mAb and effector gene co-transfection on a single vector would allow the effector gene expression to facilitate the cell selection process. By evaluating the pools recovered, the impact of effector gene overexpression on the CHO host's recovery and adaption to stable mAb production could be assessed. Although sequential stable transfections would be an informative research exercise, co-transfection would be more applicable to industry development pipelines.

7.2.4 Scale-up validation and mechanistic analysis of the top performing disaggregases from neurological disease models

From several screening rounds evaluating of a broad library of proteopathic disease associated disaggregases, 38 hit compounds were found to improve product quality and/or titre in an aggregate prone DTE mAb model. Despite external restrictions preventing aggregate analysis of the tertiary screen, the presented results strongly support the use of such compounds as CHO engineering tools, and indirectly indicate overlapping mechanisms of aggregation. In addition to completing the postponed work, further validation and characterisation of the effects of hit

compounds is required to facilitate their use as cell engineering tools for the production of therapeutic proteins.

Firstly, the top performing compounds identified from HTP screening experiments require evaluation in multiple cell models. A common trend throughout this thesis and the CHO engineering literature is the product specificity of identified solutions. Without any previous examples evaluating the effect of proteopathic disease disaggregases on mAb production, it is hypothesised this trend will be maintained. Nevertheless, evaluation in production systems with differing expression difficulties, antibody modalities and host cell backgrounds is required to confidently address the underlying hypothesis advocating, the use of such compounds in a broad CHO engineering context.

Secondly, select compounds need to be evaluated in an appropriate model of large scale production. Although HTP screens are useful tools to rapidly evaluate many experimental conditions simultaneously, they lack the precise control systems found in large scale bioreactors to maximise performance and product yield. The AMBR-15 HTP automated bioreactor system is designed to accurately model the conditions of larger scale bioreactors, and offers similar process controls such as online monitoring of glucose, lactate, pH and dissolved gasses. Evaluation in an AMBER, or similar model system would confirm whether performance improvements are equally applicable to highly optimised production systems.

Lastly, aggregation is only one of several metrics to evaluate product quality. As described in Cao et al. 2018, the engineered cystine residues in $CHO_{BIS\text{-}A}$ are also susceptible to cysteinylation or glutathionylation. This leads in monomer size variants in addition to dimerisation as a result of intermolecular disulphide bond formation. As both monomer variants exhibit reduced bioactivity, these are treated as product impurities and need to be minimised. Therefore, the quantification and evaluation of monomer variants is crucial to accurately evaluate the effect of compounds on overall $mAb_{BIS\text{-}A}$ quality.

7.2.5 Utilising proteopathic disease disaggregases as a standardised screening tool to rapidly improve the production of new DTE molecules

One of the key advantages of chemical engineering approaches is the speed in which compounds can be evaluated. Equivalent genetic approaches require vectorology, transient assessment and stable integration in order to solve any CHO engineering challenge. Although useful for host cell engineering, these steps are too time-consuming to be incorporated into industry cell line development processes.

After scale-out and scale-up applicability has been demonstrated, a library of compounds can be selected as a standardised screening tool to improve the production of new DTE therapeutics. The probability of at least one compound achieving the desired effect will be high with a moderate sized library, if compounds are systematically selected for diversity. Furthermore, the effective concentration ranges of each compound can be accurately characterised, minimising the number of experimental conditions required.

By restricting the scale, problematic DTE molecules can be screened in a single HTP experiment to identify hit compounds, followed by process optimisation in a model of large scale production. Importantly this can be run in parallel to the normal cell line development workflow with no impact on overall timelines.

Appendix A

Supplementary Figures

A.1 Chapter 3 Supplementary Figures

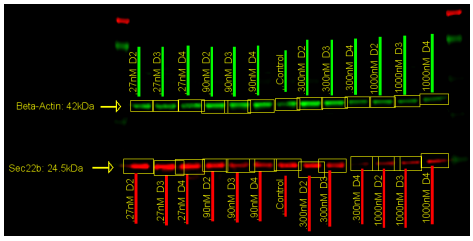

(a) SEC22B small interfering RNA (siRNA)

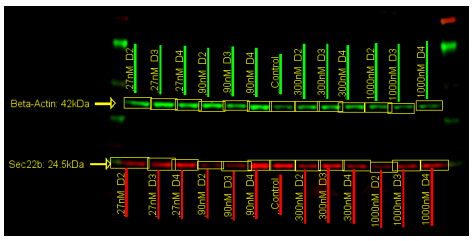

(b) SEC22B endoribonuclease prepared small interfering siRNA (esiRNA)

Figure A.1: Quantitative western blots to evaluate RNAi knock-down efficiency. Figure shows example blots for knock-down with SEC22B siRNA (**a**) and SEC22B esiRNA (**b**). CHO_{T2} cells were electroporated with 0 nM to 800 nM of Ribonucleic Acid (RNA) and seeded at 0.5×10^6 cells.ml^{-1} in 96-Deep Well Plates (DWPs). Samples were taken 2, 3, and 4 days post-transfection and triplicates pooled for western blot analysis..

A.2 Chapter 4 Supplementary Figures

Table A.1: Differentially regulated genes in CHO_{ETE} associated with Monoclonal Antibody (mAb) folding and assembly.
A complete list of the genes identified through the bioinformatic analysis of the CHO_{ETE} RNA Sequencing (RNAseq) dataset from Geoghegan et al. 2018. Columns containing' Gene Ontology (GO) hits' and fold change conditions indicated the respective number of associated GO terms from section 4.2.1.1, and the number of assessed differential expression criteria met section 4.2.1.3.

Gene ID (ENSCGRG)	Gene Symbol	GO Hits	FC Conditions	Gene ID (ENSCGRG)	Gene Symbol	GO Hits	FC ≥1.666 Hits
1018265	Amfr	1	2	1003994	Hyou1	1	2
1012473	Atf6b	1	2	1021781	Mesd	1	2
1018239	B2M	1	2	1024712	Mkks	1	1
1012370	Bak1	1	2	1014713	P3h1	1	2
1011816	Bax	1	1	1013338	P4hb	1	2
1020181	Calr	1	2	1008721	Pdia3	1	2
1017710	Canx	1	2	1005477	Pdia4	2	2
1011598	Creb3l1	1	1	1017472	Pdia6	1	2
1015590	Ddit3	1	2	1024356	PEX19	1	1
1019161	Dffa	1	1	1010542	Pfdn4	1	1
1024828	Dnajb11	1	1	1016773	Pfdn5	1	1
1024374	Dnajc10	1	2	1001849	Pfdn6	1	2
1020922	Dnajc5	1	2	1022765	Pofut2	1	2
1023828	Erlec1	1	2	1018105	Ppib	1	2
1003211	Ern1	1	2	1009299	Prdx4	1	1
1025067	Ero1lb	2	2	1012267	Ptpn1	1	2
1019603	Erp44	2	1	1000642	Ranbp2	1	1
1021447	Fkbp4	1	1	1016511	Sec61a1	1	1
1021370	Fkbp9	1	2	1009803	Syvn1	1	1
1014239	Hsp90aa1	1	1	1008911	Tbl2	1	1
1023543	Hsp90b1	1	2	1023992	Tor1b	1	1
1013777	Hspa5	3	2	1020169	Uggt1	1	2
1015556	Hspb1	1	1	1015026	Wrb	1	1

Table A.2: Final library of 17 effector genes associated with mAb folding and assembly.
The library of effector genes are described by their gene ID and symbol. The mean abundance was calculated from early- and late-stage culture transcript abundances for CHO_{ETE}. Differential regulation was defined as a fold change $\geq$1.66 in at least one condition as defined by eqs. (4.1) to (4.3) using CHO_{ETE} transcriptomics data (Geoghegan et al. 2018). The sensitivity score is a measure of the responsiveness of CHO_{ETE} or $CHO_{BIS\text{-}A}$ to titration of each effector gene.

Gene ID	Gene	Mean Abundance	Differential Regulation (Fold Change)			Sensitivity Score	
(ENSCGRG)	Symbol	(FPKM)	Early Culture	Late Culture	Throughout Culture	CHO_{ETE}	$CHO_{BIA\text{-}A}$
1013777	Bip	1047.76	1.147	0.969	0.845	0.0175	0.0088
1020181	Calr	813.54	0.474	0.498	1.052	0.0255	0.0208
1017710	Canx	346.26	1.330	1.120	0.842	0.0175	0.0139
1024828	Erdj3	105.43	0.916	0.881	0.963	0.0345	0.0245
1006614	Erdj4	14.51	0.628	0.911	1.450	0.0265	0.0304
1024374	Erdj5	94.93	0.486	0.545	1.121	0.0462	0.0211
1011686	Ero1l	61.93	0.796	0.499	0.627	0.0491	0.0202
1025067	Ero1lb	18.04	1.133	0.545	0.481	0.0160	0.0070
1023543	Grp94	525.79	0.707	0.338	0.478	0.0157	0.0337
1003994	Hyou1	454.67	0.927	0.591	0.637	0.0218	0.0175
1013338	P4hb	560.34	0.381	0.488	1.282	0.0139	0.0168
1005477	Pdia4	245.83	0.345	0.320	0.926	0.0116	0.0080
1017472	Pdia6	828.90	0.610	0.346	0.567	0.0148	0.0095
1018105	Ppib	227.20	0.557	0.437	0.786	0.0207	0.0300
1009299	Prdx4	336.48	0.867	0.389	0.448	0.0172	0.0071
1023834	Srp14	57.31	0.810	0.429	0.530	0.0278	0.0247
1019438	Xbp1	40.83	0.642	0.247	0.384	0.0270	0.0276

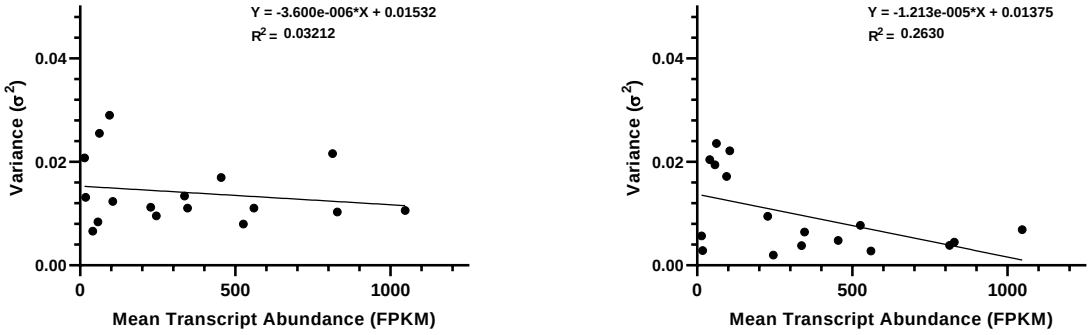

(a) IVCD **(b)** Titre

Figure A.2: Scatter plots of mean transcript abundance against Integral Viable Cell Density (IVCD) and titre variance in CHO_{ETE}.
Scatter plots shows the relationship between mean transcript abundance (calculated from Geoghegan et al. 2018) and the calculated IVCD (**a**) and titre (**b**) variance (σ^2) in CHO_{ETE} for each effector gene. Linier regressions were performed (black lines) with the R^2 values and line equations displayed.

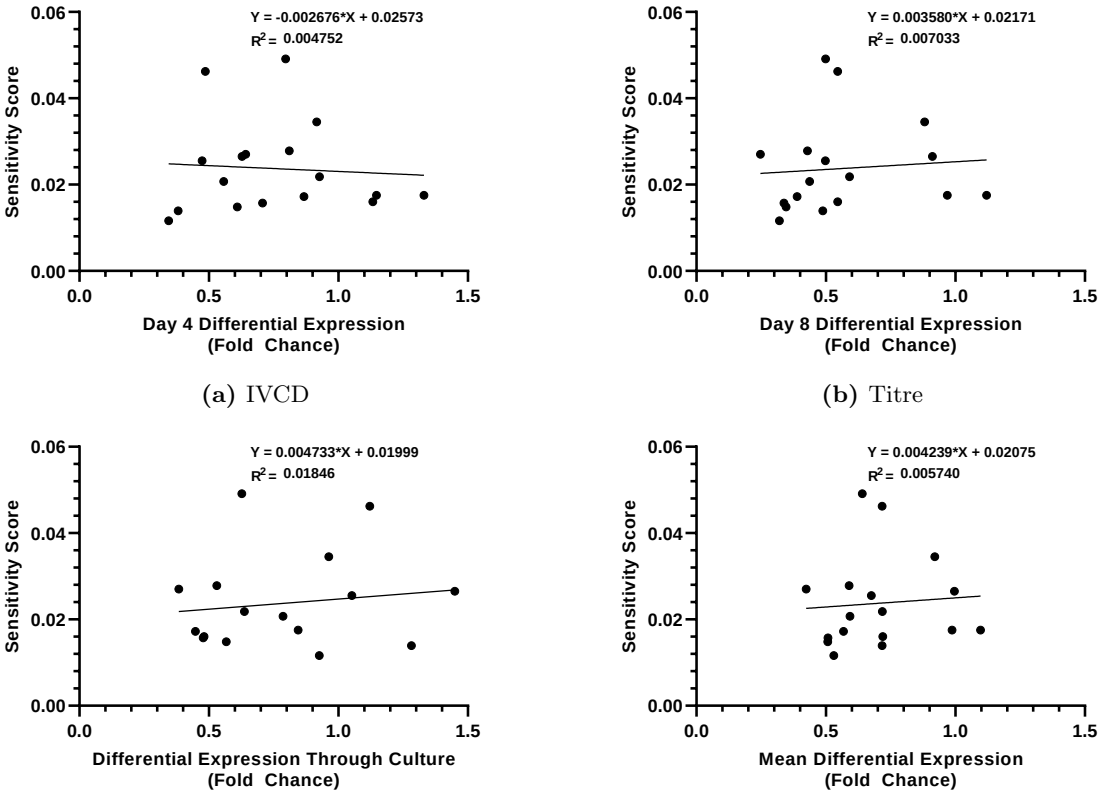

(a) IVCD **(b)** Titre

(c) IVCD **(d)** Titre

Figure A.3: Scatter plots of differential expression metrics against the calculated sensitivity score in CHO_{ETE}.
Scatter plots shows the relationship between the differential expression on day 4 (**a**), day 8 (**b**), throughout culture (**c**) and the mean of a-c (**d**) (calculated from Geoghegan et al. 2018) and the calculated sensitivity score in CHO_{ETE} for each effector gene. Linier regressions were performed (black lines) with the R^2 values and line equations displayed.

A.3 Chapter 6 Supplementary Figures

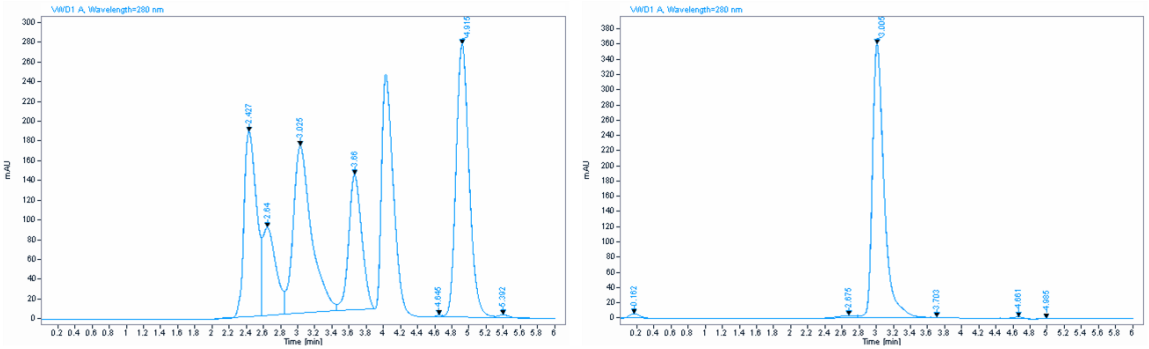

(a) Bio-Rad Protein Standard **(b)** NIP228 control

Figure A.4: Preliminary screen: Example High-Performance Liquid Size Exclusion Chromatography (HPL-SEC) traces of a Bio-Rad Gel Filtration Protein Standard and protein-A purified NIP228 control.
Plots show the traces from a Bio-Rad Gel Filtration Protein Standard (**a**) and protein-A purified NIP228 control(**b**) which were run before and after each 96-well plate of experimental $mAb_{BIS\text{-}A}$ samples.

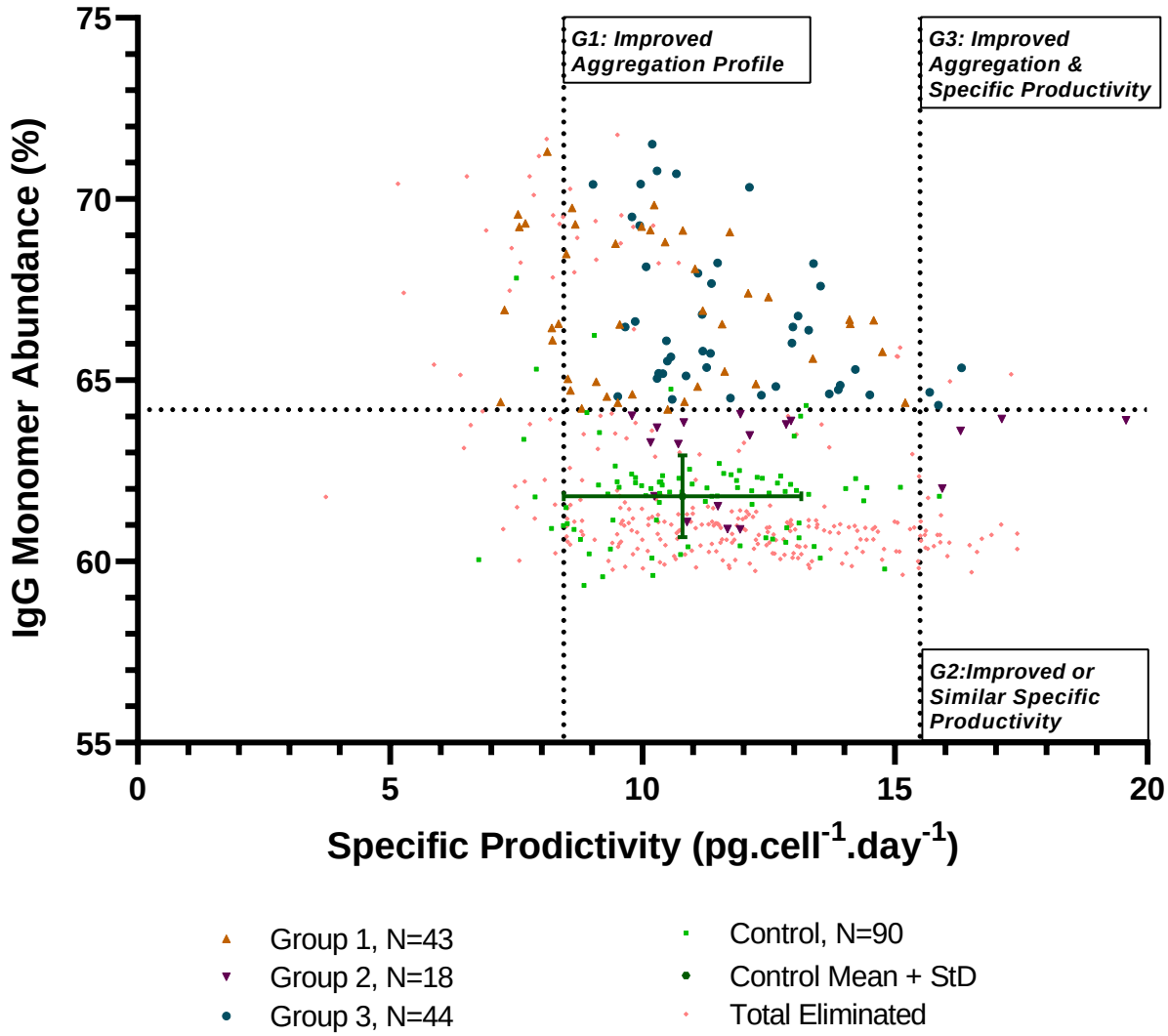

Figure A.5: Primary screen: Assessing the distribution of the compounds impact on specific productivity.
Graph displays the relationship between specific productivity and IgG monomer abundance for the hits as grouped in previous analysis and conditions previously eliminated, relative to the control population. Dotted lines are described by eqs. (6.3), (A.1) and (A.2).

$$x = qP_{Mean} - qP_{StD} \tag{A.1}$$
$$= 8.43\ pg.cell^{-1}.day^{-1}$$

$$x = qP_{Mean} + 2 \cdot qP_{StD} \tag{A.2}$$
$$= 15.494$$

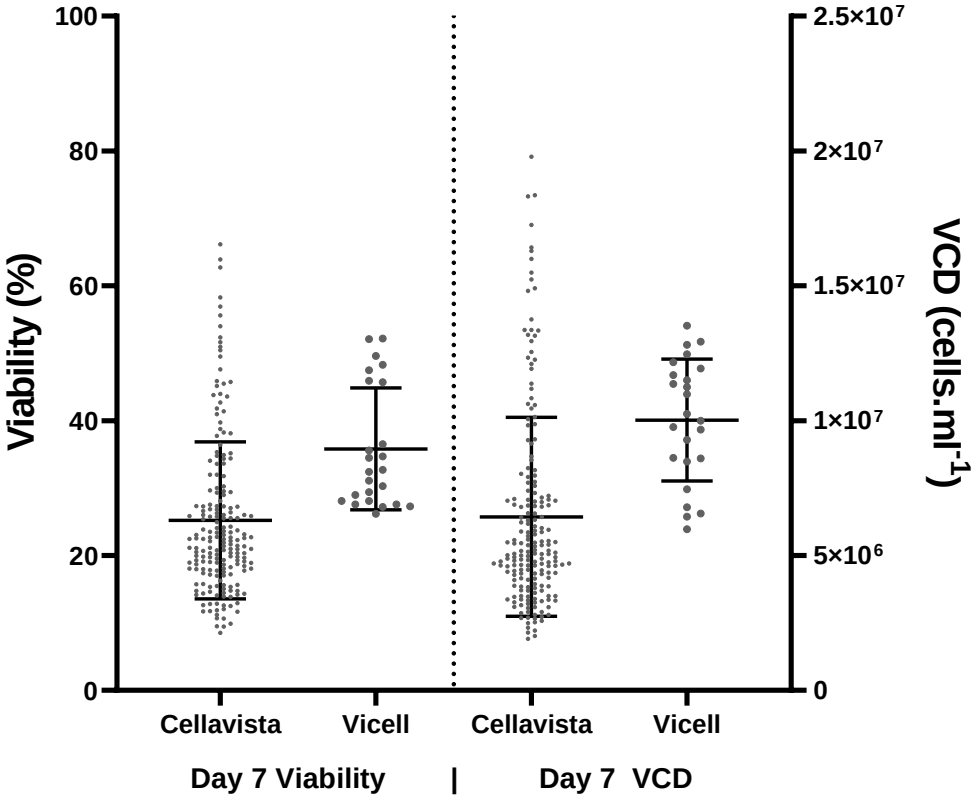

Figure A.6: Secondary screen: Comparison of the Vi-CELL and Cellavista for measuring VCD and cell viability.
The graph displays the viability and VCD of the control population as measured by the CellaVista and the Vi-CELL on day 7 post seed. The 24 Vi-CELL measurements are discrete from the control population used for the screen. Error bars represent the mean and StD of the populations.

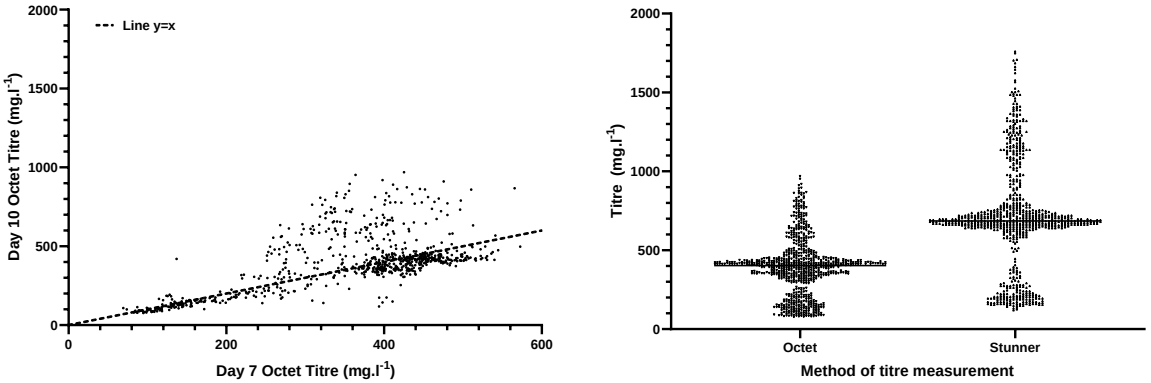

(a) Measured day 10 titre **(b)** Calculated day 10 titre

Figure A.7: Secondary screen: Evaluating methods for measuring product titre.
(**a**) Titre on day 10 measured by the Octet in relation to the day 7 Octet titre measurement with the plotted line at $x = y$ represents an equal titre at the respective time points. (**b**) Comparison of the titre on day 10 measured by Octet and Stunner with bars representing the mean of 769 purifications.

Appendix B

Synthetic Gene Constructs and esiRNA Sequences

B.1 Synthetic Gene Constructs

Table B.1: Comprehensive list of genes screened in Chapter 4.
Table includes target gene with synthesised sequence accession numbers, species, protein sequence modifications and an overview of protein function.

Gene Name	NCBI Accession No.	Species	Protein Sequence	Function	Previous Application in CHO Cell Engineering
BIP	NM-05347	Human	Full ORF	ER molecular chaperone with major roles in folding and assembly of proteins in the ER, misfolded protein degradation and UPR activation.	Borth et al. 2005; Cartwright et al. 2020; Johari et al. 2015; Pybus et al. 2014
CALR	NM-04343	Human	Full ORF	ER molecular lectin chaperone with holdase/foldase function, role in protein folding quality control, preventing aggregation and retaining incorrectly folded proteins for degradation.	Chung et al. 2004
CANX	NM-01746	Human	Full ORF	ER molecular lectin chaperone with holdase/foldase function, role in protein folding quality control, preventing aggregation and retaining incorrectly folded proteins for degradation.	Chung et al. 2004
CYP-B	NM-00942	Human	Full ORF	ER PPIase with a role in catalysing folding of proline-containing proteins.	Johari et al. 2015; Pybus et al. 2014
DNAJB9	NM-12328	Human	Full ORF	Co-chaperone for BIP that acts as a key repressor of theIRE1-mediated UPR. Also involved in ERAD of misfolded proteins.	
DNAJB11	NM-16306	Human	Full ORF	Co-chaperone for HSPA5 required for proper folding, trafficking or degradation of proteins. Binds directly to both unfolded proteins destined for ERAD and nascent unfolded peptide chains.	

Gene Name	NCBI Accession No.	Species	Protein Sequence	Function	Previous Application in CHO Cell Engineering
DNAJC10	NM-18981	Human	Full ORF	Ensures efficient folding of proteins in the ER by catalyzing the removal of non-native disulfide bonds. Also involved in ERAD by reducing incorrect disulfide bonds in misfolded glycoproteins. Interacts directly with BIP.	
ERO1A	XM-07651327	CHO	Full ORF	Oxidoreductase with a role in disulphide bond formation in assembling proteins in ER. Reoxidises P4HB and is required for the proper folding of immunoglobulins.	K. Cain et al. 2013; Mohan et al. 2007
ERO1B	XM-03507583	CHO	Full ORF	Oxidoreductase with a role in disulphide bond formation in assembling proteins in ER. Reoxidises P4HB and a range of other PDI enzymes, but at a lower rate.	
GRP94	NM-03299	Human	Full ORF	ATPase activity. Roles in folding and stabilising other proteins, in processing and transport of secreted proteins and in ERAD.	
HYOU1	NM-06389	Human	Full ORF	ER molecular chaperone associated with protein folding and secretion. Cytoprotective role, reducing hypoxia- induced apoptosis.	
P4HB	NM-00918	Human	Full ORF	Catalyses the formation and rearrangement of disulphide bonds within protein assembly within the ER. Role in inhibiting aggregation of misfolded proteins	Borth et al. 2005; R. Davis et al. 2000; Johari et al. 2015; Mohan et al. 2007

Gene Name	NCBI Accession No.	Species	Protein Sequence	Function	Previous Application in CHO Cell Engineering
PDIA4	NM-04911	Human	Full ORF	ER PDI, catalyses disulphide bond formation in protein folding. At high concentrations, functions as a chaperone that inhibits aggregation of misfolded proteins. At low concentrations, facilitates aggregation.	
PDIA6	XM-27424676	CHO	Full ORF	May function as a chaperone that inhibits aggregation of misfolded proteins. Negatively regulates the UPR.	
PRDX4	NM-06406	Human	Full ORF	An antioxidant enzyme (peroxidase) which reduces hydrogen peroxide and a PDI oxidation enzyme (works in cooperation with ERO1A). Role in activating transcription factor NF-kappaB.	
SRP14	NM-01024649	CHO	Full ORF	Part of the signal recognition particle which targets secretory proteins into the ER Role in nascent protein transfer into ER and elongation arrest, binds to RNA.	Cartwright et al. 2020; Le Fourn et al. 2014
XBP1s	NM-01244049	CHO	Spliced variant of XBP1s	Transcription factor part of UPR, working downstream of IRE1/ATF6, role in increasing protein folding and secretion within ER. Increases the capacity of the ER, up-regulates transcription of ER components.	Becker et al. 2008; Becker et al. 2010; K. Cain et al. 2013; Cartwright et al. 2020; Johari et al. 2015; Ku et al. 2008; Pybus et al. 2014; Tigges and Fussenegger 2006

B.2 Synthesised esiRNA Sequences

Table B.2: Sequences of esiRNAs designed against genes described in B.1 for screening in Chapter 4.
Table includes gene names, accession numbers, and sequence information. Additional growth arrest inducing positives control esiRNAs are appended to the bottom.

Gene Name	NCBI Accession No.	Transcript Length (bp)	esiRNA Length (bp)	Designed esiRNA Sequence
BIP	NM-005347	4027	170	GCAGGCCCAGTTGTCACCTCCCCAGAACATCTTCCCATGGATTCTGACACTGTTGACTCTTCAGACTC CGAGTCTGATATCCTTTTGGGCATTCTGGACAAGTTGGACCCTGTCATGTTTTTCAAATGTCCATCCC CAGAGTCTGCCAATCTGGAGGAACTCCCAGAGGT
CALR	NM-004343	691	307	AGGGCCCAAAGGGCCTAAGGACCGTGGTGAGCTGGAGTCTTGCCTTTTCTGCTTTGTTTTCTTTTAAG TCAGTCTGGCTGTGAACTTAGTCTCCTAAACAGCTGAGGTACAGGTGCAACGCACTCCTCATCCTGGG CCGGCTGAAGGGTGTGTCTGCGGTGGTGGGGGTCCGAGGGCACATTGGCGGAAGAAGTGCAACTGGAA GCGGAAGCCCCGCCCATCGCAGGCGAGACTTCCGGCTGTAACCGCTTGCAGCGGCTTCTGCTGACGGA GTCGGAACCGGCGGAGCTCAGGATGGTGTTGCTCG
CANX	NM-001746	4835	292	GAACCAAAATATGCTCTGAAGCCTAATTTGGTCAGAACCCCCAAATCTTAAAGGTTTTACTGGTATTG AAATTACAAACTTCACTTGCTAGTCCAAGGATTGGTTGAGGATTGTTAAGATTGCTTTCCTAAGGAAA GGGATGAGAGCTAGGTAATCAATATGATCAATGAGGATTTTGTCCAGTGCTAACATGAAATTCAGTAC TGTCCAAAGATGGGTGTTTTGTAACTGAACAACCAACCAGCTGTAAGATTAGTTTACTTACTGGTAGA CTTGAGGCTGGGAGGTGGTG
CYP-B	NM-000942	6767	317	ATATATTTGCCCACCATATATCATGTAGTCTTTTGTGACTCAATCCTTTCATTTTGCATGTTTTCAGG TTTCATCCATGTAGGGTCACTGAATGACATTCCCCTATGTAGATGAACCATGTTTTATACTCATCAGA CATCTGCATTGTTCCTACCTATGAACATGTACAAGATCAAACAAATTAATATGATGACTTACATCTTG GTGTTTGTTGGGAGAAACCTAGAATGAGAATTGCTGGAACATACACTGAGGAACTGCCAGCCAGACTG GGTTTCAAAGCAGCTGCATGATTTTATATGCCCCAGATACATGAG
DNAJB9	NM-012328	4705	162	CTGCCTTCTGAGTGCTGGGATAAAGGTATGCAACAACACCACCTGCCAGTATGCATTTCTGACACACT CATGACTTACGTGTATGTGTGTTGAGTGTGATTATGTGGTTGTATGGGAGAGTGTCTTTGTTTTTACA TCTATCCAGCCCCAAATTGAAATTGG

Gene Name	NCBI Accession No.	Transcript Length (bp)	esiRNA Length (bp)	Designed esiRNA Sequence
DNAJB11	NM-016306	1776	254	AAGGGAAGTGGTTACTGTGTTTACTCCTGGTCCTTGGAACTGTAGCTGTTCAGGCTCATGATGGACAT GATGATGACATGATTGATATTGAAGATGATCTTGATGATGTTATTGAAGAGGTAGAAGATTCGAAATC GAAATCAGATTCCAGTACTCCTCCATCTCCAAAGGTTACCTACAAAGCTCCAGTTCCAACAGGGGAGG TTTATTTTGCTGACTCCTTTGACAGAGGGTCTCTATCAGGGTGGATTTTA
DNAJC10	NM-018981	3721	165	TTTTTACTGGTGTTTGTCTTAATTCTCCTTTAGCCCTCAACCTCCTGGCTTCTCATTTTGAATCAACA TCTTTCCCTATGTCCCTTTTCTCTATCCAACCCCTGGTCACAACCCTCCCAACTTCAGGAACGGGTGT GGAGGAAAAGTCCTAGGCTTGAGATTTCA
ERO1A	XM-007651327	1530	170	AGAACGGTCATTGATTATAATGGTGAGCGGACGCTAGACGGCTTTAAGAAATTCCTGGAGAGTGGTGG CCAGGACGGTGCAGGAGACGACGATGACATGGATCTAGAAGAAGCTTTAGAGCCAGACATGGAGGAAG ATGATGATCAGAAAGCTATAAAGGACGAATTGTA
ERO1B	XM-003507583	1950	183	TCCAAGTATGAGCCCAGGAGCAATGTGATGGATGTTCAGGGTTCCACAGAGCCATCAGCCATTAAGGA CTATGTGGTGAAACATGCTTTGCCTCTGGTGGGCCACCGAAAAACCTCCAATGATGCCAAGCGGTACA CCAAGCGCCCTCTGGTGGTTGTATACTACAGTGTGGACTTCAGCTTT
GRP94	NM-003299	3006	160	ACCTGGAGCCAGAATGGGCCACTGCAGCCACAGAGGTAAAGGAGCAAACGAAGGGGAAAGTAAAGCTG GCAGCCGTGGACGCTACGGTGAACCAGGTCCTGGCCAACCGGTATGGGATTAGAGGATTCCCTACAAT CAAGATATTTCAGAAAGGCGAGGC
HYOU1	NM-006389	825	160	GAAGGAACAGCTGTGATAAATGGAGAATTCAAGGAGCTGAAACTGACTGACTATCGTGGGAAATACTT AGTTTTCTTCTTCTACCCACTCGATTTCACTTTTGTATGTCCAACTGAAATCATTGCCTTCGGTGACC GAATTGAAGAATTCAGATCTATAA
P4HB	NM-000918	6007	317	TACAAATTTTAATACACCAAATCCCATATGATAAAGCTAGGTGAATTATGTCTTAAGCTTCTGAAACT AGAGTTGTATTTAAGATGATATGATAAAAATAAATCTAAGGTAACTGTGGCAAGTGTTTTATAGTAAA ATTCTAAGAGGCTCATCAATAAACCCATGGCCAACAGCCTAAAAACACCAATGCATTTTCATTAGCCT TGCTTGCAAAAGGAAATACAGAACTCCCACTTAGATTTGAATTTTAGATAAGCAACTAGCTTTCTTTT AAGTGTAATTTGTATGCAGTATTAGGGCTCTATTTATACTAAAAG
PDIA4	NM-004911	1573	163	GGCATTCAAATAAGTACTTGCAAGCAGCAAACAATACCAAAGAATTGGAAGACTGTGAGCAGGCTAAC AAGCTGGGCGCCATCAATAGTACATTAAGTAATGAAAGCAAAGAAGCATTCATTGACTGGGCAAGATA TGATGACTCACAGGATCACTTTTGTGA

Gene Name	NCBI Accession No.	Transcript Length (bp)	esiRNA Length (bp)	Designed esiRNA Sequence
PDIA6	XM-027424676	2763	317	GGAGCAGAGACCAGGTTGCACAAGTTTCTATGAAGTAAATTACAAAGCAGGTTACAGGAGCCACAGTG TGGCCTCAAAGGACAGCAGGAGGAACGTGCTGGTGTGAACTTAGAGGCATGTCTCACTCACCTGGGGA AGGGGTGTAAACGTAGGGGTCCATACAGAAGCCAATGACCGGCCGGTGGTGCAGTTGTGAGCTGTGAG GAGGAAAGGAGTAGTGAACCATGAGTGGAGATGTGGCAGAGCAAAAACTAAGAACCAAGATCAACAAG GACCCACAAAGGAAAGAACTAGAAAACAGGTTGCTGGCTCCCTCC
PRDX4	NM-006406	2302	317	TCTGCTAATTTAAAATCGCATGCCCTGTAGCACCTGTGACTTGGGTTGCTAAATGTCTGTGAAACTGT AATTGAGTCAGTCAGTGAAAGAGACAACAGGCTTTTGGCTAATTGCCACTGAATGCTTTAGAAACTGC TGGTTTGATACCACAAAAAGATGCCTCTTCAGTAGAATTGGTGTAACAGGAATGATTGTATTGCACGT AGTTAAGCTGAAAAAGTTTAAAGCTTATGGTGAAATATTGCCAAGAGATTGTGTGTTTGGCCCTGCGC TAATGGTTTTGTATGATCAAAATCATAGCTACATGAATATCTTTT
SRP14	NM-001024649	1456	160	AGCAAAAGAAGGTGTCAAGCAGCTACTCAAACAAGGATCAGTGCAGAAGGAATTGACATGAAAACATT GCACTCTAGTGACCCACTGAGCACTTTGAAGCTGCTGCTGGCTGAAATCACTGATAGGCACCAGGGAA CCAAGGATGTCCAGAGGCCAGCCA
XBP1s	NM-001244049	5451	317	AGATCCTGTTTTGTATATGTGAGCACACAATGCAGTTACCGTTCCTAACCAACTTCTTGAATCATGAC TAATAATGGCAAAATCTTTTCATATATTGCACTTTGAAAGCCTAGAATTTCTTTTTAAATGGCTTGTT TATGTGAAATTCCCCAAATGGATGCCTAATGAAGTCTTACTTAGTAAAAGAATACTAATGTACTAGTT GGGAGCATACTGCTGTACTGGGCAACAGATGTACAAGAGAGCCTATAGGCTCCTCTCCTGTCACAAAC TATAAATAGTGGATAGGTACTTAGATTACTGCCTGCAACTACTGC
SKA3	XM-003500423	1289	206	TTTTTCCAGAAGTATGGCTATCAGTCACGAGACAAAGAAGAGTCAGGATGTGAGCACAAAGTCAGTGA CTCAGCCTCGGAGTTGGATGTGTGTGAAGACCTTCAGATGCCTGGTGTGGAGGGTGATCTGTCCGATC CATGTGTTCCAAGCAGTTCTGTTTCTGAAAATCTCCTACTACGCAGCCCACAGCTTTCAGATTTTGGA CT
PLK4	XM-027391931	2787	305	TGGGAGAAACTAATGAGCACAAAACCGATAACCCAAGCAGAGATTTCCAGGGCTATCCAGATTCACGG GACATGTTAAGAAATGCTTGGACTGATACAAGAGCCACCAAGAATGCTGATAATTCTGCTAATGTTCA TCCTGTAAACCAGCTGAGTACGACAAAGTTTACTATGACTGCACATCATAGTAAACCTGAGATTATTC AACAAGAGCTGGCCTTCCATCCTCATTCTGAACAAAGCAAGAAGAGGAGTATGGAGTCAACACTGGGT CACCAGAAACCTTCCTTACGAAGCATTACATCT

Appendix C

List of Chemical Supplements

C.1 Proteostasis Regulators (Plate *et al.* 2016)

Table C.1: Source and supplier information of compounds selected from (Plate, Cooley, et al. 2016) for use as Chinese Hamster Ovary (CHO) cell culture enhancers.
Includes Internal chemical index, source chemical index, IUPAC nomenclature, compound molecular weight, CAS number and supplier for each compound. Compounds were re-suspended at 20mM concentration in DMSO upon arrival and stored at -20°C.

Index	Source Index	IUPAC Name	Molecular Weight	CAS No.	Vendor
C1	5	4-bromo-N'-butylbenzohydrazide	271.2	537672-41-6	Life Chemicals, Ontario, Canada
C2	132	1-(4-fluorophenyl)-3-[(2-hydroxy-5-methylphenyl)amino]-2-propen-1-one	271.3	692275-04-0	ChemBridge, CA, USA
C3	145	N-(2-hydroxy-5-methylphenyl)-5-propylisoxazole-3-carboxamide	260.3	912799-53-2	Chemical Diversity, CA, USA
C4	147	N-(2-hydroxy-5-methylphenyl)-3-phenylpropanamide	255.3	393121-74-9	ChemBridge, CA, USA
C5	148	N-(2-hydroxy-5-methylphenyl)-2-((5-methyl-4-nitro-1H-pyrazol-3-yl)thio)acetamide	322.3	702665-14-3	Chemical Diversity, CA, USA
C6	238	3-(3-chlorophenyl)-5-(4-hydroxybenzylidene)-2,4-imidazolidinedione	314.7	97310-82-2	ChemBridge, CA, USA
C7	263	2-hydroxybenzaldehyde-(4-nitrophenyl)hydrazone	257.2	3155-24-6	Life Chemicals, Ontario, Canada

C.2 Compounds Sourced from AstraZeneca Open Innovation

Table C.2: Information sheet for preliminary hit compounds in chapter 6.
The table contains the internal compound index, mechanistic category, and the phenotypic toxicities rescued by compounds in the 'Phenotypic Hit' category. The 'hit group' by which each compound was identified in section 6.2.2.4 is listed along with the assessed concentrations in the secondary and tertiary screening rounds. During the preliminary screen every compound was evaluated at 10.00 μM and 100.00 μM Molecular weights have been restricted to the nearest whole number for intellectual property protection purposes.

Compound ID	M.W.	Compound Category	Phenotypic Hit Assays (Toxicities Rescued)	Preliminary Hit Group	Secondary Screen Concentrations (μM)			Tertiary Screen Concentrations (μM)		
M1	316	Phenotypic Hit	C9orf72-PR50 & FUS	G3	100.00	25.00	6.25	20.00	6.00	1.80
M2	349	Phenotypic Hit	C9orf72-PR50 & FUS	G3	100.00	25.00	6.25	40.00	12.00	3.60
M3	284	Phenotypic Hit	FUS	G1	100.00	25.00	6.25	40.00	12.00	3.60
M4	382	Phenotypic Hit	TDP-43	G3	100.00	25.00	6.25	40.00	12.00	3.60
M5	914	Rapamycin	n/a	G3	100.00	25.00	6.25	40.00	12.00	3.60
M6	388	HSP90 modulators	n/a	G3	100.00	25.00	6.25	20.00	6.00	1.80
M7	349	Phenotypic Hit	TDP-43 and FUS	G3	100.00	25.00	6.25		n/a	
M8	241	Phenotypic Hit	FUS	G3	100.00	25.00	6.25		n/a	
M9	572	Phenotypic Hit	TDP-43	G3	100.00	25.00	6.25	100.00	30.00	9.00
M10	281	Phenotypic Hit	TDP-43	G1	100.00	25.00	6.25	100.00	30.00	9.00
M11	409	Phenotypic Hit	FUS	G1	100.00	25.00	6.25	40.00	12.00	3.60
M12	306	HSP90 modulators	n/a	G1	100.00	25.00	6.25	200.00	60.00	18.00
M13	356	Phenotypic Hit	TDP-43	G3	100.00	25.00	6.25	40.00	12.00	3.60
M14	449	Phenotypic Hit	TDP-43	G3	100.00	25.00	6.25	40.00	12.00	3.60
M15	365	Phenotypic Hit	TDP-43	G3	100.00	25.00	6.25		n/a	
M16	312	Htt Aggregation (BMCL)	n/a	G3	100.00	25.00	6.25	20.00	6.00	1.80
M17	386	DisAgg. Stress Granules	n/a	G3	100.00	25.00	6.25	200.00	60.00	18.00
M18	347	DisAgg. Stress Granules	n/a	G3	100.00	25.00	6.25	200.00	60.00	18.00
M19	402	p38 MAPK inhibitors	n/a	G3	100.00	25.00	6.25	200.00	60.00	18.00
M20	958	Rapamycin Analogue	n/a	G3	100.00	25.00	6.25	100.00	30.00	9.00
M21	418	HSP90 modulators	n/a	G1	100.00	25.00	6.25		n/a	

Compound ID	M.W.	Compound Category	Phenotypic Hit Assays (Toxicities Rescued)	Preliminary Hit Group	Secondary Screen Concentrations (μM)			Tertiary Screen Concentrations (μM)		
M22	463	Phenotypic hit	TDP-43, C9orf72-PR50 & FUS	G3	100.00	25.00	6.25	40.00	12.00	3.60
M23	434	DisAgg. Stress Granules	n/a	G3	100.00	25.00	6.25	40.00	12.00	3.60
M24	388	RIPK1 modulators	n/a	G2	100.00	25.00	6.25	40.00	12.00	3.60
M25	288	Htt Aggregation (BMCL)	n/a	G1		n/a		100.00	30.00	9.00
M26	342	Phenotypic Hit	TDP-43	G3	100.00	25.00	6.25	40.00	12.00	3.60
M27	396	Phenotypic Hit	TDP-43	G3	100.00	25.00	6.25	40.00	12.00	3.60
M28	412	Phenotypic Hit	TDP-43	G2	100.00	25.00	6.25	40.00	12.00	3.60
M29	320	Htt Aggregation (BMCL)	n/a	G3	100.00	25.00	6.25	40.00	12.00	3.60
M30	404	p38 MAPK inhibitors	n/a	G3	100.00	25.00	6.25	40.00	12.00	3.60
M31	413	Phenotypic Hit	TDP-43 , C9orf72-PR50 & FUS	G3	100.00	25.00	6.25	100.00	30.00	9.00
M32	803	FKBP12 inhibitors	n/a	G2	100.00	25.00	6.25	40.00	12.00	3.60
M33	283	DisAgg. Stress Granules	n/a	G3	100.00	25.00	6.25	40.00	12.00	3.60
M34	392	Phenotypic Hit	FUS	G2	100.00	25.00	6.25	40.00	12.00	3.60
M35	356	Phenotypic Hit	FUS	R	100.00	25.00	6.25	40.00	12.00	3.60
M36	436	p38 MAPK inhibitors	n/a	G3	100.00	25.00	6.25	200.00	60.00	18.00
M37	333	Phenotypic Hit	TDP-43	G3	100.00	25.00	6.25	100.00	30.00	9.00
M38	315	Phenotypic Hit	FUS	G3	100.00	25.00	6.25		n/a	
M39	327	Phenotypic Hit	FUS	G3	100.00	25.00	6.25	40.00	12.00	3.60
M40	656	FKBP12 inhibitors	n/a	R	50.00	12.50	3.13		n/a	
M41	466	Htt Aggregation (BMCL)	n/a	G3	50.00	12.50	3.13		n/a	
M42	278	β-amyloid binders	n/a	G1	50.00	12.50	3.13	40.00	12.00	3.60
M43	383	Phenotypic Hit	FUS	R	50.00	12.50	3.13	100.00	30.00	9.00
M44	1202	Cyclophilin inhibitors	n/a	G1	50.00	12.50	3.13	20.00	6.00	1.80
M45	397	Phenotypic Hit	C9orf72-PR50 & FUS	G1	50.00	12.50	3.13	20.00	6.00	1.80
M46	443	Phenotypic Hit	TDP-43	G1	50.00	12.50	3.13	200.00	60.00	18.00
M47	442	Phenotypic Hit	TDP-43	G1	50.00	12.50	3.13	40.00	12.00	3.60
M48	388	Phenotypic Hit	FUS	G1	50.00	12.50	3.13	200.00	60.00	18.00
M49	329	Htt Aggregation (BMCL)	n/a	G3	50.00	12.50	3.13	8.00	2.40	0.72
M50	259	ALS aggregation inhib. (JMC)	n/a	G1	50.00	12.50	3.13	200.00	60.00	18.00

Compound ID	M.W.	Compound Category	Phenotypic Hit Assays (Toxicities Rescued)	Preliminary Hit Group	Secondary Screen Concentrations (μM)			Tertiary Screen Concentrations (μM)		
M51	338	DisAgg. Stress Granules	n/a	G1	50.00	12.50	3.13		n/a	
M52	331	Phenotypic Hit	C9orf72-PR50 & FUS	G1	50.00	12.50	3.13	200.00	60.00	18.00
M53	237	Phenotypic Hit	FUS	G3	50.00	12.50	3.13		n/a	
M54	1202	Cyclophilin inhibitors	n/a	R	50.00	12.50	3.13	200.00	60.00	18.00
M55	449	HSF1 activators	n/a	R	6.13	1.53	0.38	8.00	2.40	0.72
M56	301	Phenotypic Hit	TDP-43 & FUS	R	6.13	1.53	0.38		n/a	
M57	330	HSF1 activators	N/A	R	6.13	1.53	0.38		n/a	
M58	297	Phenotypic Hit	TDP-43	R	6.13	1.53	0.38		n/a	
M59	327	HSF1 activators	n/a	R	6.13	1.53	0.38		n/a	
M60	351	Phenotypic Hit	FUS	G1	6.13	1.53	0.38		n/a	
M61	426	HSF1 activators	n/a	G1	6.13	1.53	0.38		n/a	
M62	230	RIPK1 modulators	n/a	G1	6.13	1.53	0.38	8.00	2.40	0.72
M63	358	p38 MAPK inhibitors	n/a	R	100.00	25.00	6.25	100.00	30.00	9.00
M64	331	RIPK1 modulators	n/a	R	100.00	25.00	6.25	100.00	30.00	9.00

Appendix D

AppNote: Assessing the Reproducibility of the Opentrons OT2 Liquid Handler

Automated, Rapid & Reproducible Measurement of Immunoglobulin G using Opentrons OT-2 liquid handling robot and Valita®TITER and Valita®TITER Plus

Application Note

O. Swindley, H. Byrne

Introduction

Biologic drugs are the largest and fastest growing segment of the Pharmaceutical industry, with sales of €500bn and an annual growth of 8 % pa[1]. Their ability to target diseases with high specificity results in improved safety and effectiveness. However, this increases the cost of manufacturing significantly over their predecessors.

Every manufacturing process for potential biologics begins with cell line development, whether for clinical trials or market launch.

During cell line selection, thousands of single cell clones are screened for optimal growth and Immunoglobulin G (IgG) production attributes to identify those best suited to manufacturing pipelines. This process requires accurate and reproducible methodologies to ensure successful outcomes.

Commonly used methods for IgG quantification require either high-cost, specialist equipment or skilled personnel. Examples include High-Performance Liquid Chromatography (HPLC) and surface interferometry, or time-consuming assays such as Enzyme-Linked Immunosorbent Assay (ELISA). Although an ELISA is a well-established plate-based method for protein quantification, it is a lengthy multi-step process.

This article demonstrates the benefits of Valita®TITER assay range when combined with Opentrons OT-2 automation technology and software. When used alongside the Molecular Devices multi-mode iD5 plate reader, this platform provides a cost-effective reproducible solution for accurate IgG quantification throughout drug manufacturing. The data presented here shows the advantages of integrating bench-top automation into micro-titre plate-based assay work flows.

Opentrons OT-2 Liquid Handler

The Opentrons OT-2 is a fully customisable, fast, precise and low-cost bench-top liquid handler with the flexibility to run any plate protocols. Equipped with 2 pipetting arms and 11 lab ware positions, large protocols can be completed without intervention.

Protocol development with the Opentrons Python API 2.0 offers good flexibility and control over experimental work flows. Alternatively, a graphical protocol designer allows quick generation of straight forward processes. The protocol used here, in addition to numerous others used at the University of Sheffield, are freely available for use on GitHub[3] and are fully customizable via Opentrons API. This is integrated with the flexible Labware Creator, to easily import custom equipment.

Valita®TITER and Valita®TITER Plus Assay Principle

Valita®TITER and Valita®TITER Plus are rapid, high-throughput assays; quantifying IgG-Constant Domain of Antibody (Fc) interactions with a fluorescently labelled derivative of protein G via fluorescence polarization (Fluorescence Polarization (FP)).

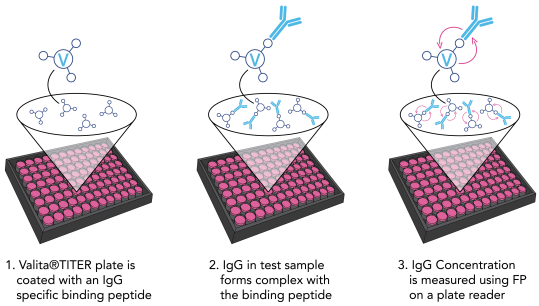

Figure D.1: Assay Schematic of Valita®TITER assay for IgG quantification using Fluorescence Polarization[4].
Each well of the plate is pre-coated with a fluorescently labelled Fc-specific probe (1). An IgG sample binds to the probe (2). Binding is measured via fluorescence polarization and rotational diffusion (3).

FP effectively analyses changes in the size of molecules. "Fixed" fluorophores are excited by polarized light and preferentially emit light in the same plane of polarization. The rotation of the molecules between absorption and emission of the photon results in "twisting" the polarization of the light. Small molecules tumble faster in solution than larger molecules. Hence, the change in molecule size upon the fluorophore-IgG binding can be detected using the degree of light de-polarization. When the fluorescently labelled IgG-binding peptide is unbound it tumbles rapidly, depolarizing the light more than when bound to an IgG.

The detection of FP involves excitation of the solution with plane polarized light and subsequent measurement of emitted light intensity in both the parallel (polarized proportion) and perpendicular (depolarized portion) planes to the exciting light. The FP is expressed as a normalised difference of the two intensities, typically expressed in milli-polarization units (Milli-Polarisation Units (mP)).

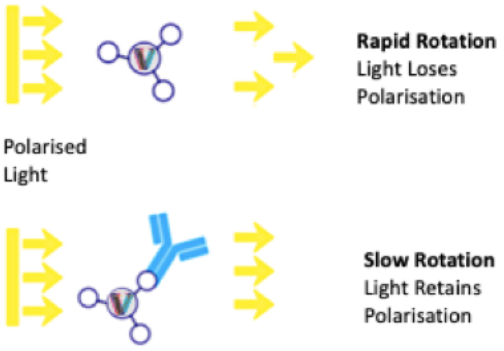

Figure D.2: Valita®TITER assay principle[4].
The assay applies fluorescence polarization to quantify IgG. Small, unbound molecules rotate rapidly in solution (top), while large, bound molecules rotate slowly (bottom).

Materials and Methods

Materials:

- Valita®TITER [Gen 2] Plus Assay kit;
- Valita®TITER [Gen 2] Assay Kit;
- Molecular Devices iD5 Multimode Plate reader;
- Opentrons OT-2 Robot;
- Native Human IgG1 standard (BioRad, Product Code: 5172-9017);
- CD-CHO medium (GibcoTM, Catalog No. 10743);
- Trough 12-channel (Axygen, Product No. RES-MW12-HP-SI);
- Nunc 96-well U-bottom plate (Thermo Scientific™, Catalog No. 168136);
- Optifit tips, 0.5 µl to 200 µl (Sartorius, Catalog No. 790201)

Method:

Human IgG standard was re-solubilised in Phosphate-Buffered Saline (PBS) to a concentration of $(5.00 \pm 0.05)\,\mathrm{mg.ml^{-1}}$ as per the manufacturer's instructions. Further dilutions to working concentrations were carried out in CD-CHO media.

The OT-2 trough was loaded with CD-Chinese Hamster Ovary (CHO) media and Human IgG1 standard, at $200\,\mathrm{mg.l^{-1}}$ or $2000\,\mathrm{mg.l^{-1}}$ for the Valita®TITER and Valita®TITER Plus assays respectively. The protocol was performed using the 8-channel P300 pipetting arm. All aspects were performed by the OT-2 as follows:

1. Media was added to columns 2-12, and IgG1 standard to column 1 of the sample plate.
2. A serial dilution of the IgG standard was performed across columns 1-11 of the sample plate, resulting in 8 independent serial dilutions. Column 12 contains assay blanks.
3. Media was added to the Valita®TITER or Valita®TITER Plus plates to reconstitute the probe.
4. Samples were added to the Valita®TITER or Valita®TITER Plus plates and mixed thoroughly by pipetting.
5. Plates were incubated at room temperature for 30 minutes and read on the iD5 plate reader using the appropriate FP method (outlined in Table 1 and 2).

The full python script for this work can be found on GitHub[3].

The OT-2 took 15 minutes to prepare each 96-well plate for analysis and could perform up to 3 assays consecutively without user intervention. The same experimental procedures as described were completed by an experienced human operator, defined as having completed at least 20 Valita®TITER or Valita®TITER Plus assays.

Table D.1: Instrument settings for Valita®TITER assay Fluorescence Polarization measurement on the iD5 reader

Setting	**Molecular Devices iD5**
Mode	Fluorescence Polarization
Excitation (nm)	485 (adjustable bandwidth)
Emission (nm)	535 (adjustable bandwidth)
Gain	Low
G-factor	1.00
Attenuation	1 OD
Integration time (ms)	400
Read Height (mm)	4.66

Table D.2: Instrument settings for Valita®TITER Plus Assay Fluorescence Polarization measurement on the iD5 reader

Setting	**Molecular Devices iD5**
Mode	Fluorescence Polarization
Excitation (nm)	485 (adjustable bandwidth)
Emission (nm)	535 (adjustable bandwidth)
Gain	Low
G-factor	1.00
Attenuation	3 OD
Integration time (ms)	400
Read Height (mm)	4.66

Results

An investigation was carried out into the technical reproducibility of replicate IgG standard curve samples prepared using the Opentrons OT-2 vs a human operator. These were analysed by Valita®TITER and Valita®TITER Plus assays. Technical reproducibility was determined by comparing the average StD and CV obtained between replicate samples across three plates at varying IgG concentrations.

Figure D.3 provides an overview of the OT-2 performance. The average StD and CV for each concentration was calculated for the

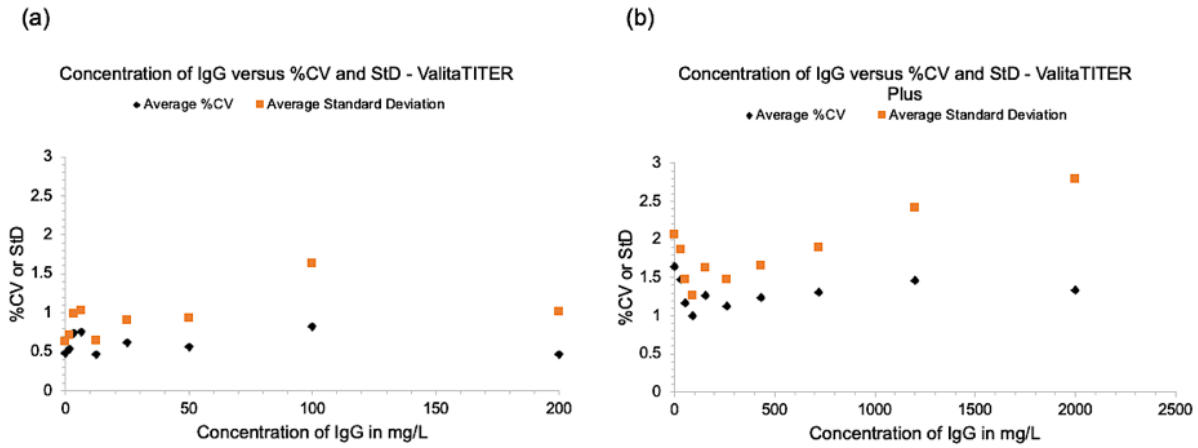

Figure D.3: Investigation into the technical reproducibility when prepared by the Opentrons OT-2 liquid handling robot.
Investigation into the technical reproducibility of Valita®TITER (a) and Valita®TITER Plus (b) for IgG quantification when prepared by the Opentrons OT-2 liquid handling robot and analysed using Molecular Devices iD5 multimode plate reader. Reproducibility was determined by comparing the average Standard Deviation (StD) and Coefficient of Variation (CV) obtained between replicate samples across three plates at varying IgG concentrations..

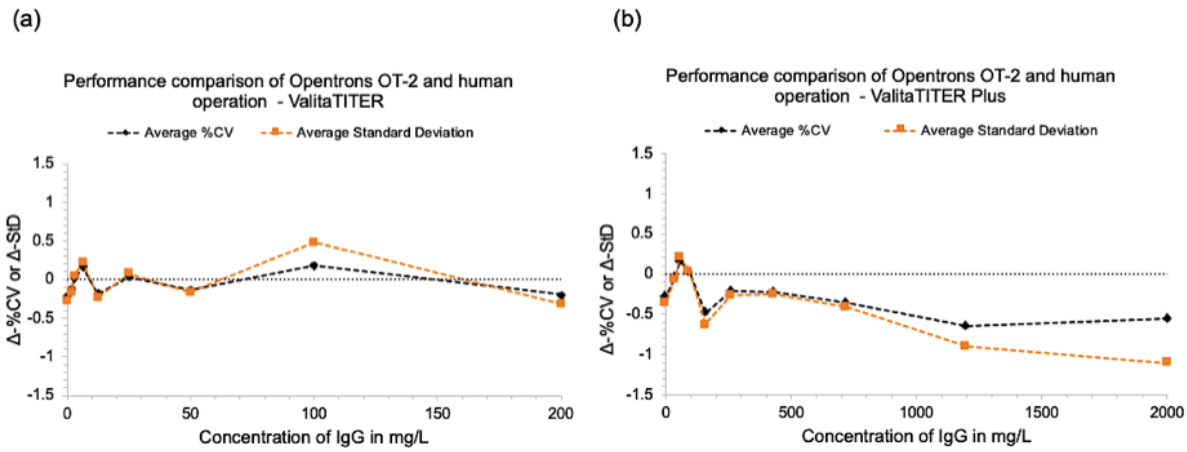

Figure D.4: Performance assessment of the Opentrons OT-2 liquid handling robot in comparison to an experienced human operator for Valita®TITER (a) and Valita®TITER Plus (b).
IgG was quantified by analysis on the Molecular Devices iD5 multi-mode plate reader. The average StD and CV between replicate samples was obtained across three plates at varying IgG concentrations. The dotted line at y=0 represents the StD or CV of the manual assays. The Change in Standard Deviation (Δ-StD) and Change in Coefficient of Variation (ΔCV) represent the change in StD and CV, calculated by the normalisation of the Opentrons OT-2 dataset against the manual dataset.

replicate plates. These were then averaged and plotted as the inter-plate average versus concentration of IgG (in $mg.l^{-1}$).

The Valita®TITER (Figure D.3a) StD and CV weighted inter-plate averages (total average of individually averaged values) obtained were 0.95 mP and 0.61 % respectively. The Valita®TITER Plus (Figure D.3b) the weighted inter-plate averages were 1.48 mP and 1.04 % respectively.

In comparison the weighted inter-plate average StD and CV respectively for a human operator were 0.98 mP and 0.66 % for Valita®TITER, and 1.85 mP and 1.30 % for Valita®TITER Plus.

The performance of the Opentrons OT-2 and the human operator were directly compared in Figure D.4. The Δ-StD and ΔCV represent the change in StD and CV of the OT-2 dataset when normalised against the manual dataset, represented by the dotted line at y=0. The Δ-StD and Change in Coefficient of Variation (Δ-%CV) of the OT-2 in comparison with the human operator is shown for the Valita®TITER assay (Figure D.4a) and Valita®TITER Plus assay (Figure D.4b). The average inter-plate Δ-StD and ΔCV obtained was −0.04 mP and −0.06 % for Valita®TITER, and −0.37 mP and −0.26 % for Valita®TITER, respectively.

Discussion and Conclusions

The accurate and reproducible quantification of IgG is essential throughout drug discovery and development. The results presented here demonstrate that the addition of automation into experimental work flows can offer several key advantages such as increased work flow capacity, whilst maintaining or improving reproducibility and reliability of data.

From the presented data, it can be concluded that the Opentrons OT-2 liquid handling robot performs the Valita®TITER assays with the same consistency and precision as a human operator, with very similar StD and %CV values observed across the assay concentration range. Additionally, when performing the Valita®TITER Plus assay, the Opentrons OT-2 outperformed the human operator reducing both the StD and Percentage Coefficient of Variation (%CV) in 80 % of the data points along the standard curve.

Combining the Valita®TITER assay range with Opentrons OT-2 liquid handling robot provides a cost effective, reproducible solution to the accurate quantification of IgG throughout drug manufacturing, with the benefit of freeing up user time.

Abbreviations

ELISA	Enzyme-Linked Immunosorbent Assay
FP	Fluorescence Polarization
HPLC	High-Pressure Liquid Chromatography
IgG	Immunoglobulin G
PBS	Phosphate-Buffered Saline
mP	Milli-polarization Units
StD	Standard Deviation
Δ-StD	Change in Standard Deviation
CV	Coefficient of Variation
ΔCV	Change in Coefficient of Variation

About the Authors

Oscar Swindley is a final year PhD student at the Department of Chemical and Biological Engineering, University of Sheffield. He works on genetic and chemical manipulation of monoclonal antibody folding and assembly processes, alongside optimisation and integration of automation procedures.

Dr. Hannah Byrne is the Head of Biological Sciences at Valitacell Ltd. She studied Analytical Chemistry at Dublin City University and has a PhD in Biochemistry. Valitacell is a growing biotechnology company developing innovative technologies to aid and improve drug discovery and development.

Contact Information

Oscar Swindley
PhD Student
Chemical and Biological Engineering
University of Sheffield
Mappin St | Sheffield | S1 3JD | England
Email: oswindley1@sheffield.ac.uk

Dr Hannah Byrne
Head of Science
VALITACELL | NIBRT
Fosters Avenue | Blackrock
Dublin | Ireland
Tel: +353 (0) 1 215 8130
Email: info@valitacell.com

References

1. `https://www.mckinsey.com/industries/pharmaceuticals-and-medical-products/our-insights/rapid-growth-in-biopharma`
2. `https://docs.opentrons.co./v2`
3. `https://github.com/OscarSwindley/Opentrons_Protocols_API2.0`
4. `https://www.valitacell.com`

The University Of Sheffield.

Appendix E

Opentrons OT-2 Liquid Handler Python Scripts

E.1 Valaitacell-Opentrons App Note

```
#Readme:
#Protocol: Valitatiter Assay, full plate standard curve for ValitaCell Opentrons Assessment
#Author: Oscar Swindley <oswindley1@sheffield.ac.uk>
#Proceed with caution if any modifications are made (dilutions, volumes, not full plate)
# Version 4.0
# Date: 30Jan20
#Enjoy!!!

#Notes:
#Please confirm 'labware' matches labwere section below, including correct tip box types and tip sizes
#For trough (Volumes in 25% excess):
    #CD-CHO = Cols 2-4. Min volume 18.0ml
    #IgG Standard at final concentration = Col 1. Min volume 7.5ml
#Current protocol for nunc 96 well plates, check dimensions if using different plates

# imports
from opentrons import protocol_api

# metadata
metadata = {
    'apiLevel': '2.0',
    'protocolName': 'ValitaTiterAssay_1in20',
    'author': 'Oscar Swindley <oswindley1@sheffield.co.uk>',
    'description': 'First python protocol, ValitaTiterAssay, 1in15 sample dilution',
}
def run(protocol: protocol_api.ProtocolContext):

    # labware: Labware used in the protocol is loaded
    plate_dil_1 = protocol.load_labware('nunc_96_ubottom', '4')
    plate_vt_1 = protocol.load_labware('valitacell_96_wellplate_150ul', '1')
    plate_dil_2 = protocol.load_labware('nunc_96_ubottom', '5')
    plate_vt_2 = protocol.load_labware('valitacell_96_wellplate_150ul', '2')
    plate_dil_3 = protocol.load_labware('nunc_96_ubottom', '6')
    plate_vt_3 = protocol.load_labware('valitacell_96_wellplate_150ul', '3')
    tip200_1 = protocol.load_labware('opentrons_96_filtertiprack_200ul', '7')
    tip200_2 = protocol.load_labware('opentrons_96_filtertiprack_200ul', '10')
    tip200_3 = protocol.load_labware('opentrons_96_filtertiprack_200ul', '11')
    tip200_4 = protocol.load_labware('opentrons_96_filtertiprack_200ul', '9')
    trough = protocol.load_labware('axygen_12_reservior_22ml', '8')

    # pipettes and settings
    p300m = protocol.load_instrument('p300_multi', mount='right',
     tip_racks=[tip200_1, tip200_2, tip200_3, tip200_4])
    p300m.flow_rate.aspirate = 100
    p300m.flow_rate.dispense = 200
    p300m.maximum_volume = 200
    p300m.minimum_volume = 15


    def VT_SC_Plate(trough_well, plate_dil, plate_vt): #FDefines running of VT_SC_Plate as a function
        #Step1: Fill Dilution media to cols 2-12
        p300m.pick_up_tip()
        for i in range(11):
            p300m.aspirate(100, trough.wells()[trough_well])
            p300m.move_to(trough.wells()[trough_well].top(-20))
            protocol.delay(seconds=1)
            p300m.dispense(100, plate_dil.wells()[8*(i+1)])
            protocol.delay(seconds=1)
```

```
        p300m.blow_out()
    p300m.drop_tip()

    #Step2: Add 222ul Standard to dil_plate Col-1
    p300m.pick_up_tip()
    p300m.mix(10, 190, trough.wells()[0])
    protocol.delay(seconds=1)
    p300m.blow_out(trough.wells()[0].top())
    p300m.transfer(100, trough.wells()[0], plate_dil.wells()[0], new_tip='never')
    protocol.delay(seconds=1)
    p300m.blow_out()
    p300m.transfer(122, trough.wells()[0], plate_dil.wells()[0], new_tip='never')
    protocol.delay(seconds=1)
    p300m.blow_out()
    p300m.drop_tip()

    #Step3: Dilute at ration of 0.6 accross cols 1-11
    p300m.pick_up_tip()
    for i in range(10):
        p300m.transfer(122, plate_dil.wells()[8*i], plate_dil.wells()[8*(i+1)], mix_after=(6, 180),
         new_tip='never')
        protocol.delay(seconds=1)
        p300m.blow_out(plate_dil.wells()[8*(i+1)].top())
    p300m.drop_tip()
    protocol.home()

   #Step3: Add 60ul VT-Buff to VT plate
    p300m.well_bottom_clearance.dispense = 7
    p300m.pick_up_tip()
    for i in range(12):
        p300m.aspirate(60, trough.wells()[trough_well])
        p300m.move_to(trough.wells()[trough_well].top(-20))
        protocol.delay(seconds=1)
        p300m.dispense(60, plate_vt.wells()[8*i])
        protocol.delay(seconds=1)
        p300m.blow_out(plate_vt.wells()[8*i].top())
    p300m.drop_tip()
    p300m.well_bottom_clearance.dispense = 1
    protocol.home()

    #Step 4: Add 60ul Dil.Sample to VT plate + mix.
    for i in range(12):
        p300m.pick_up_tip()
        p300m.mix(5, 60, plate_dil.wells()[8*i])
        p300m.blow_out(plate_dil.wells()[8*i].top())
        p300m.transfer(60, plate_dil.wells()[8*i], plate_vt.wells()[8*i], mix_after=(6, 80),
         new_tip='never')
        protocol.delay(seconds=1)
        p300m.blow_out(plate_vt.wells()[8*i].top())
        p300m.drop_tip()

VT_SC_Plate(2, plate_dil_1, plate_vt_1) #Call function to runn VT_SC_Plate
protocol.home()
VT_SC_Plate(3, plate_dil_2, plate_vt_2)
protocol.home()
VT_SC_Plate(4, plate_dil_3, plate_vt_3)
#End of Protocol
```

E.2 Lonza HTP Electroporation

```
#Readme:
#Protocol: 96well nucleofection with seeding into 24 SWP's (70ul)
#Author: Oscar Swindley <oswindley1@sheffield.ac.uk>
#Please confirm 'labware' matches labwere section below
#Proceed with caution if any modifications are made (dilutions, volumes, not full plate)
#Date: 05Feb2020
#Enjoy!!!

#README:
#First run prerequisite protocol 24well_Plate_Seed for the required plates (multiples of 4)
#Trough requires 'Nucleofection Solution' in 'A1' at start
#'Resuspended cells' in 'A2' (add when prompted), and pre-gassed media to 'A3' when prompted
#TIPRACK: RESET tip200_1 (slot 7) requires only odd rows (A. C, E, G), tip300_2 (slot 10) even rows (B, D, F, H).
#This allows transfer from 96-well-plate to 24-well-plates

# imports
from opentrons import protocol_api
from itertools import product
# metadata
metadata = {
    'apiLevel': '2.0',
    'protocolName': '96well_nucleofection_into24swps',
    'author': 'Oscar Swindley <oswindley1@sheffield.co.uk>',
    'description': 'Lonza Nucelofection protocol with 1.5-fold excess seeded into 24-SWP's'
    }

def run(protocol: protocol_api.ProtocolContext):
    # labware
    plate_stock = protocol.load_labware('cornering_96_wellplate_500ul', '9')
    plate_dna = protocol.load_labware('nunc_96_ubottom', '6')
    plate_nuc = protocol.load_labware('lonza_96_electroporation', '3')
    trough = protocol.load_labware('axygen_12_reservior_22ml', '8')
    tip200_1 = protocol.load_labware('opentrons_96_filtertiprack_200ul', '7')
    tip200_2 = protocol.load_labware('opentrons_96_filtertiprack_200ul', '10')
    tip200_3 = protocol.load_labware('opentrons_96_filtertiprack_200ul', '11')
    plate24_1A = protocol.load_labware('nunc_24_pseudo_a', '1')
    plate24_2B = protocol.load_labware('nunc_24_pseudo_b', '2')
    plate24_3A = protocol.load_labware('nunc_24_pseudo_a', '4')
    plate24_4B = protocol.load_labware('nunc_24_pseudo_b', '5')

    # pipettes (& settings if different to defaults)
    p300m = protocol.load_instrument('p300_multi', mount='right', tip_racks=[tip200_1, tip200_2])
    p300m.flow_rate.aspirate = 100
    p300m.flow_rate.dispense = 200
    p300m.maximum_volume = 200
    p300m.minimum_volume = 15

    p50m = protocol.load_instrument('p50_multi', mount='left', tip_racks=[tip200_1, tip200_3])

#Step 1: Distrubute Nuc Solution to DNA plate
    p50m.pick_up_tip()
    for i in range(4):
        p50m.aspirate(45, trough.wells()[0])
        p50m.dispense(38, plate_dna.wells()[8*i])
        protocol.delay(seconds=1)
        p50m.blow_out(trough.wells()[0].top())
    p50m.drop_tip()
```

```
    #Step 2: Distrubute DNA/RNA mix to DNA Plate
    for i in range(4):
        p50m.pick_up_tip()
        p50m.mix(3, 50, plate_stock.wells()[8*i])
        protocol.delay(seconds=1)
        p50m.blow_out(plate_stock.wells()[8*i].top())
        p50m.transfer(7, plate_stock.columns()[i], plate_dna.columns()[i], mix_after=(1, 40), new_tip='never')
        protocol.delay(seconds=1)
        p50m.blow_out(plate_dna.wells()[8*i].top())
        p50m.drop_tip()

    # Intervention 1: Insert pause to comfirm cells ready in trough column 2
    protocol.pause()
    protocol.comment('ATTENTION: Ensure below criteria are met prior to resuming protocol.
       Resuspended cells added to trough, position 8, column 2. Once complete click resume')

#Step 3: Mix cells + transfer to DNA plate
    p300m.pick_up_tip()
    p300m.well_bottom_clearance.aspirate = 2
    p300m.well_bottom_clearance.dispense = 10
    for j in range(15):
    p300m.aspirate(190, trough.wells_by_name()['A2'], rate=3.0)
    p300m.dispense(190, trough.wells_by_name()['A2'], rate=3.0)
    protocol.delay(seconds=1)
    p300m.blow_out(trough.wells_by_name()['A2'].top())
    p300m.touch_tip()
    p300m.drop_tip()
    p300m.flow_rate.aspirate = 150
    p300m.flow_rate.dispense = 200
    p300m.well_bottom_clearance.aspirate = 1
    p300m.well_bottom_clearance.dispense = 1

    for i in range(4):
        p50m.pick_up_tip()
        p50m.well_bottom_clearance.aspirate = 2
        p50m.well_bottom_clearance.dispense = 10
        for j in range(5):
         p50m.aspirate(50, trough.wells_by_name()['A2'], rate=5.0)
         p50m.dispense(50, trough.wells_by_name()['A2'], rate=5.0)
        p50m.well_bottom_clearance.aspirate = 1
        p50m.well_bottom_clearance.dispense = 1
        protocol.delay(seconds=1)
        p50m.blow_out(trough.wells_by_name()['A2'].top())
        p50m.transfer(45, trough.wells('A2'), plate_dna.wells()[8*i], new_tip='never',
           mix_after=(2, 50), touch_tip=True)
        protocol.delay(seconds=1)
        p50m.blow_out(plate_dna.wells()[8*i])
        p50m.drop_tip()

    #Step 4: Distribute cells to nucleofection plate
    for i in range(4): # loop for 4 columns on DNA setup plate
        p50m.pick_up_tip()
        p50m.mix(10, 50, plate_dna.wells()[8*i], rate=5.0)
        protocol.delay(seconds=1)
        p50m.blow_out(plate_dna.wells()[8*i].top())
        for j in range(3): # Subloop for 3 replicates
            p50m.mix(4, (50-10*j), plate_dna.wells()[8*i], rate=5.0)
            p50m.blow_out(plate_dna.wells()[8*i].top())
            protocol.delay(seconds=1.0)
            p50m.well_bottom_clearance.dispense = 2.5
            p50m.aspirate(25, plate_dna.wells()[8*i])
```

```
        p50m.dispense(20, plate_nuc.wells()[8*(3*i+j)])
        protocol.delay(seconds=1.5)
        p50m.well_bottom_clearance.dispense = 1
        p50m.blow_out(plate_dna.wells()[8*i].top())
    p50m.drop_tip()

#Intervention 3: Insert pause for electroporation
protocol.pause()
protocol.comment('ATTENTION: Ensure below criteris are met prior to resuming protocol.
   Perform electroporation and return nucleofection plate to position 3.
   During electroporation, add pregassed media to trough, position 8, col 3.
   Once complete click resume.')

#Step 5: Add 80ul media to all wells
p300m.well_bottom_clearance.dispense = 12
p300m.pick_up_tip()
for i in range(12):
    p300m.aspirate(80, trough.wells()[2])
    p300m.dispense(80, plate_nuc.wells()[8*i])
    protocol.delay(seconds=1)
    p300m.blow_out(plate_nuc.wells()[8*i].top())
p300m.drop_tip()
p300m.well_bottom_clearance.dispense = 1
protocol.home()

#Intervention 4: Reset tipracks for seeding
protocol.pause()
protocol.comment('ATTENTION: Ensure below criteria are met prior to resuming protocol.
   Please reset tipracks as detailed below ready for seeding of cells.
   tip200_1 (slot 7) Only odd rows or tips.
   tip200_2 (slot 10) requires only even rows of tips.
   Extended details in ReadME section of script.
   Once complete click resume.')
p300m.reset_tipracks() # Reset tipracks

#Step 8: Seed into 24SWPs
List_plate = [(0, plate24_1A, tip200_1),(0, plate24_2B, tip200_2),
  (6, plate24_3A, tip200_1), (6, plate24_4B, tip200_2)]

for (j, plate24, tip), i in product(List_plate, range(6)):
    isource = plate24.wells()[4*(i)]
    idest_nuc = plate_nuc.wells()[8*(i+j)]

    p300m.well_bottom_clearance.aspirate = 2.5
    p300m.well_bottom_clearance.dispense = 2.5
    p300m.pick_up_tip(tip['A' + str(i+j+1)])
    for m in range(10):
        p300m.aspirate(70, idest_nuc, rate=2.0)
        p300m.dispense(70, idest_nuc, rate=2.0)
    protocol.delay(seconds=1.0)
    p300m.blow_out(plate_nuc.wells()[8*(j+i)].top())
    protocol.delay(seconds=1.0)
    p300m.aspirate(70, idest_nuc, rate=0.5)
    p300m.well_bottom_clearance.aspirate = 1.0
    p300m.well_bottom_clearance.dispense = 1.0
    p300m.dispense(70, isource)
    p300m.mix(2, 190, isource)
    protocol.delay(seconds=1.0)
    p300m.blow_out(isource.top())
    p300m.drop_tip()
#END SCRIPT!!!
```

E.3 Addition of culture media to 24-Shallow Well Plates (SWPs)

```
Readme:
#Protocol: 24Well plate seeding (630ul)
#Author: Oscar Swindley <oswindley1@sheffield.ac.uk>
#Please confirm 'labware' matches labwere section below
#Proceed with caution if any modifications are made
#Date: 05Feb2020
#Enjoy!!!

#README:
# trough  CD-CHO to columns 9 to 12 (18ml) for 4 plates
# Can seed 4 plates at a time
#TIPRACKS SETUP, Only include ODD rows of tips (A,C,E,G)

# imports
from opentrons import protocol_api
from itertools import product

# metadata
metadata = {
    'apiLevel': '2.0',
    'protocolName': '24 _well_plate_seed',
    'author': 'Oscar Swindley <oswindley1@sheffield.co.uk>',
    'description': '24Well plate seeding'}

def run(protocol: protocol_api.ProtocolContext):
    # labware
    trough = protocol.load_labware('axygen_12_reservior_22ml', '8')
    tip300_1 = protocol.load_labware('opentrons_96_tiprack_300ul', '7')
    tip300_2 = protocol.load_labware('opentrons_96_tiprack_300ul', '10')
    plate24_1A = protocol.load_labware('nunc_24_plate', '1')
    plate24_2A = protocol.load_labware('nunc_24_plate', '2')
    plate24_3A = protocol.load_labware('nunc_24_plate', '4')
    plate24_4A = protocol.load_labware('nunc_24_plate', '5')

    # pipettes
    p300m = protocol.load_instrument('p300_multi', mount='right', tip_racks=[tip300_1, tip300_2])
    p300m.flow_rate.aspirate = 200
    p300m.well_bottom_clearance.aspirate = 2
    p300m.well_bottom_clearance.dispense = 2

    #Step 1: Create list of trough wells and plate names:
    list_plate1 = [(11, plate24_1A), (10, plate24_2A), (9, plate24_3A), (8, plate24_4A)]

  # Creates function to seed plates.
    for (col, plate24_1), j in product(list_plate1, range(6)):
        p300m.pick_up_tip()
        for i in range(3):
            p300m.aspirate(20, trough.wells()[col].top())
            p300m.aspirate(210, trough.wells()[col])
            p300m.move_to(trough.wells()[col].top(-20))
            protocol.delay(seconds=1.0)
            p300m.dispense(220, plate24_1.wells()[4*j].top())
            protocol.delay(seconds=1.0)
            p300m.blow_out(plate24_1.wells()[4*j].top())
        p300m.drop_tip()
    # End Script
```

E.4 Mid culture sampling and addition of feed

```
#Readme:
#Protocol: 24SWP sampling for Iprasense 100um (1in2), supernatants
#Author: Oscar Swindley <oswindley1@sheffield.ac.uk>
#Proceed with caution if any modifications are made
#Version 1.0
#Date: 05Feb2020
#Enjoy!!!

#README:
#trough requires CD-CHO in A1
#When prompted  feed will be added to A3, RNA later and PBS to A5 and A6.
#tip300_1 (slot 7) requires only odd tips (A. C, E, G), tip300_2 (slot 10) requires even (B, D, F, H).
#nunc24swp-pseudoA/B is physicaly the same plate type as nunc24swp.
#Intentional miss-calibration allows compiling of 24-well-plates into 96-well-plates
#Remember to load second ip-slide after 1st is complete
#FOLLOW TIPRACK RESET INSTRUCTIONS CAREFULLY

# imports
from opentrons import protocol_api
from itertools import product
from opentrons import types

# metadata
metadata = {
    'apiLevel': '2.0',
    'protocolName': 'IprasenseSampling_24swp',
    'author': 'Oscar Swindley <oswindley1@sheffield.co.uk>',
    'description': 'Sampling 24_shallow_well_plate cultures for measurements on the iprasense
    (including a dilution step) and western blot sample collection.}

def run(protocol: protocol_api.ProtocolContext):
    # labware
    plate_pel = protocol.load_labware('nunc_96_ubottom', '9')
    plate_dil = protocol.load_labware('nunc_96_ubottom', '6')
    plate_ip = protocol.load_labware('iprasense_48_slide', '3')
    trough = protocol.load_labware('axygen_12_reservior_22ml', '8')
    tip300_1 = protocol.load_labware('opentrons_96_tiprack_300ul', '7')
    tip300_2 = protocol.load_labware('opentrons_96_tiprack_300ul', '10')
    tip200_1 = protocol.load_labware('opentrons_96_filtertiprack_200ul', '11')

    plate24_1A = protocol.load_labware('nunc_24_pseudo_a', '1')
    plate24_2B = protocol.load_labware('nunc_24_pseudo_b', '2')
    plate24_3A = protocol.load_labware('nunc_24_pseudo_a', '4')
    plate24_4B = protocol.load_labware('nunc_24_pseudo_b', '5')

    # pipettes (& settings if different to defaults)
    p300m = protocol.load_instrument('p300_multi', mount='right', tip_racks=[tip300_1, tip300_2])
    p50m = protocol.load_instrument('p50_multi', mount='left', tip_racks=[tip200_1])


    #Protocol Start!!!:
    #Step 1: Fill Dilution plate with 30ul media per well
    p50m.pick_up_tip()
    for i in range(12):
        p50m.aspirate(35, trough.wells('A1'))
        p50m.dispense(30, plate_dil.columns()[i])
        protocol.delay(seconds=0.5)
        p50m.blow_out(trough.wells('A1'))
```

```
p50m.return_tip()
p50m.reset_tipracks()

#Step 2: Mix and transfer 300ul 24wp_culture 1 to supernatant plate, transfer 30ul into dilution plate
List_plate = [(0, plate24_1A, tip300_1, 0, 0), (3, plate24_1A, tip300_1, 1, 0),
   (0, plate24_2B, tip300_2, 0, 0), (3, plate24_2B, tip300_2, 1, 0),
   (0, plate24_3A, tip300_1, 2, 6), (3, plate24_3A, tip300_1, 3, 6),
   (0, plate24_4B, tip300_2, 2, 6), (3, plate24_4B, tip300_2, 3, 6)]
              #In list arguments 1-4 are: 24SWP number, 24SWP name, tiprack, column offset adjuster

p300m.well_bottom_clearance.aspirate = 1.0
p300m.well_bottom_clearance.dispense = 2.5
for (j, plate24, tip, k, l), i in product(List_plate, range(3)):
    isource = plate24.wells()[4*(i+j)]
    idest_intermediate = plate_dil.wells()[8*(i+j+l)]
    idest_wb = plate_pel.wells()[8*k]

    well_edge_x1 = isource.bottom().move(types.Point(x=5.5, y=0, z=1.5))   # defines well edges
    well_edge_x2 = isource.bottom().move(types.Point(x=-5.5, y=0, z=1.5))
    well_edge_y1 = isource.bottom().move(types.Point(x=0, y=3.75, z=1.5))
    well_edge_y2 = isource.bottom().move(types.Point(x=0, y=-3.75, z=1.5))


    p300m.pick_up_tip(tip['A' + str(i+k*3+1)]) #Selects tip to pick up
    p300m.mix(1, 300, isource, rate=2.0)
    for r in range(2):
        p300m.aspirate(290, well_edge_x1, rate=2.0)
        p300m.dispense(300, well_edge_x2, rate=3.0)
        p300m.aspirate(290, well_edge_y1, rate=2.0)
        p300m.dispense(300, well_edge_y2, rate=3.0)
        p300m.aspirate(290, well_edge_x2, rate=2.0)
        p300m.dispense(300, well_edge_x1, rate=3.0)
        p300m.aspirate(290, well_edge_y2, rate=2.0)
        p300m.dispense(300, well_edge_y1, rate=3.0)
    p300m.mix(1, 300, isource, rate=2.0)
    protocol.delay(seconds=1.0)
    p300m.blow_out(isource.top())
    p300m.transfer(30, isource, idest_intermediate, mix_after=(2, 45), new_tip='never')
    protocol.delay(seconds=1)
    p300m.blow_out(idest_intermediate.top())
    p300m.mix(1, 300, isource, rate=2.0)
    protocol.delay(seconds=1.0)
    p300m.blow_out(isource.top())
    p300m.transfer(75, isource, idest_wb, new_tip='never')
    protocol.delay(seconds=1)
    p300m.blow_out(idest_wb.top())
    p300m.drop_tip()
p300m.well_bottom_clearance.aspirate = 1.0
p300m.well_bottom_clearance.dispense = 1.0

#Intervention 1:
protocol.home()
protocol.pause("ATTENTION: Replace 'tiprack-300-1' in 'slot 7' as follows:
     Cols 1+2 odd rows, 3+4 even rows, rest of rack full.
     Replace 'tiprack-300-2' in slot 2 with a full rack.
     Insert IP slide into slot 3 for odd wells.
     Add feed to trough.A3")

p300m.reset_tipracks()

 #Step 4: Feed Plates
```

```
def Feed_Plate(plate_name):
    p300m.pick_up_tip()
    for i in range(6):
        p300m.aspirate(10, trough.wells()[2].top())
        p300m.aspirate(140, trough.wells()[2], rate=0.7)
        p300m.move_to(trough.wells()[2].top(-20))
        protocol.delay(seconds=1.0)
        p300m.dispense(150, plate_name.wells()[4*i])
        protocol.delay(seconds=1.0)
        p300m.blow_out(plate_name.wells()[4*i].top())
    p300m.drop_tip()

p300m.well_bottom_clearance.aspirate = 1.0
p300m.well_bottom_clearance.dispense = 15.0
Feed_Plate(plate24_1A)
Feed_Plate(plate24_3A)
Feed_Plate(plate24_2B)
Feed_Plate(plate24_4B)

p300m.well_bottom_clearance.aspirate = 1.0
p300m.well_bottom_clearance.dispense = 1.0
protocol.home()

#Function_create: Load into IP_slide
def IP_slide_load(x):
    for i in range(6):
        p50m.pick_up_tip()
        p50m.mix(8, 50, plate_dil.wells()[8*(2*i+x)], rate=4.0)
        protocol.delay(seconds=1)
        p50m.blow_out(plate_dil.wells()[8*(2*i+x)].top())
        p50m.aspirate(10, plate_dil.wells()[8*(2*i+x)].top())
        p50m.flow_rate.aspirate = 25
        p50m.flow_rate.dispense = 2.5
        p50m.aspirate(9.0, plate_dil.wells()[8*(2*i+x)])
        p50m.dispense(30, plate_ip.wells()[8*(2*i+x)])
        protocol.delay(seconds=1.0)
        p50m.flow_rate.aspirate = 50
        p50m.flow_rate.dispense = 100
        p50m.drop_tip()

#Step 3: Load into IP_slide 1, swaps slides, load IP_slide 2
IP_slide_load(0)
protocol.pause()
protocol.comment("ATTENTION: Replace loaded iprasense slide with empty slide.
  Once complete click resume.
  Once protocol resumes, run IP_slide one on Iprasense")

IP_slide_load(1)
protocol.home()
protocol.pause()
protocol.comment("ATTENTION: Replace dilution plate with empty nunc_96U
   to take samples for qPCR")

#Step 4: Seperate 60ul from WB samples for qPCR
for i in range(4):
    p300m.pick_up_tip()
    p300m.mix(4, 200, plate_pel.wells()[8*i])
    protocol.delay(seconds=1.0)
    p300m.blow_out(plate_pel.wells()[8*i].top())
    p300m.transfer(60, plate_pel.wells()[8*i], plate_dil.wells()[8*i], new_tip='never')
    protocol.delay(seconds=1)
```

```
    p300m.blow_out(plate_dil.wells()[8*i].top())
    p300m.drop_tip()

protocol.home()
protocol.pause()
protocol.comment("ATTENTION: Remove western blot at qPCR plates, pellet cells and return.
   Add 8ml RNA_Later to trough A5. Add 8ml ice cold PBS to trough A6")

#Step 5: Add PBC to western blot samples and mix, Add RNA later to qPCR samples
p300m.well_bottom_clearance.aspirate = 1.0
p300m.well_bottom_clearance.dispense = 9.0
p300m.flow_rate.aspirate = 150
p300m.flow_rate.dispense = 50

p300m.pick_up_tip()
for i in range(4):
    p300m.transfer(100, trough.wells('A6'), plate_pel.wells()[8*i], new_tip='never')
    protocol.delay(seconds=1)
    p300m.blow_out(plate_pel.wells()[8*i].top())
p300m.drop_tip()

p300m.pick_up_tip()
for i in range(4):
    p300m.transfer(100, trough.wells('A5'), plate_dil.wells()[8*i], new_tip='never')
    protocol.delay(seconds=1)
    p300m.blow_out(plate_dil.wells()[8*i].top())
p300m.drop_tip()

#END SCRIPT!!!
```

E.5 Harvest of 24-SWPs

```
#ReadME:
#Protocol: OS 24SWP Harvest Protocol. Iprasense load(100um 1in2) and supernatant collection
#Author: Oscar Swindley <oswindley1@sheffield.ac.uk>
#Proceed with caution if any modifications are made (dilutions, volumes, not full plate)
#Date: 05Feb20
#Enjoy!!!

#README:
#trough requires CD-CHO in col-1 for Iprasense intermediate plate dilution.
#tip300_1 (slot 7) requires only  tips (A. C, E, G), tip300_2 (slot 10) requires even tips (B, D, F, H).
#Robot will pause for all interventions. Read on-screen instructions carefully

# imports
from opentrons import protocol_api
from itertools import product
from opentrons import types

# metadata
metadata = {
    'apiLevel': '2.0',
    'protocolName': '24SWP harvest_with_IprasenseSampling_and_Titre_Sampling',
    'author': 'Oscar Swindley <oswindley1@sheffield.co.uk>',
    'description': 'Harvest 4 24_shallow_well_plate cultures for measurements on the iprasense.
         Includes 1in2 dilution step. This require tricking the OT2 to use multichannels on 24
         well plate. Also includes collecting supernatant samples for titre assays'}

def run(protocol: protocol_api.ProtocolContext):
    # labware
    plate_pel = protocol.load_labware('corning_96_wellplate_360ul_flat', '9')
    plate_dil = protocol.load_labware('nunc_96_ubottom', '6')
    plate_ip = protocol.load_labware('iprasense_48_slide', '3')
    trough = protocol.load_labware('axygen_12_reservior_22ml', '8')
    tip300_1 = protocol.load_labware('opentrons_96_tiprack_300ul', '7')
    tip300_2 = protocol.load_labware('opentrons_96_tiprack_300ul', '10')
    tip200_1 = protocol.load_labware('opentrons_96_filtertiprack_200ul', '11')

    plate24_1A = protocol.load_labware('nunc_24_pseudo_a', '1')
    plate24_2B = protocol.load_labware('nunc_24_pseudo_b', '2')
    plate24_3A = protocol.load_labware('nunc_24_pseudo_a', '4')
    plate24_4B = protocol.load_labware('nunc_24_pseudo_b', '5')

    # pipettes (& settings if different to defaults)
    p300m = protocol.load_instrument('p300_multi', mount='right', tip_racks=[tip300_1, tip300_2])
    p50m = protocol.load_instrument('p50_multi', mount='left', tip_racks=[tip200_1])


    #Protocol Start!!!:
    #Step 1: Fill Dilution plate with 30ul media per well
    p50m.pick_up_tip()
    for i in range(12):
        p50m.aspirate(35, trough.wells()[0])
        p50m.dispense(30, plate_dil.wells()[8*i])
        protocol.delay(seconds=0.5)
        p50m.blow_out(trough.wells()[0])
    p50m.return_tip()
    p50m.reset_tipracks()
```

```
#Step 2: Mix and transfer 300ul 24wp_culture into supernatant plate, transfer 30ul to dilution plate
List_plate = [(plate24_1A, tip300_1, 0), (plate24_2B, tip300_2, 0),
   (plate24_3A, tip300_1, 6), (plate24_4B, tip300_2, 6)]
            #In list arguments 1-4 are: 24SWP number, 24SWP name, tiprack, column offset adjuster

p300m.well_bottom_clearance.aspirate = 1.0
p300m.well_bottom_clearance.dispense = 2.5
for (plate24, tip, j), i in product(List_plate, range(6)):
    isource = plate24.wells()[4*(i)]
    idest_intermediate = plate_dil.wells()[8*(i+j)]
    idest_supernatant = plate_pel.wells()[8*(i+j)]

    well_edge_x1 = isource.bottom().move(types.Point(x=5.5, y=0, z=1.5))
    well_edge_x2 = isource.bottom().move(types.Point(x=-5.5, y=0, z=1.5))
    well_edge_y1 = isource.bottom().move(types.Point(x=0, y=3.75, z=1.5))
    well_edge_y2 = isource.bottom().move(types.Point(x=0, y=-3.75, z=1.5))

    p300m.pick_up_tip(tip['A' + str(i+j+1)])       #Chooses tip to pick up
    p300m.mix(1, 300, isource, rate=2.0)
    for r in range(2):
        p300m.aspirate(290, well_edge_x1, rate=2.0)
        p300m.dispense(300, well_edge_x2, rate=3.0)
        p300m.aspirate(290, well_edge_y1, rate=2.0)
        p300m.dispense(300, well_edge_y2, rate=3.0)
        p300m.aspirate(290, well_edge_x2, rate=2.0)
        p300m.dispense(300, well_edge_x1, rate=3.0)
        p300m.aspirate(290, well_edge_y2, rate=2.0)
        p300m.dispense(300, well_edge_y1, rate=3.0)
    p300m.mix(1, 300, isource, rate=2.0)
    protocol.delay(seconds=1.0)
    p300m.blow_out(isource.top())
    p300m.transfer(30, isource, idest_intermediate, mix_after=(2, 45), new_tip='never')
    protocol.delay(seconds=1)
    p300m.blow_out(idest_intermediate.top())
    p300m.mix(1, 300, isource, rate=2.0)
    protocol.delay(seconds=1.0)
    p300m.blow_out(isource.top())
    p300m.transfer(300, isource, idest_supernatant, new_tip='never')
    protocol.delay(seconds=1)
    p300m.blow_out(idest_supernatant.top())
    p300m.drop_tip()
p300m.well_bottom_clearance.aspirate = 1.0
p300m.well_bottom_clearance.dispense = 1.0

#Function_create: Load into IP_slide
def IP_slide_load(x):
    for i in range(6):
        p50m.pick_up_tip()
        p50m.mix(8, 50, plate_dil.wells()[8*(2*i+x)], rate=4.0)
        protocol.delay(seconds=1)
        p50m.blow_out(plate_dil.wells()[8*(2*i+x)].top())
        p50m.aspirate(10, plate_dil.wells()[8*(2*i+x)].top())
        p50m.flow_rate.aspirate = 25
        p50m.flow_rate.dispense = 2.5
        p50m.aspirate(9.0, plate_dil.wells()[8*(2*i+x)])
        p50m.dispense(30, plate_ip.wells()[8*(2*i+x)])
        protocol.delay(seconds=1.0)
        p50m.flow_rate.aspirate = 50
        p50m.flow_rate.dispense = 100
        p50m.drop_tip()
```

```
#Step 3: Load into IP_slide 1 - odd numbers
protocol.home()
protocol.pause()
protocol.comment("ATTENTION: Insert IP_slide 1 into position 3 (odd columns)")
IP_slide_load(0)
protocol.home()
protocol.pause()
protocol.comment("ATTENTION: Remove IP_slide 1 to read and replace with IP_slide 2.
   Remove supernatant plate and pellet cells")
IP_slide_load(1)

#Step 5: Transfer supernatant into new plate
protocol.home()
protocol.pause()
protocol.comment("1: Remove IP_slide 2 to read.
   2: Replace IP dilution plate with fresh nunc-96U for supernatant transfer.
   3: Replace tip300_1 in 'slot 7' with a full rack")

p300m.reset_tipracks() # Reset tipracks
p300m.flow_rate.aspirate = 50
p300m.well_bottom_clearance.aspirate = 2.5
p300m.well_bottom_clearance.dispense = 1
for i in range(12):
    p300m.pick_up_tip()
    p300m.transfer(190, plate_pel.wells()[8*i], plate_dil.wells()[8*i], new_tip='never')
    protocol.delay(seconds=1)
    p300m.blow_out(plate_dil.wells()[8*i].top())
    p300m.drop_tip()
#End Protocol!!!
```

E.6 ValitaTITER Assay - Variable Sample Dilution

```
#Readme:
#Protocol: Valitatiter Assay, full plate with 1in20 dilution
#Author: Oscar Swindley <oswindley1@sheffield.ac.uk>
#Proceed with caution if any modifications are made (dilutions, volumes, not full plate)
# Version 4.0
# Date: 25Dec2019
#Enjoy!!!

#Notes:
#Please confirm 'labware' matches labwere section below, including correct tip box types and tip sizes
#Trough (Volumes in 25% excess): CD-CHO = Col1 min volume 18.0ml, VT_Buff = Col3 min volume 7.2ml

# For amending sample dilution, specify sample (s) and diluent (d) volumes here:
s = 10
d = 100-s

# imports
from opentrons import protocol_api

# metadata
metadata = {
    'apiLevel': '2.0',
    'protocolName': 'ValitaTiterAssay_1in20',
    'author': 'Oscar Swindley <oswindley1@sheffield.co.uk>',
    'description': 'First python protocol, ValitaTiterAssay, 1in15 sample dilution',
}
def run(protocol: protocol_api.ProtocolContext):

    # Labware in the protocol is loaded, format: variable = labware.load('labware name', 'Position on deck')
    plate_sample = protocol.load_labware('corning_96_wellplate_360ul_flat', '1')
    plate_dil = protocol.load_labware('nunc_96_ubottom', '5')
    plate_vt = protocol.load_labware('valitacell_96_wellplate_150ul', '2')
    tip300_1 = protocol.load_labware('opentrons_96_tiprack_300ul', '7')
    tip300_2 = protocol.load_labware('opentrons_96_tiprack_300ul', '10')
    tip10_1 = protocol.load_labware('opentrons_96_tiprack_10ul', '11')
    trough = protocol.load_labware('axygen_12_reservior_22ml', '8')

    # pipettes and settings
    p300m = protocol.load_instrument('p300_multi', mount='right', tip_racks=[tip300_1, tip300_2])
    p10m = protocol.load_instrument('p10_multi', mount='left', tip_racks=[tip10_1])

    #Step1: Fill Dilution plate 142.5ul
    p300m.distribute(d, trough.wells('A1'), plate_dil.wells(), touch_tip=True)

    #Step2: Add 7.5ul Sample to Dilution Plate
    p10m.transfer(s, plate_sample.wells(), plate_dil.wells(), mix_before=(3, 10),
       mix_after=(1, 10), blow_out=True, new_tip='always')

    #Step3: Add 60ul VT-Buff to VT plate
    p300m.well_bottom_clearance.dispense = 5
    p300m.distribute(60, trough.wells('A1'), plate_vt.wells(), touch_tip=True)
    p300m.well_bottom_clearance.dispense = 1

    #Step 4: Add 60ul Dil.Sample to VT plate + mix.
    p300m.transfer(60, plate_dil.wells(), plate_vt.wells(), mix_before=(3, 60),
        mix_after=(5, 60), blow_out=True, new_tip='always', touch_tip=True)

    #End of Protocol
```

Bibliography

Allier, C. et al. (2017). "Imaging of dense cell cultures by multiwavelength lens-free video microscopy". In: *Cytometry Part A* 91.5, pp. 433–442. DOI: 10.1002/cyto.a.23079.

Allier, Cedric et al. (2018). "Lens-free Video Microscopy for the Dynamic and Quantitative Analysis of Adherent Cell Culture". In: *Journal of visualized experiments : JoVE* 132, e56580. DOI: 10.3791/56580.

Altamirano, C., C. Paredes, A. Illanes, J. J. Cairó, and F. Gòdia (2004). "Strategies for fed-batch cultivation of t-PA producing CHO cells: Substitution of glucose and glutamine and rational design of culture medium". In: *Journal of Biotechnology* 110.2, pp. 171–179. DOI: 10.1016/j.jbiotec.2004.02.004.

Altamirano, Claudia, Andrés Illanes, Rossana Canessa, and Silvana Becerra (2006). "Specific nutrient supplementation of defined serum-free medium for the improvement of CHO cells growth and t-PA production". In: *Electronic Journal of Biotechnology* 9.1, pp. 61–67. DOI: 10.2225/vol9-issue1-fulltext-8.

Ambros, Victor, Rosalind C. Lee, Ann Lavanway, Peter T. Williams, and David Jewell (2003). "MicroRNAs and other tiny endogenous RNAs in C. elegans". In: *Current Biology* 13.10, pp. 807–818. DOI: 10.1016/S0960-9822(03)00287-2.

Andya, James D., Chung C. Hsu, and Steven J. Shire (2003). "Mechanisms of aggregate formation and carbohydrate excipient stabilization of lyophilized humanized monoclonal antibody formulations". In: *AAPS Journal* 5.2, p. 21. DOI: 10.1208/ps050210.

Appenzeller-Herzog, Christian and Lars Ellgaard (2008). *The human PDI family: Versatility packed into a single fold*. DOI: 10.1016/j.bbamcr.2007.11.010.

Arden, Nilou and Michael J. Betenbaugh (2004). "Life and death in mammalian cell culture: Strategies for apoptosis inhibition". In: *Trends in Biotechnology* 22.4, pp. 174–180. DOI: 10.1016/j.tibtech.2004.02.004.

Bagasra, Omar and Kiley R. Prilliman (2004). "RNA interference: The molecular immune system". In: *The Histochemical Journal* 35.6, pp. 545–553. DOI: 10.1007/s10735-004-2192-8.

Bai, Jianwu, Katharine J. Sepp, and Norbert Perrimon (2009). "Culture of drosophila primary cells dissociated from gastrula embryos and their use in rnai screening". In: *Nature Protocols* 4.10, pp. 1502–1512. DOI: 10.1038/nprot.2009.147.

Baik, Jong Youn, Leyla Gasimli, et al. (2012). "Metabolic engineering of Chinese hamster ovary cells: Towards a bioengineered heparin". In: *Metabolic Engineering* 14.2, pp. 81–90. DOI: 10.1016/j.ymben.2012.01.008.

Baik, Jong Youn and Kelvin H. Lee (2018). "Growth Rate Changes in CHO Host Cells Are Associated with Karyotypic Heterogeneity". In: *Biotechnology Journal* 13.3, pp. 13–16. DOI: 10.1002/biot.201700230.

Bandaranayake1, Ashok D. and Steven C. Almo (2014). "Recent advances in mammalian protein production". In: *FEBS Lett.* 588.2, pp. 253–260. DOI: 10.1038/jid.2014.371. arXiv: NIHMS150003.

Barnes, Louise M. and Alan J. Dickson (2006). *Mammalian cell factories for efficient and stable protein expression*. DOI: 10.1016/j.copbio.2006.06.005.

Barron, Niall, Noelia Sanchez, Paul Kelly, and Martin Clynes (2011). "MicroRNAs: Tiny targets for engineering CHO cell phenotypes?" In: *Biotechnology Letters* 33.1, pp. 11–21. DOI: 10.1007/s10529-010-0415-5.

Bartlett, Derek W and Mark E Davis (2006). "Insights into the kinetics of siRNA-mediated gene silencing from live-cell and live-animal bioluminescent imaging." In: *Nucleic acids research* 34.1, pp. 322–33. DOI: 10.1093/nar/gkj439.

Bass, B. L. (2001). *The short answer*. DOI: 10.1038/35078175.

Bayat, Hadi, Saghar Hossienzadeh, Eśhagh Pourmaleki, Roshanak Ahani, and Azam Rahimpour (2018). "Evaluation of different vector design strategies for the expression of recombinant monoclonal antibody in CHO cells". In: *Preparative Biochemistry & Biotechnology* 48.2, pp. 160–164. DOI: 10.1080/10826068.2017.1421966.

Becker, Eric, Lore Florin, Klaus Pfizenmaier, and Hitto Kaufmann (2008). "An XBP-1 dependent bottle-neck in production of IgG subtype antibodies in chemically defined serum-free Chinese hamster ovary (CHO) fed-batch processes". In: *Journal of Biotechnology* 135.2, pp. 217–223. DOI: 10.1016/j.jbiotec.2008.03.008.

— (2010). "Evaluation of a combinatorial cell engineering approach to overcome apoptotic effects in XBP-1(s) expressing cells". In: *Journal of Biotechnology* 146.4, pp. 198–206. DOI: 10.1016/j.jbiotec.2009.11.018.

Berger, Audrey, Valérie Le Fourn, Jacqueline Masternak, Alexandre Regamey, Iris Bodenmann, Pierre Alain Girod, and Nicolas Mermod (2020). "Overexpression of transcription factor Foxa1 and target genes remediate therapeutic protein production bottlenecks in Chinese hamster ovary cells". In: *Biotechnology and Bioengineering* 117.4, pp. 1101–1116. DOI: 10.1002/bit.27274.

Bernier, Virginie, Monique Lagacé, Daniel G. Bichet, and Michel Bouvier (2004). "Pharmacological chaperones: Potential treatment for conformational diseases". In: *Trends in Endocrinology and Metabolism* 15.5, pp. 222–228. DOI: 10.1016/j.tem.2004.05.003.

Bird, Robert E. et al. (1988). "Single-chain antigen-binding proteins". In: *Science* 242.4877, pp. 423–426. DOI: 10.1126/science.3140379.

Blair, Laura J., Jeremy D. Baker, Jonathan J. Sabbagh, and Chad A. Dickey (2015). "The emerging role of peptidyl-prolyl isomerase chaperones in tau oligomerization, amyloid processing, and Alzheimer's disease". In: *Journal of Neurochemistry* 133.1, pp. 1–13. DOI: 10.1111/jnc.13033.

Borth, Nicole, Diethard Mattanovich, Renate Kunert, and Hermann Katinger (2005). "Effect of increased expression of protein disulfide isomerase and heavy chain binding protein on

antibody secretion in a recombinant CHO cell line". In: *Biotechnology Progress* 21.1, pp. 106–111. DOI: 10.1021/bp0498241.

Boutros, Michael and Julie Ahringer (2008). "The art and design of genetic screens: RNA interference". In: *Nature Reviews Genetics* 9.7, pp. 554–566. DOI: 10.1038/nrg2364.

Bové, Jordi, Marta Martínez-Vicente, and Miquel Vila (2011). "Fighting neurodegeneration with rapamycin: Mechanistic insights". In: *Nature Reviews Neuroscience* 12.8, pp. 437–452. DOI: 10.1038/nrn3068.

Bradáč, Ivan, Radka Svobodová Vařeková, Michael Wacenovsky, Michal Škrdla, Martin Plchút, and Martin Polčík (2007). "siRNA selection criteria-Statistical analyses of applicability and significance". In: *Biochemical and Biophysical Research Communications* 359.1, pp. 83–87. DOI: 10.1016/j.bbrc.2007.05.056.

Brake, Olivier ter, Karen 't Hooft, Ying Poi Liu, Mireille Centlivre, Karin Jasmijn von Eije, and Ben Berkhout (2008). "Lentiviral vector design for multiple shRNA expression and durable HIV-1 inhibition". In: *Molecular Therapy* 16.3, pp. 557–564. DOI: 10.1038/sj.mt.6300382.

Brown, Adam J. and David C. James (2016). "Precision control of recombinant gene transcription for CHO cell synthetic biology". In: *Biotechnology Advances* 34.5, pp. 492–503.

Budge, James D. et al. (2020). "Engineering of Chinese hamster ovary cell lipid metabolism results in an expanded ER and enhanced recombinant biotherapeutic protein production". In: *Metabolic Engineering* 57, pp. 203–216. DOI: 10.1016/j.ymben.2019.11.007.

Butler, M. and A. Meneses-Acosta (2012). *Recent advances in technology supporting biopharmaceutical production from mammalian cells*. DOI: 10.1007/s00253-012-4451-z.

Cain, Chris (2011). "Crossing over to bispecificity". In: *Science-Business eXchange* 4.28, pp. 783–783. DOI: 10.1038/scibx.2011.783.

Cain, Katharine et al. (2013). "A CHO cell line engineered to express XBP1 and ERO1-Lα has increased levels of transient protein expression". In: *Biotechnology Progress* 29.3, pp. 697–706. DOI: 10.1002/btpr.1693.

Calamini, Barbara et al. (2012). "Small-molecule proteostasis regulators for protein conformational diseases". In: *Nature Chemical Biology*. DOI: 10.1038/nchembio.763.

Calfon, Marcella, Huiqing Zeng, Fumihiko Urano, Jeffery H. Till, Stevan R. Hubbard, Heather P. Harding, Scott G. Clark, and David Ron (2002). "IRE1 couples endoplasmic reticulum load to secretory capacity by processing the XBP-1 mRNA". In: *Nature* 415.6867, pp. 92–96. DOI: 10.1038/415092a.

Calin, George Adrian et al. (2004). "Human microRNA genes are frequently located at fragile sites and genomic regions involved in cancers". In: *Proceedings of the National Academy of Sciences of the United States of America* 101.9, pp. 2999–3004. DOI: 10.1073/pnas.0307323101.

Camire, Joseph, Dongjoo Kim, and Soonjo Kwon (2017). "Enhanced production of recombinant proteins by a small molecule protein synthesis enhancer in combination with an antioxidant in recombinant Chinese hamster ovary cells". In: *Bioprocess and Biosystems Engineering* 40.7, pp. 1049–1056. DOI: 10.1007/s00449-017-1767-1.

Cao, Mingyan et al. (2018). "Characterization and analysis of scFv-IgG bispecific antibody size variants". In: *mAbs* 10.8, pp. 1236–1247. DOI: 10.1080/19420862.2018.1505398.

Caraveo, Gabriela et al. (2017). "FKBP12 contributes to α-synuclein toxicity by regulating the calcineurin-dependent phosphoproteome". In: *Proceedings of the National Academy of Sciences of the United States of America* 114.52, E11313–E11322. DOI: 10.1073/pnas.1711926115.

Carlage, Tyler, Rashmi Kshirsagar, Li Zang, Vijay Janakiraman, Marina Hincapie, Yelena Lyubarskaya, Andy Weiskopf, and William S. Hancock (2012). "Analysis of dynamic changes in the proteome of a Bcl-XL overexpressing Chinese hamster ovary cell culture during exponential and stationary phases". In: *Biotechnology Progress* 28.3, pp. 814–823. DOI: 10.1002/btpr.1534.

Cartwright, Joseph F. et al. (2020). "A platform for context-specific genetic engineering of recombinant protein production by CHO cells". In: *Journal of Biotechnology* 312, pp. 11–22. DOI: 10.1016/j.jbiotec.2020.02.012.

Castanotto, Daniela et al. (2007). "Combinatorial delivery of small interfering RNAs reduces RNAi efficacy by selective incorporation into RISC". In: *Nucleic Acids Research* 35.15, pp. 5154–5164. DOI: 10.1093/nar/gkm543.

Chaika, Nina V. et al. (2012). "MUC1 mucin stabilizes and activates hypoxia-inducible factor 1 alpha to regulate metabolism in pancreatic cancer". In: *Proceedings of the National Academy of Sciences of the United States of America* 109.34, pp. 13787–13792. DOI: 10.1073/pnas.1203339109.

Chang, Jiasong, Xiaoxu Chen, Ruolin Wang, Run Shi, Xiaogang Wang, Wei Lu, Sanyuan Ma, and Qingyou Xia (2020). "High-throughput screening identifies two novel small molecule enhancers of recombinant protein expression". In: *Molecules* 25.2. DOI: 10.3390/molecules25020353.

Chen, Guo Fang, Ting Hai Xu, Yan Yan, Yu Ren Zhou, Yi Jiang, Karsten Melcher, and H. Eric Xu (2017). "Amyloid beta: Structure, biology and structure-based therapeutic development". In: *Acta Pharmacologica Sinica* 38.9, pp. 1205–1235. DOI: 10.1038/aps.2017.28.

Chen, Jialong, Yixian Ren, Chen Gui, Menglan Zhao, Xian Wu, Kanmin Mao, Wenjun Li, and Fei Zou (2018). "Phosphorylation of Parkin at serine 131 by p38 MAPK promotes mitochondrial dysfunction and neuronal death in mutant A53T α-synuclein model of Parkinson's disease". In: *Cell Death and Disease* 9.6, pp. 1–15. DOI: 10.1038/s41419-018-0722-7.

Chen, John J., Joseph C. Genereux, Song Qu, John D. Hulleman, Matthew D. Shoulders, and R. Luke Wiseman (2014). "ATF6 activation reduces the secretion and extracellular aggregation of destabilized variants of an amyloidogenic protein". In: *Chemistry and Biology* 21.11, pp. 1564–1574. DOI: 10.1016/j.chembiol.2014.09.009.

Chen, Lihua and Beidong Liu (2017). "Relationships between Stress Granules, Oxidative Stress, and Neurodegenerative Diseases". In: *Oxidative Medicine and Cellular Longevity* 2017. DOI: 10.1155/2017/1809592.

Chiang, Wei Chieh, Carissa Messah, and Jonathan H. Lin (2012). "IRE1 directs proteasomal and lysosomal degradation of misfolded rhodopsin". In: *Molecular Biology of the Cell* 23.5, pp. 758–770. DOI: 10.1091/mbc.E11-08-0663.

Christiansen, Jason and Ayyappan K Rajasekaran (2004). *Biological impediments to monoclonal antibody-based cancer immunotherapy.*

Chung, Joo Young, Seung Wook Lim, Yeon Joo Hong, Sun Ok Hwang, and Gyun Min Lee (2004). "Effect of Doxycycline-Regulated Calnexin and Calreticulin Expression on Specific Thrombopoietin Productivity of Recombinant Chinese Hamster Ovary Cells". In: *Biotechnology and Bioengineering* 85.5, pp. 539–546. DOI: 10.1002/bit.10919.

Cortez, Leonardo and Valerie Sim (2014). "The therapeutic potential of chemical chaperones in protein folding diseases." In: *Prion* 8.2, p. 197. DOI: 10.4161/PRI.28938.

Cromwell, Mary E.M., Eric Hilario, and Fred Jacobson (2006). "Protein aggregation and bioprocessing". In: *AAPS Journal* 8.3. DOI: 10.1208/aapsj080366.

Cuadrado-Tejedor, M., A. Garcia-Osta, A. Ricobaraza, J. Oyarzabal, and R. Franco (2011). "Defining the Mechanism of Action of 4-Phenylbutyrate to Develop a Small-Molecule-Based Therapy for Alzheimers Disease". In: *Current Medicinal Chemistry* 18.36, pp. 5545–5553. DOI: 10.2174/092986711798347315.

Cuenda, Ana and Simon Rousseau (2007). *p38 MAP-Kinases pathway regulation, function and role in human diseases*. DOI: 10.1016/j.bbamcr.2007.03.010.

Cunnea, Paula M. et al. (2003). "ERdj5, an endoplasmic reticulum (ER)-resident protein containing DnaJ and thioredoxin domains, is expressed in secretory cells or following ER stress". In: *Journal of Biological Chemistry* 278.2, pp. 1059–1066. DOI: 10.1074/jbc.M206995200.

Dadehbeigi, Nazanin and Alan J. Dickson (2015). "Chemical manipulation of the mTORC1 pathway in industrially relevant CHOK1 cells enhances production of therapeutic proteins". In: *Biotechnology Journal* 10.7, pp. 1041–1050. DOI: 10.1002/biot.201500075.

Daga, Neha et al. (2018). "Growth-restricting effects of siRNA transfections: A largely deterministic combination of off-target binding and hybridization-independent competition". In: *Nucleic Acids Research* 46.18, pp. 9309–9320. DOI: 10.1093/nar/gky798.

Das, Atze T., Xue Zhou, Stefan W. Metz, Monique A. Vink, and Ben Berkhout (2016). "Selecting the optimal Tet-On system for doxycycline-inducible gene expression in transiently transfected and stably transduced mammalian cells". In: *Biotechnology Journal* 11.1, pp. 71–79. DOI: 10.1002/biot.201500236.

Davis, R., K. Schooley, B. Rasmussen, J. Thomas, and P. Reddy (2000). "Effect of PDI overexpression on recombinant protein secretion in CHO cells". In: *Biotechnology Progress* 16.5, pp. 736–743. DOI: 10.1021/bp000107q.

Denli, Ahmet M., Bastiaan B.J. Tops, Ronald H.A. Plasterk, René F. Ketting, and Gregory J. Hannon (2004). "Processing of primary microRNAs by the Microprocessor complex". In: *Nature* 432.7014, pp. 231–235. DOI: 10.1038/nature03049.

DeRisi, Joseph L., Vishwanath R. Iyer, and Patrick O. Brown (1997). "Exploring the metabolic and genetic control of gene expression on a genomic scale". In: *Science* 278.5338, pp. 680–686. DOI: 10.1126/science.278.5338.680.

Di, Xiao Jing, Ya Juan Wang, Dong Yun Han, Yan Lin Fu, Adam S. Duerfeldt, Brian S.J. Blagg, and Ting Wei Mu (2016). "Grp94 protein delivers γ-aminobutyric acid type A (GABAA) receptors to Hrd1 protein-mediated endoplasmic reticulumassociated degradation". In: *Journal of Biological Chemistry* 291.18, pp. 9526–9539. DOI: 10.1074/jbc.M115.705004.

Dias-Gunasekara, Sanjika et al. (2005). "Tissue-specific expression and dimerization of the endoplasmic reticulum oxidoreductase Ero1β". In: *Journal of Biological Chemistry* 280.38, pp. 33066–33075. DOI: 10.1074/jbc.M505023200.

Dickens, Jennifer A et al. (2016). "The endoplasmic reticulum remains functionally connected by vesicular transport after its fragmentation in cells expressing Z-alpha1-antitrypsin." In: *FASEB journal : official publication of the Federation of American Societies for Experimental Biology*, pp. 1–16. DOI: 10.1096/fj.201600430R.

Dimasi, Nazzareno, Ryan Fleming, Carl Hay, Rob Woods, Linda Xu, Herren Wu, and Changshou Gao (2015). "Development of a Trispecific Antibody Designed to Simultaneously and Efficiently Target Three Different Antigens on Tumor Cells". In: *Molecular Pharmaceutics* 12.9, pp. 3490–3501. DOI: 10.1021/acs.molpharmaceut.5b00268.

Distefano, Johanna K (2019). "Disease Gene Identii cation Methods and Protocols Second Edition Methods in Molecular Biology 1706". In: pp. 1–9. DOI: 10.1007/978-1-4939-7471-9.

Du, Heng, Lan Guo, et al. (2008). "Cyclophilin D deficiency attenuates mitochondrial and neuronal perturbation and ameliorates learning and memory in Alzheimer's disease". In: *Nature Medicine* 14.10, pp. 1097–1105. DOI: 10.1038/nm.1868.

Du, Heng and Shirley Shi Du Yan (2010). *Mitochondrial permeability transition pore in Alzheimer's disease: Cyclophilin D and amyloid beta*. DOI: 10.1016/j.bbadis.2009.07.005.

DuRose, Jenny B., Arvin B. Tam, and Maho Niwa (2006). "Intrinsic capacities of molecular sensors of the unfolded protein response to sense alternate forms of endoplasmic reticulum stress". In: *Molecular Biology of the Cell* 17.7, pp. 3095–3107. DOI: 10.1091/mbc.E06-01-0055.

E. Yanos, Melana, Christopher F. Bennett, and Matt Kaeberlein (2012). "Genome-Wide RNAi Longevity Screens in Caenorhabditis elegans". In: *Current Genomics* 13.7, pp. 508–518. DOI: 10.2174/138920212803251391.

Echeverri, Christophe J. et al. (2006). "Minimizing the risk of reporting false positives in large-scale RNAi screens". In: *Nature Methods* 3.10, pp. 777–779. DOI: 10.1038/nmeth1006-777.

Ecker, Dawn M., Susan Dana Jones, and Howard L. Levine (2015). "The therapeutic monoclonal antibody market". In: *mAbs* 7.1, pp. 9–14. DOI: 10.4161/19420862.2015.989042.

Elbashir, Sayda M., Jens Harborth, Winfried Lendeckel, Abdullah Yalcin, Klaus Weber, and Thomas Tuschl (2001). "Duplexes of 21-nucleotide RNAs mediate RNA interference in cultured mammalian cells". In: *Nature* 411.6836, pp. 494–498. DOI: 10.1038/35078107.

Elouahabi, Abdelatif and Jean Marie Ruysschaert (2005). *Formation and intracellular trafficking of lipoplexes and polyplexes*. DOI: 10.1016/j.ymthe.2004.12.006.

Elshereef, Abdalla A., André Jochums, Antonina Lavrentieva, Lena Stuckenberg, Thomas Scheper, and Dörte Solle (2019). "High cell density transient transfection of CHO cells for TGF-β1 expression". In: *Engineering in Life Sciences* 19.11, pp. 730–740. DOI: 10.1002/elsc.201800174.

Fire, A., S. Xu, M. K. Montgomery, S. A. Kostas, S. E. Driver, and C. C. Mello (1998). "Potent and specific genetic interference by double-stranded RNA in caenorhabditis elegans". In: *Nature* 391.6669, pp. 806–811. DOI: 10.1038/35888.

Fischer, Simon, René Handrick, and Kerstin Otte (2015). *The art of CHO cell engineering: A comprehensive retrospect and future perspectives.* DOI: 10.1016/j.biotechadv.2015.10.015.

Fischer, Simon and Kerstin Otte (2019). "CHO Cell Engineering for Improved Process Performance and Product Quality". In: *Cell Culture Engineering.* Wiley, pp. 207–250. DOI: 10.1002/9783527811410.ch9.

Freund, Nathaniel W. and Matthew S. Croughan (2018). "A simple method to reduce both lactic acid and ammonium production in industrial animal cell culture". In: *International Journal of Molecular Sciences* 19.2. DOI: 10.3390/ijms19020385.

Genereux, Joseph C et al. (2015). "Unfolded protein response-induced ¡scp¿ER¡/scp¿ dj3 secretion links ¡scp¿ER¡/scp¿ stress to extracellular proteostasis". In: *The EMBO Journal* 34.1, pp. 4–19. DOI: 10.15252/embj.201488896.

Geoghegan, Darren, Claire Arnall, Diane Hatton, Joanne Noble-Longster, Christopher Sellick, Tarik Senussi, and David C. James (2018). "Control of amino acid transport into Chinese hamster ovary cells". In: *Biotechnology and Bioengineering* 115.12, pp. 2908–2929. DOI: 10.1002/bit.26794.

Gifford, J., A. Albee, ZW. Deeds, B. Delong, K. Kao, S. Ross, and MV. Caple (2005). "An Efficient Approach to Cell Culture Medium Optimization — A Statistical Method to Medium Mixing". In: *Animal Cell Technology Meets Genomics.* Springer-Verlag, pp. 549–553. DOI: 10.1007/1-4020-3103-3_108.

Giorgetti, Sofia, Claudio Greco, Paolo Tortora, and Francesco Antonio Aprile (2018). *Targeting amyloid aggregation: An overview of strategies and mechanisms.* DOI: 10.3390/ijms19092677.

Goh, John S.Y., Peiqing Zhang, Kah Fai Chan, May May Lee, Sing Fee Lim, and Zhiwei Song (2010). "RCA-I-resistant CHO mutant cells have dysfunctional GnT I and expression of normal GnT I in these mutants enhances sialylation of recombinant erythropoietin". In: *Metabolic Engineering* 12.4, pp. 360–368. DOI: 10.1016/j.ymben.2010.03.002.

Graham, Ryan J., Hemlata Bhatia, and Seongkyu Yoon (2019). "Consequences of trace metal variability and supplementation on Chinese hamster ovary (CHO) cell culture performance: A review of key mechanisms and considerations". In: *Biotechnology and Bioengineering* 116.12, pp. 3446–3456. DOI: 10.1002/bit.27140.

Grandjean, Julia M.D. et al. (2020). "Pharmacologic IRE1/XBP1s activation confers targeted ER proteostasis reprogramming". In: *Nature Chemical Biology.* DOI: 10.1038/s41589-020-0584-z.

Greenberg, Andrew S., David Avila, Marianne Hughes, Austin Hughes, E. Churchill McKinney, and Martin F. Flajnik (1995). "A new antigen receptor gene family that undergoes rearrangement and extensive somatic diversification in sharks". In: *Nature* 374.6518, pp. 168–173. DOI: 10.1038/374168a0.

Gu, Jijie and Tariq Ghayur (2012). "Generation of dual-variable-domain immunoglobulin molecules for dual-specific targeting." In: *Methods in enzymology* 502, pp. 25–41. DOI: 10.1016/B978-0-12-416039-2.00002-1.

Güler-Gane, Gülin, Sara Kidd, Sudharsan Sridharan, Tristan J. Vaughan, Trevor C. I. Wilkinson, and Natalie J. Tigue (2016). "Overcoming the Refractory Expression of Secreted Recombinant Proteins in Mammalian Cells through Modification of the Signal Peptide and Adjacent Amino Acids". In: *PLOS ONE* 11.5. Ed. by Mark J van Raaij, e0155340. DOI: 10.1371/journal.pone.0155340.

Gulis, Galina, Kelly Cristina R. Simi, Renata R. de Toledo, Andrea Q. Maranhao, and Marcelo M. Brigido (2014). "Optimization of heterologous protein production in Chinese hamster ovary cells under overexpression of spliced form of human X-box binding protein". In: *BMC Biotechnology* 14. DOI: 10.1186/1472-6750-14-26.

Gunasekaran, Kannan et al. (2010). "Enhancing antibody Fc heterodimer formation through electrostatic steering effects: Applications to bispecific molecules and monovalent IgG". In: *Journal of Biological Chemistry* 285.25, pp. 19637–19646. DOI: 10.1074/jbc.M110.117382.

Haas, Alexander K., Shin Ichiro Yoshimura, David J. Stephens, Christian Preisinger, Evelyn Fuchs, and Francis A. Barr (2007). "Analysis of GTPase-activating proteins: Rab1 and Rab43 are key Rabs required to maintain a functional Golgi complex in human cells". In: *Journal of Cell Science* 120.17, pp. 2997–3010. DOI: 10.1242/jcs.014225.

Hackl, Matthias, Nicole Borth, and Johannes Grillari (2012). *MiRNAs - pathway engineering of CHO cell factories that avoids translational burdening.* DOI: 10.1016/j.tibtech.2012.05.002.

Hamada, Makiko et al. (2002). "Effects on RNA interference in gene expression (RNAi) in cultured mammalian cells of mismatches and the introduction of chemical modifications at the 3'-ends of siRNAs". In: *Antisense and Nucleic Acid Drug Development* 12.5, pp. 301–309. DOI: 10.1089/108729002761381285.

Hammond, Stephanie and Kelvin H. Lee (2012). "RNA interference of cofilin in Chinese hamster ovary cells improves recombinant protein productivity". In: *Biotechnology and Bioengineering* 109.2, pp. 528–535. DOI: 10.1002/bit.23322.

Han, Dong-Yun, Xiao-Jing Di, Yan-Lin Fu, and Ting-Wei Mu (2015). "Combining valosin-containing protein (VCP) inhibition and suberanilohydroxamic acid (SAHA) treatment additively enhances the folding, trafficking, and function of epilepsy-associated γ-aminobutyric acid, type A (GABAA) receptors." In: *The Journal of biological chemistry* 290.1, pp. 325–37. DOI: 10.1074/jbc.M114.580324.

Hansen, Henning Gram, Claes Nymand Nilsson, et al. (2015). "Versatile microscale screening platform for improving recombinant protein productivity in Chinese hamster ovary cells". In: *Scientific Reports* 5.December, pp. 1–12. DOI: 10.1038/srep18016.

Hansen, Henning Gram, Nuša Pristovšek, Helene Faustrup Kildegaard, and Gyun Min Lee (2017). "Improving the secretory capacity of Chinese hamster ovary cells by ectopic expression of effector genes: Lessons learned and future directions". In: *Biotechnology Advances* 35.1, pp. 64–76. DOI: 10.1016/j.biotechadv.2016.11.008.

Harding, Heather P., Yuhong Zhang, Anne Bertolotti, Huiqing Zeng, and David Ron (2000). "Perk is essential for translational regulation and cell survival during the unfolded protein response". In: *Molecular Cell* 5.5, pp. 897–904. DOI: 10.1016/S1097-2765(00)80330-5.

Harreither, Eva et al. (2015). "Microarray profiling of preselected CHO host cell subclones identifies gene expression patterns associated with in-creased production capacity". In: *Biotechnology Journal* 10.10, pp. 1625–1638. DOI: 10.1002/biot.201400857.

Hatahet, Feras and Lloyd W. Ruddock (2009). *Protein disulfide isomerase: A critical evaluation of its function in disulfide bond formation.* DOI: 10.1089/ars.2009.2466.

Hayes, N. V.L., C. M. Smales, and P. Klappa (2010). "Protein disulfide isomerase does not control recombinant IgG4 productivity in mammalian cell lines". In: *Biotechnology and Bioengineering* 105.4, pp. 770–779. DOI: 10.1002/bit.22587.

Hendershot, Linda M. (2004). "The ER chaperone BiP is a master regulator of ER function". In: *Mount Sinai Journal of Medicine* 71.5, pp. 289–297.

Henschel, Andreas, Frank Buchholz, and Bianca Habermann (2004). "DEQOR: A web-based tool for the design and quality control of siRNAs". In: *Nucleic Acids Research* 32.WEB SERVER ISS. Pp. 113–120. DOI: 10.1093/nar/gkh408.

Hergesheimer, Rudolf C., Anna A. Chami, Denis Reis De Assis, Patrick Vourc'h, Christian R. Andres, Philippe Corcia, Débora Lanznaster, and Hélène Blasco (2019). "The debated toxic role of aggregated TDP-43 in amyotrophic lateral sclerosis: A resolution in sight?" In: *Brain* 142.5, pp. 1176–1194. DOI: 10.1093/brain/awz078.

Holliger, Philipp and Peter J. Hudson (2005). "Engineered antibody fragments and the rise of single domains". In: *Nature Biotechnology* 23.9, pp. 1126–1136. DOI: 10.1038/nbt1142.

Holliger, Philipp, Terence Prospero, and Greg Winter (1993). ""Diabodies": Small bivalent and bispecific antibody fragments". In: *Proceedings of the National Academy of Sciences of the United States of America* 90.14, pp. 6444–6448. DOI: 10.1073/pnas.90.14.6444.

Homann, Stefanie et al. (2017). "A novel rapid and reproducible flow cytometric method for optimization of transfection efficiency in cells". In: *PLOS ONE* 12.9. Ed. by Guangyu Wu, e0182941. DOI: 10.1371/journal.pone.0182941.

Hu, Guang, Jonghwan Kim, Qikai Xu, Yumei Leng, Stuart H Orkin, and Stephen J Elledge (2009). "A genome-wide RNAi screen identifies a new transcriptional module required for self-renewal". In: *Genes and Development* 23.7, pp. 837–848. DOI: 10.1101/gad.1769609.

Hughes, J. P., S. S. Rees, S. B. Kalindjian, and K. L. Philpott (2011). *Principles of early drug discovery.* DOI: 10.1111/j.1476-5381.2010.01127.x.

Hutvágner, György, Martin J Simard, Craig C Mello, and Phillip D Zamore (2004). "Sequence-Specific Inhibition of Small RNA Function". In: *PLoS Biology* 2.4. Ed. by Gerald Joyce, e98. DOI: 10.1371/journal.pbio.0020098.

Hwang, H. W. and J. T. Mendell (2006). *MicroRNAs in cell proliferation, cell death, and tumorigenesis.* DOI: 10.1038/sj.bjc.6603023.

Hwang, Su Jeong, Choon Ju Jeon, Sung Min Cho, Gyun Min Lee, and Sung Kwan Yoon (2011). "Effect of chemical chaperone addition on production and aggregation of recombinant flag-tagged COMP-angiopoietin 1 in chinese hamster ovary cells". In: *Biotechnology Progress* 27.2, pp. 587–591. DOI: 10.1002/btpr.579.

Hwang, Sun Ok, Joo Young Chung, and Gyun Min Lee (2003). "Effect of doxycycline-regulated ERp57 expression on specific thrombopoietin productivity of recombinant CHO cells". In: *Biotechnology Progress* 19.1, pp. 179–184. DOI: 10.1021/bp025578m.

Imai-Nishiya, Harue, Katsuhiro Mori, Miho Inoue, Masako Wakitani, Shigeru Iida, Kenya Shitara, and Mitsuo Satoh (2007). "Double knockdown of α1,6-fucosyltransferase (FUT8) and GDP-mannose 4,6-dehydratase (GMD) in antibody-producing cells: A new strategy for generating fully non-fucosylated therapeutic antibodies with enhanced ADCC". In: *BMC Biotechnology* 7.1, p. 84. DOI: 10.1186/1472-6750-7-84.

Ishino, Tetsuya et al. (2013). "Engineering a monomeric Fc domain modality by N-glycosylation for the half-life extension of biotherapeutics". In: *Journal of Biological Chemistry* 288.23, pp. 16529–16537. DOI: 10.1074/jbc.M113.457689.

Jadhav, Vaibhav et al. (2013). "CHO microRNA engineering is growing up: Recent successes and future challenges". In: *Biotechnology Advances* 31.8, pp. 1501–1513. DOI: 10.1016/j.biotechadv.2013.07.007.

Jazayeri, Seyedeh Hoda, Amir Amiri-Yekta, Salahadin Bahrami, Hamid Gourabi, Mohammad Hossein Sanati, and Mohammad Reza Khorramizadeh (2018). *Vector and Cell Line Engineering Technologies Toward Recombinant Protein Expression in Mammalian Cell Lines.* DOI: 10.1007/s12010-017-2689-8.

Johari, Yusuf B., Scott D. Estes, Christina S. Alves, Marty S. Sinacore, and David C. James (2015). "Integrated cell and process engineering for improved transient production of a "difficult-to-express" fusion protein by CHO cells". In: *Biotechnology and Bioengineering* 112.12, pp. 2527–2542. DOI: 10.1002/bit.25687.

Kallunki, Tuula, Marin Barisic, Marja Jäättelä, and Bin Liu (2019). "How to Choose the Right Inducible Gene Expression System for Mammalian Studies?" In: *Cells* 8.8, pp. 1–16. DOI: 10.3390/cells8080796.

Kalsi, Devika (2018). "High-throughput platform development for Chinese Hamster Ovary (CHO) cell culture performance enhancement using small molecules". In:

Kampinga, Harm H. and Elizabeth A. Craig (2010). *The HSP70 chaperone machinery: J proteins as drivers of functional specificity.* DOI: 10.1038/nrm2941.

Kanehisa, Minoru and Susumu Goto (2000). *KEGG: Kyoto Encyclopedia of Genes and Genomes.* DOI: 10.1093/nar/28.1.27.

Kaufman, Randal J. (1999). "Stress signaling from the lumen of the endoplasmic reticulum: Coordination of gene transcriptional and translational controls". In: *Genes and Development* 13.10, pp. 1211–1233. DOI: 10.1101/gad.13.10.1211.

Kelley, Brian (2009). "Industrialization of mAb production technology: The bioprocessing industry at a crossroads". In: *mAbs* 1.5, pp. 440–449. DOI: 10.4161/mabs.1.5.9448.

Khan, Aly A., Doron Betel, Martin L. Miller, Chris Sander, Christina S. Leslie, and Debora S. Marks (2009). "Transfection of small RNAs globally perturbs gene regulation by endogenous microRNAs". In: *Nature Biotechnology* 27.6, pp. 549–555. DOI: 10.1038/nbt.1543.

Kiese, Sylvia, Astrid Papppenberger, Wolfgang Friess, and Hanns Christian Mahler (2008). "Shaken, not stirred: Mechanical stress testing of an IgG1 antibody". In: *Journal of Pharmaceutical Sciences* 97.10, pp. 4347–4366. DOI: 10.1002/jps.21328.

Kim, Jee Yon, Yeon Gu Kim, and Gyun Min Lee (2012). *CHO cells in biotechnology for production of recombinant proteins: Current state and further potential.* DOI: 10.1007/s00253-011-3758-5.

Kim, Sung Hyun and Gyun Min Lee (2007). "Down-regulation of lactate dehydrogenase-A by siRNAs for reduced lactic acid formation of Chinese hamster ovary cells producing thrombopoietin". In: *Applied Microbiology and Biotechnology* 74.1, pp. 152–159. DOI: 10.1007/s00253-006-0654-5.

Kittler, Ralf et al. (2004). "An endoribonuclease-prepared siRNA screen in human cells identifies genes essential for cell division". In: *Nature* 432.7020, pp. 1036–1040. DOI: 10.1038/nature03159.

Klanert, Gerald et al. (2019). "A cross-species whole genome siRNA screen in suspension-cultured Chinese hamster ovary cells identifies novel engineering targets". In: *Scientific Reports* 9.1. DOI: 10.1038/s41598-019-45159-2.

Korennykh, Alexei V., Pascal F. Egea, Andrei A. Korostelev, Janet Finer-Moore, Chao Zhang, Kevan M. Shokat, Robert M. Stroud, and Peter Walter (2009). "The unfolded protein response signals through high-order assembly of Ire1". In: *Nature* 457.7230, pp. 687–693. DOI: 10.1038/nature07661.

Ku, Sebastian C.Y., Daphne T.W. Ng, Miranda G.S. Yap, and Sheng-Hao Chao (2008). "Effects of overexpression of X-box binding protein 1 on recombinant protein production in Chinese hamster ovary and NS0 myeloma cells". In: *Biotechnology and Bioengineering* 99.1, pp. 155–164. DOI: 10.1002/bit.21562.

Kumar, Niraj, Patrick Gammell, Paula Meleady, Michael Henry, and Martin Clynes (2008). "Differential protein expression following low temperature culture of suspension CHO-K1 cells". In: *BMC Biotechnology* 8, p. 42. DOI: 10.1186/1472-6750-8-42.

Kunert, Renate and David Reinhart (2016). "Advances in recombinant antibody manufacturing." In: *Applied microbiology and biotechnology* 100.8, pp. 3451–61. DOI: 10.1007/s00253-016-7388-9.

Kuo, Timothy T. and Victoria G. Aveson (2011). "Neonatal Fc receptor and IgG-based therapeutics". In: *mAbs* 3.5, pp. 422–430. DOI: 10.4161/mabs.3.5.16983.

Kupferschmidt, Kai (2013). "A lethal dose of RNA". In: *Science* 341.6147, pp. 732–733. DOI: 10.1126/science.341.6147.732.

LaFleur, David W. et al. (2013). "Monoclonal antibody therapeutics with up to five specificities Functional enhancement through fusion of target-specific peptides". In: *mAbs* 5.2, pp. 208–218. DOI: 10.4161/mabs.23043.

Lalonde, Marie Eve and Yves Durocher (2017). "Therapeutic glycoprotein production in mammalian cells". In: *Journal of Biotechnology* 251.December 2016, pp. 128–140. DOI: 10.1016/j.jbiotec.2017.04.028.

Le Fourn, Valérie, Pierre-Alain Alain Girod, Montse Buceta, Alexandre Regamey, and Nicolas Mermod (2014). "CHO cell engineering to prevent polypeptide aggregation and improve therapeutic protein secretion". In: *Metabolic Engineering* 21, pp. 91–102. DOI: 10.1016/J.YMBEN.2012.12.003.

Lee, A.-H., N. N. Iwakoshi, and L. H. Glimcher (2003). "XBP-1 Regulates a Subset of Endoplasmic Reticulum Resident Chaperone Genes in the Unfolded Protein Response". In: *Molecular and Cellular Biology* 23.21, pp. 7448–7459. DOI: 10.1128/mcb.23.21.7448-7459.2003.

Lee, Jong Kil and Nam Jung Kim (2017). "Recent advances in the inhibition of p38 MAPK as a potential strategy for the treatment of Alzheimer's disease". In: *Molecules* 22.8. DOI: 10.3390/molecules22081287.

Lee, Kyung Ha et al. (2016). "C9orf72 Dipeptide Repeats Impair the Assembly, Dynamics, and Function of Membrane-Less Organelles". In: *Cell* 167.3, 774–788.e17. DOI: 10.1016/j.cell.2016.10.002.

Lee, Wing-Hin, Ching-Yee Loo, Mary Bebawy, Frederick Luk, Rebecca Mason, and Ramin Rohanizadeh (2013). "Curcumin and its Derivatives: Their Application in Neuropharmacology and Neuroscience in the 21st Century". In: *Current Neuropharmacology* 11.4, pp. 338–378. DOI: 10.2174/1570159x11311040002.

Lesueur, Léa L., Lluis M. Mir, and Franck M. André (2016). "Overcoming the Specific Toxicity of Large Plasmids Electrotransfer in Primary Cells In Vitro". In: *Molecular Therapy - Nucleic Acids* 5.3, e291. DOI: 10.1038/mtna.2016.4.

Li, Ji and Zuojin Liu (2015). "[Comparison of efficiency and cytotoxicity of different transfection reagents in transfecting RIP140-siRNA into Kupffer cells]." In: *Nan fang yi ke da xue xue bao = Journal of Southern Medical University* 35.12, pp. 1694–700.

Li, Yunxia et al. (2019). "Enhanced production of anti-PD1 antibody in CHO cells through transient co-transfection with anti-apoptotic gene Bcl-XL combined with rapamycin". In: *Processes* 7.6, pp. 1–9. DOI: 10.3390/pr7060329.

Lim, Sing Fee, Kok Hwee Chuan, Sen Liu, Sophia O.H. Loh, Beatrice Y.F. Chung, Chin Chew Ong, and Zhiwei Song (2006). "RNAi suppression of Bax and Bak enhances viability in fed-batch cultures of CHO cells". In: *Metabolic Engineering* 8.6, pp. 509–522. DOI: 10.1016/J.YMBEN.2006.05.005.

Lim, Yiping, Niki S. C. Wong, Yih Yean Lee, Sebastian C. Y. Ku, Danny C. F. Wong, and Miranda G. S. Yap (2010). "Engineering mammalian cells in bioprocessing – current achievements and future perspectives". In: *Biotechnology and Applied Biochemistry* 55.4, pp. 175–189. DOI: 10.1042/ba20090363.

Lin, Jonathan H., Han Li, Yuhong Zhang, David Ron, and Peter Walter (2009). "Divergent effects of PERK and IRE1 signaling on cell viability". In: *PLoS ONE* 4.1. Ed. by Andreas Bergmann, e4170. DOI: 10.1371/journal.pone.0004170.

Lin, Nan et al. (2015). "Chinese hamster ovary (CHO) host cell engineering to increase sialylation of recombinant therapeutic proteins by modulating sialyltransferase expression". In: *Biotechnology Progress* 31.2, pp. 334–346. DOI: 10.1002/btpr.2038.

Lin, Z. Ping, Yashang Lee, Fang Lin, Michael F. Belcourt, Peining Li, Joseph G. Cory, Peter M. Glazer, and Alan C. Sartorelli (2011). "Reduced level of ribonucleotide reductase R2 subunits increases dependence on homologous recombination repair of cisplatin-induced DNA damage". In: *Molecular Pharmacology* 80.6, pp. 1000–1012. DOI: 10.1124/mol.111.074708.

Liu, Guangbo, Alyssa N. Coyne, Fen Pei, Spencer Vaughan, Matthew Chaung, Daniela C. Zarnescu, and J. Ross Buchan (2017). "Endocytosis regulates TDP-43 toxicity and turnover". In: *Nature Communications* 8.1. DOI: 10.1038/s41467-017-02017-x.

Liu, Justin K.H. (2014). *The history of monoclonal antibody development - Progress, remaining challenges and future innovations.* DOI: 10.1016/j.amsu.2014.09.001.

Madeira, Fábio et al. (2019). "The EMBL-EBI search and sequence analysis tools APIs in 2019". In: *Nucleic Acids Research* 47.W1, W636–W641. DOI: 10.1093/nar/gkz268.

Mahboubi, Hicham and Ursula Stochaj (2017). *Cytoplasmic stress granules: Dynamic modulators of cell signaling and disease*. DOI: 10.1016/j.bbadis.2016.12.022.

Martens, Tobias, Nils Ole Schmidt, Carmen Eckerich, Regina Filibrandt, Mark Merchant, Ralph Schwall, Manfred Westphal, and Katrin Lamszus (2006). "A novel one-armed anti-c-Met antibody inhibits glioblastoma growth in vivo". In: *Clinical Cancer Research* 12.20 PART 1, pp. 6144–6152. DOI: 10.1158/1078-0432.CCR-05-1418.

Maurisse, Rosalie, David De Semir, Hamid Emamekhoo, Babak Bedayat, Alireza Abdolmohammadi, Hooman Parsi, and Dieter C. Gruenert (2010). "Comparative transfection of DNA into primary and transformed mammalian cells from different lineages". In: *BMC Biotechnology* 10.1, p. 9. DOI: 10.1186/1472-6750-10-9.

Mcintyre, Glen J., Allison J. Arndt, Kirsten M. Gillespie, Wendy M. Mak, and Gregory C. Fanning (2011). "A comparison of multiple shRNA expression methods for combinatorial RNAi". In: *Genetic Vaccines and Therapy* 9, p. 9. DOI: 10.1186/1479-0556-9-9.

Meng, Zhongji and Mengji Lu (2017). *RNA interference-induced innate immunity, off-target effect, or immune adjuvant?* DOI: 10.3389/fimmu.2017.00331.

Merquiol, Emmanuelle, Dotan Uzi, Tobias Mueller, Daniel Goldenberg, Yaakov Nahmias, Ramnik J. Xavier, Boaz Tirosh, and Oren Shibolet (2011). "HCV causes chronic endoplasmic reticulum stress leading to adaptation and interference with the unfolded protein response". In: *PLoS ONE* 6.9. DOI: 10.1371/journal.pone.0024660.

Milstein, C and A C Cuello (1983). "Hybrid hybridomas and their use in immunohistochemistry." In: *Nature* 305.5934, pp. 537–40.

Mittal, Vivek (2004). "Improving the efficiency of RNA interference in mammals". In: *Nature Reviews Genetics* 5.5, pp. 355–365. DOI: 10.1038/nrg1323.

Mohan, Chaya, Soon Hye Park, Joo Young Chung, and Gyun Min Lee (2007). "Effect of doxycycline-regulated protein disulfide isomerase expression on the specific productivity of recombinant CHO cells: Thrombopoietin and antibody". In: *Biotechnology and Bioengineering* 98.3, pp. 611–615. DOI: 10.1002/bit.21453.

Mohr, Stephanie, Chris Bakal, and Norbert Perrimon (2010). "Genomic Screening with RNAi: Results and Challenges". In: *Annual Review of Biochemistry* 79.1, pp. 37–64. DOI: 10.1146/annurev-biochem-060408-092949.

Mohr, Stephanie E., Jennifer A. Smith, Caroline E. Shamu, Ralph A. Neumüller, and Norbert Perrimon (2014). "RNAi screening comes of age: Improved techniques and complementary approaches". In: *Nature Reviews Molecular Cell Biology* 15.9, pp. 591–600. DOI: 10.1038/nrm3860.

Moore, Chris B., Elizabeth H. Guthrie, Max Tze Han Huang, and Debra J. Taxman (2010). "Short hairpin RNA (shRNA): design, delivery, and assessment of gene knockdown." In: *Methods in molecular biology (Clifton, N.J.)* 629, pp. 141–158. DOI: 10.1007/978-1-60761-657-3_10.

Mori, Katsuhiro et al. (2004). "Engineering Chinese hamster ovary cells to maximize effector function of produced antibodies using FUT8 siRNA". In: *Biotechnology and Bioengineering* 88.7, pp. 901–908. DOI: 10.1002/bit.20326.

Morris, Jill A., Andrew J. Dorner, Chris A. Edwards, Linda M. Hendershott, and Randal J. Kaufman (1997). "Immunoglobulin binding protein (BiP) function is required to protect cells from endoplasmic reticulum stress but is not required for the secretion of selective proteins". In: *Journal of Biological Chemistry* 272.7, pp. 4327–4334. DOI: 10.1074/jbc.272.7.4327.

Mortazavi, Mehri, Mohammad Ali Shokrgozar, Soroush Sardari, Kayhan Azadmanesh, Reza Mahdian, Hooman Kaghazian, Seyed Nezamedin Hosseini, and Mohammad Hossein Hedayati (2019). "Using chemical chaperones to increase recombinant human erythropoietin secretion in CHO cell line". In: *Preparative Biochemistry and Biotechnology* 49.6, pp. 535–544. DOI: 10.1080/10826068.2018.1479865.

Mu, Ting Wei, Derrick Sek Tong Ong, Ya Juan Wang, William E. Balch, John R. Yates, Laura Segatori, and Jeffery W. Kelly (2008). "Chemical and Biological Approaches Synergize to Ameliorate Protein-Folding Diseases". In: *Cell* 134.5, pp. 769–781. DOI: 10.1016/j.cell.2008.06.037.

Mu, Ting-Wei, Derrick Sek Tong Ong, Ya-Juan Wang, William E. Balch, John R. Yates, Laura Segatori, and Jeffery W. Kelly (2008). "No Title". In: *Cell* 134.5.

Muchowski, Paul J. and Jennifer L. Wacker (2005). "Modulation of neurodegeneration by molecular chaperones". In: *Nature Reviews Neuroscience* 6.1, pp. 11–22. DOI: 10.1038/nrn1587.

Mullick, Alaka et al. (2006). "The cumate gene-switch: A system for regulated expression in mammalian cells". In: *BMC Biotechnology* 6.1, p. 43. DOI: 10.1186/1472-6750-6-43.

Muyldermans, S., T. Atarhouch, J. Saldanha, J. A.R.G. Barbosa, and R. Hamers (1994). "Sequence and structure of vh domain from naturally occurring camel heavy chain immunoglobulins lacking light chains". In: *Protein Engineering, Design and Selection* 7.9, pp. 1129–1135. DOI: 10.1093/protein/7.9.1129.

Neef, Danial, Alex Jaeger, and Dennis Thiele (2012). "Heat shock transcription factor 1 as a therapeutic target in neurodegenerative diseases". In: *Nat Rev Drug Discov.* 1023.12, pp. 930–944. DOI: 10.1038/jid.2014.371. arXiv: NIHMS150003.

Neumüller, Ralph A. and Norbert Perrimon (2011). "Where gene discovery turns into systems biology: Genome-scale RNAi screens in Drosophila". In: *Wiley Interdisciplinary Reviews: Systems Biology and Medicine* 3.4, pp. 471–478. DOI: 10.1002/wsbm.127.

Ngantung, Frederyk A., Peter G. Miller, Fikile R. Brushett, Goh Lin Tang, and Daniel I.C. Wang (2006). "RNA interference of sialidase improves glycoprotein sialic acid content consistency". In: *Biotechnology and Bioengineering* 95.1, pp. 106–119. DOI: 10.1002/bit.20997.

Nguyen, Lap Thi, Kazutaka Atobe, Jose Mario Barichello, Tatsuhiro Ishida, and Hiroshi Kiwada (2007). "Complex formation with plasmid DNA increases the cytotoxicity of cationic liposomes". In: *Biological and Pharmaceutical Bulletin* 30.4, pp. 751–757. DOI: 10.1248/bpb.30.751.

Nijwening, Jeroen H. and Roderick L. Beijersbergen (2010). "Using large-scale RNAi screens to identify novel drug targets for cancer". In: *IDrugs* 13.11, pp. 772–777.

Nishimiya, Daisuke, Takashi Mano, Kenji Miyadai, Hiroko Yoshida, and Tohru Takahashi (2013). "Overexpression of CHOP alone and in combination with chaperones is effective in improving antibody production in mammalian cells". In: *Applied Microbiology and Biotechnology* 97.6, pp. 2531–2539. DOI: 10.1007/s00253-012-4365-9.

Nishitoh, Hideki, Masao Saitoh, Yoshiyuki Mochida, Kohsuke Takeda, Hiroyasu Nakano, Mike Rothe, Kohei Miyazono, and Hidenori Ichijo (1998). "ASK1 is essential for JNK/SAPK activation by TRAF2". In: *Molecular Cell* 2.3, pp. 389–395. DOI: 10.1016/S1097-2765(00)80283-X.

Opentrons (2020).

Oslowski, Christine M and Fumihiko Urano (2011). "Measuring ER stress and the unfolded protein response using mammalian tissue culture system." In: *Methods in enzymology* 490, pp. 71–92. DOI: 10.1016/B978-0-12-385114-7.00004-0.

Ovcharenko, Dmitriy, Richard Jarvis, Scott Hunicke-Smith, Kevin Kelnar, and David Brown (2005). "High-throughput RNAi screening in vitro: From cell lines to primary cells". In: *RNA* 11.6, pp. 985–993. DOI: 10.1261/rna.7288405.

Ozcan, Umut, Erkan Yilmaz, Lale Ozcan, Masato Furuhashi, Eric Vaillancourt, Ross O Smith, Cem Z Görgün, and Gökhan S Hotamisligil (2006). "No Title". In: 313.5790. DOI: 10.1126/science.1128294.

Pacholewska, Alicja (2017). ""Loget" - a Uniform Differential Expression Unit to Replace "logFC" and "log2FC"". In: *Matters* 3.10, e201706000011. DOI: 10.19185/matters.201706000011.

Pan, Xiao, Mathieu Streefland, Ciska Dalm, René H. Wijffels, and Dirk E. Martens (2017). "Selection of chemically defined media for CHO cell fed-batch culture processes". In: *Cytotechnology* 69.1, pp. 39–56. DOI: 10.1007/s10616-016-0036-5.

Pasettoa, Matteo, Antonella Antignani, Pinar Ormanoglub, Eugen Buehlerb, Rajarshi Guhab, Ira Pastana, Scott E. Martinb, and David J. FitzGeralda (2015). "Whole-genome RNAi screen highlights components of the endoplasmic reticulum/Golgi as a source of resistance to immunotoxin-mediated cytotoxicity". In: *Proceedings of the National Academy of Sciences of the United States of America* 112.10, E1135–E1142. DOI: 10.1073/pnas.1501958112.

Patel, Yash D. (2018). "Design and characterisation of multi-gene expression vectors for CHO cell engineering". PhD thesis. Sheffield: Iniversity of Sheffield.

Peng, Lin, Wendian Xiong, Yanfei Cai, Yun Chen, Yang He, Jianfeng Yang, Jian Jin, and Huazhong Li (2017). "A simple, rapid method for evaluation of transfection efficiency based on fluorescent dye". In: *Bioengineered* 8.3, pp. 225–231. DOI: 10.1080/21655979.2016.1222995.

Peng, Ren-Wang and Martin Fussenegger (2009). "Molecular engineering of exocytic vesicle traffic enhances the productivity of Chinese hamster ovary cells". In: *Biotechnology and Bioengineering* 102.4, pp. 1170–1181. DOI: 10.1002/bit.22141.

Pérez-Rodriguez, Saumel, María de Jesús Ramírez-Lira, Mauricio A. Trujillo-Roldán, and Norma A. Valdez-Cruz (2020). "Nutrient supplementation strategy improves cell concentration and longevity, monoclonal antibody production and lactate metabolism of Chinese hamster ovary cells". In: *Bioengineered* 11.1, pp. 463–471. DOI: 10.1080/21655979.2020.1744266.

Perrimon, Norbert, Jian Quan Ni, and Lizabeth Perkins (2010). *In vivo RNAi: today and tomorrow.* DOI: 10.1101/cshperspect.a003640.

Plate, Lars, Christina Cooley, et al. (2016). "Small molecule proteostasis regulators that reprogram the ER to reduce extracellular protein aggregation". In: *eLife* 5.2016JULY, pp. 1–26. DOI: 10.7554/eLife.15550.

Plate, Lars and R Luke Wiseman (2017). "Regulating Secretory Proteostasis through the Unfolded Protein Response: From Function to Therapy". In: *Cell Press* 27.10. DOI: 10.1016/j.tcb.2017.05.006.

Portilho, Newton and Andrea Almeida (2011). "Maize Transformation to Obtain Plants Tolerant to Viruses by RNAi Technology". In: *Genetic Transformation*. InTech. DOI: 10.5772/24613.

Pybus, Leon P., Greg Dean, Nathan R. West, Andrew Smith, Olalekan Daramola, Ray Field, Stephen J. Wilkinson, and David C. James (2014). "Model-directed engineering of "difficult-to-express" monoclonal antibody production by Chinese hamster ovary cells". In: *Biotechnology and Bioengineering* 111.2, pp. 372–385. DOI: 10.1002/bit.25116.

Rader, Ronald A (2008). "(Re)defining biopharmaceutical". In: *Nature Biotechnology* 26.7, pp. 743–751. DOI: 10.1038/nbt0708-743.

Rahimi, P., V. Iranpur Mobarakeh, S. Kamalzare, F. Sajadian Fard, R. Vahabpour, and R. Zabihollahi (2018). "Comparison of transfection effi ciency of polymer-based and lipid-based transfection reagents". In: *Bratislava Medical Journal* 119.11, pp. 701–705. DOI: 10.4149/BLL_2018_125.

Rahimpour, Azam (2017). "Evaluation of Chemical Chaperones on the Transient Expression in Chinese Hamster". In: *Journal of Global Pharma Technology* 0.0.

Rahimpour, Azam, Behrouz Vaziri, Reza Moazzami, Leila Nematollahi, Farzaneh Barkhordari, Leila Kokabee, Ahmad Adeli, and Fereidoun Mahboudi (2013). "Engineering the Cellular Protein Secretory Pathway for Enhancement of Recombinant Tissue Plasminogen Activator Expression in Chinese Hamster Ovary Cells: Effects of CERT and XBP1s Genes". In: 23.8, pp. 1116–1122.

Reynolds, Angela, Devin Leake, Queta Boese, Stephen Scaringe, William S. Marshall, and Anastasia Khvorova (2004). "Rational siRNA design for RNA interference". In: *Nature Biotechnology* 22.3, pp. 326–330. DOI: 10.1038/nbt936.

Ridgway, John B.B., Leonard G. Presta, and Paul Carter (1996). "'Knobs-into-holes' engineering of antibody C(H)3 domains for heavy chain heterodimerization". In: *Protein Engineering* 9.7, pp. 617–621. DOI: 10.1093/protein/9.7.617.

Riechmann, Lutz, Michael Clark, Herman Waldmann, and Greg Winter (1988). "Reshaping human antibodies for therapy". In: *Nature* 332.6162, pp. 323–327. DOI: 10.1038/332323a0.

Rinderspacher, Alison et al. (2009). "Potent inhibitors of Huntingtin protein aggregation in a cell-based assay". In: *Bioorganic and Medicinal Chemistry Letters* 19.6, pp. 1715–1717. DOI: 10.1016/j.bmcl.2009.01.087.

Ritacco, Frank V., Yongqi Wu, and Anurag Khetan (2018). *Cell culture media for recombinant protein expression in Chinese hamster ovary (CHO) cells: History, key components, and optimization strategies.* DOI: 10.1002/btpr.2706.

Root, David E., Nir Hacohen, William C. Hahn, Eric S. Lander, and David M. Sabatini (2006). "Genome-scale loss-of-function screening with a lentiviral RNAi library". In: *Nature Methods* 3.9, pp. 715–719. DOI: 10.1038/nmeth924.

Ryno, Lisa M., R. Luke Wiseman, and Jeffery W. Kelly (2013). "Targeting unfolded protein response signaling pathways to ameliorate protein misfolding diseases". In: *Current Opinion in Chemical Biology* 17.3, pp. 346–352. DOI: 10.1016/j.cbpa.2013.04.009.

Sarkar, Sovan, Gauri Krishna, Sara Imarisio, Shinji Saiki, Cahir J. O'Kane, and David C. Rubinsztein (2008). "A rational mechanism for combination treatment of Huntington's disease using lithium and rapamycin". In: *Human Molecular Genetics* 17.2, pp. 170–178. DOI: 10.1093/hmg/ddm294.

Saurabh, Satyajit, Ambarish S. Vidyarthi, and Dinesh Prasad (2014). *RNA interference: Concept to reality in crop improvement*. DOI: 10.1007/s00425-013-2019-5.

Scekic-Zahirovic, Jelena et al. (2016). "Toxic gain of function from mutant FUS protein is crucial to trigger cell autonomous motor neuron loss". In: *The EMBO Journal* 35.10, pp. 1077–1097. DOI: 10.15252/embj.201592559.

Schwarz, Dianne S., György Hutvágner, Benjamin Haley, and Phillip D. Zamore (2002). "Evidence that siRNAs function as guides, not primers, in the Drosophila and human RNAi pathways". In: *Molecular Cell* 10.3, pp. 537–548. DOI: 10.1016/S1097-2765(02)00651-2.

Shen, Ying, Laurent Meunier, and Linda M. Hendershot (2002). "Identification and characterization of a novel endoplasmic reticulum (ER) DnaJ homologue, which stimulates ATPase activity of BiP in vitro and is induced by ER stress". In: *Journal of Biological Chemistry* 277.18, pp. 15947–15956. DOI: 10.1074/jbc.M112214200.

Shoulders, Matthew D. et al. (2013). "Stress-Independent Activation of XBP1s and/or ATF6 Reveals Three Functionally Diverse ER Proteostasis Environments". In: *Cell Reports* 3.4, pp. 1279–1292. DOI: 10.1016/j.celrep.2013.03.024.

Shuen, W. H., R. Kan, Z. Yu, H. L. Lung, and M. L. Lung (2015). "Novel lentiviral-inducible transgene expression systems and versatile single-plasmid reporters for in vitro and in vivo cancer biology studies". In: *Cancer Gene Therapy* 22.4, pp. 207–214. DOI: 10.1038/cgt.2015.9.

Shukla, Abhinav A, Leslie S Wolfe, Sigma S Mostafa, and Carnley Norman (2017). "Evolving trends in mAb production processes". In: *Bioengineering & Translational Medicine* 2.November 2016, pp. 58–69. DOI: 10.1002/btm2.10061.

Shukla, Surendra K. et al. (2015). "MUC16-mediated activation of mTOR and c-MYC reprograms pancreatic cancer metabolism". In: *Oncotarget* 6.22, pp. 19118–19131. DOI: 10.18632/oncotarget.4078.

Sigoillot, Frederic D. and Randall W. King (2011). "Vigilance and validation: Keys to success in RNAi screening". In: *ACS Chemical Biology* 6.1, pp. 47–60. DOI: 10.1021/cb100358f.

Singh, Pankaj K., Randall E. Brand, and Kamiya Mehla (2012). "MicroRNAs in pancreatic cancer metabolism". In: *Nature Reviews Gastroenterology and Hepatology* 9.6, pp. 334–344. DOI: 10.1038/nrgastro.2012.63.

Sioud, Mouldy (2011). "Promises and challenges in developing RNAi as a research tool and therapy." In: *Methods in molecular biology (Clifton, N.J.)* Vol. 703, pp. 173–187. DOI: 10.1007/978-1-59745-248-9_12.

Smith, Jennifer A., Elizabeth A. White, Mathew E. Sowa, Maria L.C. Powell, Matthias Ottinger, J. Wade Harper, and Peter M. Howley (2010). "Genome-wide siRNA screen identifies SMCX, EP400, and Brd4 as E2-dependent regulators of human papillomavirus oncogene expression". In: *Proceedings of the National Academy of Sciences of the United States of America* 107.8, pp. 3752–3757. DOI: 10.1073/pnas.0914818107.

Smith, Karen T. and Jerry L. Workman (2012). "Chromatin Proteins: Key Responders to Stress". In: *PLoS Biology* 10.7, e1001371. DOI: 10.1371/journal.pbio.1001371.

Smith, Steven E., Susana Granell, Laia Salcedo-Sicilia, Giovanna Baldini, Gustavo Egea, Jeff H. Teckman, and Giulia Baldini (2011). "Activating transcription factor 6 limits intracellular accumulation of mutant α 1-antitrypsin Z and mitochondrial damage in hepatoma cells". In: *Journal of Biological Chemistry* 286.48, pp. 41563–41577. DOI: 10.1074/jbc.M111.280073.

Sung, Hoon Back, Kyungho Lee, Elizabeth Vink, and Randal J. Kaufman (2006). "Cytoplasmic IRE1α-mediated XBP1 mRNA splicing in the absence of nuclear processing and endoplasmic reticulum stress". In: *Journal of Biological Chemistry* 281.27, pp. 18691–18706. DOI: 10.1074/jbc.M602030200.

Sung, Yun Hee, Jae Seong Lee, Soon Hye Park, Jane Koo, and Gyun Min Lee (2007). "Influence of co-down-regulation of caspase-3 and caspase-7 by siRNAs on sodium butyrate-induced apoptotic cell death of Chinese hamster ovary cells producing thrombopoietin". In: *Metabolic Engineering* 9.5-6, pp. 452–464. DOI: 10.1016/j.ymben.2007.08.001.

Tabar, Mehdi Sharifi, Mahdi Hesaraki, Fereshteh Esfandiari, Fazel Sahraneshin Samani, Haghighat Vakilian, and Hossein Baharvand (2015). "Evaluating electroporation and lipofectamine approaches for transient and stable transgene expressions in human fibroblasts and embryonic stem cells". In: *Cell Journal* 17.3, pp. 438–450. DOI: 10.22074/cellj.2015.5.

Takagi, Yasuhiro, Takuya Kikuchi, Ryuta Wada, and Takeshi Omasa (2017). "The enhancement of antibody concentration and achievement of high cell density CHO cell cultivation by adding nucleoside". In: *Cytotechnology* 69.3, pp. 511–521. DOI: 10.1007/s10616-017-0066-7.

Tansey, E M and P P Catterall (1994). "Monoclonal antibodies: A witness seminar in contemporary medical history". In: *Medical History* 38.3, pp. 322–327. DOI: 10.1017/S0025727300036632.

Tavender, Timothy J. and Neil J. Bulleid (2010). "Molecular mechanisms regulating oxidative activity of the Ero1 family in the endoplasmic reticulum". In: *Antioxidants and Redox Signaling* 13.8, pp. 1177–1187. DOI: 10.1089/ars.2010.3230.

Theis, Mirko and Frank Buchholz (2011). "High-throughput RNAi screening in mammalian cells with esiRNAs". In: *Methods* 53.4, pp. 424–429. DOI: 10.1016/j.ymeth.2010.12.021.

Thuerauf, Donna J, Marie Marcinko, Peter J Belmont, and Christopher C Glembotski (2007). "Effects of the isoform-specific characteristics of ATF6α and ATF6β on endoplasmic reticulum stress response gene expression and cell viability". In: *Journal of Biological Chemistry* 282.31, pp. 22865–22878. DOI: 10.1074/jbc.M701213200.

Tigges, Marcel and Martin Fussenegger (2006). "Xbp1-based engineering of secretory capacity enhances the productivity of Chinese hamster ovary cells". In: *Metabolic Engineering* 8.3, pp. 264–272. DOI: 10.1016/j.ymben.2006.01.006.

Tiscornia, Gustavo, Oded Singer, Masahito Ikawa, and Inder M. Verma (2003). "A general method for gene knockdown in mice by using lentiviral vectors expressing small interfering RNA". In: *Proceedings of the National Academy of Sciences of the United States of America* 100.4, pp. 1844–1848. DOI: 10.1073/pnas.0437912100.

Todd, Tiffany W. and Janghoo Lim (2013). *Aggregation formation in the polyglutamine diseases: Protection at a cost?* DOI: 10.1007/s10059-013-0167-x.

Tran, Nham, Mitch Raponi, Ian W. Dawes, and Greg M. Arndt (2004). "Control of specific gene expression in mammalian cells by co-expression of long complementary RNAs". In: *FEBS Letters* 573.1-3, pp. 127–134. DOI: 10.1016/j.febslet.2004.07.075.

Trummer, Evelyn et al. (2008). "Transcriptional profiling of phenotypically different Epo-Fc expressing CHO clones by cross-species microarray analysis". In: *Biotechnology Journal* 3.7, pp. 924–937. DOI: 10.1002/biot.200800038.

Urano, Fumihiko, Xiao Zhong Wang, Anne Bertolotti, Yuhong Zhang, Peter Chung, Heather P. Harding, and David Ron (2000). "Coupling of stress in the ER to activation of JNK protein kinases by transmembrane protein kinase IRE1". In: *Science* 287.5453, pp. 664–666. DOI: 10.1126/science.287.5453.664.

Valitacell (2020).

Vázquez-Rey, María and Dietmar A. Lang (2011). "Aggregates in monoclonal antibody manufacturing processes". In: *Biotechnology and Bioengineering* 108.7, pp. 1494–1508. DOI: 10.1002/bit.23155.

Vembar, Shruthi S. and Jeffrey L. Brodsky (2008). "One step at a time: Endoplasmic reticulum-associated degradation". In: *Nature Reviews Molecular Cell Biology* 9.12, pp. 944–957. DOI: 10.1038/nrm2546.

Walsh, Gary (Biochemist) (2003). *Biopharmaceuticals : biochemistry and biotechnology*. J. Wiley, p. 551.

Wang, Tian Yun and Xiao Guo (2020). "Expression vector cassette engineering for recombinant therapeutic production in mammalian cell systems". In: *Applied Microbiology and Biotechnology* 104.13, pp. 5673–5688. DOI: 10.1007/s00253-020-10640-w.

Ward, E. Sally, Detlef Güssow, Andrew D. Griffiths, Peter T. Jones, and Greg Winter (1989). "Binding activities of a repertoire of single immunoglobulin variable domains secreted from Escherichia coli". In: *Nature* 341.6242, pp. 544–546. DOI: 10.1038/341544a0.

Waza, Masahiro, Hiroaki Adachi, Masahisa Katsuno, Makoto Minamiyama, Fumiaki Tanaka, Manabu Doyu, and Gen Sobue (2006). *Modulation of Hsp90 function in neurodegenerative disorders: A molecular-targeted therapy against disease-causing protein.* DOI: 10.1007/s00109-006-0066-0.

Weber, Wilfried and Martin Fussenegger (2004). "Inducible gene expression in mammalian cells and mice." In: *Methods in molecular biology (Clifton, N.J.)* 267, pp. 451–466. DOI: 10.1385/1-59259-774-2:451.

Wen, Xinmei et al. (2014a). "Antisense proline-arginine RAN dipeptides linked to C9ORF72-ALS/FTD form toxic nuclear aggregates that initiate invitro and invivo neuronal death". In: *Neuron* 84.6, pp. 1213–1225. DOI: 10.1016/j.neuron.2014.12.010.

— (2014b). "Antisense proline-arginine RAN dipeptides linked to C9ORF72-ALS/FTD form toxic nuclear aggregates that initiate invitro and invivo neuronal death". In: *Neuron* 84.6, pp. 1213–1225. DOI: 10.1016/j.neuron.2014.12.010.

Weng, Yanjie, Ying Shi, Xi Xia, Wenjuan Zhou, Hongyan Wang, and Changyu Wang (2017). "A multi-shRNA vector enhances the silencing efficiency of exogenous and endogenous genes in human cells". In: *Oncology Letters* 13.3, pp. 1553–1562. DOI: 10.3892/ol.2017.5672.

Wesolowski, Janusz et al. (2009). "Single domain antibodies: Promising experimental and therapeutic tools in infection and immunity". In: *Medical Microbiology and Immunology* 198.3, pp. 157–174. DOI: 10.1007/s00430-009-0116-7.

Wilkinson, Ian C., Susan B. Fowler, et al. (2013). "Monovalent IgG4 molecules: Immunoglobulin Fc mutations that result in a monomeric structure". In: *mAbs* 5.3, pp. 406–417. DOI: 10.4161/mabs.23941.

Wilkinson, Ian C., Catherine J. Hall, et al. (2009). "High resolution NMR-based model for the structure of a scFv-IL-1β complex: Potential for NMR as a key tool in therapeutic antibody design and development". In: *Journal of Biological Chemistry* 284.46, pp. 31928–31935. DOI: 10.1074/jbc.M109.025304.

Wiseman, R Luke, Evan T Powers, Joel N Buxbaum, Jeffery W Kelly, and William E Balch (2007). "An Adaptable Standard for Protein Export from the Endoplasmic Reticulum". In: *Cell* 131.4, pp. 809–821. DOI: 10.1016/j.cell.2007.10.025.

Wlaschin, Katie F. and Wei Shou Hu (2007). "Engineering cell metabolism for high-density cell culture via manipulation of sugar transport". In: *Journal of Biotechnology* 131.2, pp. 168–176. DOI: 10.1016/j.jbiotec.2007.06.006.

Wolozin, Benjamin and Pavel Ivanov (2019). "Stress granules and neurodegeneration". In: *Nature Reviews Neuroscience* 20.11, pp. 649–666. DOI: 10.1038/s41583-019-0222-5.

Wong, Danny Chee Furng, Kathy Tin Kam Wong, Peter Morin Nissom, Chew Kiat Heng, and Miranda Gek Sim Yap (2006). "Targeting early apoptotic genes in batch and fed-batch CHO cell cultures". In: *Biotechnology and Bioengineering* 95.3, pp. 350–361. DOI: 10.1002/bit.20871.

Wu, Suh-Chin (2009). "RNA interference technology to improve recombinant protein production in Chinese hamster ovary cells". In: *Biotechnology Advances* 27, pp. 417–422. DOI: 10.1016/j.biotechadv.2009.03.002.

Wu, W. (2004). "A novel approach for evaluating the efficiency of siRNAs on protein levels in cultured cells". In: *Nucleic Acids Research* 32.2, 17e–17. DOI: 10.1093/nar/gnh010.

Wurm, Florian M. (2004). "Production of recombinant protein therapeutics in cultivated mammalian cells". In: *Nature Biotechnology* 22.11, pp. 1393–1398. DOI: 10.1038/nbt1026.

Xia, Xu Gang, Hongxia Zhou, and Zuoshang Xu (2006). "Multiple shRNAs expressed by an inducible pol II promoter can knock down the expression of multiple target genes". In: *BioTechniques* 41.1, pp. 64–68. DOI: 10.2144/000112198.

Xu, Jianlin, Peifeng Tang, Andrew Yongky, Barry Drew, Michael C. Borys, Shijie Liu, and Zheng Jian Li (2019). "Systematic development of temperature shift strategies for Chinese hamster ovary cells based on short duration cultures and kinetic modeling". In: *mAbs* 11.1, pp. 191–204. DOI: 10.1080/19420862.2018.1525262.

Xu, Xun et al. (2011). "The genomic sequence of the Chinese hamster ovary (CHO)-K1 cell line". In: *Nature Biotechnology* 29.8, pp. 3–5. DOI: 10.1038/nbt.1932.

Yancey, Paul H., Mary E. Clark, Steven C. Hand, R. David Bowlus, and George N. Somero (1982). "Living with water stress: Evolution of osmolyte systems". In: *Science* 217.4566, pp. 1214–1222. DOI: 10.1126/science.7112124.

Yang, Zhang et al. (2015). "Engineered CHO cells for production of diverse, homogeneous glycoproteins". In: *Nature Biotechnology* 33.8, pp. 842–844. DOI: 10.1038/nbt.3280.

Yates, Andrew D. et al. (2020). "Ensembl 2020". In: *Nucleic Acids Research* 48.D1, pp. D682–D688. DOI: 10.1093/nar/gkz966.

Yee, Joon Chong, Marcela De Leon Gatti, Robin J. Philp, Miranda Yap, and Wei Shou Hu (2008). "Genomic and proteomic exploration of CHO and hybridoma cells under sodium butyrate treatment". In: *Biotechnology and Bioengineering* 99.5, pp. 1186–1204. DOI: 10.1002/bit.21665.

Yee, Joon Chong, Ziomara P. Gerdtzen, and Wei-Shou Hu (2009). "Comparative transcriptome analysis to unveil genes affecting recombinant protein productivity in mammalian cells". In: *Biotechnology and Bioengineering* 102.1, pp. 246–263. DOI: 10.1002/bit.22039.

Yi, Rui, Brian P. Doehle, Yi Qin, Ian G. Macara, and Bryan R. Cullen (2005). "Overexpression of Exportin 5 enhances RNA interference mediated by short hairpin RNAs and microRNAs". In: *RNA* 11.2, pp. 220–226. DOI: 10.1261/rna.7233305.

Yoshida, Hiderou (2007). "ER stress and diseases". In: *FEBS Journal* 274.3, pp. 630–658. DOI: 10.1111/j.1742-4658.2007.05639.x.

Yoshida, Hiderou, Toshie Matsui, Nobuko Hosokawa, Randal J. Kaufman, Kazuhiro Nagata, and Kazutoshi Mori (2003). "A time-dependent phase shift in the mammalian unfolded protein response". In: *Developmental Cell* 4.2, pp. 265–271. DOI: 10.1016/S1534-5807(03)00022-4.

Yoshida, Hiderou, Toshie Matsui, Akira Yamamoto, Tetsuya Okada, and Kazutoshi Mori (2001). "XBP1 mRNA is induced by ATF6 and spliced by IRE1 in response to ER stress to produce a highly active transcription factor". In: *Cell* 107.7, pp. 881–891. DOI: 10.1016/S0092-8674(01)00611-0.

Young, Lydia M., Alison E. Ashcroft, and Sheena E. Radford (2017). *Small molecule probes of protein aggregation*. DOI: 10.1016/j.cbpa.2017.06.008.

Zhang, Liang, Andreas Castan, Joanne Stevenson, Nathalie Chatzissavidou, Francisco Vilaplana, and Veronique Chotteau (2019). "Combined effects of glycosylation precursors and lactate on the glycoprofile of IgG produced by CHO cells". In: *Journal of Biotechnology* 289.November 2018, pp. 71–79. DOI: 10.1016/j.jbiotec.2018.11.004.

Zhang, Peiqing, Diana Lifen Tan, Desmond Heng, Tianhua Wang, Mariati, Yuansheng Yang, and Zhiwei Song (2010). "A functional analysis of N-glycosylation-related genes on sialylation of recombinant erythropoietin in six commonly used mammalian cell lines". In: *Metabolic Engineering* 12.6, pp. 526–536. DOI: 10.1016/j.ymben.2010.08.004.

Zhang, Yinan et al. (2012). "Chiral cyclohexane 1,3-diones as inhibitors of mutant SOD1-dependent protein aggregation for the treatment of ALS". In: *ACS Medicinal Chemistry Letters* 3.7, pp. 584–587. DOI: 10.1021/ml3000963.

Zou, Gang Ming (2010). "RNAi in stem cells: Current status and future perspectives". In: *Methods in Molecular Biology*. Vol. 650, pp. 3–14. DOI: 10.1007/978-1-60761-769-3_1.